

Advanced Ziegler-Natta catalyst tools to empower polypropylene innovators

Jose M. Rego, John Kaarto, Amaia Montoya,

W.R. GRACE Co., 7500 Grace Drive, Columbia, MD
21044, USA

Abstract

GRACE has developed advanced internal donor, external donor, support and process aids technologies that afford enhanced value for polypropylene (PP) producers, converters, brand owners and ultimately consumers. These advanced Ziegler-Natta (ZN) building blocks make possible innovation in the polypropylene (PP) industry to address the needs of the highly complex PP market. This presentation reviews some of these technologies and showcases how GRACE ZN catalyst technology enables innovative product features such as ultra-high clarity thermoformed parts, low temperature no-break and high MFR reactor TPO injection molding grades for automotive and low blooming injection molded articles for packaging applications.

Introduction

W.R. GRACE (GRACE hereafter) is the leading third party PP catalyst supplier licensor of polypropylene (PP). This leadership position is the result of targeted acquisitions that have afforded the broadest catalyst portfolio in the industry and, most importantly, because of GRACE's relentless commitment to catalyst innovation that can enable our customers globally. In this connection, GRACE's innovation approach is to understand and address market needs. In the SPE PO 2015 Conference, we presented GRACE's four market themes pictorial that has become our innovation compass [1] for catalyst development efforts. Figure 1 shows those four innovation themes that revolve around developing: (i) stronger materials that enable down-gauging (lighter theme); (ii) materials with rheological features that make it possible to increase fabrication rates (faster); (iii) materials with less catalyst residuals, lower Volatile Organic Compounds (VOC) content, lower taste and odor by avoiding peroxide cracking and non-Phthalate based (cleaner); and (iv) materials with higher transparency (clearer). These themes are still the dominant innovation drivers in 2016.

Market drivers are a key part of the innovation process, but technology capability is critical to being able to provide solutions that enable PP producers, converters and brand owners. In this regard, GRACE has developed a ZN

catalyst technology platform that enables catalyst innovation to address market known and unknown needs.

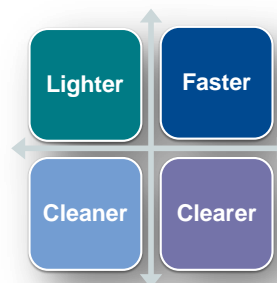


Figure 1: Innovation themes that drive the PP industry since 2005 (market research by GRACE).

This paper discusses tools that GRACE uses to enable catalyst technology development and provides several examples of PP innovation enabled by GRACE catalyst technology.

GRACE ZN Tools

GRACE has built a PP catalyst innovation tool box over the last 10 years that has made us the leading third party supplier globally. Figure 2 shows a high level view of the tool box that GRACE uses to address product needs for different applications and process requirements for the different processes used by PP producers (UNIPOL® PP, SPHERIPOL, INNOVENE, NOVOLLEN, HYPOL, SPHERIZONE ...). Some more details of these options are provided later in the text. The selection of catalyst components has a substantial influence on PP products that can be made and also on the operability and the cost in use of the PP manufacturing units. Regarding the former, how the catalyst is built will influence MFR capability, isotacticity range, Molecular Weight Distribution (MWD), ethylene-propylene rubber (EPR) content capability and ethylene distribution. Catalysts can be assembled to address the commodity markets, or differentiated spaces or both (the ideal concept of one catalyst for all applications). In relation to how the catalyst components listed in Figure 2 can affect plant operability and cost in use, this is done by tailoring catalyst productivity, catalyst life time and catalyst particle size.

The internal donor captures much of the attention of research groups in academia and industry. It is certainly a key element of the ZN technology, but other elements (support, external donors and process aids) are also critical to providing the desired performance. GRACE has developed internal donor technology that is considered as the 6th generation catalyst platform because of very high productivities, broad XS capability, excellent H₂ response and best in class operability. This platform was discovered

by using high throughput tools that have allowed GRACE to have access to an extensive library of internal donors that will enable constant innovation in years to come. Figure 3 shows a “shotgun” plot of polydispersity index (PDI) versus XS that includes a large number of the internal donors in the GRACE library and highlights the ability that GRACE has to be the industry leading innovator. The CONSISTA® catalyst commercialized in 2012 for the UNIPOL® PP process is one of the points in this plot. It should be noted that all internal donors in Figure 3 are non-phthalate in nature.

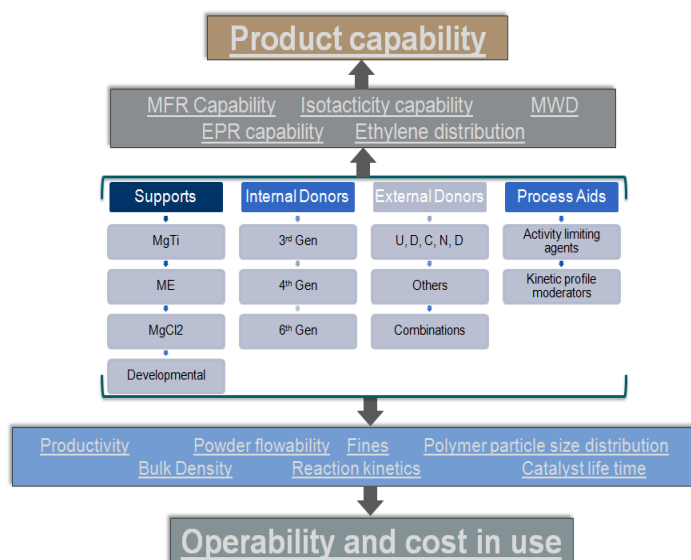


Figure 2: GRACE catalyst innovation tool box and product and process properties impacted.

Other recent innovations that are also very exciting from an innovation perspective is the discovery activity moderators that provide high flexibility to meet the needs of different processes used in the industry.

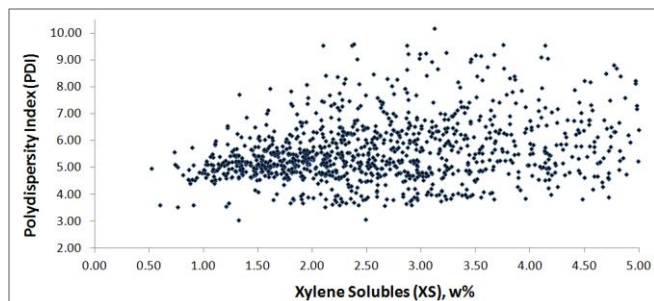


Figure 3: Shotgun plot that shows GRACE's internal donor capability. All internal donors in this plot are non-phthalate in nature.

Showcases

Ultra-clear PP thermoformed articles

The food packaging industry is looking for PP offerings that can provide enhanced clarity and top load of thermoformed articles to compete with PET. The main drivers for this interest are that PET has very high density and it is difficult to process.

Ethylene random copolymers (e-RCP) do not seem to meet the requirements that are given in Figure 4 for a deep drawn article (cup). Grace has developed a butene random copolymer (b-RCP) based on 6th generation catalyst technology to address this market need. The key working hypothesis for this development work is that GRACE's 6th generation catalyst affords a more random distribution of both comonomer which translates into smaller crystal domains that translates into lower haze. In addition, b-RCP affords higher modulus which translates into higher top load.

Figure 5 shows the results obtained for a number of e-RCP and b-RCP with and without clarifier. It is important to note that thermoformed cups were made and analyzed at the Milliken Research Center in Spartanburg, South Carolina (see Appendix for details). As can be seen from Figure 5, only the cups made with clarified b-RCP fall inside the performance requirements of this development.

This enhanced behavior could be explained as a result of the pending ethyl groups in b-RCP been more prompt to participate in the lamellar crystalline phase rather than in the amorphous phase which can result in faster crystallization rates vs e-RCP. Faster crystallization rates can help freeze the orientation introduced during the thermoforming step which, in turn, can translate into increased modulus. In addition, the presence of advanced clarifiers can decrease crystal size to sub-micron levels, which combined with a lower concentration of amorphous phase can lead to enhanced haze. The latter effect could be related to a lower concentration of refractive index change interfaces.

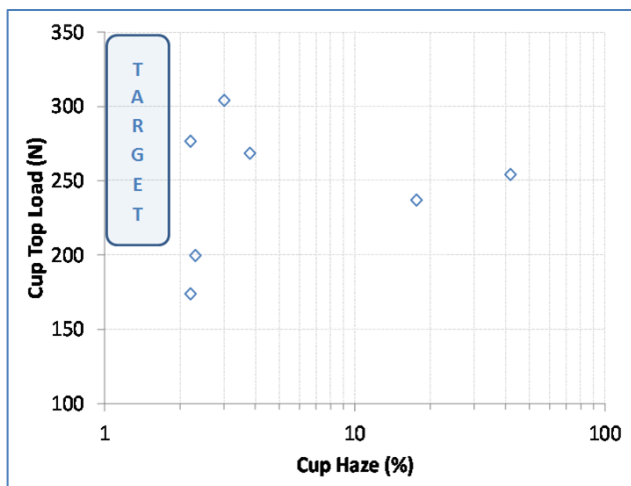


Figure 4: Pictorial representation of target cup top load and haze. The blue diamond's correspond to cups produced with commercial ethylene random copolymers (e-RCP).

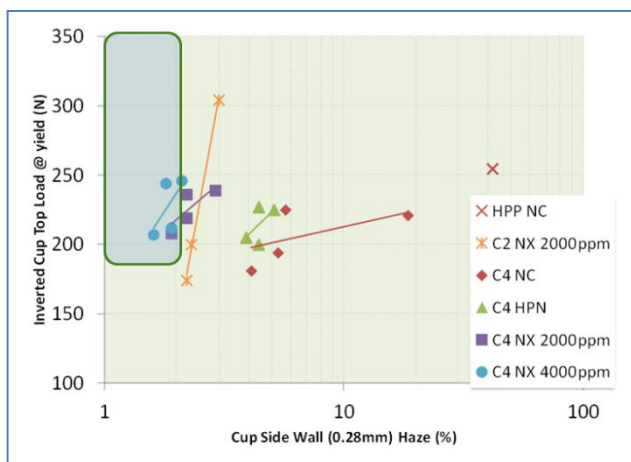


Figure 5: Cup top load versus side wall haze for the different prototypes tested in this development study. NC = no clarifier; HPN = HPN 600ei; NX = NX8000; C2 = ethylene-RCP; C4 = butene-RCP.

High MFR in-reactor TPO's

One of the trends in the automotive industry is high melt flow rate (MFR) in-reactor TPO to enable shorter injection molding cycle time of large intricate parts. TPO is defined here as an impact copolymer (ICP) that shows no break behavior. The no break requirement is temperature dependent and the industry speaks about room temperature, 0 °C, -20 °C and -30 °C no break performance. The main design parameters for no-break performance are EPR content (EPR^c) and EPR particle size distribution. EPR^c is limited by powder flowability that is controlled by catalyst technology and process hardware considerations. In this example, EPR^c is limited to 33 w%. The EPR particle size distribution is controlled

by thermodynamic and kinetic factors. The latter relate to the compatibility of the two phases which can be moderated by adjusting the ethylene content in the EPR and the former depends on shear forces in the extruder and viscosity differences between rubber (discontinuous) and matrix (continuous) phases. This has been described generically by Taylor's empirical relationship of domain break up (eq. [1])

$$d \propto \frac{G}{\gamma} \frac{\eta_R}{\eta_M} \dots [1]$$

Where \underline{d} is the EPR average particle size, $\underline{\eta}$ is the EPR (R) or the matrix (M) viscosity, \underline{G} is the HPP/EPR interfacial tension and γ is the shear rate. The viscosity ratio η_R/η_M can be converted to a ratio of the TPO MFR (MFR^T) and the MFR of the matrix (MFR^M) and this ratio is denoted in this paper as β/α ratio.

Figure 6 shows the master lines of MFR^T versus MFR^M for different β/α ratios. The typical β/α working range is from 1 to 3 with most products being in the 1.5 to 2.5 bracket. It is apparent from this Figure 6 that a MFR^T = 20 g/10 min will require a MFR^M of 20 g/10min for $\beta/\alpha = 1$, of ~ 40 g/10min for $\beta/\alpha = 2$ and of ~ 100 g/10min for $\beta/\alpha = 3$. Higher MFR^T will demand even higher MFR^M. To make this kind of MFR^T, it is necessary to use a catalyst with enhanced MFR response. The Grace 6th generation catalyst platform provides this capability and enables high MFR^T in-reactor TPO. Figure 7 shows the room temperature izod as a function of MFR for a number of 6th generation catalyst based r-TPOs at three β/α ratios (modeled values obtained from empirical correlations). All these r-TPO's in Figure 7 exhibit the same EPR^c (33 w%).

It appears from Figure 7 that room temperature no-break r-TPO's having a MFR as high as 30 g/10 min can be produced with GRACE catalyst technology.

Low blooming technology e-RCP

The third and final showcase included in this paper is the development of low blooming RCP technology for food packaging applications. Blooming is a thin layer of chemical products that migrate to the part as a function of service temperature and time. The research work done for this development showed that blooming is primarily related to PP oligomers and other ethylene-propylene chains and not to additives used in this application. This thin layer changes the optical properties of the part (increases haze) and this is the way performance is measured (see additional details in Appendix). The GRACE 6th generation catalyst enables the control of XS in RCP to achieve ratios of XS to ethylene content (Et) (XS/Et) even < 1 at certain Et levels. Figure 8 shows the

level of haze change after treating molded parts to 55 °C temperature for 24 hours as a function of the XS/Et ratio. A haze change of 15 % is considered acceptable by brand owners in this application. space. As can be seen from this Figure, the RCP materials that fall within the acceptable range are those with an XS/Et ratio < 1.5.

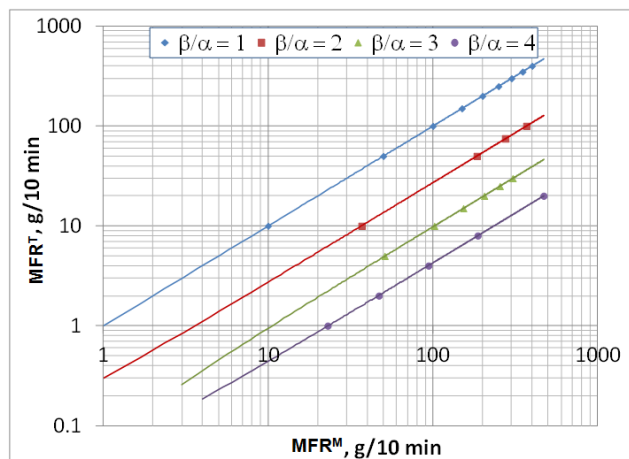


Figure 6: MFR^T versus MFR^M for different β/α ratios.

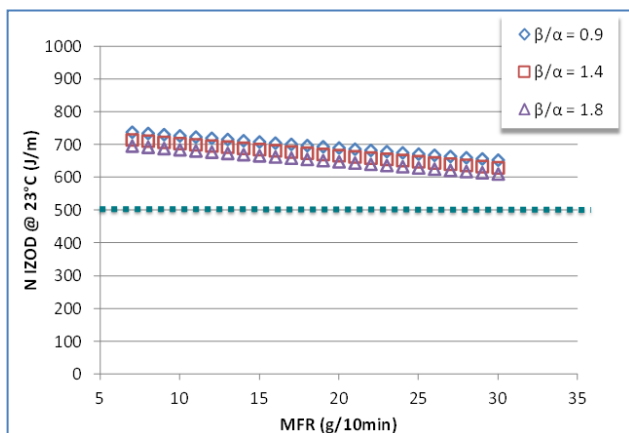


Figure 7: Room temperature izod as a function of MFR for modeled r-TPO's (empirical correlations done on 6th generation based TPO's). EPR^c is 33 w% for all modeled systems in the graph.

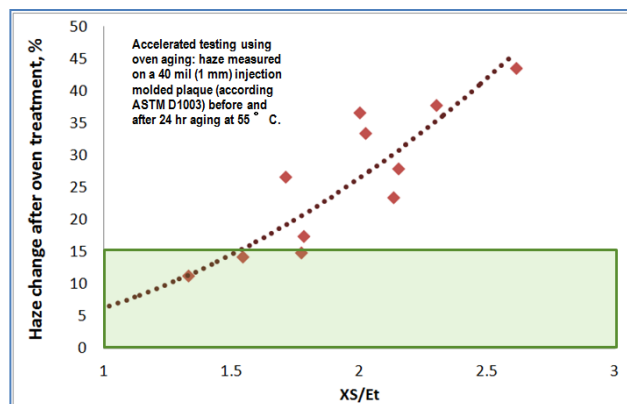


Figure 8: % change in haze after oven treatment as a function of the XS/Et ratio for different RCP prototypes studied in this showcase.

Conclusions

Grace has developed advanced internal donor, external donor, support and process aids technologies that afford enhanced value for PP producers, converters, brand owners and ultimately consumers. These advanced ZN building blocks make it possible to address the needs of the highly complex PP market. This presentation showcased how GRACE ZN catalyst technology enables innovative product features such as ultra-high clarity thermoformed parts, low temperature no-break and high MFR reactor TPO injection molding grades for automotive and low blooming injection molded articles for packaging applications.

Acknowledgements

The authors would like to thank Milliken for making available to GRACE their sheet extrusion and thermoforming lines as well as testing labs for the development work of the ultra-clear RCP.

References

- 1) Kaarto, J., Van Egmond, J., Rego, J.M., Williams, C., SPE PO Houston Conference 2015,
- 2) Cheruvather, A. V., Langer, E. H. G., Niemantsverdriet, H. J. W., and Thune, P. C., *Langmuir*, 2012, 28(5), 2643.
- 3) Turunen, A., Linnolahti, M., Karttunen, V. A., Pakkanen, T. A., Denifl, P., and Leinonen, T., *Journal of Molecular Catalysts A: Chemical*, 2011, 334 (1), 103.
- 4) Kuklin, M. S., Bazhenov, A. S., Denifl, P., Leinonen, T., Linnolahti, M., and Pakkanen, T. A., *Surface Science*, 2015, 625, 5.
- 5) Andoni, A., Chadwick, J. C., Niemantsverdriet, H. J. W., Thune, P. C., *Journal of Catalysts*, 2008, 257(1), 81.
- 6) Bazhenov, A.S., Denifl, P., Leinonen, T., Pakkanen, A., Linnolahti, M., Pakkanen, T.A.; J. Phys. Chem. C2014, 118, 27878-27883

Appendix

Raw materials

R-TPO, e-RCP and b-RCP were made in GRACE pilot plant set ups. All materials were formulated with anti-oxidants (Irganox 1010 and Irgafos 168) and an acid scavenger (calcium stearate or ZnO or DHT4A). HPN 600ei and NX8000 were kindly provided by Milliken. Additives were dispersed in the polymers using lab twin screw extruders.

Methods

Properties tested are shown in Table 1 as well as the standard methods used. The r-TPO and low blooming projects testing was performed in GRACE Labs.

Table 1: Properties tested and test methods

Property	Method
Flexural Modulus, MPa	ASTM D790
Notched Izod Impact, J/m	ASTM D256
MFR, g/10 min	ASTM D1238
XS, w%	ASTM D5492
Haze in injection molded plaques	ASTM D1003

XS were measured with a Viscotek instrument equipped with Flow Injection Polymer Analyzer. Sample preparation is very similar to what is described in the ASTM method D5492.

Ethylene content in the r-TPO, b-RCP, and e-RCP, ethylene content in the r-TPO EPR and r-TPO EPR content were measured with FTIR methods developed for GRACE catalysts systems.

Blooming on e-RCP 1 mm plaques was measured by placing the molded plaques in an oven at 55 °C for 24 h and measuring haze before and after the oven treatment and calculating the % change.

The b-RCP thermoforming work was conducted at the Milliken lab in Spartanburg, South Carolina. An in-line sheet forming and thermoforming process was used to produce deep draw cups. Cast-sheet was produced by feeding PP formulated pellets to a sheet forming line. The line is composed with three major sections (1) a single screw extruder (2) a coat hanger-manifold die and (3) a water bath and a set of chill-rolls. The 1.9 mm thick sheet was fed into an Illig RDM-54K solid phase former equipped with upper and lower infrared ceramic heaters. Sheet forming and thermoforming were set at similar conditions for all samples each time. The molded cups were 139 mm tall and 500 ml in volume with a mouth diameter of 93 mm and a bottom diameter of 59 mm. Cup optics were measured at the same height where wall thickness is around 275 μm . Wall thickness reduction is about 7 fold at this location. Clarity and haze were measured with a BYK Gardner Plus haze meter using ASTM method D1003-11.

ADVANCES IN HDPE TECHNOLOGY FOR LARGE DIAMETER PE100 PIPE APPLICATIONS

*Cliff Mure, Univation Technologies - Middlesex, NJ, USA
Predrag Micic, Qenos Pty Ltd - Melbourne, Victoria, Australia*

Abstract

Although bimodal HDPE has been well-established in PE100 pipe applications since the 1990's, continued advances in catalyst and polymerization process technology in recent years have led to further improvements in mechanical properties and extrusion processability. Univation Technologies has commercialized the PRODIGY™ BMC-200 Catalyst System to produce a bimodal PE100 material in a single gas-phase reactor. This new bimodal HDPE material exhibits an excellent balance of mechanical properties along with a unique rheology which delivers advantages in the pipe extrusion process. The molecular weight distribution resulting from this bimodal catalyst system yields processing advantages that include high output, low melt temperature, and high melt strength. The high melt strength of the extrudate provides improved wall thickness distribution, which facilitates the production of large diameter pipes. In addition to mechanical properties and extrusion processability, the quality of joints of pipes and fittings is a critical element of pipe performance and/or integrity. Electrofusion and butt fusion trials were conducted in order to successfully validate compatibility of large diameter pipes produced with the BMC-200 PE100 with other PE100 materials and with commercially-available fittings.

Introduction

PE pipes have been in use for more than 50 years, delivering excellent performance. Today polyethylene is a well-established material for gas and water supply systems, waste water disposal and sewage systems, as well as numerous industrial applications such as transport of slurries in mining and for coal seam gas. PE piping systems, also in larger nominal diameters, have become a common preference in tenders and specifications by civil engineering firms for large scale irrigation projects.

Traditionally, these bimodal polyethylenes have been produced only in multiple reactor configurations (Figure 1). These staged-reactor systems produce excellent products for applications including film, blow molding and PE100 pipe. However, the process is more

complicated and requires more capital than a single reactor system.

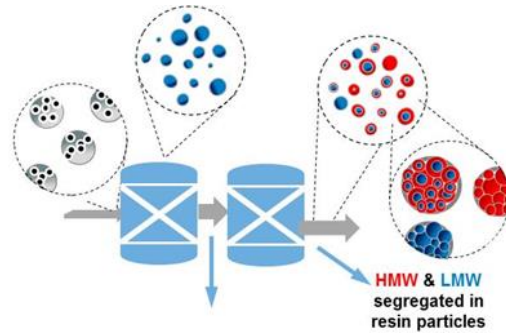


Figure 1. Staged-Reactor Bimodal HDPE Polymerization Process

Recently, Univation Technologies has developed a two component catalyst system that produces a bimodal molecular weight distribution with a desirable comonomer distribution (Figure 2). The two catalyst components produce different, controlled, polymer chains under specific reaction conditions. The first catalyst component (component A) produces high molecular weight polymer chains. Catalyst component B produces low molecular weight polymer chains. Component A has a high affinity for comonomer which is essential for formation of tie molecules and promoting excellent slow crack growth resistance. Component B also incorporates some comonomer, but less than that of component A.

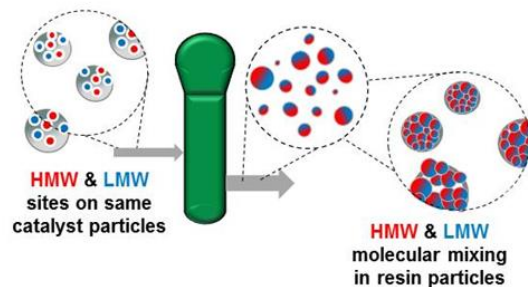


Figure 2. Single-Reactor PRODIGY BMC-200 Polymerization Process

Polyethylene products for various applications are produced by varying the split (ratio of HMW/LMW polymer components), spread (ratio of the molecular weights of the components), the overall molecular weight, and the comonomer content. These polymer attributes are controlled by varying the ratio of the catalyst components, the reaction temperature, and the gas composition in the reactor. The overall molecular weight distribution is relatively broad resulting in good extrusion processability. Figure 3 shows the typical distributions of molecular weight and comonomer for polyethylene produced with the PRODIGY BMC-200 Bimodal Catalyst System. This combination of molecular weight distribution and comonomer distribution results in an excellent balance of stiffness (pressure rating), slow crack growth resistance (SCGR), resistance to rapid crack propagation (RCP), and extrusion processability.

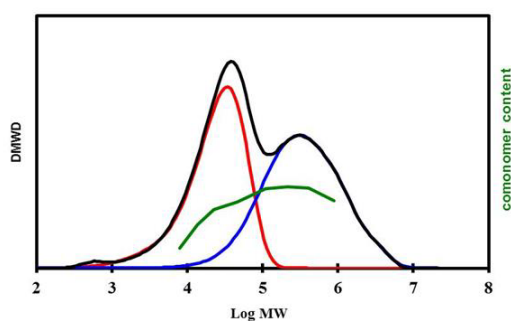


Figure 3. MWD and Comonomer Distribution for PRODIGY PE100 Resin

Polymer Properties

The PRODIGY BMC-200 PE100 resin, when first introduced, had a melt index MFR_5 that was outside the range specified in the ISO water and gas product standards, ISO 4427 and ISO 4437. The 2007 versions of these ISO standards specified the MFR_5 range of 0.2 to 1.4. The melt index for the PRODIGY PE100 product was outside this range because the polymer was designed for the end-use properties and processability by optimizing the individual component Mw's and MWD's, the split, and the comonomer content. However, simply specifying the resin's melt index and density are not sufficient for designing bimodal or multimodal polymer products for demanding applications such as PE100 pipe.

The MFR_5 of the PRODIGY PE100 product is in the range of 0.15 to about 0.18 compared to the lower limit of 0.2 in the earlier ISO standards. Consequently, the melt flow ratio is somewhat higher than that of other PE100 materials. The MFR_5 range in the ISO standards was eventually modified in order to accommodate lower melt

index materials such as PRODIGY PE100. This is discussed further later in the paper; there was a significant amount of fusion compatibility testing done in order to support the petition to make the change. Overall, the PRODIGY PE100 material meets or exceeds the critical pipe properties required for PE100 applications, including long-term hydrostatic strength MRS10, slow crack growth resistance, and resistance to rapid crack propagation.

The combination of the low MFR_5 and the characteristic molecular weight distribution gives the PRODIGY PE100 resin some unique properties. In the extrusion of pipes, especially large pipes, the flow characteristics at different rates is important. At high shear rates, it is desirable to have a relatively low viscosity to enable low head pressure and good extruder output. The flow of the polymer as it exits the die is also critical. At the die exit, the shear rate is relatively low. Gravity acts on the extrudate as it flows from the die exit to the first cooling tank. Therefore, it is desirable to have high viscosity at low shear rate in order to prevent sag, a flow of the extrudate from top to bottom. Commercially-available "low sag" PE100 materials exhibit high viscosity at low shear rates.

The rheology of the PRODIGY PE100 exhibits a high degree of shear thinning. The complex viscosity, measured at 190°C, is shown in Figure 4. The competitive PE100 used for comparison is a popular "low sag" grade. At relatively high shear rates or frequencies in the dynamic rheology test, the complex viscosity of the PRODIGY PE100 is similar to that of the competitive PE100. However, at low frequencies, measured down to 0.01 s⁻¹, the complex viscosity of the PRODIGY PE100 is significantly higher than that of competitive PE100 material. Thus, the PRODIGY PE100 exhibits a unique balance of high viscosity at low frequency and desirably low viscosity at high frequency.

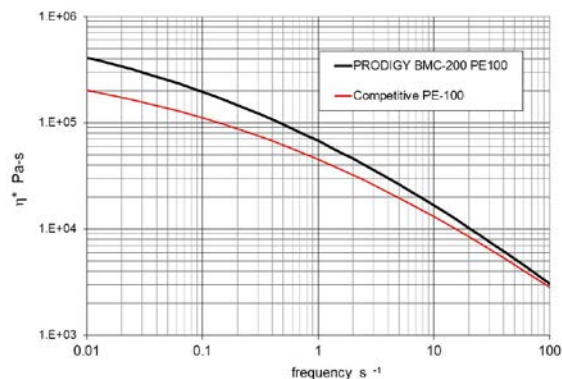


Figure 4. Complex Viscosity Tested at 190°C

The melt flow of the PE100 materials may also be characterized using a Rheotens rheometer to measure the melt strength in the lab. In this test, the extrudate from the rheometer is pulled at a constant acceleration rate while the force in the extrudate is recorded. Figure 5 shows the melt strength tested at 190°C comparing the PRODIGY PE100 to four competitive PE100 product grades, including “low sag” materials. The melt strength of the PRODIGY PE100 is significantly higher than that of the competitive grades. In pipe extrusion, depending on the specific extruder and operating conditions, a given material may be extruded at a range of melt temperature. Therefore, the melt strength test has been conducted at a range of temperatures with the same trends between the materials.

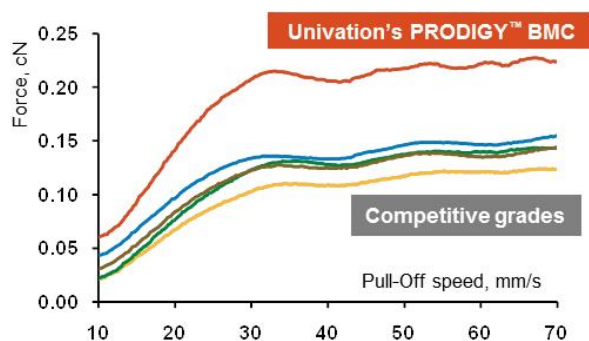


Figure 5. Rheotens Melt Strength at 190°C for PE100 Materials

In the commercialization of the PRODIGY PE100 material, demonstrations of fusion compatibility for both butt welding and electrofusion were done. In these fusion processes, the polymer at the interface is melted and then cooled while in contact with either another pipe or a fitting. Therefore, the melting and cooling characteristics of pipe materials are important to the fusion process. The melting and cooling of polyethylene is characterized in the lab by differential scanning calorimetry (DSC). In the DSC test, the heat flow is measured as the polymer is melted, cooled, and then re-melted. Figure 6 shows the DSC scans for the PRODIGY PE100 and for a competitive PE100 resin. The thermal behavior is similar with respect to positions of melting and cooling peaks as well as the area under the peaks. This data demonstrates that the overall crystallinity and thermal properties of these materials are similar. This is significant because pipes and fittings may be produced from different PE100 materials but the DSC data demonstrates they will heat and cool in a similar manner. This was demonstrated with successful electrofusion of PRODIGY PE100 pipes to fittings produced with another PE100 material.

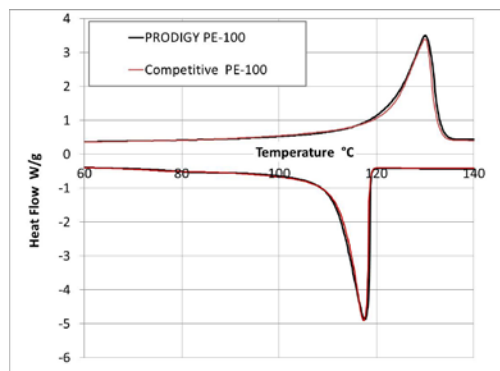


Figure 6. DSC Heating and Melting Behavior

Pipe Extrusion Characteristics

The extrusion performance of PRODIGY PE100 is advantaged, in particular for fast extrusion of large, thick wall pipes. The unique rheology results in a relatively high specific output and low melt temperature and subsequently faster cooling rates. The output of many pipe extrusion operations is constrained by the capacity to cool the pipe downstream of the die. Figure 7 shows the specific output and melt temperature of the PRODIGY PE100 along with 5 other commercial PE100 materials. This data was generated from an extrusion trial run on a 90 mm diameter grooved barrel extruder in commercial operation. This trial produced 250 mm SDR11 pipes. These extrusion characteristics enable good control of the wall thickness and ovality, two properties important for efficient and high quality pipe joining.

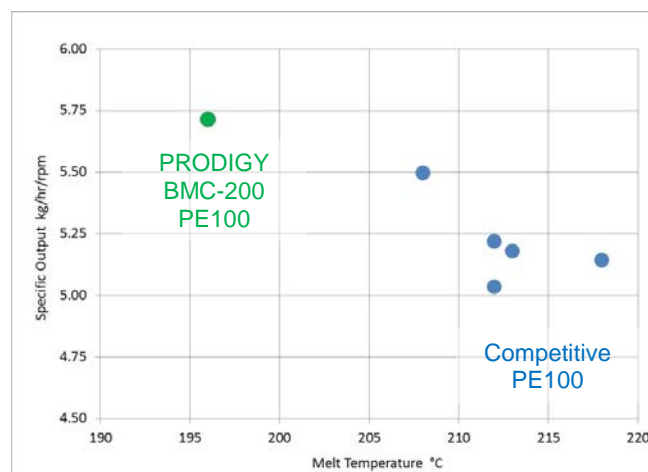


Figure 7. Specific Output and Melt Temperature During Production of 250 mm Diameter SDR11 Pipes

Case Studies of Large PE100 Pipes

In 2011, Hunter Water in Australia evaluated options to replace an old 900 mm diameter steel water pipeline that, because of the age of the pipe and corrosion, required regular maintenance and repair. PE100 pipe was chosen for its flexibility, corrosion resistance, and ability to use advanced installation techniques. HDF145B PE100 material, produced by Qenos Ltd in Australia with the PRODIGY catalyst, was chosen to produce the 1,000 mm diameter PN16 pipes.¹ The new pipeline installation achieved some significant environmental benefits.

The route of the pipeline was through a sensitive wetlands area and the new underground installation minimized disturbance to the local environment. The old pipeline used a bridge to cross a river. The bridge was replaced with the PE100 pipe which was installed under the river bed using horizontal directional drilling (HDD). In order to perform the HDD installation, about 300 meters of the pipe was assembled by butt fusion using standard welding parameters. The welding operation is shown in Figure 8. Figure 9 shows the length of 1,000 mm diameter PE100 pipe attached to a steel puller as it is readied for HDD installation. The toughness of the PE100 material allows this type of installation. The pipe is subjected to high tensile stresses as it is pulled through the pilot hole. Further, the pipe may be scratched or gouged as it is pulled through; the high resistance to slow crack growth ensures that the pipe is still suitable for long-term service after installation.



Figure 8. Butt Welding of 1,000 mm diameter pipes in the field



Figure 9. A 300 meter long length of pipe prepared for HDD installation

Another PE100 installation success story in Australia was achieved in 2012. The heaviest rainfall recorded in the Melbourne area in 133 years caused the breach of a levee and the water from the Morwell River flooded an open-cut coal mine. The coal from this mine directly supplied a power plant on the same site which was supplying a significant portion of the electricity for the state of Victoria.²

In order to alleviate the flooding in the mine and power plant, an emergency response team devised a solution to dewater the mine and to divert the flow of the river. Dams were constructed and PE100 pipes (500 mm and 630 mm diameter) produced with HDF145B from Qenos (produced with PRODIGY BMC Catalyst) were used to transport the water out of the mine (Figure 10). The second phase of the project was to divert the entire flow of the river around the affected area using PE100 pipes. This phase of the project used 1,600 mm diameter PE100 pipes to transport the 800 million liters per day of water (maximum flow of 2,800 million liters per day).



Figure 10. PE100 pipes used to dewater the mine

The emergency response team evaluated options to alleviate the flooding and to divert the river flow. Several factors dictated that PE100 pipe would be the optimum solution for the problem. PE100 provides the mechanical properties required for the water distribution application – pressure rating, impact resistance, slow crack growth resistance. The PE100 pipes offer ease of installation relative to other materials, with the ability to handle long lengths of pipes due to its light weight and the ability to butt weld in the field in order to produce leak free joints.

The Qenos HDF145B material, produced with PRODIGY BMC-200 Catalyst Technology, was selected specifically for the application. Delivery time was critical. The ability to extrude with high rates at relatively low melt temperature allowed the fastest possible production of pipes. The excellent extrusion characteristics ensured optimum performance in the field installation. The exceptional melt strength resulted in a very uniform wall thickness distribution and tight control of the ovality of the pipes. In large pipe installations, if wall thickness distribution is not substantially uniform, the pipes need to be routed to match up thicknesses of the pipes being joined. However, because of the successful production of consistent pipe with the Qenos HDF145B material, the pipes were produced within specifications, eliminating the need to field rout the pipes in the fusion process. This greatly facilitated the installation process. Figure 11 shows the 1,600 mm diameter pipes being butt welded in the field. The timeline of the project, including the diversion of the river flow, was 2 months; because of the fast response, the power supply to Melbourne and the state of Victoria was uninterrupted.

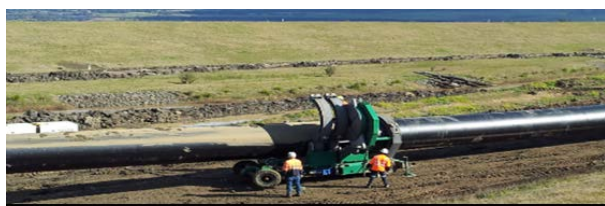


Figure 11. Field butt welding of 1,600 mm diameter pipes for river diversion

Pipe Standards

The plastic pipe industry has successfully developed standards to ensure durability and high reliability and to ensure regulation and adherence to specifications. This was possible due to a strong commitment from the entire value chain including raw material suppliers, product manufacturers, test laboratories, and end users. In turn, standards have created the incentive for suppliers to improve material performance, and for manufacturers to develop more innovative products.

PE materials are only partly defined by melt flow ratio and density; the resin's molecular structure can be more specifically tailored to meet the performance demands of specific applications. Therefore, it is important that standards and specifications for pipe products specify adequate requirements to ensure that only the highest performance materials conform and are specified.

The latest editions of system standards ISO 4427-1/2/3/5:2007 PE water and ISO 4437-1/2/3/4/5:2014 gas reflect the advancements in PE100 material performance and the successful field experience with lower MFR₅ (< 0.2 g/10min) bimodal PE100 resins over the last decade. For example, the 2007 versions of these standards specified an MFR₅ range of 0.20 - 1.40 g/10min. The current versions of the standards allow the use of materials with MFR down to 0.15 g/10min as per the following extract from Table 1 in ISO 4437. With regard to a pipe system made with such PE100, "attention is drawn to the fusion compatibility" as shown in note 9 in the following table.

Table 1. Melt Index Specified Per ISO 4437:2014

Characteristic	Requirement ^a	Test parameters		Test method
		Parameter	Value	
Melt mass-flow rate (MFR) for PE 80 and 100	0,20 to 1,40 g/10 min ^a Maximum deviation of ± 20 % of the nominated value	Load	5 kg	ISO 1133-1
		Test temperature	190 °C	
		Time	10 min	
		Number of test pieces ^b	According to ISO 1133-1	

^a Materials of nominated value $0,15 \leq \text{MFR} < 0,20$ may be introduced, in such case attention is drawn to the fusion compatibility subclause 4.5. The lowest MFR value resulting from the maximum lower deviation of the nominated value to be not less than 0,15.

Standards also cover advancements in product capability to make large diameter pipes. Even for large dimensions, electrofusion (EF) welding is an indispensable joining method. Today, electrofusion fittings are used for pipe with diameters up to 800 mm in the form of couplers for axial joints and saddle components for branches and connections. Permissible operating pressures of up to 2,500 kPa (water) and 1,000 kPa (gas) have become a norm. Operating practices in some applications like coal seam gas in Australia are moving towards even higher pressures of 1,600 kPa for the transport of gas. Therefore, it is critical to ensure that good integrity EF joints are formed even with the combination of very large pipes and lower MFR₅ (< 0.2 g/10min) PE100.

In the electrofusion process, heat is generated internally by wires embedded in the fitting. Tight tolerances on the roundness of the pipes and the gap between the fitting and pipe are critical. However, as pipes get larger, the

specified dimensional tolerances increase.³ Therefore, improvements in consistency of the dimensions of large pipes achieved through the extrusion process are essential for success in the EF process.

Electrofusion and Joints integrity testing program

A test program to validate the EF compatibility of the PRODIGY PE100 with commercial EF fittings was coordinated between Univation Technologies, Qenos (resin manufacturer), pipe extrusion companies and fittings manufacturers.

The test program involved manufacture of SDR17 pipes, using the PRODIGY PE100 material, in four different diameters: 800 mm, 630 mm, 560 mm and 110 mm. Pipes were extruded as part of commercial production at pipe manufacturers Vinidex (630SDR17 and 560SDR17) and ZEIT (800SDR17 and 110SDR17). Additional details of the test program were presented at the Plastic Pipes XVIII Conference in 2016.³

Table 2 outlines some of the EF test conditions. A majority of the investigation was conducted at Plasson (Israel) using electrofusion coupler and saddle type joining and product testing on SDR17 pipes in diameters of 800 mm, 630 mm, 560 mm and 110 mm; with some conducted at Friatec. Both Plasson and Friatec used “off-the-shelf” fittings produced with their standard PE100 materials. Figures 12 and 13 show, respectively, a 630 mm diameter coupler getting hydrostatically tested and a 110 mm diameter saddle assembly getting ready for product testing at Plasson testing premises in Israel.⁴ The 800 mm diameter electrofusion coupler testing program was performed by Friatec and SKZ Institute in Germany.⁵

The Plasson program investigated EF weld temperatures from -10° to +45°C, varying the gap between pipe and fitting as well as different weld energy inputs. Electrofusion weld integrity was assessed via pipe hydrostatic pressure testing per EN 12201-3, Decohesion and selected Strip Bend tests according to ISO 21751.

Table 2. Electrofusion Testing Program Parameters

Pipe Diameter, mm	Pipe Wall, mm	Pipe MFR5	Fitting type/ Dimensions	Weld conditions	Hydrostatic test conditions	Decohesion
110	7	0.160	Coupler 110SDR11 (PE100) Tapping Saddle 110x40SDR11 (PE100)	2xMin + 1xMax ¹ Min+Max ¹	80°C/1000hrs/ 6.3bar ²	After hydr. test
560	35	0.150	Coupler 560SDR11 (PE100)	Min+Max ¹	80°C/1000hrs/ 6.3bar ²	After hydr. test
630	40	0.196	Coupler 630SDR11 (PE100) Tapping Saddle 630x110SDR11 (PE100)	Min+Max ¹	80°C/1000hrs/ 6.3bar ²	After hydr. test ³
800	50	0.165	Coupler 800SDR17 (PE100)	“Standard”	80°C/1000hrs/ 5.0bar	After hydr. test

¹Min and Max outline the most extreme weld conditions, as per below:

Minimum weld conditions:

- Weld temperature: -10°C
- Gap: Maximum gap between fitting and pipe (pipe machined to simulate the situation where the fitting is at its upper internal diameter tolerance, pipe at its minimal external diameter as defined by the standard + removal of 0.6 mm off the pipe diameter to simulate pipe scraping)
- Weld energy: minimum possible energy input which is calculated taking into account the controller lower energy tolerance (as defined in the standard) and the product highest resistance allowed based on the product definition

Maximum weld conditions:

- Weld temperature: +45°C
- Gap: Maximum gap between fitting and pipe (pipe machined to simulate the situation where the fitting is at its upper internal diameter tolerance, pipe at its minimal external diameter as defined by the standard + removal of 0.6 mm off the pipe diameter to simulate pipe scraping)
- Weld energy: maximum possible energy input which is calculated taking into account the controller upper energy tolerance as defined in the standard, and the product lowest resistance allowed based on the product definition

²The test conditions were set in accordance with the pipe SDR/PN rating as in EN 12201

³On the 630 mm diameter saddle, a strip bend test was performed according to ISO 21751



Figure 12. 630SDR17 Gas Pipe and Electrofusion Coupler During Hydrostatic Pressure Testing



Figure 13. 110SDR17 Water Pipe and Tapping Saddle Electrofusion Assembly Ready For Product Testing

The EF assemblies were tested in the hydrostatic pressure test under the conditions given in Table 2. Additionally, the EF assemblies were also tested in a decohesion test; the joints should exhibit ductility in the decohesion test. All results from the testing program recorded PASS, demonstrating high quality electrofusion capability for joining of large diameter thick walled pipes made using a PE100 with $MFR_5 < 0.2$ g/10min. Comments from the test laboratories on the test performance results were that electrofusion fittings have all coped well with welding to pipes manufactured using this PE100 material with MFR_5 as low as 0.15 g/10min.

Conclusions

- Using PRODIGY BMC-200 Catalyst Technology, PE100 pipe resin with excellent mechanical properties has been developed and is commercially produced.
- The extrusion characteristics of the PRODIGY PE100 resin are unique, facilitating the extrusion of large thick pipes.
- The recent change in standards ISO 4427 and ISO 4437 to include a provision for PE100 resins

with $MFR_5 < 0.2$ g/10min reflects the intent of standards to keep pace with the development and innovations associated with pipe materials.

- The electrofusion work demonstrates that high quality joints can be produced with pipes made from PE100 with $MFR_5 < 0.2$ g/10min and commercially available electrofusion fittings
- It is possible to join using electrofusion very large and thick wall pipes as demonstrated by extensive product testing of electrofusion assemblies with pipe of sizes up to 800 mm in diameter and up to 50 mm in wall thickness

References

1. P. Micic, T. Campbell, Challenging installation of large diameter HDPE pipe by directional drilling provides a comprehensive water management solution and an improved environmental outcome, Plastic Pipes Symposium XVI Conference Proceedings, September 24-26, 2012
2. P. Micic, G. Beckton, 1600mm PE Pipe Installation Saves Power Supply in Victoria, Australia, Plastic Pipes Symposium XVII Conference Proceedings, September 22-24, 2014.
3. R. Eckert, Jointing of Large Bore PE Pipes; "Think Big" ... and Even Bigger!, Plastic Pipes Symposium XVI Conference Proceedings, September 24-26, 2012
4. P. Micic, C. Mure, Electrofusion Joining Performance of Very Large Pressure Pipes Produced with a $MFR_5 < 0.2$ g/10 min PE100, Plastic Pipes Symposium XVIII Conference Proceedings, September 12-14, 2016.
5. Plasson Israel test report: "Fusion compatibility of pipes produced of Qenos HDF 145B HDPE with PLASSON EF fittings" (2014)
6. Friatec Germany test report: FRIALEN-Safety Fittings "Fusibility of pipes with $MFR_5 < 0.2$ g/10min"; FRIALEN Info Nr. 49 (2014).

TMPRODIGY is a trademark of Univation Technologies, LLC.

DEVELOPMENT OF A NOVEL SOLID-TYPE MAO ACTIVATOR FOR OLEFIN POLYMERIZATIONS

Eiichi Kaji and Yujin Takemoto, Tosoh Finechem Corporation, Shunan, Yamaguchi, JP

Abstract

Methylaluminoxane (MAO) supported on SiO_2 (SiO_2/MAO) has been widely used as an effective activator for slurry and gas phase processes in homogeneous polymerization systems. Extensive research has been conducted to improve catalyst performances of a metallocene complex combined with SiO_2/MAO . Nevertheless, strong requirements to develop more effective solid activators than SiO_2/MAO still exist.

We have developed an original and unique solidified MAO (Solid MAO) produced by a self-aggregation method which is significantly different from previous experiments. The size of particles obtained can be well controlled by modifying the reaction conditions. Solid MAO having both functions of support and activator of a metallocene complex, shows high performances in olefin polymerization as compared to SiO_2/MAO .

Introduction

Methylaluminoxane ($[\text{-Al(Me)-O-}]_n$, MAO) which is produced by partially hydrolyzed compound of trimethylaluminum, is known as an effective activator of metallocene complex for olefin polymerization. In order to control polymer morphology, MAO has been generally supported on some solid compounds with controlled shape, such as SiO_2 , Al_2O_3 and similar supports to form solid-type catalyst.

In case of SiO_2 , it is necessary to calcinate it under defined conditions (time, temperature etc.) to control a concentration of hydroxyl group on the solid surface. In addition, MAO supported on SiO_2 generally shows lower activity compared to MAO itself. Higher activity of a catalyst is very important to reduce the amount of residue of inorganic compounds such as SiO_2 in the polymer produced because inorganic residue sometimes causes product defects such as fish eyes in polymer film. Higher activity also has a positive impact on the cost effectiveness of the catalyst system.

From these viewpoints, there have been some proposals to obtain MAO solidified without a support such as SiO_2 in order to enhance the activity. The following are representative examples.

(i) utilization of pre-polymerization [1]

(ii) utilization of MAO micelle in fluorinated organic solvent [2]

(iii) utilization of nonionic surfactant [3]

(iv) utilization of poor solvent [4]

First, we have carried out a supplementary experiment according to the literature [4]. Solidification using a poor solvent and MAO, gave aggregated particles with varying sizes as seen in SEM image (figure 1). Then, we tried to find a new method to make solidified MAO having higher particle uniformity than any methods reported so far.

I have originally found that solidified MAO particles can be obtained by heating of specific MAO solution without any additives and supports which showed extremely high activities for olefin polymerization when combined with metallocene complex. We named the resultant product Solid MAO for this novel solidified MAO. In this paper, our advances of Solid MAO development will be reported in detail.

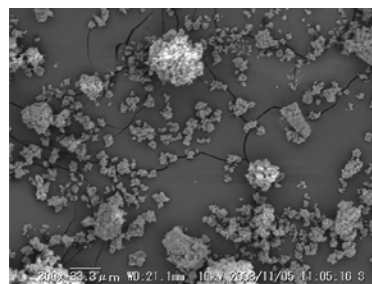


Figure 1. SEM image of solid-type MAO with varying particle sizes as produced according to the literature [4].

Experiments

All experiments have been conducted under dry nitrogen gas. The typical synthetic procedure is described hereunder.

1) Synthesis of MAO toluene solution for Solid MAO production [5]

Trimethylaluminum and dehydrated toluene were added into a flask with a condenser, a thermometer and a stirring device. The solution was cooled to around 15°C . Benzoic acid was added slowly to the solution so that the temperature range was controlled from 15 to 23°C . After this addition, the solution was heated at 60 to 80°C to form MAO structure.

2) Synthesis of Solid MAO [5]

MAO toluene solution obtained above was added into the similar reactor vessel and heated for 8hrs at 100°C under moderate stirring. Then, Solid MAO particles could be prepared by self-aggregation of MAO.

3) Preparation of metallocene complex supported Solid MAO catalyst

Metallocene toluene slurry was added to Solid MAO toluene slurry under moderate stirring for 24hrs at ambient temperature. Zr content and Al content in the catalyst prepared were quantitatively analyzed by an induced coupled plasma measurements of the hydrolyzed sample.

4) Ethylene polymerization

Dehydrated hexane was added into an autoclave reactor with a thermometer and a stirring device. Then, triethylaluminum as a scavenger was added. After ethylene replacement, the catalyst was added. The polymerization was started at 70 °C to pressurize to 0.7MPa by ethylene gas and conducted for 1hr at the temperature.

Results and Discussions

1) Preparation of Solid MAO

MAO itself is almost insoluble in aromatic solvents like toluene. This means that MAO shows solubility in some solvents by coordination of trimethylaluminum. Taking this into consideration, a hypothesis was built that MAO solution having less residual trimethylaluminum, would be suitable for Solid MAO production. So, we have tried to prepare Solid MAOs by using MAO solutions with different Al/O molar ratio. The SEM images of Solid MAOs prepared by using various MAO solutions are shown below.

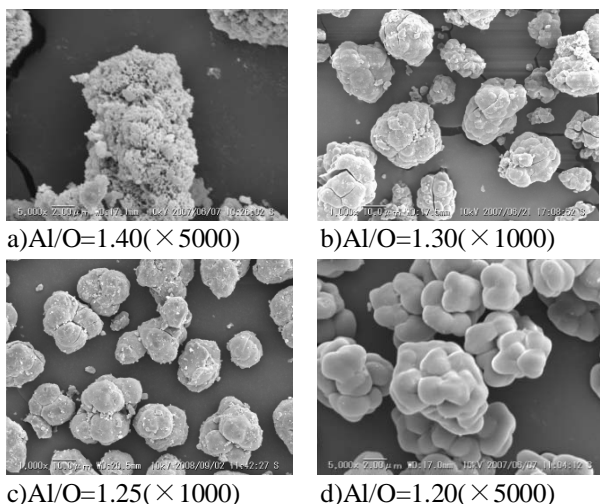


Figure 2. SEM images of Solid MAOs prepared by using various MAO solutions with different Al/O molar ratios.

As shown in the SEM images, the Solid MAO particle structures changed drastically. As Al/O molar ratio was decreased, the uniformity of Solid MAO particle could be improved. According to the results, we believe that MAO solution with decreased trimethyl-aluminum content is suitable for Solid MAO production because residual trimethylaluminum might be an inhibition factor for solidification of MAO.

2) Results of ethylene polymerizations using metallocene supported Solid MAO catalysts

The Solid MAO (6.1μm, Al content 41wt% in solid) base catalysts with various metallocene complexes were prepared and those catalytic activities were evaluated for ethylene polymerization. The results are shown in table 1.

Table 1. Results of ethylene polymerizations using Solid MAO base catalysts.

Metallocene complex	Activity, kg/g-cat · hr	BD* ¹ , g/cc
<i>rac</i> -Et(Ind) ₂ ZrCl ₂	9,000	0.39
Ind ₂ ZrCl ₂	9,000	0.37
(1,3-Me ₂ Cp)ZrCl ₂	6,300	0.41
(<i>n</i> BuCp) ₂ ZrCl ₂	12,000	0.39
Ref.* ²	1,100	0.34
<i>rac</i> -Et(Ind) ₂ ZrCl ₂		

*1 : Bulk density of polymer, *2 : SiO₂/MAO used (Al content 13.9wt% in solid)

It was concluded from this table that Solid MAO base catalysts showed higher activities and BDs than that of SiO₂/MAO. The aluminum content in Solid MAO was almost 3 times higher than SiO₂/MAO. But taking that difference into consideration, Solid MAO still showed higher activity.



Figure 3. SEM image of polymer obtained by using *rac*-Et(Ind)₂ZrCl₂ supported Solid MAO catalyst shown in table 1 (x300).

SEM image of polymer particles is shown in figure 3. As understood in this image, the polymers seem to have replicas of Solid MAO particles. Additionally, it was recognized that the polymer particles produced have high homogeneity. Neither fine particles nor coarse particles are observed.

Solid MAO particle size can be well controlled by changing some solidification conditions like agitation speed. As usually observed, Solid MAO catalytic activities also decreased as the particle size increases. The results are shown in figure 4 (conventional, blue line). We have found a novel solidification procedure which gave Solid MAO that maintained high activity even with increased particle size (improved, red line). The detailed procedure can be reported after the publication of the patent. It is noteworthy that metallocene catalyst supported on Solid MAO by the improved procedure gives ethylene polymer with high BD. This means that structure and active sites of Solid MAO can be changed by the solidification procedures.

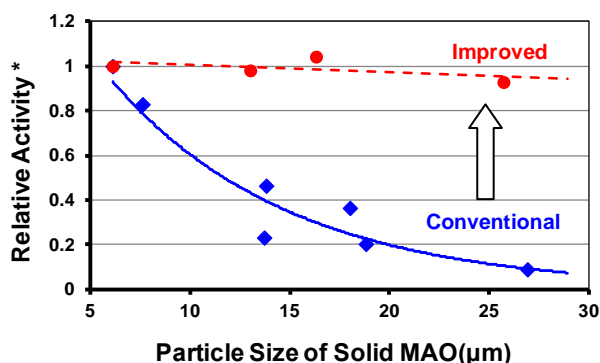


Figure 4. Relationship between particle size of Solid MAO and relative activity showing maintenance of high activity with increased particle size with the improved procedure.

*Activity of Solid MAO for that of 6.1μm in a diameter.

3) Some analyses of Solid MAOs

3-1) BET analyses

BET analyses of Solid MAOs were conducted using N₂ gas to understand the structure of Solid MAO. The results of relative surface area and micropore volume are shown in table 2.

Table 2. Results of BET analysis of Solid MAO.

Average particle diameter, d(50), μm	Relative surface area, m ² /g	Pore volume, cm ³ /g
5.7	475	0.26
7.6	484	0.28
14.2	472	0.25
20.0	382	0.21
30.0	424	0.23

From this table, the relative surface areas of Solid MAOs were around 350 to 500m²/g and its pore volume were around 0.2 to 0.3cm³/g. These results showed that Solid MAOs tested have large specific surface area comparable to SiO₂ normally used as an inorganic support and smaller pore volume than SiO₂.

3-2) Solid State NMR measurements

We have conducted solid state NMR analyses of Solid MAO and SiO₂/MAO to find any differences. The results are shown in figure 5 and 6.

In both solid-type MAOs, there was one peak derived from methyl groups of MAO having the same chemical shift (around -5ppm). It was considered that these methyl groups were deemed to be in similar environments by NMR measurement. The strength of peaks could reflect aluminum contents in the solids. But there was no difference among the samples due to the same circumstances of methyl groups in the solids.

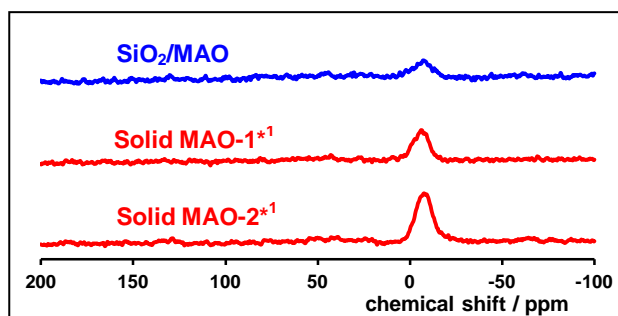


Figure 5. ¹³C CP/MAS NMR spectra of Solid MAO and SiO₂/MAO showing the -5 ppm shifts from MAO methyl groups.

*1 : Al content in Solid MAO-2 was higher than Solid MAO-1.

²⁷Al MAS NMR spectra of Solid MAOs and SiO₂/MAO were also measured. The result shows in figure 6. There were two peaks (around 35ppm and -15ppm) in SiO₂/MAO, whereas a single peak (around -4ppm) in Solid MAO. We currently consider that four coordinated and six coordinated Al sites exist in SiO₂/MAO. In contrast, six coordinated Al sites mainly exist in Solid MAO. We are continuing examination of the structure of active sites on Solid MAO in greater detail.

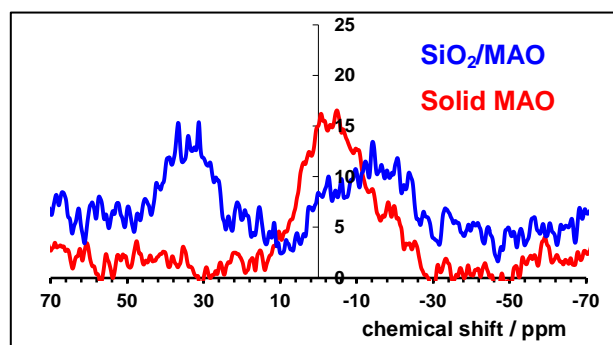


Figure 6. ²⁷Al MAS NMR spectra of Solid MAO and SiO₂/MAO indicating coordinated Al sites.

3-3) TEM analysis

We have measured TEM images of Solid MAO to obtain some information on primary particles. The results are shown in figure 7 and 8.

From figure 7, it seems that Solid MAO is composed of aggregate of small primary particles and the sizes of the primary particles are estimated about 15 to 30nm. In addition, we have found new results on Solid MAO structure from further detailed TEM observation. That is, some lattice patterns were found in the primary particles of Solid MAO in TEM image as you can see in the red circles of figure 8. Most parts of Solid MAO were non-crystallized solid which did not have any lattice pattern (figure 9). At first, I supposed that these lattice patterns might be derived from crystallized MAO itself. As far as I know, there is no report on crystallized MAO. So, we have examined to give light on the structure having lattice patterns shown here.

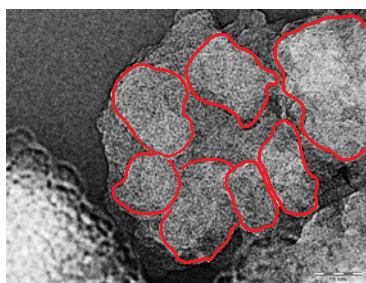


Figure 7. TEM image of Solid MAO-1($\times 300,000$).

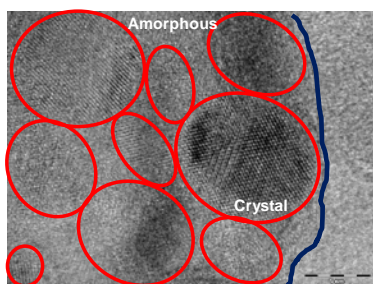


Figure 8. TEM image of Solid MAO-1($\times 500,000$).

*Deep blue line shows a border of Solid MAO particle and a supporting film for TEM measurement.

To confirm what the existence of lattice patterns in Solid MAO means, the electron diffraction (ED) pattern was simulated from the lattice pattern and compared to that of some known compounds. As a result, it was concluded that the ED pattern of alumina with corundum structure was identified to simulated ED pattern of crystal phase in Solid MAO. This means that alumina structure exists in Solid MAO. The existence of alumina structure in Solid MAO is thought to enhance the strength of this solid-type activator.

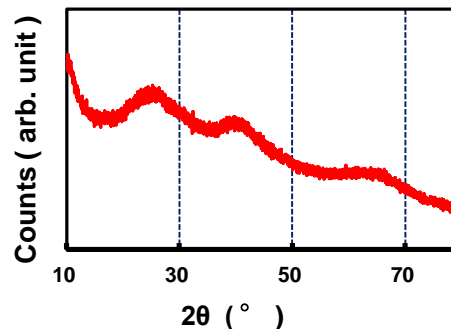


Figure 9. XRD measurement of Solid MAO.

Conclusions

Metallocene catalysts supported on Solid MAO showed higher activity than SiO_2/MAO base catalyst in ethylene polymerization and also gave good morphology of polymer produced. In addition, we have found a novel solidification procedure to obtain larger size Solid MAO showing high activity and gives polyethylene with high BD.

There are still some unknowns to elucidate on Solid MAO structure and its active sites. But it is assumed that Solid MAO base catalyst might have a different active site from one of SiO_2/MAO base catalyst from the data of ^{27}Al MAS NMR spectroscopy. In addition, the existence of alumina structure in Solid MAO was found by TEM analyses and may contribute to the formation and performances of Solid MAO.

We continue exploring Solid MAO to elucidate the structure and to enhance the catalytic performance.

Acknowledgements

We would like to thank Michael East and Steve White for helpful discussions to prepare the manuscript.

References

1. S.P. Diefenbach, U.S. Patent 6,730,758 (2004).
2. L. Resconi, P. Castro and L. Huhtanen, E. Patent 2,383,299 (2011).
3. B. Lu, J. Wang, X. Hong and Z. Jing, J. Patent 9216908 (1997).
4. M. Kioka and N. Kashiwa, J. Patent H07-042301(1995).
5. E. Kaji, E. Yoshioka, U.S. Patent 8,404,880 (2013).

Scented Polyolefins from Ziegler-Natta Catalysts

*Dennis B. Malpass
Serenity Consulting
(Email: kaw62jry@gmail.com)*

*Society of Plastics Engineers (SPE)
Polyolefins International Conference
Houston, TX
February 26-March 1, 2017*

Abstract

Each year, transition metal catalysts are used on six continents to manufacture millions of tons of polyolefins. Ziegler-Natta catalysts are, by far, the most important. Since the inception of the polyolefins industry based on Ziegler-Natta catalysts in the 1950s, aluminum alkyls have been indispensable. That remains so today. This paper describes aluminum alkyls that function as cocatalysts and leave residues in the polymer that are converted to compounds which impart a scent to the polymer. Suitable cocatalysts may be produced in-house from readily available precursors using well-established methods. Alternatively, such cocatalysts may be obtained from metal alkyl manufacturers.

Though scented polyolefins have been available for many years, techniques used to produce them have changed little. Typically, methods involve post-reactor blending of virgin resin with masterbatches containing aroma compounds [1]. This paper describes use of aluminum alkyls to produce scented polyolefins manufactured with Ziegler-Natta catalysts. A convenient way to illustrate the technology is to consider the case study of citronellol, also known as 3,7-dimethyl-6-octen-1-ol. Citronellol is a well-established scent compound with a floral, rose-like aroma and is used in perfumery and insect repellants. (Commercially available citronellol is a mixture of stereoisomers.) Cocatalyst may be produced by reaction of a terpene with triisobutylaluminum (TIBAL) using technology disclosed in expired patents by Karl Ziegler and discussed by Ziegler in an American Chemical Society review published in 1960 [2].

A crucial aspect of the method described here is as follows: After the raw polymer is exposed to ambient air, cocatalyst residues generate the scent agent in the usual course of the process. That is, after the polymer is produced, it is simply handled by standard procedures. Cocatalyst residues will oxidize and hydrolyze to produce scent compounds. Scent agents will be dispersed evenly throughout the polymer. Routine handling usually involves pneumatic conveyance and pelletization, during which the polymer is exposed to ambient air. Alternatively, simple steps (discussed below) may be taken to facilitate oxidation/hydrolysis of cocatalyst residues. In either case, post-reactor blending and masterbatches are obviated.

Scented polyolefins could add value to the millions of pounds of film used to produce trash bags, grocery bags and merchandise ("T-shirt") bags. Scents may also enhance marketability of disposable diapers and personal hygiene products.

Perhaps an even more important possible application is the life-saving potential of citronellol-scented polyolefin in insecticide-treated nets for prevention of diseases spread by mosquitoes. (Citronellol is a well-known mosquito repellent.)

Background for This Paper

When I was just beginning my career as an industrial chemist in the 1970s, among my early assignments was to work with a company in the flavor and fragrance industry. The company wanted to explore whether an aluminum alkyl might afford advantages as a route to citronellol, a well-established F&F product. The project was a technical success and progressed to the plant trial stage, but economics did not warrant changing from their existing technology. The project was terminated.

The aluminum alkyl intermediate was assigned the moniker “tricitronellylaluminum” (TCAL, pronounced “tee cal,” discussed below), but was never offered to the polyolefins industry for use as a cocatalyst. There were several reasons for this, including:

- TCAL was unproven as a cocatalyst for Ziegler-Natta catalysts,
- TCAL was costlier than conventional aluminum alkyl cocatalysts.

At the time, there was little incentive for polyolefin producers to evaluate TCAL as a cocatalyst for ZN polymerizations. We eventually tested TCAL using a supported ZN polyethylene catalyst. I recall that TCAL functioned reasonably well as a cocatalyst, though the activity was somewhat lower than results with triethylaluminum (TEAL). Polyethylene from the experiment was stored in a large evaporating dish in a vacuum desiccator jar. When the cover was removed, the polymer exuded the distinct scent of lemon. Since citronellol is reported to have a floral, rose-like aroma [3], the product may have been partially converted to citronellal, reported to have an intense lemon scent [4].

Though TCAL has received little attention for many years, the cursory experiment above demonstrated that TCAL and similar aluminum alkyls might be useful for introducing scents to polyolefins. The method constitutes a simple means of adding value to polyolefins for several niche applications, identified later in this paper. Technology used to produce TCAL and similar compounds is in the public domain, since relevant patents expired decades ago. The aluminum alkyls could be easily produced in-house or provided by existing industrial manufacturers of metal alkyls.

In recent years, I approached several companies that are either directly or indirectly involved in the polyolefins industry. None was interested in scented polyolefins, so I decided to appeal to a broader audience at the SPE conference on polyolefins.

What is the intent of this paper? My hope is to generate interest in a simple, convenient method to introduce scents to polyolefins for use in selected applications, for example, in LLDPE trash bags. Perhaps an even more important application is bed netting that may be produced with citronellol-scented polyolefin fibers which could potentially save lives in countries afflicted by mosquito-borne diseases, such as malaria, yellow fever and dengue fever. Such netting would be an environmentally friendly way of introducing mosquito repellent and obviate the soaking of nets in noxious insecticides. Other applications of scented polyolefins may occur to marketing experts in attendance at this conference. From a personal standpoint, it will be profoundly gratifying in my senectitude to play a role in bringing value-added products to market, particularly one that might save lives.

Introduction

The global plastics business is enormous. The demand in 2015 was estimated to have been about 240 million metric tons for the major plastics [5], or about 70 pounds for every man, woman and child in the world. Polyolefins accounted for nearly $\frac{2}{3}$ of the total, or about 151 million metric tons. All industrial polyolefins require a catalyst or an initiator to effect the polymerization of ethylene and propylene. Transition metal catalysts are, by far, the most important, accounting for about 86% of the global output of polyolefins.

Polyethylene was first manufactured on a large scale in 1939 and the product was then known as “high pressure polyethylene” [6]. Now known as low density polyethylene (LDPE), it remains industrially important today, though it is largely peripheral to the motif of this paper. LDPE and closely related products, such as EVA (ethylene-vinyl acetate copolymer), are manufactured at high pressures and temperatures using free radical initiators, almost exclusively organic peroxides. All other versions of polyethylene (HDPE, MDPE, HMW-HDPE, LLDPE, etc.) and the various forms of polypropylene (HP, RCP and ICP) are produced with transition metal catalysts.

Dr. Clifford Lee, VP of Townsend Solutions, estimates that about 280 billion pounds of HDPE, LLDPE and PP were produced in 2015 [7]. HDPE, LLDPE and PP are fabricated into a diverse range of consumer goods using a variety of processing methods. For example, large amounts of (~80%) of LLDPE go into blown film applications. Significant amounts of HDPE (25-30%) and PP (15-20%) are also fabricated into film. Dr. Lee estimates that the global production of HDPE and LLDPE in 2015 was about 151 billion pounds and all forms of polypropylene totaled about 129 billion pounds [7].

Two types of transition metal catalysts account for the vast majority of polyolefins manufactured in the world today: Ziegler-Natta and chromium catalysts [8]. For HDPE, chromium supported on silica (“Phillips”) catalysts are narrowly favored over Ziegler-Natta catalysts. In large measure, this is because chromium catalysts produce HDPE with broad molecular weight distribution which enhances processibility while retaining mechanical properties. It is estimated that slightly more than half of the global production of HDPE employs chromium catalysts. However, ZN catalysts are dominant in LLDPE, accounting for about 84% of the total. In polypropylene, ZN catalysts are even more dominant, accounting for more than 97% of total PP production. Collectively, for the manufacture of HDPE, LLDPE and PP, transition metal catalysts are used in the following approximate proportions:

Ziegler-Natta:	78%
Cr (“Phillips”):	17%
Single Site:	5%

Polyolefins incorporating fragrances have been described in the literature for many years. A case in point is a patent issued in 1971 disclosing post-reactor blending of polyethylene of small particle size with a scent agent [9]. Polyethylene particles were ground to a fine powder (200 mesh was preferred). A masterbatch was prepared by blending 30% of a fragrance compound with fine HDPE powder. The fragrance-containing masterbatch was then blended with virgin LDPE to achieve a polyethylene composition containing about 3000 ppm scent agent. Though the patent describes a process for production of scented polyolefins, there are significant differences relative to the process discussed in this paper:

- The method described in this paper does not require grinding or milling.

- Masterbatches containing 30-40% (300,000 to 400,000 ppm) of fragrance compounds are not required.
- Concentration of scent agent in the final polyolefin composition in the aluminum alkyl route is an order of magnitude lower.

Ziegler-Natta Catalysts

What are known today as “Ziegler-Natta catalysts” were discovered in 1953 by German chemist Karl Ziegler. Because a preliminary experiment with propylene was deemed to have been unsuccessful (a conclusion later realized to be in error), Ziegler decided to focus on ethylene polymerization and return to propylene later [10, 11]. Giulio Natta was then Director of the Institute of Industrial Chemistry at the Milan Polytechnic Institute and a consultant to Montecatini. In 1952, Natta attended a lecture delivered by Ziegler in Frankfurt during which he learned of Ziegler’s success with the oligomerization of ethylene by the so-called growth (“aufbau”) reaction [10]. (The “aufbau” reaction foreshadowed Ziegler’s later discoveries on ethylene polymerization.) Natta influenced Montecatini to engage Ziegler as a consultant and to obtain commercial rights to Ziegler’s technology in Italy. The consulting agreement allowed Natta access to Ziegler’s discoveries on what was termed “transformation of olefins.” Using catalysts described by Ziegler for ethylene polymerization, Natta polymerized propylene and determined the crystal structure of stereoregular polypropylene. This work was done before Ziegler had returned to study the applicability of his catalysts to propylene polymerization. This sequence of events ended the previously close personal relationship between Ziegler and Natta [10]. Nonetheless, Ziegler and Natta were jointly awarded the 1963 Nobel Prize in chemistry. Today, ZN catalysts are used globally for production of millions of tons of polyethylene and polypropylene.

Ziegler-Natta catalysts may be broadly defined as binary combinations of a transition metal compound from Groups 3-12 of the Periodic Table with an organometallic compound from Groups 1, 2 or 13 [12]. Substantial reactions take place between the transition metal and organometallic components resulting in predominantly inorganic compositions that function as polymerization catalysts. Many modern ZN catalysts are produced using titanium tetrachloride (TiCl_4 , or “tickle 4”) and TEAL, both clear, colorless liquids. Though TiCl_4 is sometimes (erroneously) called the “catalyst,” it is more accurate to call TiCl_4 a “pre-catalyst,” since it must be transformed through reactions with TEAL. Independently, neither TiCl_4 nor TEAL is capable of producing high polymers in practical amounts. Moisture and air must be rigorously excluded during handling of ZN catalysts, because even small (ppm) amounts of water and oxygen may result in deactivation (“poisoning”) of the catalyst. Industrial ZN catalysts are often supported on silica or magnesium chloride.

Early industrial Ziegler-Natta catalysts were obtained principally by reduction of TiCl_4 using aluminum metal. They were unsupported and contained occluded AlCl_3 . These archaic catalysts were powdery, purple solids containing about 24%Ti, and exhibited low activity (usually < 2 kg polymer/g catalyst). Because of low activity, polymer produced with these primitive catalysts required post-reactor treatment to remove catalyst residues and other undesirable components.

Modern ZN catalysts are typically powdery or granular solids with a grayish or brownish tint, depending on the transition metal, the support employed and activation procedure used. Many involve titanium and are produced by techniques that enable control of

morphology and particle size. Most contain only 1-4% titanium, but provide high activities. For example, activities as high as 100 kg of PP/g of catalyst [13] have been reported (corresponding to *millions* of pounds of PP per pound of titanium). The polymers require no post-reactor treatment to remove catalyst and cocatalyst residues.

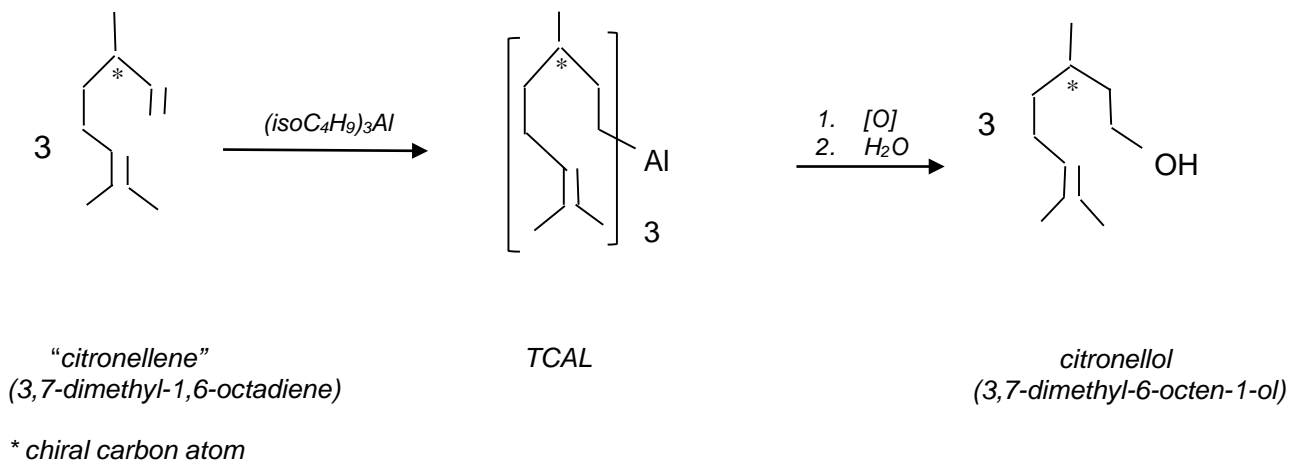
Aluminum Alkyls

Aluminum alkyls have contributed mightily to the astonishing commercial success of Ziegler-Natta catalysts, harking back to the very beginning of the polyolefins industry based on transition metal catalysts. The most important aluminum alkyl in the polyolefins industry today is TEAL, sold globally in multi-million pound/year quantities. However, TEAL and most of the industrially important aluminum alkyls are very hazardous chemicals. TEAL is both pyrophoric (ignites on exposure to air) and explosively reactive with water, as are many of the commercially significant aluminum alkyls.

Aluminum alkyl cocatalysts for ZN polymerizations are typically used in large excess relative to the transition metal. Al/transition metal ratios of 30-40 are not uncommon in industrial polyethylene processes. An excess is used to insure that sufficient aluminum alkyl is present to accomplish the three key roles that cocatalysts must fulfill [14]:

- Reduction of the transition metal compound to a lower oxidation state;
- Alkylation of the transition metal to produce active centers for polymerization;
- Scavenging of catalyst poisons, particularly water and oxygen.

Aluminum alkyls envisioned for introducing scents into polyolefins are significantly less hazardous than TEAL. They contain lower Al content and will be much less reactive with air and water. The aluminum alkyl selected for the case study is tris(3,7-dimethyl-6-octenyl)aluminum, known more simply as “tricitronellylaluminum” (TCAL). TCAL may be produced using the so-called exchange (or displacement) reaction of TIBAL with the terpene 3,7-dimethyl-1,6-octadiene (“citronellene”), chemistry developed by Ziegler in the 1950s [2, 15]. The internal double bond is virtually unreactive under conditions commonly used for exchange reactions.



TCAL is a non-viscous liquid with formula weight of 444.8 and a theoretical aluminum content of 6.07%. Handling characteristics are similar to that of a Grignard reagent. Though TCAL is air- and water-reactive, it is substantially less hazardous than TEAL. For example, the non-pyrophoric limit (NPL) of TCAL in heptane is 91%, while the NPL of TEAL in heptane is 12% (higher NPLs indicate lower reactivity [16]). The NPL of TCAL is comparable to that of the mildly air-reactive tri-*n*-decylaluminum.

The approximate concentration of citronellol within a polyolefin may be calculated using a hypothetical ethylene polymerization with a Ziegler-Natta catalyst, TCAL cocatalyst and the following assumptions:

- the catalyst contains 1.5% titanium
- the cocatalyst (TCAL) contains 6.0% Al
- the Al/Ti ratio used in the polymerization is 40, and
- the activity of the catalyst is 20,000 lb polymer/lb of catalyst.

In this illustration, the final concentration of TCAL in the polymer will be about 280 ppm. In theory, one mole of TCAL will generate 3 molar equivalents of citronellol. However, yields of alcohols *via* oxidation-hydrolysis of R₃Al compounds are known to be lowered because of free radical side reactions [17], one of which produces an aldehyde (perhaps explaining the intense lemon scent characteristic of citronellal mentioned earlier). Free radical side reactions can be minimized by introduction of catalytic amounts of titanium compounds, such as tetraisopropyl titanate (TIPT), enabling yields of >90% to be obtained [17]. Allowing for yield losses from side reactions, it is estimated that the concentration of citronellol dispersed within the polyethylene of this illustration will be about 260 ppm. The “aroma threshold limit value” for detection of citronellol is reported to range from 11 ppb to 2.2 ppm [18].

If the scent is too pronounced, the cocatalyst may be diluted with a less expensive cocatalyst such as TEAL. If concentration of scent agent needs to be increased, higher Al/transition metal ratios may be used. Ratios of 100-200 will lower polymer molecular weight marginally owing to chain transfer reactions, but should have little impact on other polymer properties. Another way to maximize scent agent would be to carry out simple post-reactor steps (though masterbatches would still not be required). For example, addition of a catalytic amount of TIPT, subsequently sparging the raw polymer with dry air, and then with water mist, should increase the concentration of scent agent.

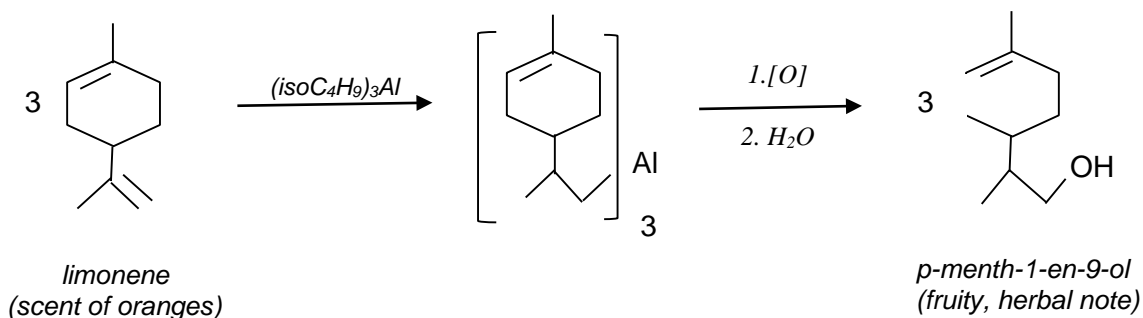
Using selected aluminum alkyls to impart scent to polyolefins may be demonstrated in small-scale polymerization tests with standard Ziegler-Natta catalysts from a range of polyolefin technologies, including Unipol®, Spheripol®, Borstar® and Hypol®. Initial demonstration of the method could be done in laboratory or pilot plant polymerization reactors [19].

Scope

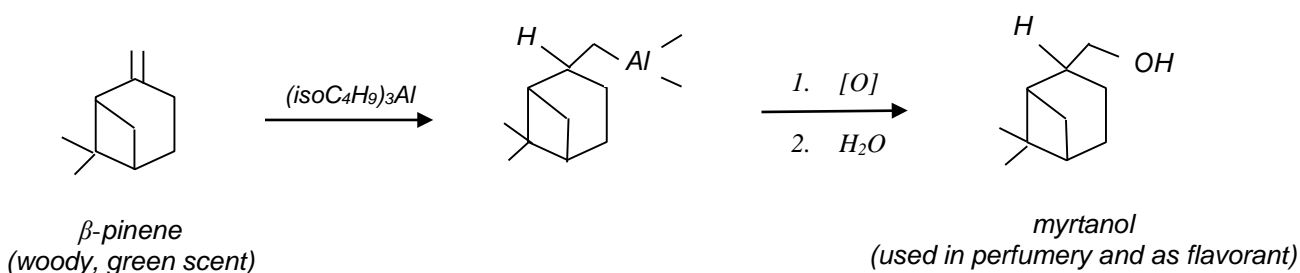
Citronellol is but one of several agents that may be used to impart a pleasant scent to polyolefins by way of aluminum alkyl cocatalysts. For example, suitable cocatalysts may be prepared by reaction of TIBAL with other terpenes or different organic compounds containing a terminal double bond. As in the TCAL case study, internal double bonds will

be essentially unreactive. In many respects, aluminum alkyls derived from terpenes will be similar to conventional R_3Al compounds. Since TCAL and the aluminum alkyls obtained from terpenes illustrated below contain no functional groups that might interfere with their performance as ZN cocatalysts, they should perform reasonably well in olefin polymerization. For interested parties, samples of scented aluminum alkyl cocatalysts can be arranged for testing.

Limonene is a cyclic terpene with the scent of oranges. It is obtained from the rinds of citrus fruits. Like citronellene, it is commercially available and can be easily converted into an aluminum alkyl that will be effective as a cocatalyst for ZN catalysts. After aging in air (and undergoing oxidation and hydrolysis), the scent compound in the polymer will be 2-(4-methylcyclohex-3-en-1-yl)propan-1-ol, also known as “*p*-menth-1-en-9-ol”, which has a distinctive fruity, herbal note.



β -Pinene is another commercially available cyclic terpene that may be readily converted into an aluminum alkyl cocatalyst. β -Pinene is obtained from pine resin and possesses a “woody, green pine-like smell” [20]. After polymerization, the aluminum alkyl will produce myrtanol which is used in perfumery and as a flavorant:



An unknown in the method disclosed here is the extent to which the scent compound may decompose during high temperature processes typically used for extrusion of polyolefins. Temperatures in excess of 200° C are routine. Like citronellol, 1-decanol (*n*-decyl alcohol) is a primary C_{10} alcohol with comparable formula weight (158.2), and is reported to decompose between 299 and 393 °C [21]. Furthermore, the atmospheric boiling point of citronellol is reported to be 225° C [22]. These data suggest that thermal stability of citronellol may not be a significant issue.

Applications

Scented polyolefins will be suitable primarily for niche markets. Key targets are polyolefin films that are fabricated into bags, personal hygiene products and other consumer goods to which a pleasant scent may add value. However, for most large-volume markets for HDPE, LLDPE and PP, scents will be superfluous. If applications are successfully developed, scented polyolefins will likely be manufactured in campaigns using standard ZN catalysts and polymerization reactors. Manufacturing facilities may be converted back to unscented products simply by dropping in a conventional cocatalyst, such as TEAL, into the process.

Polyolefin Film

Polyolefin film has been fabricated into trash bags with pleasant scents for many years. Fragrances mask malodorous refuse in trash bags. Heretofore, scents have typically been introduced by way of masterbatches in post-reactor treatments [1, 9]. Polyolefin film is also used to fabricate grocery and merchandise bags, both of which are eminently recyclable. Scents should not adversely affect recyclability of polyolefin films. (However, today only small quantities of plastic bags are recycled. Reasons for low recycle rates are varied, but include inadequate infrastructure, marginal economics and limited markets for recycled products.)

Personal Hygiene Products

Polyolefins are used to produce personal hygiene products, such as incontinence pads and sanitary napkins. They are also used in disposable diapers. Polyolefins with a scent should mitigate offensive odors from such products.

Artificial Flowers

Though a relatively small-volume application, polyolefins are used in production of artificial flowers. A pleasant scent should enhance marketability of decorative flowers.

Mosquito Bed Netting

Mosquito-borne diseases have tormented humankind for thousands of years [23]. Ancient Chinese writings described symptoms of the illness that would later become known as malaria. Malaria is spread by *Anopheles* mosquitoes infected with protozoan parasites, most notably *Plasmodium falciparum*. According to the World Health Organization (WHO, the global health organization of the United Nations), deaths from malaria in 2015 were about 438,000 [24]. However, annual worldwide deaths from malaria in the millions were not uncommon as recently as the 1930s.

Moreover, mosquitoes spread other deadly diseases such as yellow fever. An article in a chemical industry trade magazine reported in early 2016 that more than “1 million people die [annually] from mosquito-borne illnesses” [25]. Prevention of mosquito bites may save millions of lives. Mosquitoes (*Aedes aegypti*) are also responsible for spreading the Zika virus. (Though Zika causes the heartrending birth defect called microcephaly, it is rarely fatal.)

In the latter part of World War II, “dichlorodiphenyltrichloroethane” (DDT) saved the lives of innumerable servicemen in areas afflicted by malaria [26]. After the war, DDT virtually eliminated malaria in some Third World countries. Illustrative is the case history of Sri

Lanka (formerly Ceylon), a small island country about the size of West Virginia located off the southeast coast of India. Sri Lanka's history shows the ebb and flow of the dread disease over the past century. In Ceylon/Sri Lanka, DDT use began in 1946 and had nearly eliminated malaria by 1963 [27]. Resurgence of the disease occurred in the late 1960s owing to a variety of factors, including scaling back of indoor residual spraying (IRS) with DDT.

In the USA, a cooperative program involving the Center for Disease Control (CDC) and other public health agencies eliminated malaria by the late 1940s, primarily using DDT and IRS [28]. However, DDT was banned in the USA in 1972 by the first director of the EPA, William Ruckelshaus. Following the lead of the USA, other countries also banned DDT. Some Third World countries came under pressure from the USA and other major donors, who threatened to withhold food aid unless the country stopped using DDT [29]. In 2009, the United Nations stated its intent to phase-out DDT globally "by the early 2020s" [30]. Nonetheless, DDT is still being used for IRS in developing countries under exemptions from the Stockholm Convention on Persistent Organic Pollutants [31].

In the late 1950s, mosquitoes began to develop resistance to DDT [32], mostly a consequence of indiscriminate, large-scale misuse in agriculture. Because of incipient mosquito resistance and DDT bans, it has become imperative to develop alternative methods to combat malaria and other mosquito-borne illnesses.

A key alternative method involves use of nets that serve as a physical barrier to mosquitoes. Nets are intended for use over beds at night when female *Anopheles* mosquitoes seek blood meals for egg production. Insecticide-treated nets (ITN) are far more effective than untreated nets because, in addition to serving as a barrier, ITN repel and kill mosquitoes. Most bed nets are produced from polyethylene, polypropylene or polyester fibers [33]. To prepare ITN, nets are simply immersed in a water-insecticide bath and allowed to dry in air. Consequently, insecticide is merely deposited on the surface of the polymer. According to the CDC and WHO, only pyrethroids are approved for ITN at this point [33, 34].

"Mosquito nets are now a billion-dollar industry, with hundreds of millions of insecticide-treated nets passed out in recent years..." [35]. Though the latter statement may be hyperbole, it is clear that mosquito nets are vital in today's fight against malaria. Unfortunately, ITN meant to prevent nocturnal mosquito bites are being misused as fishing nets in Madagascar and other Third World countries [35].

Despite the fact that citronellol repels mosquitoes [22], it is not presently used in ITN. The principal reason is probably that citronellol is simply too volatile to exhibit longevity in ITN prepared by the immersion method. However, citronellol generated by the aluminum alkyl cocatalyst method will be uniformly distributed throughout the polymer (rather than merely deposited onto the surface, as in the immersion process). Scent agent will migrate to the surface by a process called "blooming." Instead of evaporating from the surface, it is believed that the scent agent will be slowly exuded from the polymer. Such ITN will release citronellol continually over an extended period, though long-term efficacy will have to be determined by further research. An additional advantage of ITN made from citronellol-impregnated fibers is that misuse as fishing nets would be less damaging environmentally compared to ITN produced using deleterious insecticides.

As a means of overcoming mosquito-resistance, WHO recently recommended that two insecticides be used in mosquito nets "to mitigate the risk of the development and

spread of insecticide resistance...” [34]. One of the insecticides in two-component ITN should be a citronellol-impregnated polyolefin fiber described here.

Regulatory

Judicious choice of scent agent may render regulatory barriers irrelevant. In the case study discussed above, for example, citronellol is the scent agent. Since citronellol is on the Federal Drug Administration’s “generally regarded as safe” (GRAS) list, citronellol-scented polyolefins should pose few regulatory problems.

In the section on scope above, raw materials limonene and β -pinene are also on the GRAS list and are obtained from natural sources (citrus rinds and pine oil, respectively). Furthermore, the derivatives themselves (*p*-menth-1-en-9-ol and myrtenol) are used in perfumery and food additives, implying that regulatory obstacles should be minimal.

References

1. R. Renstrom, www.plasticsnews.com/article/20080804/NEWS/308049977/scent-suppliers-smell-potential-in-plastics, August 4, 2008.
2. K. Ziegler, *Organometallic Chemistry*, ACS Monograph 147 entitled *Organo-aluminum Compounds*, H. Zeiss, editor, Reinhold, NY, 207, **1960**.
3. www.merriam-webster.com/dictionary/citronellol
4. G. Burdock, *Fenaroli’s Handbook of Flavor Ingredients*, CRC Press, 5th edition, 321, **2005**.
5. H. Rappaport, IHS, personal communication, January 5, 2016.
6. R. Seymour, *History of Polyolefins*, Reidel Publishing, R. Seymour and T. Cheng, editors, 2, **1986**.
7. C. Lee, Townsend Solutions, personal communication, February 1, 2016.
8. Single site catalysts (SSC) are also based on transition metals. In 2017, however, relatively small amounts of polyolefins are produced with SSC compared to quantities produced with other transition metal catalysts. Though SSC are increasingly important in the modern polyolefins industry, they are much less consequential than ZN and Cr catalysts, and will remain so well into the 21st century. At this point, SSC have made significant inroads into large volume applications only for LLDPE (~15%).
9. B. Gaeckel, US 3,553,296, January 5, 1971.
10. F. McMillan, *The Chain Straighteners*, The MacMillan Press Ltd., London, **1979**. McMillan’s book provides an excellent historical account of the genesis of ZN catalysts and personal interactions between Ziegler and Natta. The “falling out” between Ziegler and Natta is discussed in Chapter 8; see also the footnote on page 77.
11. For a brief discussion of the origins and characteristics of ZN catalysts, see Chapter 3 in *Introduction to Industrial Polypropylene*, D. Malpass and E. Band, Wiley-Scrivener, 59, **2012**.
12. D. Malpass and E. Band, *Introduction to Industrial Polypropylene*, Wiley-Scrivener, 61, **2012**.
13. *Ibid.*, 87 and 103.
14. *ibid.*, 125; see also D. Malpass, *Introduction to Industrial Polyethylene*, Wiley-Scrivener, 49, **2010**.
15. T. Mole and E. Jeffery, *Organoaluminium Compounds*, Elsevier, 129, **1972**; D. Malpass, L. Fannin and J. Ligi, *Kirk-Othmer Encyclopedia of Chemical Technology*, John Wiley & Sons, 3rd Edition, Vol 16, 569, **1981**. A discussion of the exchange reaction applied to the production of TEAL is available in J. Ligi and D. Malpass, *Encyclopedia of Chemical Processing and Design*, Marcel Dekker, J. McKetta and W. Cunningham, editors, Vol 3, 29, **1977**.
16. For a discussion of pyrophoricity test methods and non-pyrophoric limits, see D. Malpass, *Handbook of Transition Metal Polymerization Metal Polymerization Catalysts*, Wiley, R. Hoff and R. Mathers, editors, 551, **2010**.

17. J. Zietz, Jr., G. Robinson and K. Lindsay, *Comprehensive Organometallic Chemistry*, Vol 7, 375 and 378, **1982**.
18. G. Burdock, *Fenaroli's Handbook of Flavor Ingredients*, CRC Press, 5th edition, 324, **2005**.
19. D. Malpass and E. Band, *Introduction to Industrial Polypropylene*, Wiley-Scrivener, 217, **2012**. Chapter 10 provides a detailed discussion of equipment and procedures used for testing ZN propylene polymerization catalysts.
20. <https://en.wikipedia.org/wiki/Beta-Pinene>.
21. M. Riley and R. Anthony, *Journal of Catalysis*, Vol. 103, 87, **1987**.
22. <https://en.wikipedia.org/wiki/Citronellol>.
23. Malaria, for example, has plagued humanity for at least 500,000 years. See S. Shah, *The Fever*, Farrar, Straus and Giroux, 12, **2010**.
24. www.who.int/malaria/media/world-malaria-report-2015/en/. See also Center for Disease Control and Prevention website: www.cdc.gov/malaria/
25. M. Garcia, *Chemical & Engineering News*, 31, February 29, 2016.
26. R. Zubrin, *Merchants of Despair*, Encounter Books, 93, **2012**. DDT was introduced in January of 1944 to defeat an epidemic of typhus in Italy. DDT was later used in the Pacific theater of World War II to combat malaria.
27. <http://journals.plos.org/plosone/article?id=10.1371/journal.pone.0043162>. See also <https://www.ucsf.edu/news/2012/08/12645/malaria-nearly-eliminated-sri-lanka-despite-decades-conflict>.
28. www.cdc.gov/malaria/about/history/elimination_us.html
29. E. Zelson, *Rethinking DDT*, William & Mary Environmental Law and Policy Review, 253, **2014** (<http://scholarship.law.wm.edu/wmelpr>); see also R. Zubrin, *Merchants of Despair*, Encounter Books, 101, **2012**.
30. www.reuters.com/article/2009/05/06/us-ddt-idUSTRE54542W20090506
31. <http://www.ncbi.nlm.nih.gov/books/NBK1724/>
32. E. Miller, www.mosquitoreviews.com/DDT-resistant-mosquitoes.html, **2012**. See also www.cdc.gov/malaria/about/biology/mosquitoes/ and S. Shah, *The Fever*, Farrar, Straus and Giroux, 201, **2010**.
33. www.cdc.gov/malaria/malaria_worldwide/reduction/itn.html
34. www.who.int/mediacentre/factsheets/fs094/en
35. J. Gettelman, *New York Times*, January 24, 2015.

Acknowledgements

The author gratefully acknowledges assistance of the following associates and former colleagues in the preparation of this paper:

Dr. Elliot I. Band, AkzoNobel
Dr. Jacob George, Gulbrandsen Chemicals
Dr. Ray Hoff, Chemplex Company (retired)
Dr. Paul Jones, International Flavor & Fragrances
Dr. Clifford Lee, Townsend Solutions
J. J. Ligi, AkzoNobel (retired)
Sheila Phippeny Malpass, (slides)
Howard Rappaport, IHS

Supported Metallocene Catalyst for Long Chain Branched Polypropylene

*Iku Kozai¹⁾, Masaaki Ito¹⁾, Sachio Hotta¹⁾ and Kuninori Takahashi¹⁾
Takehiro Sagae²⁾, Shinichi Kitade²⁾ and Takao Tayano²⁾*

1) Japan Polypropylene Corporation, 1-1-1, Marunouchi, Chiyoda-ku, Tokyo 100-8251 Japan

2) R&D Division, Japan Polychem Corporation, 1 Toho-cho, Yokkaichi, Mie 510-0848 Japan

Abstract

Japan Polypropylene Corporation (JPP) and Japan Polychem Corporation (JPC) have developed a new metallocene catalyst for long chain branched polypropylene (LCB-PP). LCB structure [1] is useful for improving melt strength of linear polyolefins like polyethylene (PE) and polypropylene (PP). However it has not been sufficiently solved by catalyst technology to introduce LCB into PP main chains because selective synthesis of active vinyl macromers and following incorporation at active sites for PP main chains were very difficult. JPP and JPC successfully solved the problem by their unique metallocene complex and clay mineral technologies and launched high melt strength (HMS) PP under the brand name of WAYMAX. Rheological properties and some application examples will be also reported.

Introduction

LCB PP is one of the most interesting targets for PP manufacturers because melt-strength of general linear PP is too low for foaming application. In order to install LCB structure into PP, mainly post reactor modification technologies have been developed. Peroxide [2] or electron beam radiation [3] is usually used. However post reactor modification has some disadvantages such as poor appearance by gels, coloring by residual radicals, limited suitability for repeated extrusion and so on. In case of PE, catalytic introduction of LCB has been achieved. For example, constrained geometry complex (CGC) is widely used. On the contrary, there was no commercialized catalyst technology for LCB-PP. It might be because of essential difference in structural properties, that is, secondary carbon atoms at methyl substituents of polymer chains. Therefore new catalyst technology for selective and effective LCB installation has been desired.

JPP and JPC have developed a new catalyst system for LCB-PP based on their unique metallocene technology including clay mineral support and launched a new product lineup under the brand name of WAYMAX. Some technical features will be discussed.

Requirements and Architecture

Requirements for LCB-PP catalyst are summarized in the following three points.

1. Selective synthesis of active vinyl macromers
2. Effective incorporation of synthesized macromers
3. Overall melt flow rate (MFR) control for extrusion foaming application

Macromer synthesis reaction needs very specific catalyst behavior and decreases molecular weight of polymer chains because it accelerates elimination reaction. So if we use only the complex suitable for macromer synthesis for catalyst preparation, overall MFR of the product PP doesn't reach to necessary values for extrusion foaming. Therefore we selected the architecture for LCB-PP catalyst shown in Figure 1.

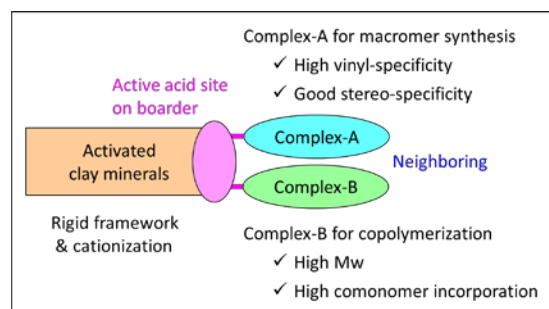


Figure 1. Architecture for LCB-PP catalyst

In-situ Macromer Synthesis

General olefin polymerization catalysts are active only for α -olefins which have a terminal double bond and inactive for internal olefins such as vinylidene compounds. In case of CGC for LCB-PE, active macromers are synthesized by β -elimination reaction at the connecting metal-carbon bond. Because PE has essentially no substituents on polymer chains, all reactions provide only active macromers. However in case of PP, there is a methyl substituent at β -position of metal-carbon bond. In addition, hydrogen extraction is much faster than methyl extraction in β -elimination reaction. Then major

products are inactive vinylidene macromers generally (Figure 2). Therefore we need to develop a very specific catalyst which promotes thermally less preferred β -methyl extraction.

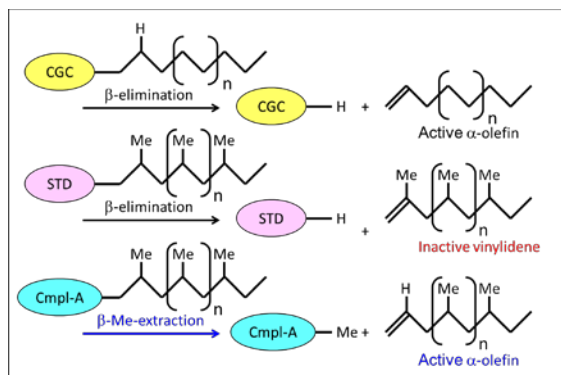


Figure 2. Difference in structure and specificity

We tried a lot of types of metallocene and found that certain complex framework worked well.

Complex		A-1	A-2	A-3
Stereo/Regio [mol%]	mm	97.6	98.0	97.8
	2-1	0.08	0.07	0.09
	1-3	0.18	0.16	0.18
Unsaturated terminal [unit/1,000unit]	1-Propenyl	0.79	0.72	0.88
	Vinylidene	N.D.	N.D.	N.D.
	1-Butenyl	N.D.	N.D.	N.D.
	<i>i</i> -Butenyl	N.D.	N.D.	N.D.
Saturated terminal [unit/1,000unit]	<i>i</i> -Butyl	1.23	1.17	1.21
	<i>n</i> -Propyl	N.D.	N.D.	N.D.
	<i>n</i> -Butyl	N.D.	N.D.	N.D.
	Et	N.D.	N.D.	N.D.

Table 1. ^{13}C -NMR analyses of PP obtained by complexes in the same category

Table 1 shows microstructures of PP obtained by some complexes in the same category supported on activated clay mineral. Polymerization was conducted without hydrogen addition. Stereospecificity is not so high but acceptable. Regiospecificity is high. Therefore we can estimate that β -elimination reaction will usually happen after regular 1-2 insertion. The most important point is unsaturated terminal structure. It is noted that only 1-propenyl structure was observed for all complexes. Hydrogen and methyl extraction at the metal-carbon bond after regular 1-2 insertion provides *i*-butenyl and 1-propenyl structure respectively. The above experimental

findings mean that only methyl substituent is extracted. Specificity of extraction is perfect. Similarly saturated terminal structure is interesting. Active sites after β -hydrogen elimination have a metal-hydrogen bond. Then regular 1-2 insertion after the reaction provides *n*-propyl terminal structure. However no *n*-propyl was observed in all samples. Observed *i*-Butyl terminal corresponds to regular 1-2 insertion after methyl extraction. As a conclusion, saturated terminal structure also shows that specificity of extraction is perfect. We selected this type of complex for LCB-PP catalyst as a potential macromer preparation site.

Macromer Incorporation

The second point is macromer incorporation. Even though macromers have an active terminal carbon-carbon double bond, only the limited conformation toward an active site is necessary for incorporation into active polymer chain. Indeed solution polymerization is relatively easier for analysis and understanding. However, we are afraid that it is not suitable for effective synthesis of LCB-PP. One of well-known advantages of solid catalysts is to accelerate reaction by concentrating substrate on its surface. If we support a pair of metallocene complexes, complex-A for macromer synthesis and complex-B for incorporation, within the close distance, macromer incorporation will be enhanced. Then we selected supported catalyst instead of solution polymerization.

Fortunately JPP and JPC had developed their original supported metallocene catalysts for propylene random copolymerization when we started this study. The fundamental framework was applied to LCB-PP catalyst. The following Figure 3 is a typical analysis result of prepared LCB-PP with the LCB-PP catalyst-I comprising complex-A, complex-B and clay mineral support according to the typical preparation recipe.

Gel permeation chromatography combined with light scattering and viscometer detectors (GPC-MALLS-V) was employed to detect LCB structure. Branching frequency is evaluated by the following equation (1):

$$g' = [\eta]_{\text{br}} / [\eta]_{\text{lin}} \quad (1)$$

where g' is a branching index, $[\eta]_{\text{br}}$ and $[\eta]_{\text{lin}}$ are intrinsic viscosity of the measured sample and reference linear PP.

It is noted that there is clear g' drop at high molecular weight region which means that the corresponding high molecular weight PP chains contain LCB considerably. Therefore our selection of supporting instead of solution was effective.

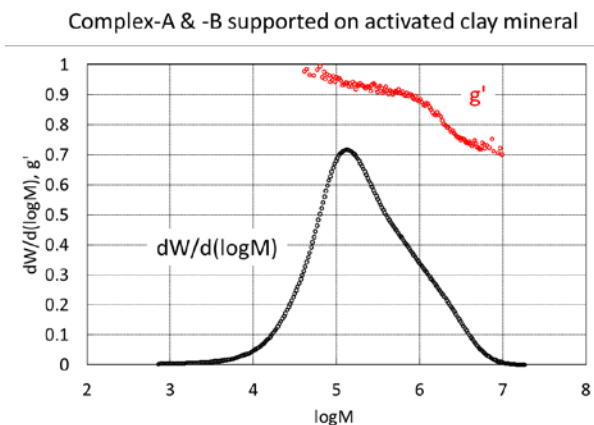


Figure 3. GPC-MALLS-V profile of LCB-PP prepared with the catalyst-I comprising complex-A, complex-B and clay mineral support.

Then we investigated influence of solid components. If we employ different types of solid activation materials, active site surroundings of supported two complexes might be different. For the purpose, we prepared the model catalyst-II supported on MAO-SiO₂ using the same mixing ratio of complex-A and complex-B as the above catalyst-I. Analysis result is shown in the following Figure 4.

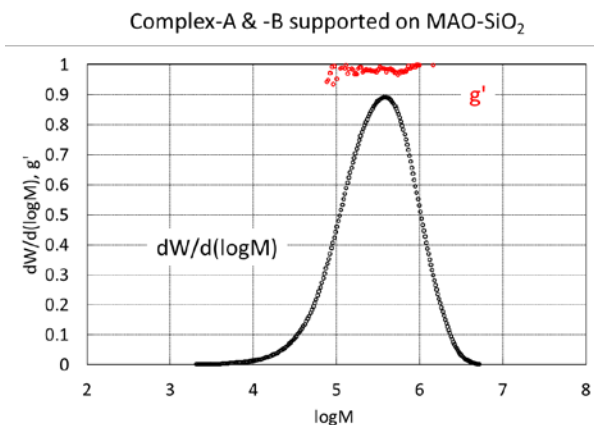


Figure 4. GPC-MALLS-V profile of the PP sample prepared with the catalyst-II comprising complex-A, complex-B and MAO-SiO₂.

Even though the same mixing ratio was employed, the PP sample doesn't contain any recognizable LCB. Therefore supported surroundings of metallocene might strongly influence on LCB preparation reaction. The authors believe that activated complex-A and -B will be located within the closer distance in the catalyst-I than in the case of catalyst-II because acid sites which cationize metallocene on activated clay minerals are concentrated

on the border [4]. The following Figure 5 is a typical AFM image of activated clay mineral. The border gets thicker than the original through some atom extraction by acid treatment. Clay minerals are not capable of activating metallocene without acid treatment in advance. Then it is rational to consider that only the chemically and physically modified part has activation ability. Therefore activated metallocene complexes are located within only the limited part, which might increase probability of preferable distance between complex-A and complex-B.

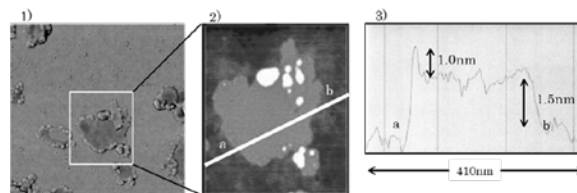


Figure 5. Typical AFM image of clay mineral platelets after acid treatment

Properties of LCB-PP

Various kinds of LCB-PP samples were prepared with the LCB catalyst described above and their rheological properties were investigated. Finally we found a good proportion of complex-A and complex-B for foaming application. Then we launched WAYMAX grades whose rheological properties are shown in the following figures.

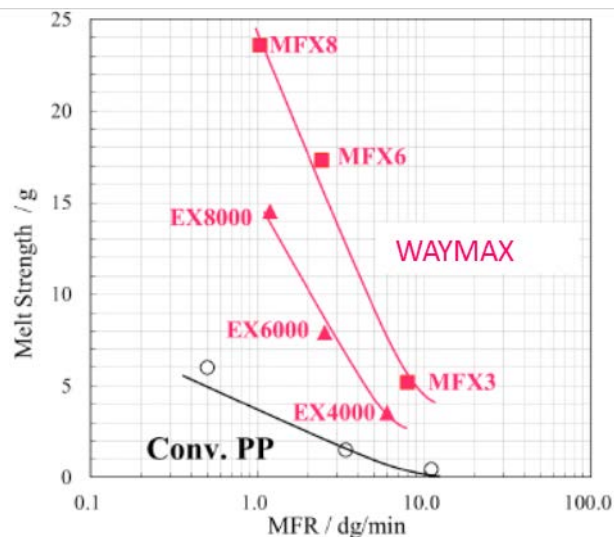


Figure 6. Melt strength of WAYMAX and conventional PP

Figure 6 shows melt strength (MS) of WAYMAX. MFR was measured according to ISO 1133 standard. CAPIROGRAPH (TOYO SEIKI SEISAKU-SHO, Ltd.) was used for MS measurement under the following conditions: capillary size: diameter: 2 mm, length: 40 mm, piston speed: 20 mm/min, barrel temperature: 230 °C. It is noted that MS is drastically enhanced compared with the conventional linear PP (a commercial grade produced with ZN catalyst) even though any post reactor reaction was employed.

Elongation viscosity shown in Figure 7 was measured with ARES rheometer combined with extensional viscosity fixture tools (TA instruments) at 180 °C and strain rate of 0.1 sec⁻¹. We can see clear "strain-hardening" which is generally required for foaming application.

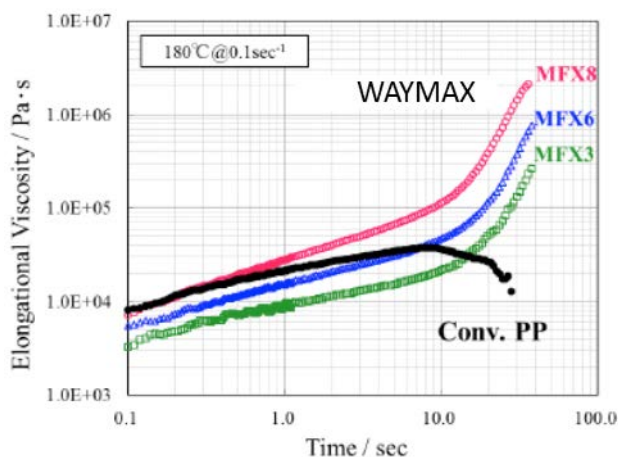


Figure 7. Elongation viscosity of WAYMAX and conventional PP

Conclusion

JPP and JPC have developed unique LCB-PP catalyst utilizing their experience and knowledge on metallocene catalyst. The architecture comprising three components, complex-A for macromer synthesis, complex-B for macromer incorporation and clay mineral support for accelerating necessary reactions, was used for catalyst development. Certain kind of complex has high specificity for active macromer synthesis. Some complexes show almost perfect specificity for thermally unfavorable β -methyl extraction reaction instead of hydrogen extraction. Clay mineral support contributes to high branching efficiency which is clearly different from unsuccessful result with MAO-SiO₂. It might be because of activation site surroundings mainly prepared on the border. The developed catalyst system is used for commercial production of HMS-PP under the brand name of

WAYMAX whose rheological properties are far different from conventional PP.

References

1. R.P. Legendijk et al., *Polymer*, **42**, 10035 (2001)
2. Japanese patent application, Hei10-330436
3. US patent 4916198.
4. T. Tayano et al., *J. Mol. Catal. A: Chem.*, **420**, 228 (2016)

NEW SOLUTIONS FOR POLYOLEFIN STABILIZATION: ADVANCED UV STABILIZER FOR MOLDING APPLICATIONS AND A UV/THERMAL STABILIZER FOR BUILDING & CONSTRUCTION

Rob Lorenzini, Jian-Yang Cho, Jerry Eng, Fadi Khawam, Sophie Poelmans

Abstract

Compounders, extruders, and molders are constantly demanding extended weatherability in polymer parts and looking for competitive advantages. New innovations are highlighted for two rapidly expanding market segments: molding and building & construction. A new stabilizer for molded products provides excellent color stability, long outdoor service life, and has broad food contact approvals. A new solution for building & construction provides outstanding UV weatherability and thermal stability for rugged applications. These new solutions deliver many advantages including the ability to meet extended warranties on roofing materials, and for molded articles, to look great and retain mechanical integrity for years.

Introduction

Polymers are inherently unstable when exposed to sunlight. Ultraviolet photons from the sun contain sufficient energy to homolytically cleave chemical bonds and form radical species. These radicals attack polymer chains, pigment, etc. in the presence of oxygen. The use of UV stabilizing chemistries is essential for outdoor polymer applications. For especially rugged applications, such as roofing materials, UV stabilizers must also factor in the ability to handle extended exposure to intense sunlight and heat, and must deliver commercial service lives in excess of 10 or more years.

As outdoor applications for polyolefins become more diverse, compounders, extruders, molders, as well as consumers, are demanding improvements in the stabilizer performance in polymer articles. For some applications, the manufacturer now guarantees the product against photobleaching and physical degradation by sunlight for a specified length of time. With minimal increases in the cost of a formulation, producers can realize the value of well-stabilized materials and products for their customers. Solvay, from the days of American Cyanamid and Cytec, is committed to delivering UV stabilizer innovations that enable customers to capture additional value from performance differentiated products.

Solvay is introducing stabilizers for different market segments: CYASORB CYNERGY SOLUTIONS® M535 Stabilizer for polyethylene injection and blow molding, and CYASORB CYNERGY SOLUTIONS® B878T Stabilizer for polyolefin construction materials that require long-term UV and heat stability for harsh conditions.

Injection Molding is the Future

From automotive interiors to packaging, injection molded parts are everywhere. The global injection molded plastic market is expected to reach 296 billion USD by 2020.¹ Much of this growth is driven by the replacement of metals and other materials with polymers, as well as precipitous general growth in Asia. The performance requirements for polyolefin injection molded articles vary drastically depending on application and producer – some products use no UV stabilizer and barely enough antioxidant to survive processing, and some high-end products require a decade or more of outdoor exposure. CYASORB CYNERGY SOLUTIONS® M535 stabilizer is a new solution recommended for general polyethylene molded articles to provide UV-8+ protection at modest loading levels.

CYASORB CYNERGY SOLUTIONS® M535 Stabilizer for UV-8+ PE Molding Applications

To test the performance of the new stabilizer, the material was extruded into HDPE along with phenolic/phosphite antioxidant and was injection molded into plaque test specimens and Type V tensile bars. All weathering in this section was performed in an Atlas Ci5000 Weatherometer using ASTM G155 Cycle 1 conditions.

In an HDPE containing 1% of a white pigment masterbatch, CYASORB CYNERGY SOLUTIONS® M535 stabilizer shows 10,000 hours of ASTM G155 weathering with 90% retention of strain at break (Figure 1). Compared to three popular competitive stabilizers, CYASORB CYNERGY SOLUTIONS® M535 stabilizer delivers equal performance at nearly half of the concentration.

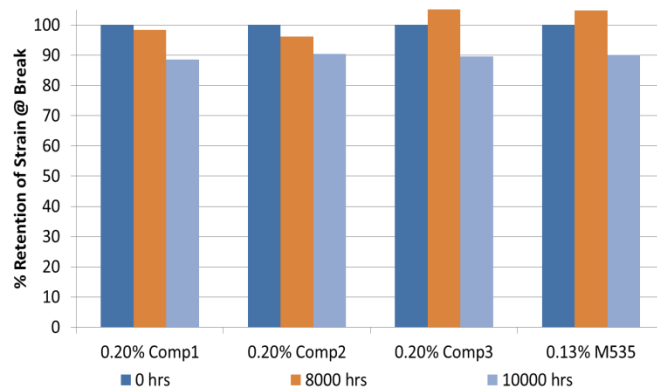


Figure 1 | Tensile data comparing CYASORB CYNERGY SOLUTIONS® M535 stabilizer to popular competitive stabilizers in HDPE with 1% white pigment masterbatch and CYANOX® 2777 antioxidant in ASTM G155 Cycle 1 Weathering

To ensure good long-term quality control, color matching is essential whenever anything is added to a polymer/pigment system, especially UV stabilizers. CYASORB CYNERGY SOLUTIONS® M535 stabilizer imparts a very low initial color in natural HDPE (Figure 2). Because CYASORB CYNERGY SOLUTIONS® M535 can be used at lower loadings than competitive solutions, a color concentrate producer could add more pigment or other additives to the formulation in lieu of stabilizer, allowing for formulation flexibility and helping to maximize value.

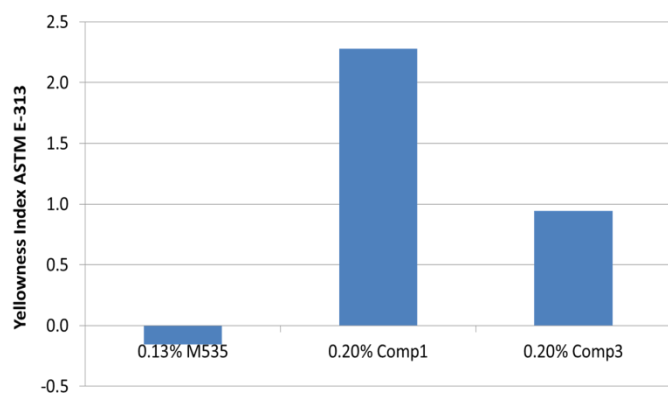


Figure 2 | Initial color of HDPE containing various stabilizers and CYANOX® 2777

In addition to low initial color, the retention of the intended initial color of a polymer article during outdoor exposure/field use is critical. CYASORB CYNERGY SOLUTIONS® M535 stabilizer demonstrates good color stability in natural HDPE (Figure 3), staying below ΔE of 2.0 after 10,000 hours of Xenon weathering.

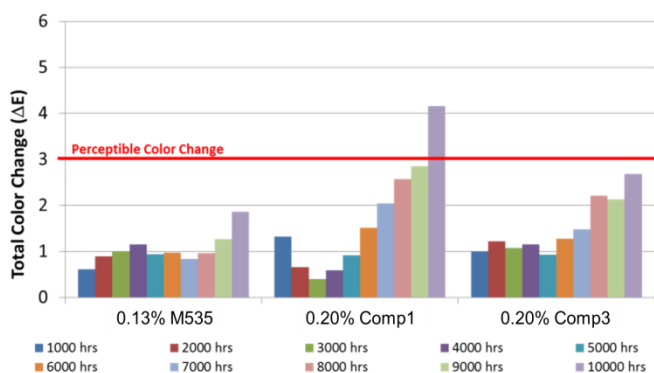


Figure 3 | Total color change in natural HDPE after 10k hours G155 weathering. Samples contain CYANOX® 2777 antioxidant.

CYASORB CYNERGY SOLUTIONS® M535 stabilizer is especially effective in preventing photo-induced color change and surface degradation (as measured by loss of gloss) in pigmented systems – color data is shown for HDPE with a phthalocyanine green-based pigment masterbatch (Figure 4), demonstrating a ΔE of 3.0 after 10,000 hours of weathering. Gloss data further demonstrates excellent surface protection (Figure 5). Again, the new stabilizer outperforms competitive systems at nearly half the loading level.

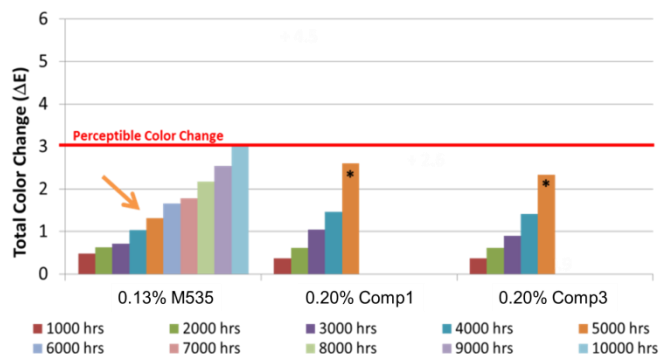


Figure 4 | Total color change in green HDPE after 10k hours G155 weathering. The (*) denotes surface crazing.

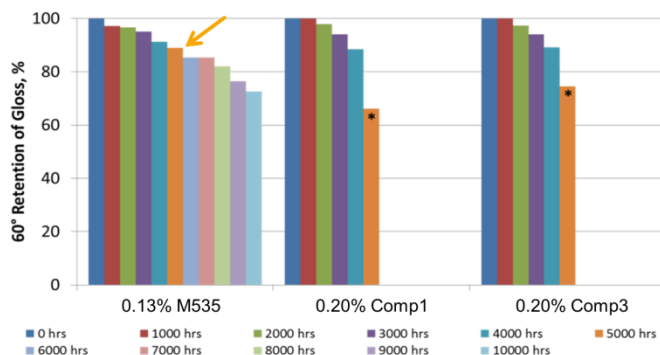


Figure 5 | 60° retention of gloss in green HDPE after 10k hours G155 weathering. The (*) denotes surface crazing.

Unique Challenges in Stabilizing Building & Construction Polymers

Polyolefins, especially TPO, TPV and TPE, are replacing other materials in construction for reasons including: their physical properties, ease of fabrication, barrier properties, relative cost effectiveness, lower weight, and recyclability. For some building applications, including roofing membranes, the performance requirements are even more demanding, with some manufacturers looking to meet and even exceed the current long-term heat aging and weather resistance specifications set forward by the ASTM (Table 1). A product that far surpasses the current long-term heat aging standards could help a producer find new markets in desert regions or in equatorial locations; at the extremes, a roof could be hotter than 90°C due to location, design, materials and radiant heat from surrounding surfaces. In addition to the aforementioned environmental stresses on roofing sheets, they will often be in contact with tar and other building materials that could contain stabilizer-inactivating chemicals.

North America ASTM D6878 Standard for Thermoplastic Based Sheet Roofing			
Test	ASTM Test Method	Test conditions	Passing requirements
Heat Aging	ASTM D573	5,376 hours at 116 °C/240 °F	>90% retained elongation and breaking strength
Weather Resistance	ASTM G155	10,080 kJ/m ² at 340 nm and 80 °C, BPT, 50 °C air temperature	7x magnification No cracks/crazing

Table 1 | Various standards for thermoplastic polyolefin sheet roofing.

CYASORB CYNERGY SOLUTIONS® B878T Stabilizer for Building & Construction Applications

The samples described in this section were prepared as follows:

- TPO resin, Mg(OH)₂, TiO₂, stabilizers
- 27 mil (~0.7mm) TPO roofing sheet for single ply membranes
- Specimens testing according to ASTM D6878 + ASTM D573
- ASTM D6878 Xenon conditions: 0.70W/m² @ 340nm, 80°C
- ASTM D573: Oven aging at 116°C and 138°C
- Tensile testing according to ASTM D751
- Color measurements according to ASTM E313

As shown in Table 1, the current UV specification for TPO sheet roofing is no cracking/crazing on a mandrel after 10,080 kJ/(m²·nm) radiant exposure @ 340nm, and the oven specification calls for 5,376 hours @ 116°C. CYASORB CYNERGY SOLUTIONS® B878T stabilizer shows no cracking or crazing over a mandrel at 3x the radiant energy of the ASTM UV specification (Figure 6). The commercial formulation failed after ~27,500 kJ/m².

ASTM UV Requirement								
↓								
kJ/m ²	2520	5040	7560	10080	20160	25200	27470	30240
B878T	Pass	Pass	Pass	Pass	Pass	Pass	Pass	Pass
Commercial Reference	Pass	Pass	Pass	Pass	Pass	Pass	Failed	Failed

Figure 6 | Results of mandrel testing after UV exposure. The (**) denotes the starting of cracking.

More quantitatively, tensile testing was used to probe the physical properties of the sheets after Xenon weathering; retention of stress at break (Figure 7) and retention of strain at break (Figure 8) are shown. The CYASORB CYNERGY SOLUTIONS® B878T-containing formulation had minimal loss of stress or strain at break after the prescribed 10,080 kJ/m², whereas the commercial reference exhibited a steady loss of stress at break over time, finally reaching ~80% retention at the ASTM minimum exposure.

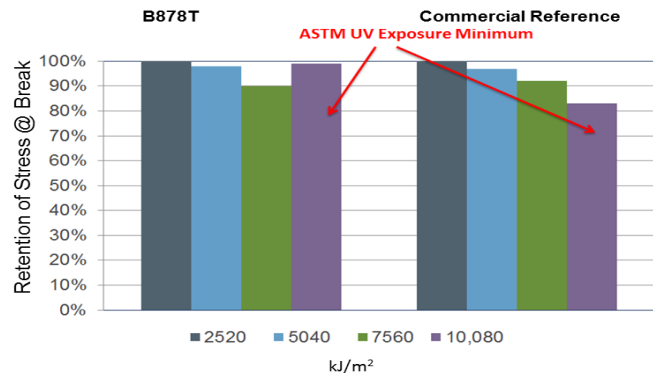


Figure 7 | TPO roofing sheet – retention of stress at break after 10,080 kJ/(m²·nm) radiant energy in an ASTM D6878 weatherometer

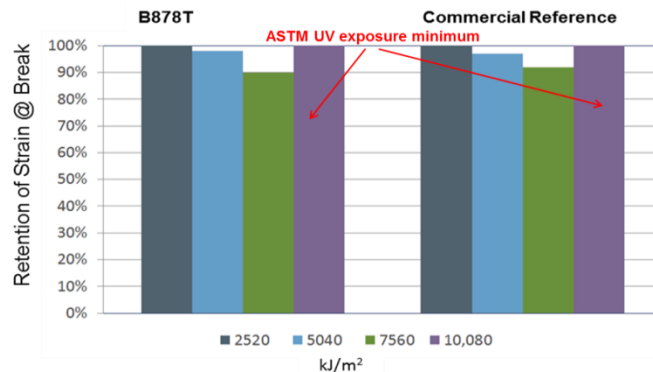


Figure 8 | TPO roofing sheet – retention of strain at break after 10,080 kJ/(m²·nm) radiant energy in an ASTM D6878 weatherometer

With respect to thermal performance, CYASORB CYNERGY SOLUTIONS® B878T stabilizer maintains over 70% retention of stress at break (Figure 9) and strain at break (Figure 10) after 7,500 hours of thermal aging at 116°C, compared to a commercial formulation that loses both properties after 3,000 hours. Tensile data from a more extreme, supplementary 138°C oven aging test shows CYASORB CYNERGY SOLUTIONS® B878T maintaining 90% retention of stress at break (Figure 11) and 70% retention of strain at break (Figure 12) after 4,000 hours compared to two competitive samples that show loss of physical properties after 2000 hours. Note that in the aforementioned studies, single ply TPO roofing sheets were used; multilayer constructions are used in most applications.

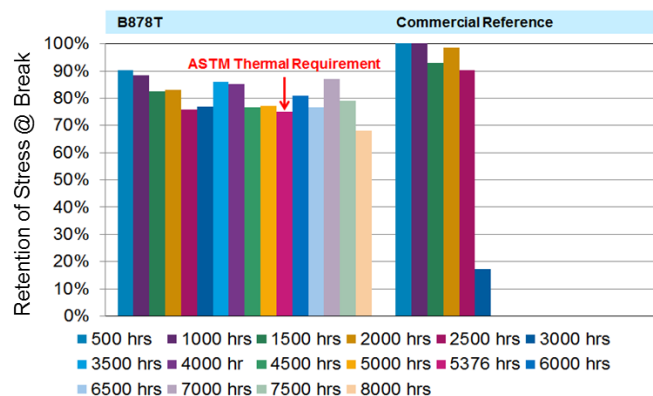


Figure 9 | 116°C oven aging of TPO roofing sheets – retention of stress at break

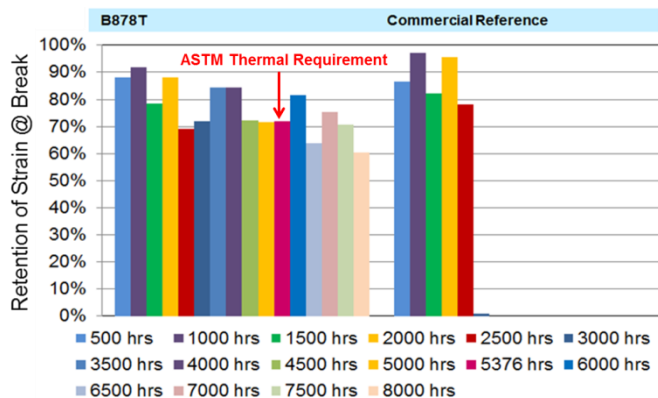


Figure 10 | 116°C oven aging of TPO roofing sheets – retention of strain at break

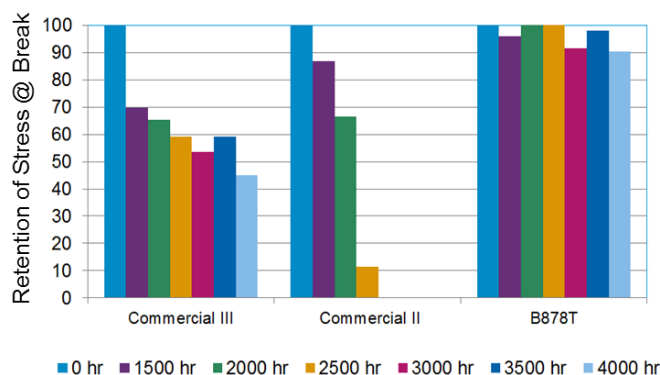


Figure 11 | 138°C oven aging of TPO roofing sheets – retention of stress at break

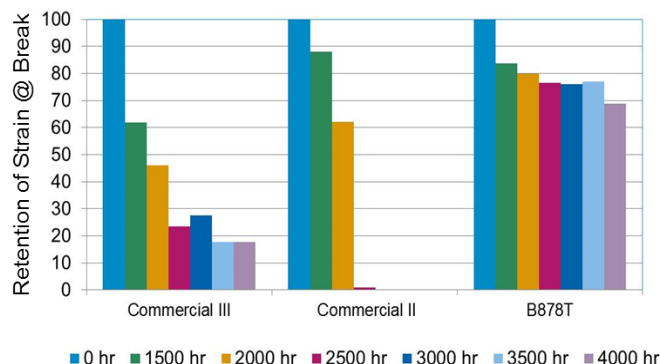


Figure 12 | 138°C oven aging of TPO roofing sheets – retention of strain at break

Conclusions

This paper highlights the UV and thermal performance of two new stabilizers: CYASORB CYNERGY SOLUTIONS® M535 stabilizer for injection and blow molding, and CYASORB CYNERGY SOLUTIONS® B878T stabilizer for demanding building & construction applications. In HDPE injection molded parts, modest levels of CYASORB CYNERGY SOLUTIONS® M535 have shown to deliver good surface protection, tensile property retention and colorfastness through various weathering experiments in an ASTM G155 Cycle 1 weatherometer. In TPO roofing materials, CYASORB CYNERGY SOLUTIONS® B878T demonstrated excellent retention of physical properties and strong resistance to cracking in both highly-intense ASTM D6878 Xenon weathering conditions and two high-temperature ovens. These new innovations in stabilizer technology and their corresponding improvements polyolefin performance highlight how Solvay is asking more from chemistry.

¹ Grand View Research Market Report, <https://www.grandviewresearch.com/press-release/global-injection-molded-plastics-market>



Solvay Technology Solutions

5 Garrett Mountain Plaza
Woodland Park, NJ 07424
custinfo@solvay.com
T: +1.973.357.3100

Recent Aspects of Polypropylene and Polyethylene Stabilization

Jungdu Kim⁽¹⁾, T. Schmutz⁽²⁾, HeeJung Kwon⁽³⁾, and K. Keck⁽³⁾

⁽¹⁾ Songwon International Americas, USA

⁽²⁾ Songwon International AG, Switzerland

⁽³⁾ Songwon Industrial, South Korea

Abstract

Polypropylene (PP) and Polyethylene (PE) in general must be stabilized during compounding, processing, storage, and service life due to their inherently limited stability against auto-oxidation. The stabilization of those substrates during compounding and conversion is rather complex, as the following performance criteria need to be fulfilled:

- Good protection of molecular weight during melt conversion
- Low initial color
- Low color development during melt conversion
- Low gasfading
- Reasonable contribution to thermal stability
- Easily adjustable Long Term Thermal Stability (LTTS).

As processing stabilizer, liquid phosphites like tris-nonylphenylphosphite (TNPP) are one of successful stabilizers for polyethylene due to its excellent price/performance balance and its good compatibility in PE.

In replacing liquid phosphite (TNPP...) a fundamental decision needs to be made, whether to remain with a liquid stabilizer or to convert to a completely solid stabilization package. The advantages and disadvantages of both approaches will be highlighted in this paper.

In addition, for cases where a pronounced service life of a plastic part is needed, high end stabilization strategies (Low VOC and gasfading) for PP are discussed.

CHANGEOVER IN A TRANSFER LINE: NUMERICAL MODELING AND EXPERIMENTAL VALIDATION

*Hyunwoo Kim, Laura Dietsche, Chris Thurber, Eric Marchbanks and Jin Wang
The Dow Chemical Company, Midland, MI*

Abstract

In industry, a broad range of polyolefin products are often processed in the same equipment with multiple changeovers daily. Changing the resins in processing equipment such as extruders, transfer lines and dies exerts cost in terms of material waste and production down time. Minimizing these losses by running the products in an optimized sequence and by designing a flow path to reduce this transition time can be a great benefit. We studied the changeover from a single or twin-screw extruder previously [1,2]. Changeover times from transfer lines and dies can be different and even longer than extruder changeover times. These downstream flow channels can have significant impacts on transient operations in the polymer processing industry.

In this study, a series of numerical simulations were conducted to determine the changeover time from a transfer line connecting an extruder to a die. The impact of the polyolefin resin properties and resin sequence on the changeover time was also studied. Congruently, the changeover time was measured experimentally using online and offline optical techniques. These numerical and experimental results provided increased understanding of the influences that resin rheology (viscosity, melt flow and shear thinning index) and resin sequencing have on changeover time. Additionally, this work supports a theoretical framework for the design of flow channels to minimize the changeover delay due to the residence time of the resin in polymer processing equipment downstream of the extruder.

Introduction

For many polymer compounding and fabrication businesses, a broad range of products are often processed in the same set of equipment with multiple changeovers daily. Resin properties and processing characteristics of the different products can vary over a broad range. Transitioning between products requires purging the previous material out from the free volume of the extruder, transfer line and die, resulting in lost production time and an increased production cost. The time needed to achieve and adequate switch out of the materials in the

polymer processing equipment can vary significantly depending on the flow rate, viscosity ratio between the resins, and flow channel design. Understanding the fundamental influence of these factors on the changeover operation is of significant practical significance and can be used to minimize the time and cost involved.

We previously studied the changeover from twin- and single-screw extruders [1,2], and identified a few important factors that can impact the extruder changeover time. A polymer discharged from the extruder will flow through the downstream flow channels such as transfer lines and dies, further increasing the changeover time. Unlike the extruder, mixing is very limited in these channels where the materials flow sequentially in a plug flow pattern. Material properties such as melt viscosity, shear thinning and viscoelasticity can be important predictors for the changeover time. The design of the flow channel is another crucial factor in the changeover operation as non-streamlined pathlines and dead volume can significantly increase the changeover time.

In this study, we developed a numerical method and an experimental protocol to determine the resin changeover time from a transfer line. A simple transfer line geometry was modeled to numerically determine a changeover time between two resins with differing rheological properties (shear viscosity and/or shear thinning index) based on a transient flow model. A die was constructed with the same transfer line flow channel to determine the changeover time experimentally. Changeover time from the transfer line was measured by online monitoring of the resin composition change before and after the transfer line using optical methods.

Governing Equations

Simulation of the flow of fluid in a transfer line involves the numerical solution of the equations governing viscous fluid flow on the specified computational domain, subject to the stated boundary conditions. Steady state and transient continuity and momentum equations as well as the transient 2-phase “volume-of-fluid” (VOF) equations [3] can be solved for the flow in a transfer line. For example steady, laminar flow of an isothermal, incompressible, non-Newtonian

fluid can be described by the following forms of the equations of continuity and motion:

$$\nabla \cdot \mathbf{v} = 0 \quad (1)$$

$$-\nabla p + \nabla \cdot \mathbf{T} = \rho \mathbf{a} \quad (2)$$

where ρ , \mathbf{v} , p , \mathbf{T} , and \mathbf{a} are the density, velocity vector, pressure, extra stress tensor, and acceleration, respectively.

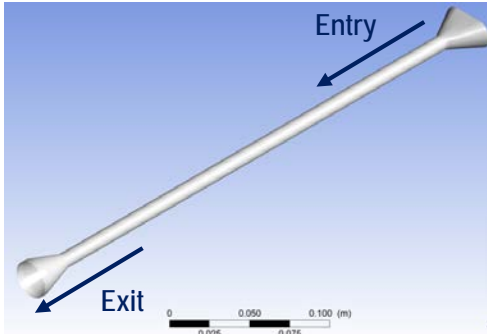
Simulation

Geometry

Two transfer line geometries used for the flow simulations are shown in Figure 1. Geometry A, shown in Figure 1a, has a 38 mm wide, 19 mm high elliptical flow inlet. It transitions to a 10 mm diameter circular channel. This 330 mm long circular channel ends with a 10 mm-to-25 mm diameter conical expansion channel.

Geometry B (Figure 1b) was used to aid in comparing the changeover times from numerical modeling and experimental measurements. A die (mimicking a transfer line) having an internal flow channel of Geometry B was designed and used for the changeover time experiments. This geometry is very similar to Geometry A in Figure 1a. This has an extended entry to transition from the twin screw tips to a 10 mm diameter circular channel. This 10 mm diameter channel is 175 mm long and ends with a 3 mm diameter orifice.

(a)



(b)

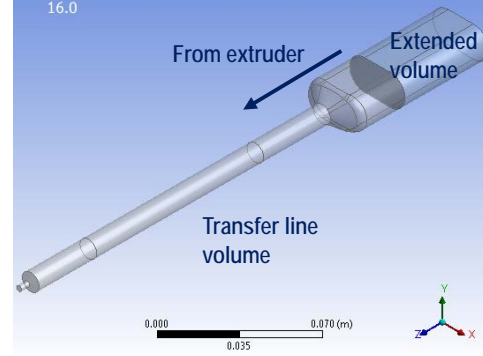


Figure 1. Two transfer line geometries, (a) Geometry A and (b) Geometry B, used for numerical modeling and changeover time experiments.

For the actual flow simulation, the inlet of these two geometries were extended to generate a fully developed inlet flow profile and to simulate the changeover time distribution from the extruder. This extended flow channel volume for Geometry B is shown in Figure 1b.

Computational Grid

The transfer line geometries were meshed using the ANSYS CFD Mesher. In order to reduce the computational time, only one quadrant of the geometry was meshed and modeled after splitting the geometry along two symmetry planes in the flow direction. An all hexahedral mesh was generated and the total mesh counts were around 120,000 elements (Geometry A) and 90,000 elements (Geometry B).

Flow Simulation

The steady or transient laminar, incompressible, isothermal flow of the non-Newtonian polymer was simulated by solving the mass and momentum equations via a finite element formulation using ANSYS Fluent. The following were the flow boundary conditions:

- Flow rate at inlet = 0.5 to 5 kg/h
- No slip boundary conditions on all transfer line walls
- Symmetry boundary conditions along symmetry planes.
- Outflow (i.e., fully developed flow condition) at transfer line exit

In order to simulate the resin changeover, a transient flow model incorporating a two-fluid “volume of fluid” (VOF) method was used to track the evolving shape of the interface between the two resins. VOF is a free-surface modelling technique to track and locate the fluid-fluid interface by solving a scalar advection equation for the volume fraction of one of the fluid phases. The overall fluid physical properties (e.g., density and viscosity)

associated with each computational cell are then determined by volume fraction based mixing rules.

The changeover simulations were initiated with a steady state model to develop an initial flow profile of the starting resin at a constant flow rate. This was followed by a transient model incorporating the VOF method, but continuing to add only the Phase 1 fluid at the inlet with the initial flow rate. Finally, the new phase (Phase 2) was introduced to the inlet of the transfer line and the transient solution was computed at every time step, typically using 0.1 to 1 s time intervals.

Changeover times were determined by setting up two solution monitors to record the area average and mass flow rate weighted average of the volume fraction of Phase 2 at the outlet at every time step. These averages are determined by surface integrals (i.e., summations) over all of the computational cell faces (or facets), i , at the outlet;

$$\text{Area average} = \frac{\sum_i \alpha_{i,2} A_i}{\sum_i A_i} \quad (3)$$

$$\text{Mass flow rate weighted average} = \frac{\sum_i \alpha_{i,2} \rho_i v_i A_i}{\sum_i \rho_i v_i A_i} \quad (4)$$

where A_i is the area of the computation facet; $\alpha_{i,2}$ and ρ_i are the volume fraction of Phase 2 and the overall fluid density respectively that are associated with the facet; and v_i is the cell velocity normal to the facet face. The area average is representative of the composition of a frozen slice of extrudate taken at the transfer line exit. In contrast, the flow rate weighted average is representative of a “mixing cup” composition measurement for the fluid extrudate collected at the exit. The VOF simulation was continued until there was no change in the Phase 2 composition at the outlet of the transfer line. CPU times to reach this new steady state were 5-10 h across 20 processors.

Experimental

Materials and Rheology

Experimental shear viscosity data for three polyethylene resins (PE) and one polystyrene (PS) resin were used for numerical modeling. Resin A is a 1.0 dg/min melt index (190 °C/2.16 kg), 0.92 g/cm³ density linear low density polyethylene (LLDPE) resin. Resin B is a 2.3 dg/min melt index, 0.917 g/cm³ density LLDPE resin. Resin C is a 1.9 dg/min melt index, 0.919 g/cm³ density low density polyethylene (LDPE) resin. Resin D is a 1.5 dg/min melt index (200 °C/5 kg) PS resin. The rheologies of the three PE resins used for changeover simulation (Resin A, B and C) at 280 °C are compared in Figure 2a. The rheology of Resin A at 243 °C and Resin

D at 233 °C used for changeover experiments are compared in Figure 2b. Temperatures were the actual melt temperatures of the polymers measured during the changeover experiments.

The rheological behaviors of the polymers were described for numerical modeling based on the Cross model:

$$\eta = \frac{\eta_o}{1 + \left(\frac{\eta_o \gamma'}{\tau^*} \right)^{1-n}} \quad (5)$$

where:

η = viscosity, Pa.s

η_o = zero shear viscosity, Pa.s

τ^* = stress constant, Pa.s

γ' = shear rate, 1/s

n = exponent

It should be noted that the trend for the PE resins based on viscosity is $A > B > C$; and the trend based on the extent of shear thinning is $C > A > B$.

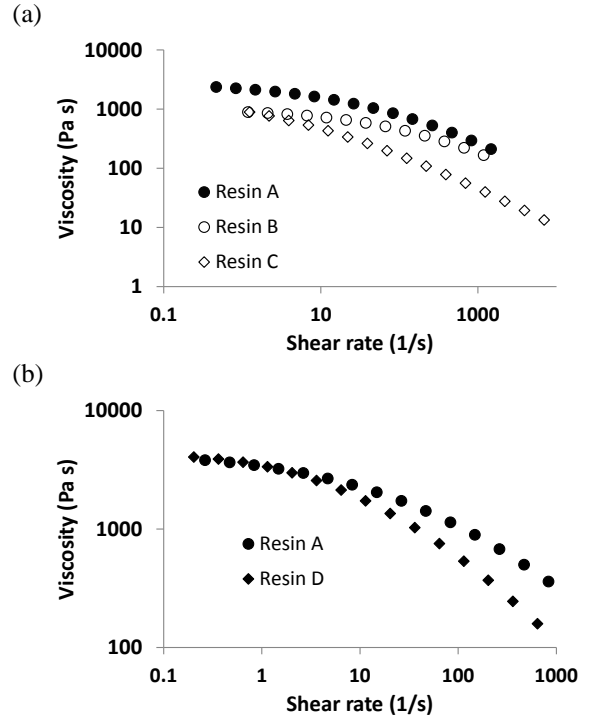


Figure 2. Resin rheology (a) for Resin A, B and C at 280 °C and (b) for Resin A at 243 °C and Resin D at 233 °C.

Changeover Experiments

Geometry B (Figure 2b) was used for the changeover experiments. The experimental set-up is illustrated in Figure 3. The transfer line (die) was connected to an 18 mm twin-screw extruder. Two optical probes were installed near the inlet and outlet of the transfer line to monitor the resin changeover based on a Raman signal. More details about the optical measurements to monitor resin changeover can be found elsewhere [1,2].

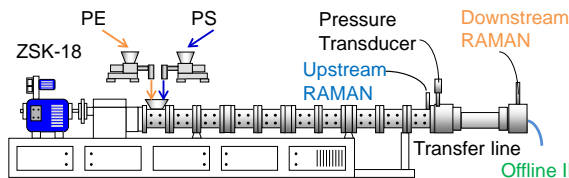


Figure 3. Experimental set-up to determine the changeover time from a transfer line.

PE (Resin A) and PS (Resin D) were selected for the changeover experiments due to their distinctive Raman response. For a typical experiment, the line was run for at least 15 minutes to ensure that steady-state conditions of either PE or PS (Phase 1) had been reached at a constant flowrate before introducing the Phase 2 material. Once steady state was reached, the feeding of Phase 1 was stopped and feeding of the new resin (Phase 2) started simultaneously at the same feed rate. Changeover from the upstream and downstream locations shown Figure 3 were monitored until > 99% changeover was obtained. During the experiment, extrudate samples were also collected from the transfer line discharge every 30 s, and the resin composition was determined off-line from Infrared (IR) measurements.

Results and Discussions

Effects of Resin Rheology on Changeover

A series of transient flow simulation based on the VOF method described above was carried out to determine the changeover times within a transfer line. Figure 4a and Figure 4b show the simulated flow profiles when Resin B (red) is changed over to Resin A (blue) and when Resin A is changed over to Resin B in transfer line Geometry A (Figure 1a) flowing at 5 kg/h. Note that the inlet of the transfer line was extended to create a fully developed velocity profile before reaching the original inlet plane. Time, $t = 0$ was defined when a fully developed profile of Phase 2 first reached the original inlet. Comparing Figure 4a and 4b suggests that the resin viscosity and resin sequencing can significantly affect the evolution of the interface for this two-phase flow system. The flow front of Phase 2 reaches the transfer line exit

around $t = 10$ s for both cases. Then the Phase 2 resin continues to replace the original Phase 1 resin within the transfer line at an increasing proportion. For the changeover from Resin B to Resin A (Figure 4a), Resin B is completely replaced by Resin A at 74 s. However, for the changeover from Resin A to Resin B (Figure 4b), changeover was never completed within a simulated time frame of 117 s. The final changeover state is a Phase 2 core stream encapsulated by a Phase 1 skin near the wall.

Figure 5 shows that resin changeover monitored at the transfer line exit based on the flow rate weighted and area average of the volume fraction of Phase 2 during the transient flow modeling. Changeover profiles can be affected by the resin sequence used for the changeover of resins with differing shear viscosities. For both cases shown in Figure 5, the flow rate weighted average increased very rapidly as soon as the Phase 2 resin reached the transfer line exit. Due to the parabolic nature of the velocity profile, Phase 2 resin in the core flows out faster at the exit plane than the Phase 1 resin near the wall. This has a strong effect on the “mixing cup” average.

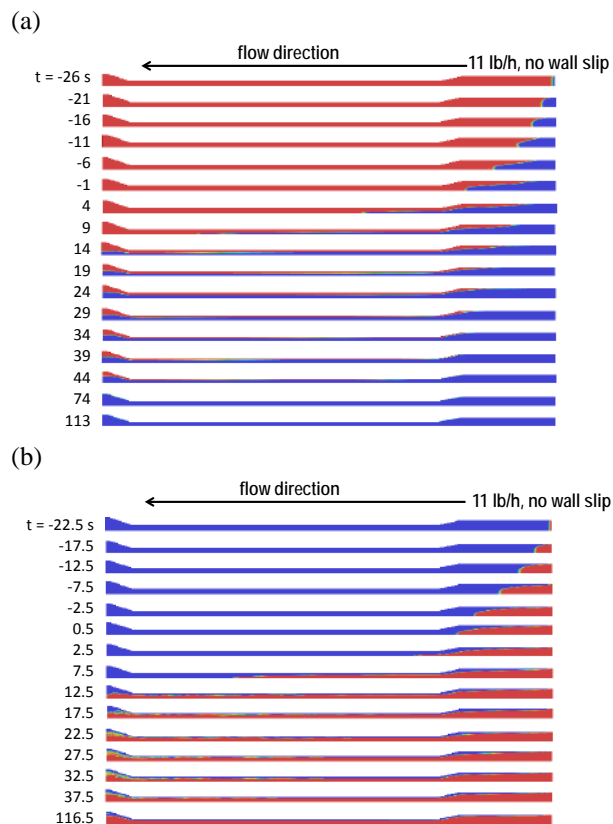


Figure 4. Changeover simulation results in a transfer line Geometry A (a) from Resin B to Resin A, and (b) from Resin A to Resin B flowing at 5 kg/h.

The trends seen for the area weighted average data were different from the flow rate weighted average data, and varied depending on the resin sequence. In this case,

the monitored average composition is not affected by the velocity profile. When a lower viscosity Resin B was switched over to a higher viscosity Resin A (Figure 5a), the area average of the volume fraction of Phase 2 increased gradually until complete changeover was achieved. However, when Resin A was changed over to Resin B (Figure 5b), the area average reached a new steady state at slightly less than 60% of complete changeover, never reaching a full changeover state even at the final simulation time of 120 s.

Table 1 summarizes times required for 97% changeover based on flow rate weighted average and area average. Changeover times determined by flow rate weighted average were shorter when a higher viscosity Resin A was switched over to a lower viscosity Resin B than for the low to high viscosity changeover. However, the changeover time based on area average of volume fraction of Phase 2 was significantly longer for the changeover from Resin A to Resins B (where a changeover of 97% was never achieved in the simulated time frame).

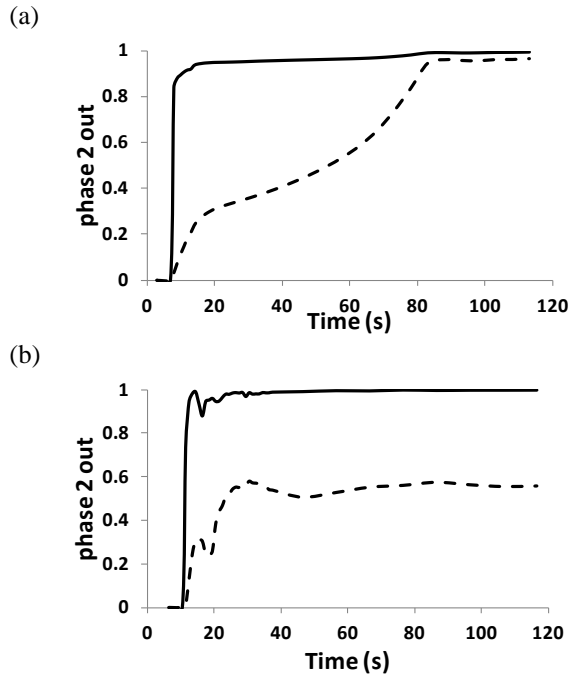


Figure 5. Changeover monitors at the transfer line exit based on flow rate weighted (solid) and area average (dashed) of volume fraction of Phase 2 from transient flow models for (a) Resin B to Resin A and for (b) Resin A to Resin B.

Table 1. Changeover time between Resin A and Resin B for > 97% conversion at transfer line exit

	Flow rate weighted avg	Area average
Resin B to Resin A	67 s	120 s
Resin A to Resin B	23 s	very long time

This difference in changeover responses depending on the resin sequence and monitors used can be explained by the resin and velocity profile of a transient two-phase flow. Figure 6 compares the velocity profiles of a two-phase flow from the exit of the transfer line plotted from the center (Position = 0) to the transfer line wall (Position = 0.0125 m) at $t = 20$ s. When a low viscosity resin (Resin B) is changed over to a high viscosity resin (Resin A), flow modeling predicted that high viscosity resin would form a core stream with a fairly flat velocity profile encapsulated by a relatively high (as compared to Figure 6b) velocity boundary layer of the low viscosity resin as illustrated in Figure 6a. Thus, a high viscosity plug flow can drag the low viscosity skin layer along, allowing for complete removal within a finite time frame. However, when a higher viscosity resin (Resin A) is changed over to a lower viscosity resin (Resin B), the transient two-phase flow consists of a low viscosity core with a more parabolic velocity flow profile (fast at the center and low near the interface) encapsulated by a very sluggish high viscosity boundary layer (Figure 6b). The low viscosity core flow moves over the almost stationary boundary layer, without removing the higher viscosity skin.

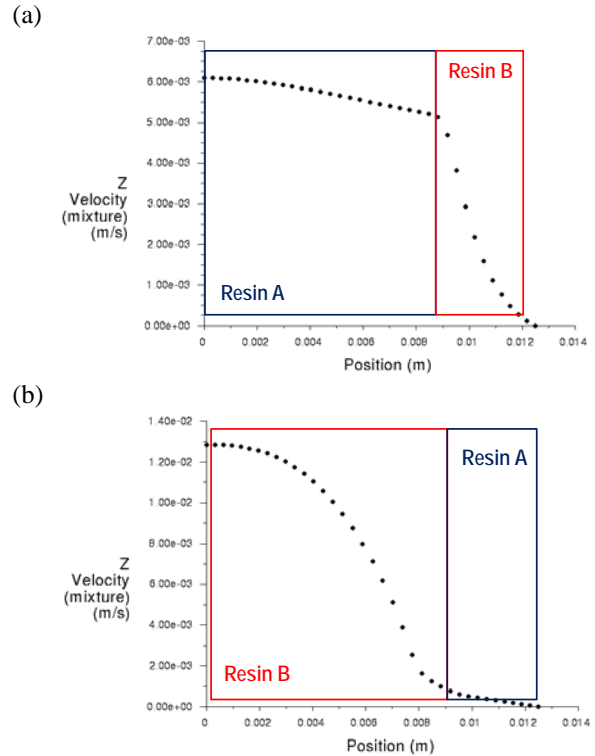


Figure 6. Two-phase velocity profiles at $t = 20$ s from the VOF transient flow modeling for (a) Resin B to Resin A and for (b) Resin A to Resin B at 5 kg/h.

A transient flow modeling was also conducted for Resin B and Resin C. As shown in Figure 2a, Resin B and Resin C have the same zero shear viscosity, but their shear thinning behaviors are distinguished in that as the

LDPE resin (Resin C) shear thins more pronouncedly compared to the LLDPE resin (Resin B). Figure 7 compares the changeover from Phase 1 to Phase 2 monitored at the transfer line exit for Resin B to Resin C (Figure 7a) and for Resin C to Resin B (Figure 7b). Depending on the extent of shear thinning and resin sequence, they exhibited dissimilar changeover profiles. For both cases, flow rate weighted average showed a sharp increase when the Phase 2 resin first reached the transfer line exit. For Resin B (LLDPE) to Resin C (LDPE), the area average of Phase 2 volume fraction gradually increased and eventually reached complete changeover. For Resin C (LDPE) to Resin B (LLDPE), the area average reached a steady state at less than 50% conversion and a complete changeover state was never achieved at the final simulation time of 130 s.

Table 2 compares the changeover results from the transient flow modeling for Resin B to Resin C and for Resin C to Resin B. These results indicate that the changeover time varies significantly depending on the resin sequence for polymers with different degree of shear thinning. The simulations predicted that it would take a longer time to change over from less shear thinning (resulting in higher viscosity) Resin B to Resin C if a flow rate weighted average of volume fraction of Phase 2 is used. However, if an area average is used, the transient model predicted a finite changeover time for Resin B to Resin C but an infinitely long time for Resin C to Resin B. This is contrary to what would be expected from the relative resin viscosities based on Table 1 trends discussed above, and suggests that the extent of shear thinning could have a stronger influence on the changeover time than the resin viscosity. It also suggests that it is the rheological nature of the skin layer (Phase 1) that dominates.

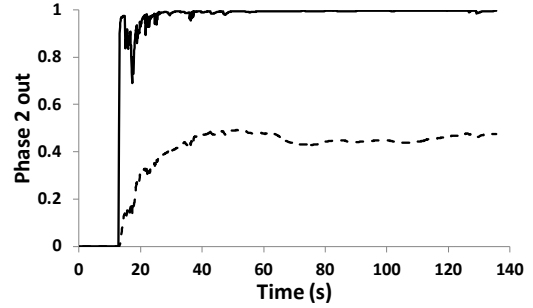
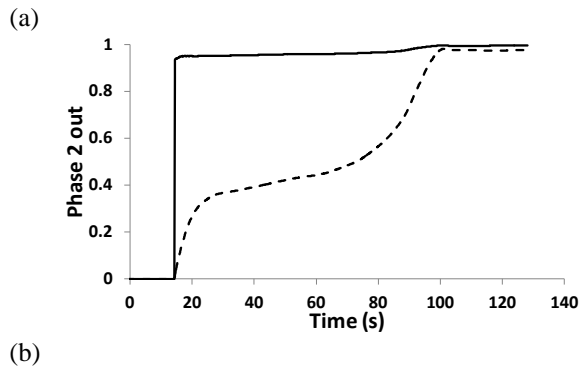
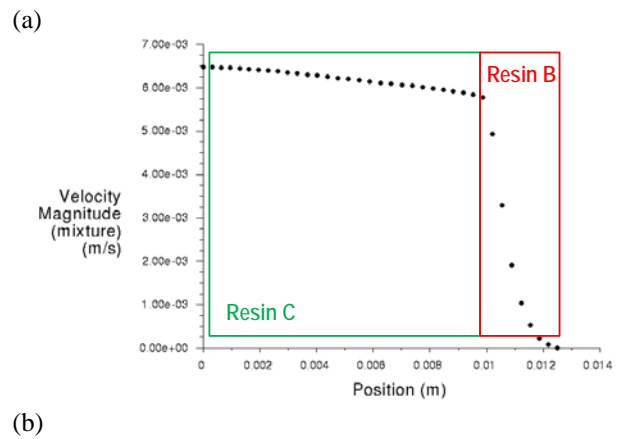


Figure 7. Changeover monitors at the transfer line exit based on flow rate weighted (solid) and area (dashed) average of volume fraction of Phase 2 from transient flow models for (a) Resin B to Resin C and for (b) Resin C to Resin B.

Table 2. Resin changeover time between Resin B and Resin C for > 97% conversion at transfer line exit

	Flow rate weighted avg	Area average
Resin B to Resin C	85 s	99 s
Resin C to Resin B	26 s	very long time

Figure 8 shows velocity profiles simulated for a two-phase transient flow for the changeover from Resin B to Resin C and from Resin C to Resin B across the transfer line exit at 5 kg/h. When compared to Figure 6b, using the same Phase 2 (core) material, we see that the velocity profile of the Phase 1 material near the wall in Figure 8b is significantly flatter for the more shear thinning (and in this case less viscous) Resin C, which in turn increases the height of the parabolic profile for the core material. Flushing out this near zero velocity skin layer will take an infinitely long time as reflected in the area average changeover time, while the flow rate weighted average will indicate that only Phase 1 is being collected (in a mixing cup) at relatively short times.



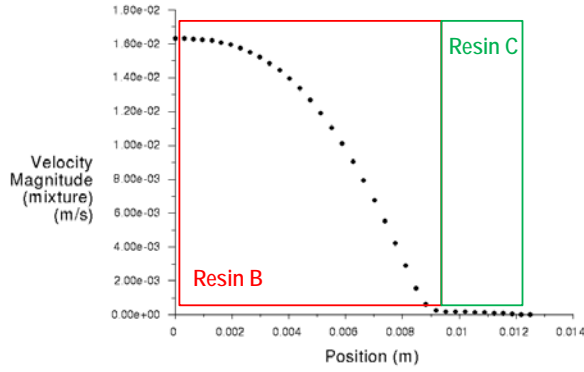


Figure 8. Two-phase velocity profile at $t = 20$ s from VOF transient flow modeling for (a) Resin B to Rein C and (b) Resin C to Resin B at 5 kg/h.

If we reconsider the results in Table 1 from a shear thinning effect standpoint, we see the same trends as seen in Table 2 in that Resin A is more shear thinning than Resin B, and the higher shear thinning skin layer tends to have a flatter velocity profile. However, the differences in the degree of shear thinning are less when comparing Resins A and B so that the viscosity effects will be more dominant.

Changeover Time Experiments

In order to validate the changeover time results from the transient flow simulation, changeover extrusion trials were conducted on a setup described in Figure 3 to determine the changeover time experimentally. The changeover between PE and PS was quantified by attaching transfer line (die) Geometry B to a twin-screw extruder and using on-line optical measurements. The changeover time from the same flow channel geometry (Figure 1b) was also estimated via flow simulation using the resin rheology data in Figure 2b. For the changeover simulations, the flow rate weighted average of volume fraction of Phase 2 was monitored at both the entry and exit of the transfer line (upstream and downstream locations in Figure 9) to quantify the changeover from the transfer line. Figure 10 compares the changeover between Resin A and Resin D determined via numerical modeling (dashed lines) and a changeover experimental trial (solid lines). For the changeover measurements from the upstream location of the transfer line, online Raman measurements were utilized. Downstream changeover was measured using offline IR measurements on extrudate samples from the die.

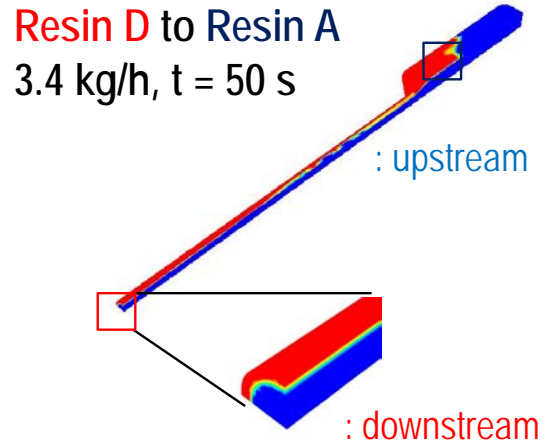
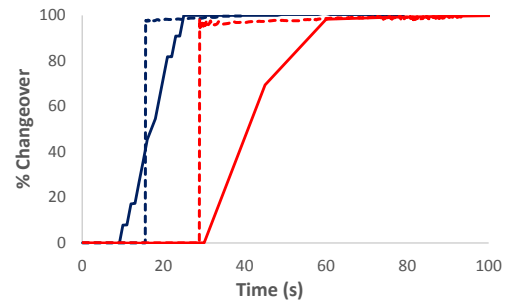


Figure 9. Transient VOF flow modeling on Geometry B for changeover from Resin D to Resin A flowing at 3.4 kg/h and upstream and downstream locations where the changeover based on flow rate weighted average of volume fraction of Phase 2 was monitored.

Figure 10 shows the % changeover versus time at two different locations, inlet (blue) and outlet of the transfer line (red); time zero represents the moment when the extruder feed stream resin switch is made. Clearly, there is a reasonable agreement between the changeover determined through numerical modeling and experimental measurement. In particular, the numerical modeling was able to predict the onset of the changeover from both upstream and downstream locations reasonably well. The main discrepancy between numerical modeling and experimental result is on the slope of the lines. Experimental results showed a more gradual change in % changeover over time while the numerical simulation based on flow rate weighted averages predicted a sudden jump from 0 to 100% changeover. This mismatch can be due to the significant phase mixing inside the extruder that leads to a broad distribution in the resin composition feeding the transfer line. Whereas, the simulations were conducted based on an assumption of an instantaneous 100% feed change between two resins that will flow sequentially from a pure Phase 1 to Phase 2 transition in a plug flow.

(a)



(b)

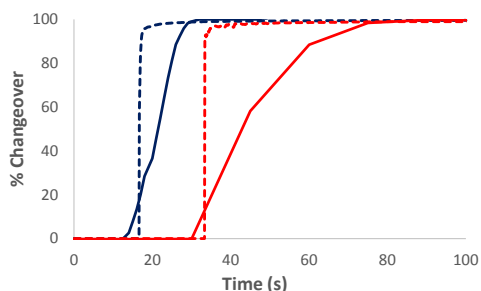


Figure 10. Changeover at 1.7 kg/h rate (a) from Resin D to Resin A and (b) from Resin A to Resin D monitored from inlet (blue) and outlet (red) of Geometry B determined from flow simulation (dashed line) and experimental measurements (solid line).

Table 3 lists experimentally and numerically determined changeover times for > 99% changeover between Resin A and Resin D from the transfer line. Changeover times were recorded from the upstream and downstream locations in Figure 9 and the differences between the upstream and downstream values are reported in Table 3. There are reasonable agreements in the changeover times determined through flow simulation and changeover experiments. Both experiments and simulation predicted faster changeover at a higher flow rate, 3.4 kg/h versus 1.7 kg/h as expected. Experiments and simulation both predicted a longer changeover for Resin A (PE) to Resin D (PS) at 3.4 kg/h, (where the shear thinning characteristics would be stronger, with Resin A being less shear thinning), and a longer changeover for Resin D to Resin A at 1.7 kg/h (where the shear thinning characteristics are weaker, with Resin D having lower viscosity).

Table 3. Time for > 99% changeover between Resin A and Resin D from a transfer line.

Changeover time (s)	Experimental		Simulation	
Flowrate (kg/h)	1.7	3.4	1.7	3.4
Resin D to Resin A	> 115	50	161	36
Resin A to Resin D	> 56	60	83	65

Conclusions

This study has shown how the resin changeover from a transfer line can be significantly affected by the resin rheology and resin sequencing. The numerical definition of changeover time; i.e., based on flow-rate average versus area average; can affect the trends observed and

needs to be taken into account when interpreting the results. When changeover time is based on flow rate weighted average (i.e., “mixing cup” composition in an extrudate), the flow simulation predicted that at similar flow conditions, switching the resins from high to low viscosity (with similar shear thinning characteristics) takes place faster than the opposite order. The reverse trend is predicted using area averages, which reflects the development of an almost stationary high viscosity skin layer that is very hard to remove from the system. When resins with different degrees of shear thinning are involved, area-average based changeover is predicted to be faster inside a transfer line when a less shear thinning (LLDPE) resin is purged out by a more shear thinning (LDPE) resin. These results suggest that higher viscosity and more shear thinning (LDPE) resins make a good purge material for lower viscosity and less shear thinning (LLDPE) resins.

Changeover time from a transfer line was also determined via experiments. However, once again the nature of the changeover time being measured needs to be understood in order to correctly interpret the results. Changeover times based on mixing cup sampling may be very different from those based on point probe measurements or frozen resin analysis. In this work, changeover times between PE and PS resins measured using an optical technique appeared to correlate well with what were estimated from numerical modeling, using flow-rate-average based predictions. Both experiments and modeling predict a longer changeover time at a lower flow rate. The results emphasize the importance of understanding the rheology and resin sequencing of polymer resins for the changeover from a transfer line. Optimizing these factors will help minimize the changeover time for the polymer processing equipment for reduced production time and cost.

References

1. J. Wang, C. Thurber, X. Chen, M. Read, N. Horstman, C. Pavliceck, J. Stanley, *SPE-ANTEC Tech. Papers*, **62**, 863 (2016).
2. C. Thurber, H. Kim, J. Wang, R. Wrisley, E. Marchbanks, *SPE Polyolefins Conference* (2017).
3. ANSYS Fluent manual, <https://support.ansys.com/portal/site/AnsysCustomerPortal>.

SIMULATION OF CO-ROTATING FULLY INTERMESHING TWIN-SCREW COMPOUNDING EXTRUDERS: ALTERNATIVES FOR PROCESS DESIGN

Paul G. Andersen, Coperion Corporation, Ramsey, NJ

Alex Utracki, Coperion Corporation, Pitman, NJ

Frank Lechner, Coperion GmbH, Stuttgart, Germany

Abstract

The co-rotating fully intermeshing twin-screw extruder is the primary production unit for compounding polymer based materials. It also has had a long term presence in processing material in the chemical and food industry and more recently in pharmaceuticals. The layout of a co-rotating twin-screw compounder for a specific processing task is primarily based on 1) the experience of the process development engineer, and 2) tests run on a lab-scale unit. Additionally, scale-up to a much larger extruder is very often required as part of the development process. Traditionally this scale up has been based on experience and classical scale-up rules.

In addition to experience and lab tests, good simulation software can help guide the development engineer in the design of initial compounding extruder configuration as well as scale-up to a commercial unit. The overall objective being to minimize risk (cost). Know-how based on experience, trials in the laboratory, production and simulation software are the preferred combination for the layout of an extrusion process.

Introduction

It has been a long standing industry goal to be able to simulate the entire compounding process from feed intake, through plastification and downstream mixing zones until the pressure built-up zone. Nevertheless, not all process sections can be described sufficiently by simulation software. This is due to several reasons such as high complexity of the computation as well as missing feedstock and product characteristic data. This later point is particularly relevant when it comes to polymer compounds containing different components such as additives, fillers, etc. However, in spite of shortcomings, 1 D and 3 D modeling is used to describe the process and can support the process engineer for the layout and scale-up of a compounding process.

Background

Co-rotating and fully intermeshing twin screw extruders, with one screw wiping the other, and both wiping the 8-shaped barrel inside, are defined by two characteristic dimensions: diameter ratio D_o/D_i and specific torque M_d/a^3 , Figure 1.

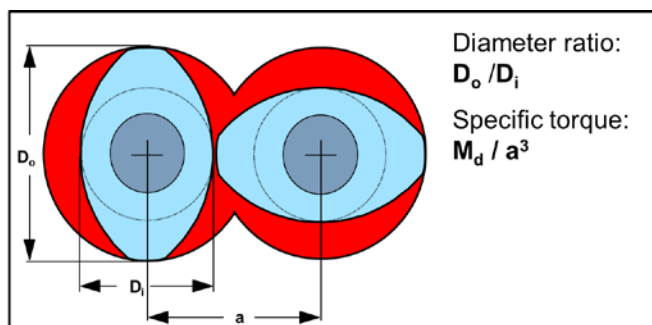


Figure 1: Character dimensions of Twin-screw Extruder

Figure 2 shows a typical set-up for compounding engineering polymers. Materials contained in the formulation are fed at precisely defined locations along the length of the process section. During the compounding process the blended ingredients pass through each of the different unit operations along the length of the extruder.

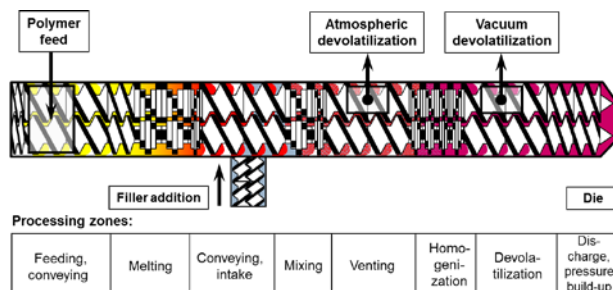


Figure 2: Process section for Compounding

For each new compounding process, the feed sequencing and unit operation need to be defined. In addition to experience and lab tests, 1 D and 3 D modeling programs are available for use to describe the process and can support the process engineer for the layout and scale-up of a compounding process. Comparison of the simulation results to real process data is strongly recommended.

One of the issues related to using simulation software is that exact conditions required to start the simulation are difficult to describe at a specific location. Therefore each unit operation has to be described separately: Feeding section, plastification, mixing, degassing and pressure built-up zone. Suitable characteristic data of all raw materials as well as of the final polymer melt are essential parameters required to use simulation software. The most important data are 1) melt density, 2) heat transfer coefficient as a function of temperature, and 3) the viscosity curve over a shear rate range from 1 1/s to 1000 1/s. The geometrical data of the co-rotating twin screw compounder is given by the individual machine supplier.

Simulation: 1D

For 1 D modeling the two most widely used commercial simulation software packages are Sigma and Ludovic. Coperion developed its own proprietary software in the late 1970s called ZSKalc. These software packages are mainly used to 1) simulate temperature profile, 2) filling degree, and 3) pressure built-up capability along the length of the process section.

The Coperion ZSKalc simulation software hierarchy is illustrated in Figure 3. Input data required are 1) machine configuration (barrels and screw), 2) process parameter (screw speed, material feed rate, material feed temperature, material pressure at the screw tip, barrel temperatures), and 3) material properties. The resultant output, material temperature, material pressure, degree of fill and specific energy input is calculated by using both analytical and numerical methods.

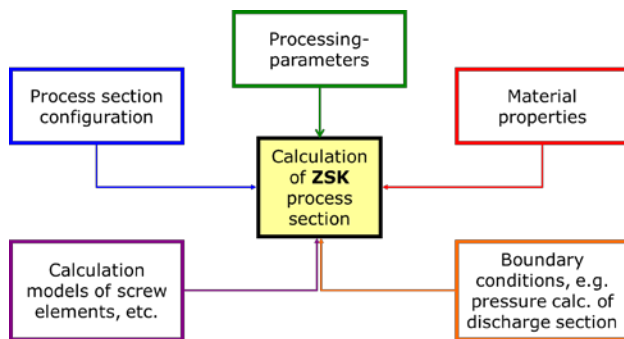


Figure 3: Data structure for ZSK calculations

Simulation: 3D

Using 3D-Modeling (finite element method) as a numerical technique is also used to simulate various process conditions. It delivers local details of a compounding process as shown in Figure 4. The pressure

distribution is depicted by gradation of colors from high pressure (orange) to low pressure (blue). The pressure drop downstream of the reverse conveying screw element can be clearly seen as well as the pressure peak in the intermeshing zone.

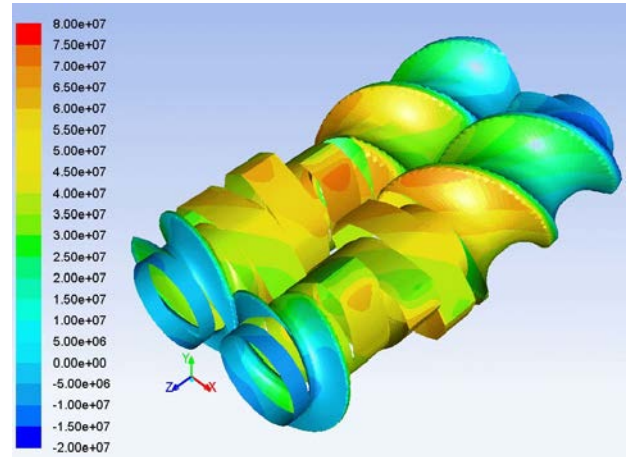


Figure 4: FEM simulation of screw element sequence

For 3 D modeling commercial and non-commercial programs are available, e.g. CFX, Fluent, OpenFoam, Star CCM, Fidap, Polyflow, and XimeX. They are mainly used to simulate local process conditions, even down to specific areas within an individual screw element.

Simulation: 1D vs. 3D

The easiest way to describe the difference between 1D and 3D simulation is as follows: 1D provides a birds-eye view of the process, but can't zoom in on local details, while 3D can provide very detailed information of the immediate surroundings, but not what is happening in the neighborhood.

Bierdel and Lechner [1] provided some excellent graphics to illustrate this difference. Figure 5 shows a sample screw sequence, a series of conveying elements followed by a restrictive element.

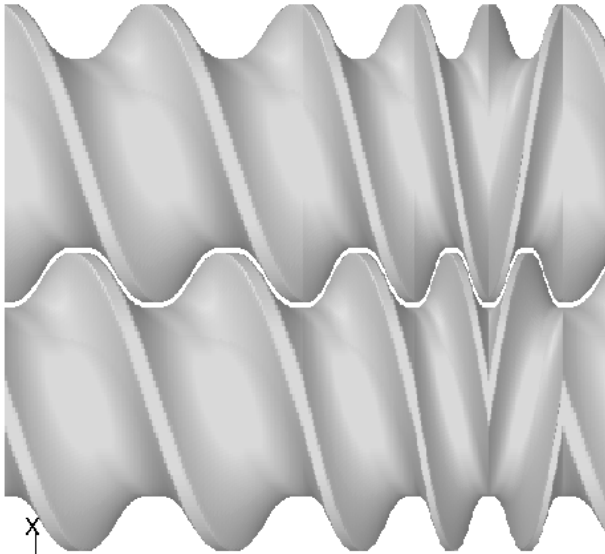


Figure 5: Screw configuration sequence.

Based on the screw configuration in Figure 5, Figure 6 depicts the overall pressure drop across the restrictive element as simulated by a 1D program. On the other hand, Figure 7 shows the 3D simulation that provides localized details of the pressure drop. As before, red orange indicates high pressure.

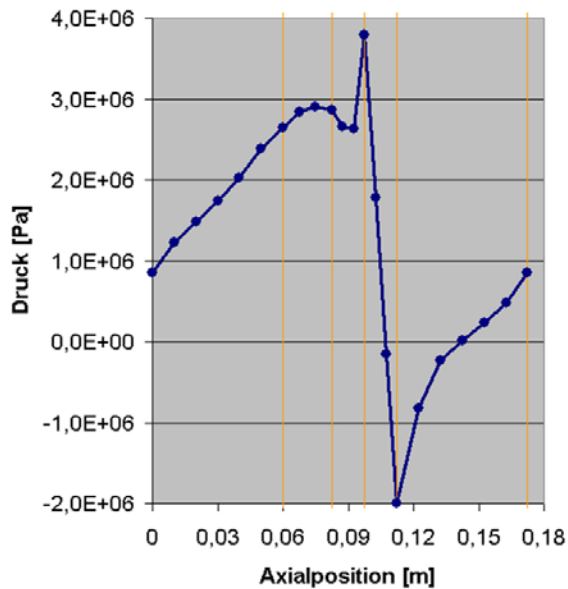


Figure 6: Pressure drop value across restrictive elements

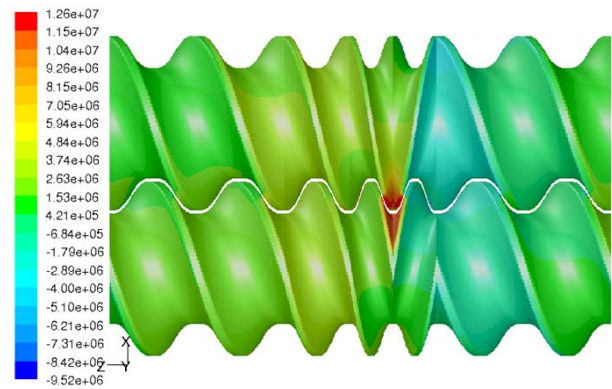
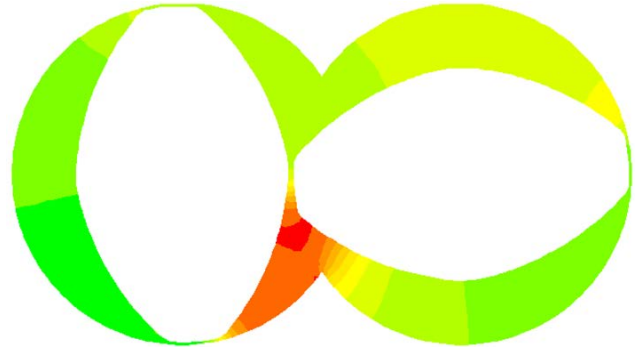


Figure 7: Pressure drop details at restrictive element.

Simulation: Feed Intake Zone

Powder conveying capacity of an extruder depends on the properties of raw materials, the screw design and process conditions. Even if one has good characterization of the raw materials such as solid density, particle size distribution, porosity, etc., feed intake behavior cannot be calculated sufficiently without data from a lab trial or production run.

The equation in Figure 8 shows that the feed intake and conveying rate inside of the process section are a function of many variables and therefore subject to fluctuation. For example, Figure 9 illustrates the change in bulk density for a powder/granule feed stock in a lab size extruder between the feed intake section to the melting zone. The change depends on the process conditions (such as speed) and geometric data (screw pitch) of the given machine system.

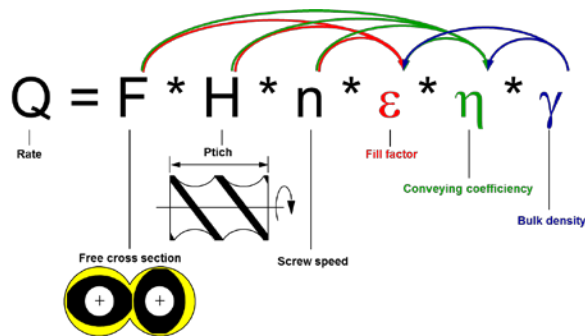


Figure 8: Conveying capacity for solids

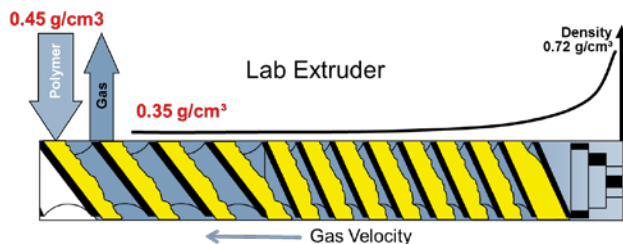


Figure 9: Powder feedstock conveying in lab compounder.

In general, for pellets feed intake limitations do not have to be considered. For powders the feed intake may become critical if the medium particle size d_{50} falls below 150 μm . The feed intake depends strongly also on the screw configuration including the design of the melting zone. A screw pitch in the feeding area of 1.7 D to 2.0 D is recommended as well as feed intake zone minimum length of 4 D.

Use of neural networks was investigated as a way to model solids conveying better [2]. The technology has shown good results if the system is “trained”. This means that actual process data has to be incorporated as an informational foundation and can then be used to simulate the process. This technique can be used to verify the scale-up from a lab test to a larger machine.

Figure 10 shows results from a ZSK 40 test where PP powder and 30% talc are fed into the main feed at Barrel 1. Simulation 1 which used a “trained” system, i.e. based on real process data input from a lab trial, shows very good results. These results are well aligned with the actual data compared to the trial data. Without real process data, the blue line shows definitely a large deviation from the reality.

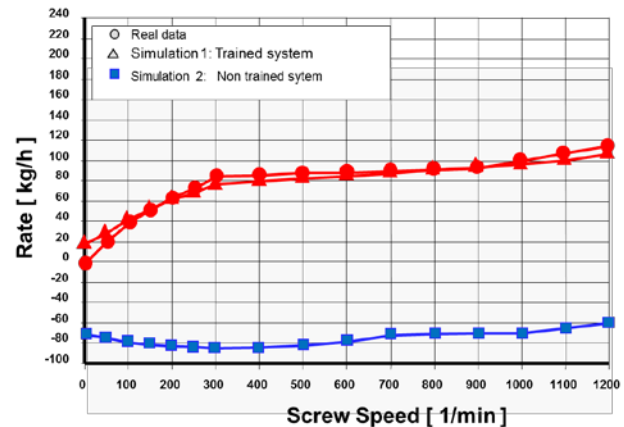


Figure 10: Simulation of Feed Intake

Simulation: Melting and Homogenization of Polymers

As shown in Figure 11, polymer entering the melting zone undergoes a phase change from solid to the melt. Still today, this phase change has not been accurately calculated by simulation software. Therefore it is important that the development engineer knows basic material properties such as melting point, viscosity, and enthalpy curves. From this data, the minimum specific energy input required can be defined and based on this the melting zone can be designed.

At the end of the melting zone the polymer should be completely molten. This strongly depends on the screw design and the process conditions. Figure 12 shows the melt quality variation of a polyethylene having experienced varying process conditions. Polymer Sample 1 shows a complete molten product at the end of the melting zone whereas Sample 4 still contains unmolten polymer as the screw speed was too low.

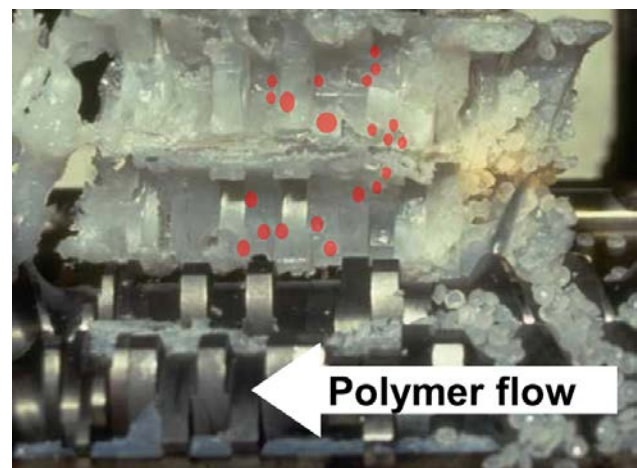


Figure 11: Melting zone showing transformation of polymer



Figure 12: Melting performance

An example of the difficulty a simulation program can have to accurately predict the melting section performance of the twin-screw compounding process, as well as the misleading information that can be provided is shown in Figure 13 a-d. The basis for this inaccuracy can be two-fold. First, the algorithm for polymer melting may be inadequate. The various calculations based on the influence of extruder operating conditions and material parameters may not have the correct balance. In addition to the model algorithm, the correct input data is critical. While it is relatively easy to provide extruder operating data, quality material data is less readily available. For example, the initial particle size of the polymer will have an influence on melting. Figure 10 depicts the melting for pellets, but many compounding lines, especially for polyolefins, process powder which flows significantly different from pellets. One can measure solids flow, heat transfer, coefficient of friction etc. in the lab, but under actual dynamic conditions, there are innumerable uncontrollable influences such as fluidization that impact actual heat transfer, coefficient of friction, etc.

The Figure 13 sequence depicts a comparison between data derived for melting HDPE based on a simulation and an actual ZSK 92 run. The percent melting of HDPE on the ZSK 92, as well as the melt temperature are almost identical between the lab extruder run versus simulation software. However, the calculated specific energy is much higher compared to the trial and does not fit with respect to the HDPE enthalpy curve. A simulated specific energy of 0.283 kWh/kg would lead to a melt temperature of almost 400°C whereas the trial as well as the simulation shows a melt temperature of 216°C and 222°C, respectively. Additionally, the model shows that the material is approximately 50% melted at the end of the first kneading block section, but is then fully melted by screw conveying elements prior to entering the second

kneading block section. The actual test data indicated some unmelt remained at discharge from the extruder.

In this example a reality check of comparing predicted temperature versus specific energy against the enthalpy curve would identify that the melt temperature and the specific energy don't agree and that one or potentially both are incorrect. Without experimental data as an anchor point it is, in most cases, difficult to know which one is closest to being correct.



Process conditions:

- Product: PP-Powder MI₂ = 2
- ZSK 92
- Screw Speed 240 rpm
- Rate: 850 kg/h

Figure 13a: Example screw configuration

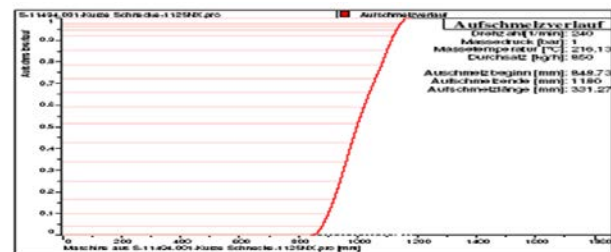


Figure 13b: Simulation of melting

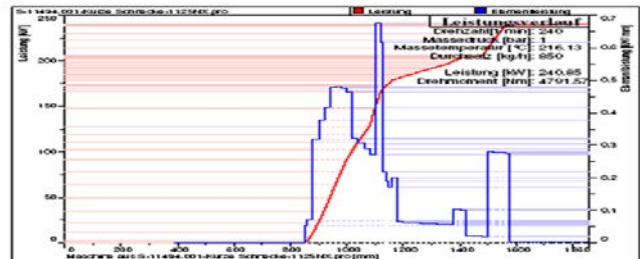


Figure 13c: Simulation of melt temp and power consumption

Results

	Sigma	Trial
Degree of plastification (%)	100	98
Melt temperature (°C)	216	222
Power consumption(kW)	240	132

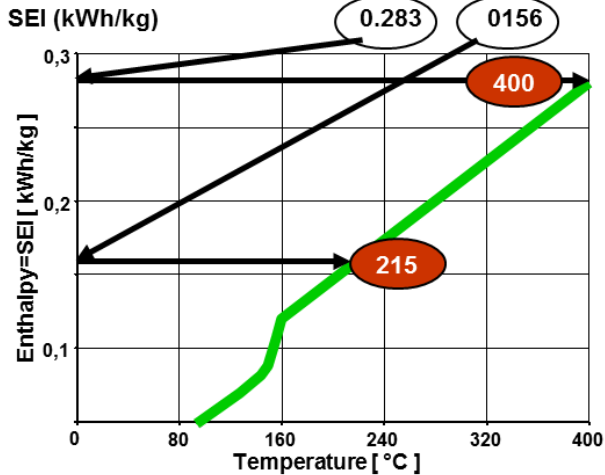


Figure 13d: Comparison of results, simulation vs. data.

Simulation: Pressure Buildup Zone

Once the polymer has been melted and mixed, simulations can perform very well if appropriate as well as accurate data is provided. Figure 14 illustrates the sub-programs that comprise ZSKalc simulation software and provide the required input parameters. These are used in consort to calculate the process:

- Exco for the screw configuration
- Propfit for the material data
- Rebex for the discharge pressure
- Geometry data of the machine

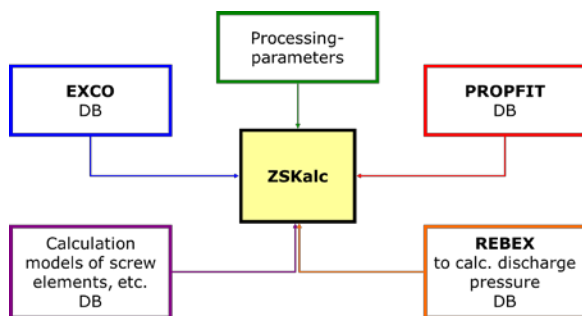


Figure 14: Coperion data structure for ZSK calculations

As an example for beneficial program utilization, back-up length and the temperature increase in the process section can be simulated very precisely if well-defined material properties are provided. This simulation software allows one to calculate the optimum screw pitch for the

pressure built-up which will minimize the back-up length and the specific energy input.

Figure 15 depicts the calculation of different parameters using ZSKalc for scale up to a ZSK 380 running 46 tonnes/hr. of melt fed LDPE.

Red – Material Temperature
Blue – Barrel Temperature
Black – Pressure
Pink – Specific Mechanical Energy
Colored Circles & Square – Run data

As can be seen from the results in Figure 10, the predicted melt temperature, discharge pressure and specific mechanical energy are virtually spot on.

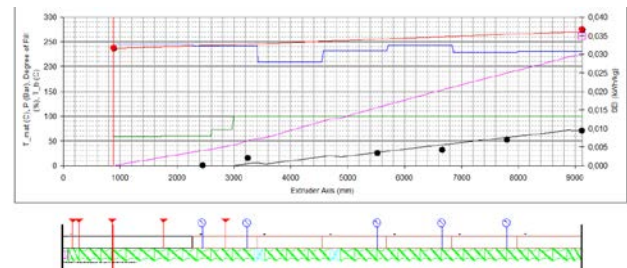


Figure 15: Simulation with ZSKalc

Summary

Using 1 D and 3 D modelling can be used to minimize the risk for process design and the scale-up. The result can only be accurate if the required parameters are provided. Finally a comparison with operation or trial data is strongly recommended.

3 D modelling delivers local details of a process section whereas 1 D modelling can provide process characteristic trends, e.g. the influence of screw speed on the specific energy input. The screw configuration in the pressure build-up zone can be designed more effectively.

References

1. M. Bierdel, F. Lechner, Scale-up mit Simulationsprogrammen: Vergleich von Simulation mit Realitaet, VDI Tagung 2013
2. U. Feuerlein, Verbesserung von Compoundiermaschinen durch Prognose der Einzugs Grenzen ueber Analytische Pulverkennwerte, Diplomarbeit – Berufsakademie Stuttgart, 2004

Biopolymer Compounds for Applications Requiring Marine Degradation

Stanley Dudek, Polymer Processing Tech., TX

Mustafa Cuneyt Coskun, Polymer Processing Tech., TX

Background

The tremendous production and consumption of plastics in various industries has led to some serious environmental concerns. The persistence of synthetic polymers in the environment poses a major threat to natural ecological systems. Therefore, some people believe that the use of biodegradable plastics is the only way to significantly reduce the environmental pollution due to plastic waste because biodegradable polymers can be environmentally friendly.

Biopolymers or bioplastics are plastics which include living microorganisms in their production process. Bioplastics have the biochemical advantage of being totally or partially produced from renewable materials such as vegetable oils, sugar cane, and cornstarch, and can be biodegradable into carbon dioxide, methane, water, and inorganic compounds.

Research studies have been performed to better understand the degradation of different degradable polymers in marine environments. Typically, these studies are performed on single polymers and not blends of polymers. In various applications, however, blends of different polymers are needed to fulfill the requirements of the application. This study was initiated to understand the biodegradation of biopolymer compounds made from blends of different biopolymers. Specifically, the mechanisms of the degradation and how the different mechanisms affect the use of the compounds in a marine environment were investigated. The specific application of netting for oyster bed rebuilding was the focus.

Introduction

Bioplastics are a form of plastic which uses living microorganisms in their production process. Some of the most commonly known bioplastics are polylactic acid (PLA), polyhydroxyalkanoates (PHA), including polyhydroxybutyrate (PHB) and copolymers of PHB, soy-based plastics, cellulose polyesters, starch-based bioplastics, and bio-polyethylene.

Degradable plastics have received global attention since they are eco-friendly and because they can decompose in nature. Both aliphatic as well as aliphatic-aromatic co-polyesters have been produced so far and have received great attention because of their degradability in the natural environment. These polymers can offer fast degradability in bioactive environments by the enzymatic reactions of microorganisms such as bacteria. In addition,

chemical hydrolysis also can break down biopolymer chains into their monomers. The chemical structure of the polymers influences the degradability of these polymers, especially the presence of functional groups and hydrophilicity-hydrophobicity balance, and by the ordered structure such as crystallinity, orientation, and other morphological properties (Chen et al. 2008). Biodegradable polymers are degradable but conventional plastics have better physical and mechanical properties (Table 1). It is increasingly important to design polymer compounds having both satisfactory mechanical properties and degradability.

Biopolymer Types-Synthetic Reactions versus Fermentation

Polylactic Acid (PLA) is a thermoplastic polyester which obtains sugar by fermentation of corn or sugar cane. Plants produce glucose (sugar) and oxygen as products of photosynthesis. Photosynthesis is performed in chloroplasts which use CO₂, water, and sun energy to produce sugar and oxygen. Corn stores the sugars which it produces in the endosperm to use it as an energy source to grow. Per the Corn Refiners Association, harvested crops are sent to processing for grinding. The starch is then extracted from the corn mixture. Starch is then hydrolyzed to glucose.

PLA production consists of three major steps after the glucose obtained. The first step is the production of lactic acid by glycolysis followed by bacterial fermentation. Glycolysis is the universal cellular metabolic process that breaks down 6-carbon glucose into two 3-carbon pyruvate molecules. In the absence of oxygen, pyruvate molecules can be converted into lactic acid by fermentation. Due to asymmetric carbon located in the lactic acid backbone, two isomer structures are available. L-Lactic acid is a mirror image of D-Lactic acid and D-Lactic acid structure is very rare in nature [1]. The second step is the purification of lactic acid and preparation of lactide. Lactide is produced by a back-biting reaction of oligomeric lactic acid. This reaction occurs by nucleophilic attacking of a hydroxyl group of lactic acid to its carboxyl group binding carbon atom site. The third step is ring-opening polymerization of the lactides (figure 1). The lactide is treated in a solvent free environment by chemicals to open the lactide rings to form a long chain polylactide polymer which can be thousands of monomers bound to each other. Thus, PLA is a synthetic polymer even though it is based on a fermentation produced bio-based material.

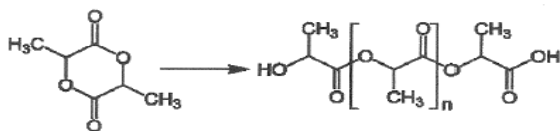


Figure 1. Structures of lactide (left) and poly-lactide (right) after ring opening polymerization. [2].

PLA can offer good thermal and mechanical properties similar to conventional plastics polyethylene, polystyrene, and polyethylene terephthalate (PET). Additionally, PLA can provide superior odor barrier properties, resistance to dairy foods with similar properties of PET and higher elasticity than Petro-based polystyrene. However, the properties of PLA highly depend on the molecular weight of polymer chain, crystallinity, and the ratio between two enantiomers, L-PLA, and D-PLA.

Polyhydroxyalkanoates (PHA) are biodegradable linear polyesters that can be obtained from several microorganisms such as bacteria, yeast, and fungi. Microorganisms can accumulate PHA's intracellularly as an energy source similar to fat storage in animals. Extraction of PHA polymers from microorganisms is done by breaking the cell walls and/or by enzymatic digestion followed by washing in a centrifuge.

Common types of PHA's are polyhydroxyvalerate (PHV), polyhydroxybutyrate (PHB), polyhydroxybutylhexanoate (PHBH) and polyhydroxybutyratevalerate (PHBV) (figure 2), PHB is a bio-polyester that can accumulate in the cytoplasm of a cell. The size of PHB particles is about 0.5 μm and, in a suitable environment, the microorganism can produce PHB up to 90% of their dry cell weight [3]. Biochemical production of PHB molecules initiates with hydrolysis of a selected carbon source to an acetate molecule. Then the cofactor enzyme (coenzyme A) binds to the acetate molecule by forming thioester bonds between the acetate and the sulfur atoms of coenzyme A. That reaction is called acetylation. Coenzyme A is a carrier of acetyl groups in biological systems assisting in the formation of acetyl-CoA which is a common molecule found in all PHA producing organisms. Two acetyl-CoA molecules convert to the dimer acetoacetyl-CoA by a reversible condensation reaction. The Acetoacetyl-CoA molecule will reduce until the monomer -3-hydroxybutyryl-CoA is obtained. Coenzyme A will then release at the last step of monomer synthesis forming -3-hydroxybutyryl which will polymerize to form Polyhydroxy butyrate (PHB). PHB molecules trapped in a cell membrane can be extracted by chemical, mechanical, or enzymatic processes which break down the cell membrane. Extracted polymers are dissolved in an appropriate solvent such a chloroform, methylene chloride or pyridine. The remaining biological structures should then be removed by filtration or centrifugation.

Degradation in a Soil Environment

Degradation is defined as a reduction in the molecular weight of the polymer. Biodegradation is defined as reduction in the molecular weight by naturally occurring microorganisms such as bacteria, fungi, and actinomycetes. Traditional plastics made from petroleum based products do not degrade quickly in the environment. As a rule, widely used plastics do not naturally biodegrade when released into the environment [5,6,7,8]. This is perhaps unsurprising, as one of the primary reasons for the popularity and widespread application of many polymers is their exceptionally high stability and durability [5,6].

There are four mechanisms by which plastics degrade in the environment: photodegradation, thermo-oxidative degradation, hydrolytic degradation, and biodegradation by microorganisms [9]. Generally speaking, the natural degradation of plastic begins with photodegradation, which leads to thermo-oxidative degradation. Ultraviolet light from the sun provides the activation energy required to initiate the incorporation of oxygen atoms into the polymer [9, 10]. This causes the plastic to become brittle and to break into smaller and smaller pieces (Figure 3), until the polymer chains reach sufficiently low molecular weight to be metabolized by microorganisms which from a bio-slime (Figure 4) on the particles [6, 9]. These microbes either convert the carbon in the polymer chains to carbon dioxide or incorporate it into biomolecules [5, 9]. However, this entire process is very slow, and it can take 50 or more years for plastic to fully degrade [11].

Organic materials completely disappear because they are a food source for the organisms in soil or marine waters. This is also true of the biopolymers. With a food/soil environment like compost, which is between 55° and 65°C and 45% to 55% moisture, organic materials will disappear in the moist, hot soil in 180 days and not leave any small fragments or residue. This is the basis behind ASTM D6400 Specification Standard for biodegradation under industrial aerobic compost conditions. The ASTM D6400 Standard requires plastic samples to convert 90% of the carbon in the plastic sample to CO_2 after 180 days while at 58°C. Because PHA is a natural polymer, synthesized by bacteria as an energy and carbon source, the ability to be degraded (consumed) is widely spread among the microorganisms in a marine environment. It is reported that many genus of microorganisms including *Alcaligenes*, *Comamonas*, *Pseudomonas*, *Streptomyces*, *Acidovorax*, *Marinobacter*, *Thermobifida*, and so on, are reported as PHB and PHA-degrading bacteria.

Degradation in a Marine Environment

Degradation in a marine environment follows a similar process to the process in soil. However, the degradation process in water is hindered by the fact that the photodegradative and thermooxidative effects are

significantly decreased in seawater due to the lower temperature and the oxygen availability. Also, there is a time delay in the formation of the bio slime especially with the polymers that require a synthetic step in their production process (figure 4). ASTM D6691 Test Method provides a description of the testing procedures that best simulate the marine environment and a method by which to measure biodegradation. ASTM D6691 Test Method is used to determine the degree and rate of aerobic biodegradation of plastic materials exposed to the indigenous population of existing sea water or synthesized sea water with a pre-grown population of an at least 10 aerobic marine microorganisms of known genera. The microorganisms are representatives of organisms in the marine water. It does not include all the species of marine organisms.

Biodegradation of a polymer sample in marine water is measured from the carbon dioxide evolution from the decaying polymer sample. ASTM D7081 specifies that 30% of the carbon in the plastic has to be converted to CO₂ after 180 days as measured by a CO₂ respirometer. ASTM D7801 further requires the test to follow the procedures specified in ASTM D6691 Test Method and that the samples also must pass the composting standard of ASTM D6400.

A variety of factors, including, but not limited to, water temperature, plastic resin type, additives, and thickness of materials, can impact marine biodegradation. Biodegradable plastics will biodegrade much faster than polyethylene. Bioplastics are hygroscopic and absorb water readily that allows the biopolymer to break into smaller pieces and initiate hydrolysis, which leads to biodegradation. Polyethylene plastic is hydrophobic and does not absorb marine water [12]. Polyhydroxyalkanoates (P3HB and PHBV), polyhydroxyvalyrate (PHV), polyhydroxybutyrate (PHB) and (PHBH) have been studied extensively for biodegradation in marine environments. PHB biodegraded in sea water at a rate of 0.6 µg/week in sea water at 25°C. PLA did not biodegrade in sea water at the same temperature [13]. PLA did not biodegrade in an anaerobic liquid environment, either. PHB biodegraded rapidly in three weeks. PHA and cellulose met the ASTM D7081 requirements for greater than 90% disintegration in three months but other industrially compostable polymers such as PLA not [14]. PHA and cellulose met the ASTM D7081 requirements for 30 percent biodegradation in six months but PLA does not [15]. PLA and PHA biodegrade and release carbon dioxide during the aerobic biodegradation process. PLA, however, requires a significant amount of hydrolysis before it can be consumed by microorganisms which would use enzymes such as esterase, lipase, and protease to further break down and consume the polymer. An esterase is a hydrolase enzyme that splits esters into an acid and an alcohol in a chemical reaction with water called hydrolysis. A wide range of different esterases exists that differ in their

substrate specificity. A lipase is an enzyme that catalyzes the hydrolysis of fats (lipids). Lipases are a subclass of the esterases. Lipases perform essential roles in the digestion, transport, and processing of dietary lipids (e.g. triglycerides, fats, oils) in most, if not all, living organisms. A protease (also called a peptidase or proteinase) is any enzyme that performs proteolysis, that is, begins protein catabolism by hydrolysis of the peptide bonds that link amino acids together in a polypeptide chain. Proteases can be found in animals, plants, fungi, bacteria, archaea, and viruses. Moreover, the original substrate of these enzymes is probably not the PLA surface. Therefore, the biodegradability of PLA and other synthetic degradable polymers are not as good as polymers produced by microorganisms via fermentation.

Degradation Testing

Based on the background information discussed above, test samples were produced from various degradable polymers. The initial samples were films that were tested to determine their degradation behavior in a marine environment. The primary focus was to determine simple tests to determine, first, if degradation is occurring, and second, how the polymer type affects the degradation mechanism. Since marine degradation can be both anaerobic as well as aerobic, methane generation was chosen as one test. The second test was the observation of physical surface changes.

The films were extrusion cast on a Brabender extruder to a thickness of 2 mils. Pieces of film, approximately 2 inches' square, were cut from the film and placed in glass jars which had been filled with water from the Gulf of Mexico. The samples were divided into two groups. One group of jars were closed and allowed to become anaerobic. The other group of jars were left open to allow air into the water. The anaerobic jars with film samples that were produced from materials made by fermentation, such as PHA and PHB, started producing a noticeable amount of methane within 30 days. The PLA did not produce noticeable methane within 30 days. Additionally, both the aerobic and anaerobic film samples that were produced from materials made by fermentation started to show the growth of a bio-slime within 15 days. Bio-slime did not exhibit itself on the PLA. This agrees with the literature. PHAs are degraded by enzymes from a wide range of bacteria and fungi. The PHBH surface is the real substrate for the enzymatic degradation. Therefore, the rate of biodegradation of PHBH is faster than PLA in the ambient environment because the PLA requires a significant reduction in molecular weight via hydrolysis before biodegradation can begin

Thicker bars were then molded to determine more about the degradation mechanisms and the degradation rates blends of the polymers. Table 2 details the degradation of a PHBH based compound. Notably, the sample took 3 months to accumulate the growth of

microorganism on its surface to then reach a faster degradation loss of 4 percent/month versus a degradation rate of 1%/month during the first three months.

Table 2. Marine Degradation Speed of PHA Based Compounds in an Aerobic Environment

Period	Day	Weight		Geometry		
		Grams	%	Thickness	Width	Length
Start	0	3.74	100	3.97	9.75	79.85
1 month	30	3.7	99	3.96	9.74	79.34
3 months	92	3.63	97	3.89	9.68	79.62
6 months	183	3.18	85	3.59	9.43	77.61
12 months	365	2.13	57	2.83	8.47	73.5

Another important observation was that the surface was significantly eroded on the PHA sample while the PLA sample did not exhibit any erosion (Figure 5). The PLA did exhibit changes due to hydrolysis as you can see by the change in opacity in Figure 6. The PHBH compound did not significantly hydrolyze.

Marine Oyster Netting

Oyster netting is used to hold in place oyster shells collected from various venues that process and serve oysters. They are then used to form new oyster beds. At the present, the netting is produced from polyethylene which can constrict the growth of the new oyster inside the netting. To resolve this issue, a netting material, based on the data developed from this study, was extruded (Figure 7) and then subjected to marine degradation testing. The results after five months were very similar to the testing done on the films and the bars. Netting is now being field tested in oyster beds along the Florida coast.

References

1. S. Pilla, *Handbook of Bioplastics and Biocomposites Engineering Applications*, Wiley, Hoboken, NJ, pp.80 (2011).
2. "Polylactic acid," http://en.wikipedia.org/wiki/Polylactic_acid (2003).
3. Q. Wang, H. Yu, Y. Xia, Z. Kang, Q. Qi, Complete PHB mobilization in *Escherichia coli* enhances the stress tolerance: a potential biotechnological application. *Microbial Cell Factories*, **8**, 47 (2009).
4. "Polyhydroxyalkanoates," <http://en.wikipedia.org/wiki/Polyhydroxyalkanoates> (2010).
5. K. Yamada-Onodera, H. Mukumoto, Y. Katsuyaya, A. Saiganji, Y. Tani, Degradation of polyethylene by a fungus, *Penicillium simplicissimum* YK. *Polym. Degrad. Stabil.*, **72**, 323-327 (2001).
6. Y. Zheng, E.K. Yanful, A.S. Bassi, A review of plastic waste biodegradation, *Crit. Rev. Biotechnol.*, **25**, 243-250 (2005).
7. M.S. Marqués-Calvo, M. Cerdà-Cuellar, D.P.R. Kint, J.J. Bou, S. Muñoz-Guerra, Enzymatic and microbial biodegradability of poly(ethylene terephthalate) copolymers containing nitrated units, *Polym. Degrad. Stabil.*, **91**, 663-671 (2006).
8. S. Bonhomme, A. Cueur, A.M. Delort, J. Lemaire, M. Sancelme, G. Scott, Environmental degradation of polyethylene, *Polym. Degrad. Stabil.*, **81**, 441-452 (2003).
9. A.L. Andrady, Microplastics in the marine environment, *Mar. Pollut. Bull.*, **62**, 1596-1605 (2011).
10. J.M. Raquez, A. Bourgeois, H. Jacobs, P. Degée, M. Alexandre, P. Dubois, Oxidative degradations of oxodegradable LDPE enhanced with thermoplastic pea starch: thermo-mechanical properties, morphology, and UV-ageing studies, *J. Appl. Polym. Sci.*, **122**, 489-496 (2011).
11. R.J. Müller, I. Kleeberg, W.D. Deckwer, Biodegradation of polyesters containing aromatic constituents, *J. Biotechnol.*, **86**, 87-95 (2001).
12. C. Bastioli, *Handbook of Biodegradable Polymers*, Rapra Technology Limited, pp. 36 (2005).
13. H. Tsuji, K. Suzuyoshi, Environmental degradation of biodegradable polyesters 1. Poly(caprolactone), poly[(R)-3-hydroxybutyrate], and poly(L-lactide) films in controlled static seawater, *Polymer Degradation and Stability*, **75**, 347-355 (2002).
14. J. Greene, Biodegradable and Oxodegradable Plastics Degradation in Compost and Marine Environments, *Proceedings of the 8th World Congress of Chemical Engineering*, Montreal, Canada, (2009).
15. J. Greene, Marine Biodegradation of PLA, PHA, and Bio-additive Polyethylene Based on ASTM D7081, *Proceedings of the SPE Global Plastics Environmental Conference*, (2011).

Tables

Table 1. Typical Material and Application Properties

Physical Properties	LDPE	PLA	PBAT	PHBH
Specific Gravity (ASTM D792)	0.92	1.26	1.23	1.2
Crystalline Melt Temperature (°C) (ASTM D3418)	110	162	126	126
Glass Transition Temperature (°C) (ASTM D792)	-70	60	-30	0
Mechanical Properties				
Tensile Yield Strength, (MPa) (ASTM D638)	26	52	38	19
Tensile Elongation, (%) (ASTM D638)	700	5	450	300
Notched Izod Impact, (J/m) (ASTM D256)	414	25	NA	48
Flexural Modulus, (MPa) (ASTM D790)	150	69	NA	800
Heat Distortion Temp. (°C) (ASTM D648)	106	60	NA	103

Figures

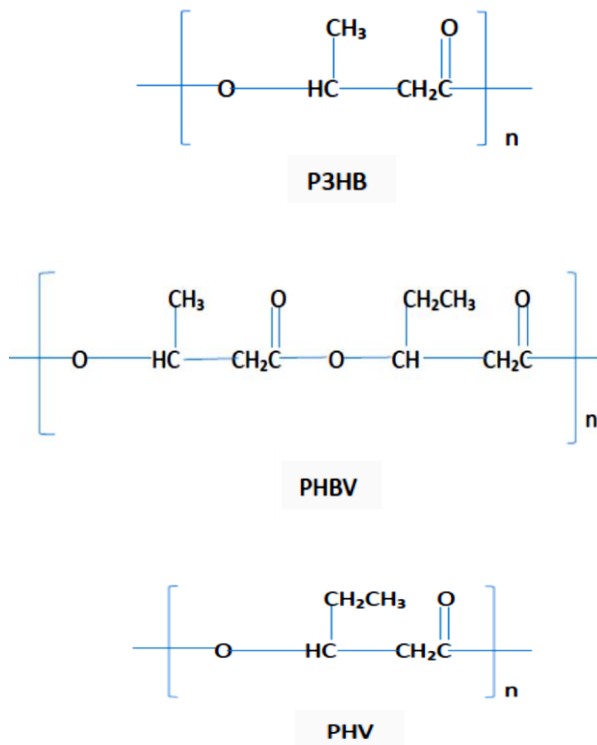


Figure 2. Structures of poly-3-hydroxyvalerate (PHV), poly-3-hydroxybutyrate (P3HB) and poly-3-hydroxybutyrate-co-3-hydroxyvalerate (PHBV). [4].



Figure 3. Biodegradation Behavior in Soil

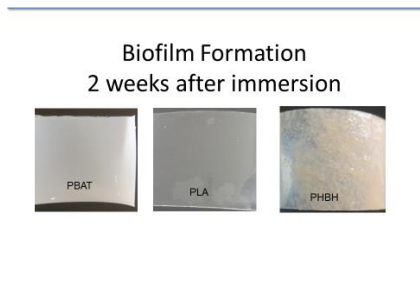


Figure 4. Biofilm Formation



Figure 7. Biopolymer Netting

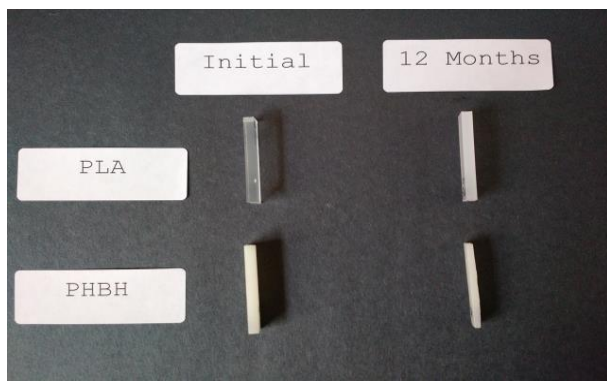


Figure 5. Surface Erosion of PLA and PHBH

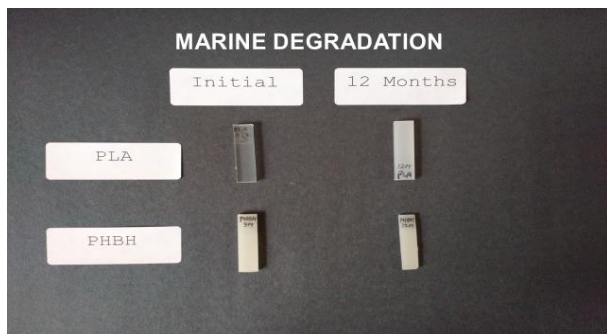


Figure 6. Opacity of PLA and PHBH

Novel plant-based dialkyl hydroxylamine antioxidant

Dr. Chingfan Chris Chiu

President

Chitec Technology Co., Ltd., Houston, Texas

Abstract

Dialkyl hydroxylamine antioxidant (AO) has received much attention from the polyolefin industry due to its super non-yellowing properties and resistance to gas fading. This AO has found wide acceptance as a standard in several high-end film and fiber applications based on polyolefins.

However, first generation hydroxylamine is based on tallow and this has raised concerns among vegetarians, some religion faiths, mad-cow disease watchers, and so on. To introduce this technology into more applications, a new type of hydroxylamine, not of animal origin, is available to the polyolefin industry.

Chitec now offers a novel plant-based hydroxylamine AO based on sustainable palm oil which has been registered with TSCA, REACH, NDSL, TCSI and FDA over the past five years.

In this presentation, the plant-based AO will be compared with the tallow-based product with respect to both composition and antioxidation efficiency.

In addition, its synergistic effect in combination with secondary AO and light stabilizer will be discussed using a melt strength model which is a critical aspect in film production.

Other experimental results will be discussed including gas fading, stretchability, retention and so forth, to show that the plant-based hydroxylamine is an ideal AO for both film and fiber production.

Introduction

Unlike commodity hindered phenolic AO, dialkyl hydroxylamine AO does not discolor when it comes in contact with NO_x. In other words, it is strongly

resistant to gas fading. This advantage makes dialkyl hydroxylamine AO popular in polyolefin-based fiber and film industries where gas fading is severe.

The structure of dialkyl hydroxylamine is hawk-shaped and is not an efficient processing stabilizer in protection of melt-flow, for example, which is critical for multiple passes testing. However, it is an excellent protector of melt-strength, which is one of the most critical properties for film and fiber processes, besides color.

In U.S. Patent No. 4,876,300, dialkyl hydroxylamine shows powerful protection of color in comparison to hindered phenolic AO or hindered amine light stabilizer (HALS). In example 29, PP that contained hindered phenolic AO + HALS went from YI=12.5 to 51.3 after five extrusions at 280°C while dialkyl hydroxylamine + HALS went merely from YI=7.4 to 9.7.

First generation hydroxylamine is a derivative of tallow amine, as described by its chemical name. The word “tallow” has raised concerns among customers especially vegetarians, some religious groups, and those concerned about mad-cow disease. A hydroxylamine antioxidant of non-animal origin has been long expected by the market.

The concept of tallow replacement has been adopted in other products, for example hydrotalcite DHT-4A was used extensively in the US five years ago. But it has been replaced by DHT-4V in almost every food contact polyolefin application, if not all, in the US nowadays. V stands for vegetable grade.

Chitec observed this opportunity and initiated a project to develop a dialkyl hydroxylamine with no animal origin in 2012. We replaced tallow amine

with palm-oil amine which not only makes it non-tallow but also green in nature as the plant-derived feedstock is sustainable. Replacing the amine raw materials also changes the composition of dialkyl hydroxylamine, hence it requires a new chemical name and a new CAS Registry Number (RN). The first generation dialkyl hydroxylamine carried the name *Amines, bis(hydrogenated tallow alkyl), oxidized* and was listed with CAS RN 143925-92-2. The vegetable version of dialkyl hydroxylamine is named slightly different; *Amines, bis(hydrogenated palm-oil alkyl) hydroxy* with a CAS RN 1374859-51-4.

Dialkyl hydroxylamine is a UVCB substance comprising at least eight constituents. Even with similar raw material, i.e. dialkylamines, the composition of palm oil-based hydroxylamine AO is still slightly different from the tallow-based one. The three major constituents are hydroxylamines, nitrones, and the raw material dialkylamines. Palm oil-based dialkyl hydroxylamine contains 73% hydroxylamines vs. 67% in the tallow-based dialkyl hydroxylamine¹. But palm oil-based dialkyl hydroxylamine has a higher content of nitrones at 14% vs. 5%. The analysis is completed by LC-MS.

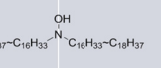
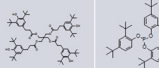
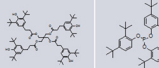
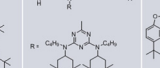


Because of the difference in composition and CAS RN/name, a complete new global registration is required for this palm oil-based hydroxylamine AO. The registration process was initiated in December 2012 by obtaining a CAS RN, and in following three years, REACH, TSCA, and NDSL were obtained in sequence. In July 2016, another milestone was achieved as this palm oil-based hydroxylamine AO acquired FDA clearance for food contact applications in PP and HDPE with a 0.1% maximum dosage. The last goal is to receive EFSA's food contact authorization in 2018 and this initiative is estimated will cost 0.5 million dollars to complete. Ever more complicated and expensive global chemical inventory registration has created a major hurdle for a small company like Chitec to innovate and invent.

Experimental section

Palm oil-based and tallow-based dialkyl hydroxylamine AOs were compared for protection of melt-strength and color. Other AO packages containing traditional phenolic AO, HALS and lactone-based AO respectively were also compared. The experiment was conducted using virgin PP (MI = 16.47) available from Formosa Plastics by using twin extruders under a nitrogen blanket.

The dosage of each AO package is 1,000 ppm. The respective composition is shown in Table 1. All of the formulations contain phosphite AO 168 as a secondary AO by varying the primary AO which is palm oil-based hydroxylamine as AO-1, tallow-based hydroxylamine as AO-2, hindered phenolic AO 1010 as AO-3, HALS-1 as AO-4, and the combination of 1010 plus a lactone-based AO as AO-5. The last two are also proprietary products of Chitec. Their chemical structures are attached. The last two were tested because they are known as AOs with high color stability. Beside the AO, all of the formulations contain 200 ppm hydrotalcide as an acid scavenger.

Table 1. Composition of AOs

	Palm-based hydroxylamine	Tallow-based hydroxylamine	1010	168	HALS-1	Lactone
						
AO-1	1			2		
AO-2		1		2		
AO-3			1	2		
AO-4				2	1	
AO-5			1	2		0.2

Melt-strength analysis

The melt-strength analysis was conducted by an elongation rheometer, the Rheotens 71.91 from Goettfert, at 180 °C. The result is shown in Figure 1. "Force" as indicated by the Y axis stands for melt-strength which is a function of velocity. Overlapping lines of AO-1, AO-2, and AO-3 indicates that palm oil-based dialkyl hydroxylamine AO, tallow-based dialkyl hydroxylamine AO, and hindered phenolic AO gave similar melt strength performance. In other words, even though they possess different structures they provide the same protection on PP's melt-strength.

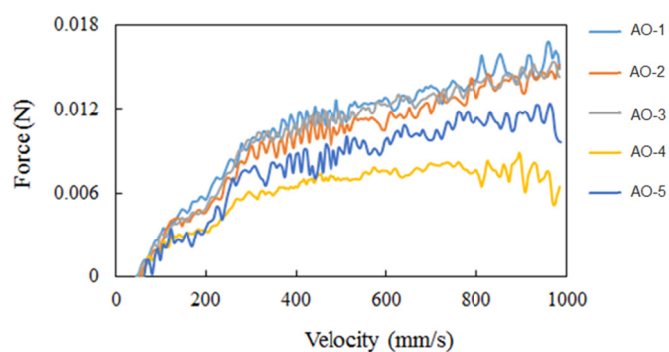


Figure 1. Results of melt-strength analysis

AO-4, where hydroxylamine AO and hindered phenolic AO were replaced by HALS, a known long-term heat stabilizer, shows a different curve

which indicates inferior melt-strength performance. In other words, HALS is not efficient in protecting melt-strength at 180 °C.

Most surprisingly, with the addition of a small amount of a novel lactone based-AO, the melt-strength of AO-5 greatly deteriorated. This is the opposite of our prediction as lactone-based AO is known to be superior as a melt-flow property protector to hindered phenolic AO. In AO-3, hindered phenolic AO shows good performance.

Shear experiments

Another way to compare these five AO packages is to run shear experiments by using high pressure capillary rheometer, Rheograph 2003 from Goettfert, at 180 °C, 190 °C and 200 °C. The results are shown in Figure 2. No meaningful differences were found among these five spectra which indicates a similar polymer structure.

Shear rate vs. viscosity

- Test equipment: High pressure capillary rheometer.
- Model: Rheotens from Gottfert
- Temp.: 180 °C, 190 °C and 200 °C

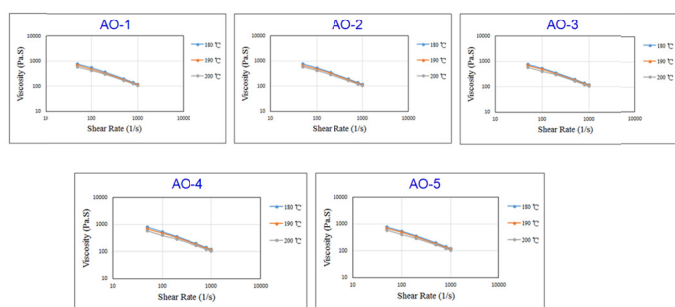


Figure 2. Result of shear experiment

Gas fading experiment

These five specimens were placed in a gas-fading reactor in which nitrogen oxides were generated by sodium nitrate reacting with sulfuric acid. The experiment ran for 24 hours at room temperature. The results are shown in Figure 3. Only the specimen containing AO-3 showed severe yellowing in contrast to the other four AO packages. This result is predictable as hindered phenolic AO is known to turn yellow on exposure to nitrogen oxide. Specimens containing AO-1 and AO-2 again are shown to be resistant to gas-fading without any visual differences. That means the byproducts of palm oil-based dialkyl hydroxylamine and tallow-based amine do not affect the performance of gas-fading resistance.

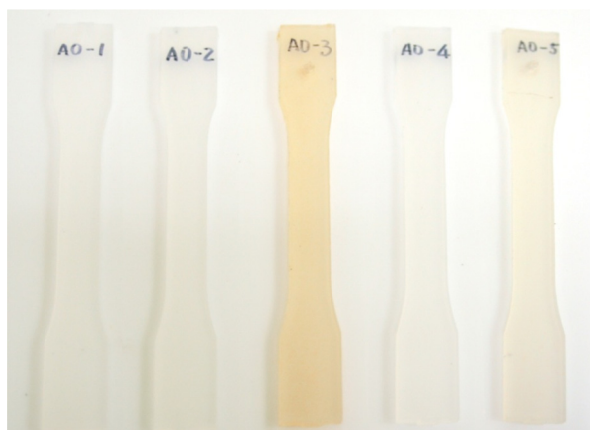


Figure 3. Results of the gas-fading experiment

Conclusion

1. A new palm oil-based dialkyl hydroxylamine AO is commercially available which is slightly different from the tallow-based predecessor in terms of composition.
2. The difference in composition between them does not affect AO efficiency in protecting melt-strength of polypropylene in combination with a secondary phosphite AO, as demonstrated by the rheometer.
3. Both palm oil-based and tallow-based dialkyl hydroxylamine AOs are highly resistant to gas fading in contrast to hindered phenolic AOs.

Reference

1. NICNAS, File No. NA/592, Full Public Report "Amines, bis(hydrogenated tallow alkyl), oxidised", May 1998.

TALC AS ANTIBLOCKING IN LLDPE: PERFORMANCE SCREENING OF DIFFERENT TALC GRADES VERSUS OTHER MINERAL ANTIBLOCKING

Piergiorgio Ercoli Malacari, IMI Fabi Spa, Milano, Italy

Abstract

As many plastic films tend to stick together, making difficult to separate film layers, some mineral additives are used to improve this situation. Specifically, in LLDPE films, micronized talc is often used as antiblocking agent. Thanks to the micro-roughness achievable on film surface, talc acts as a spacer between the film layers minimally affecting transparency and other mechanical properties. The presence of talc in the LLDPE film formulation interacts with other additives, creating a unique set of properties that makes talc a very effective additive for film applications.

In this paper different talc grades will be investigated for their intrinsic characteristics in comparison with other known mineral antiblocking additives to evaluate their effect in LLDPE film for final performances. A comprehensive evaluation of all the properties will be performed to rank each single tested additive for the antiblocking function, considering all the side properties including mineral additive abrasivity and bulk handling

A novel talc antiblocking additive characterized by free flowing appearance and dust-free behavior, for innovative solutions in talc handling will be also introduced.

Introduction

In order to prevent adjacent layers of polymer films from adhering to each other (blocking), antiblocking agents are normally incorporated into the polymer from which the film is made. The degree to which a film is susceptible to blocking is mainly determined by the smoothness of the surfaces; the smoother the surface, the greater is the degree of intimate physical contact and therefore the greater the blocking. The incorporation of tiny particles into the film allows to reduce the surface smoothness, minimizing the blocking. In general, inorganic minerals are used for this functions, such as: talc, diatomaceous earth, calcium carbonate, calcined clay and both ground and synthetic silica. The function of these finely divided particles is to produce asperities on the film surface and thus minimize the area of flat contact.

Antiblocking efficiency is only one of many performance criteria that must be considered in the selection of a right antiblock agent for polymer film. Other important properties are: clarity, coefficient of friction and interaction effects with processing aids. As some minerals could be quite hard, it is also important to consider the

effect that those additives could have in terms of equipment wearing during their incorporation into the polymeric resin. Also additive bulk properties can play a role in the overall features to be considered when an antiblock agent has to be selected, because they might affect the economy in additive dispersion.

The purpose of this study is the evaluation of different antiblocking agents, including several talc grades, dispersed in linear low density polyethylene (LLDPE), comparing different sets of properties achievable into a blown LLDPE film.

Experimental

Materials

A general purpose M.I. 1.0 g/10min butene LLDPE resin was used for both antiblocking masterbatch granules and film production. The resin is characterized by a density of 0.918 g/cc.

Different inorganic additives were used as antiblocking agents and their properties are summarized in Table 1. All of them are from natural source with the exception of amorphous synthetic silica. In this study, six different talc grades from IMI Fabi Spa were investigated versus calcium carbonate, diatomaceous earth, calcined clay and synthetic silica. The talc grades are characterized by different particle size distributions and some of the investigated grades are also coated for better dispersion in polymer and lower interaction with processing aids. In Figures 8 to 12, a SEM image at the same magnification of the five different antiblocking additives is showed for a direct visual comparison of the inorganic products.

Abrasivity test, summarized in Table 1, consists in the amount of copper abraded by a thin copper net where a water slurry of the additive has insisted for 120 minutes under a controlled contact condition. The higher the abrasivity value, the stronger the expected wearing achievable during mineral processing.

Processing

The antiblocking additives were pre-dispersed into the LLDPE resin to form a masterbatch. All the antiblocking additives were loaded into the masterbatch to achieve a final loading of 3000 ppm into the blown film. Also process stabilizers and slip agent (Erucamide at 800 ppm final loading on the film) were added to each

masterbatch. Masterbatches were produced by means of a co-rotating intermeshing twin screw extruder, purging the feeding area with nitrogen to minimize oxidation. Masterbatch was precisely mixed to the resin to achieve the final loading of 3000ppm of antiblocking additive and 800 ppm of Erucamide; the blend was extruded into a laboratory blown film line, achieving a 45 micron film.

Neat LLDPE resin (without antiblocking additives and slip agent) was extruded to achieve a reference in the study. Also a sample containing slip agent (800 ppm Erucamide) has been prepared to measure the effect of slip agent without inorganic antiblock additive (sample ID is LLDPE).

Testing

The induced blocking test procedure used the parallel plate method as per ASTM D3354, to determine the degree of blocking. In preparing the samples, squared pieces of film were cut from the layflat tubing; the double layer was separated and discharged from static charges before being reunited and conditioned in recirculating forced air oven for 24h at 60°C, under controlled pressure. All samples were tested for antiblocking final loading, to confirm the exact 3000 ppm antiblock content.

The slip performance, as measured by static coefficient of friction (COF), follows the test procedure of ASTM D1894.

Optical properties were measured according to: ASTM D1003 for transparency (haze), ASTM D2244 for color (yellowness) and ASTM D2456 for surface appearance (gloss at 60°).

Mechanical properties were tested as well, according to: ASTM D882 (tensile strength at yield – machine direction) and ASTM D1709 (dart drop test).

Results and discussion

Antiblocking properties

To compare the relative antiblocking performance of the examined inorganic additives, the induced blocking at 60°C has been used, such temperature is rather selective and it emphasizes the antiblocking efficiency. In Figure 1, the results are plotted.

It appears that the modification of neat LLDPE with slip agent makes the film opening worse (better surface adhesion), while the addition of inorganic antiblock agents improves the film separation. The worse antiblock agent in this evaluation results to be the calcined clay, followed by calcium carbonate. Talc samples are in between, while the highest efficiency is recorded by both diatomaceous earth and synthetic silica samples.

Concerning the talc samples behavior, results can be split into two groups: finer grades (NB140c and

NB140Tc) and coarser grades (all the other talc samples). In general, the coarser the talc size, the higher the antiblocking efficiency.

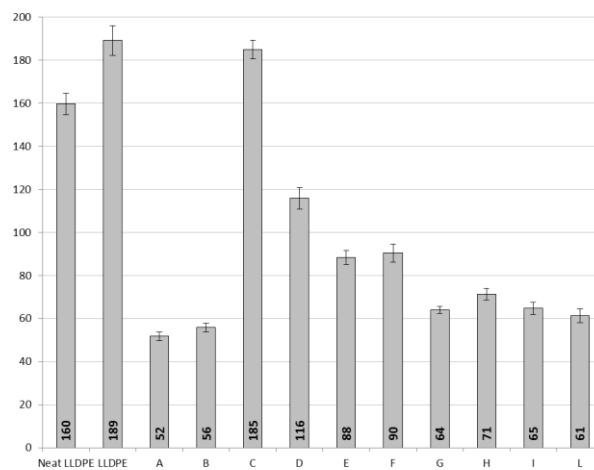


Figure 1: Antiblocking [g] after re-blocking at 60°C of 45µm LLDPE blown film, modified with 3000ppm of different antiblocking additives and 800ppm of Erucamide - according to ASTM D3354

Optical properties

The haze behavior in the study can be observed from Figure 2. The addition of additive masterbatch barely affects the transparency (LLDPE versus LLDPE) and the haze variation in the samples is mainly due to the inorganic additives themselves.

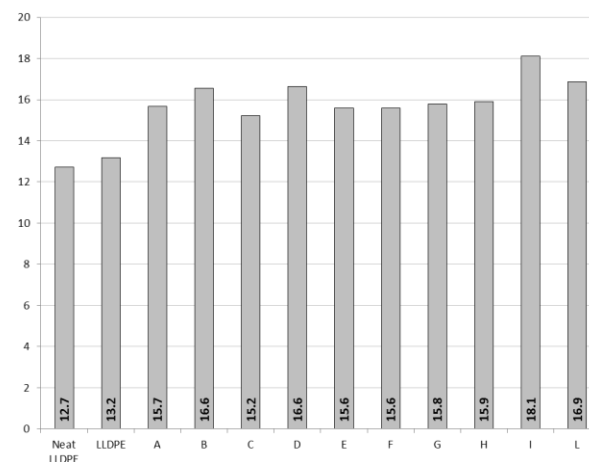


Figure 2: Haze [%] of 45µm LLDPE blown film, modified with 3000ppm of different antiblocking additives and 800ppm of Erucamide - according to ASTM D1003

The best behavior is recorded by calcined clay, followed by diatomaceous earth and fine talc. Synthetic silica performs as per calcium carbonate and the coarsest talc samples (CHB2 and NoBlock-S). In the case of talc samples, haze level achieved per same talc loading is

directly linked with the talc particle size distribution: the finer the talc size, the lower the haze.

In terms of color, the yellow index was set as indication for both process condition and additive modification. The intermediate usage of masterbatch for blown film production, didn't affect the resin color, as visible from yellowness values recorded between neat LLDPE and LLDPE (raw resin modified with masterbatch containing slip agent only).

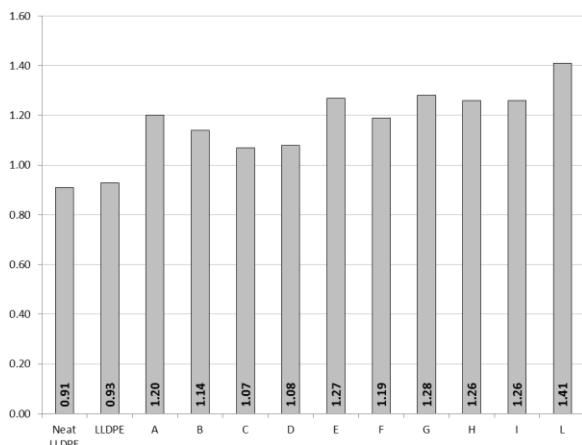


Figure 3: Yellowness [-] of 45µm LLDPE blown film, modified with 3000ppm of different antiblocking additives and 800ppm of Erucamide - according to ASTM D2244

The yellowness gap visible from Figure 3 data is due to the antiblocking additives. The more neutral additive are both calcined clay and calcium carbonate, while talc samples show the more visible variation.

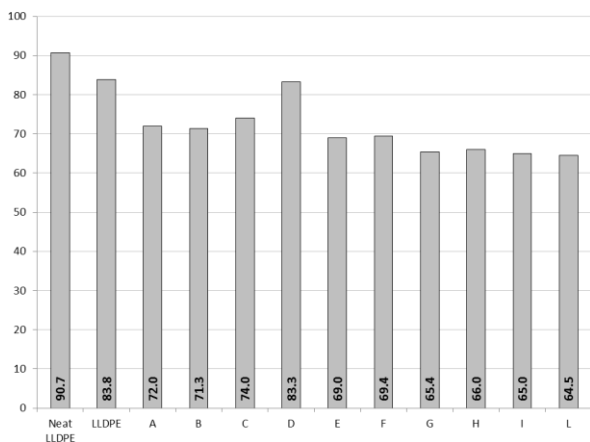


Figure 4: Gloss at 60° [%] of 45µm LLDPE blown film, modified with 3000ppm of different antiblocking additives and 800ppm of Erucamide - according to ASTM D2244

The effect of foreign particles into the LLDPE film is immediately visible on recorded gloss data; In fact, the original value of LLDPE gloss records a significant reduction once modified with additives. The slip agent itself contributes to the gloss reduction; differently from

the other antiblock additives, calcium carbonate doesn't contribute to the gloss reduction. In Figure 4, test results are summarized.

Slip properties

Slip properties were measured as per static coefficient of friction (COF). From Figure 5 it is clearly visible the improvement achieved by adding the slip agent to neat LLDPE. The further reduction is then achieved because of the micro roughness developed by the presence of inorganic antiblocking additives. The main exception can be recorded for synthetic silica that minimally improve the COF. The strong interaction existing between synthetic silica and slip agent is clear because of the extremely high specific surface of the inorganic additive: part of the slip additive was absorbed by silica, making it no longer available on the film surface. Also fine talc shows this tendency (but in minor extent). The higher micronized grade (NB140c) shows the highest COF among the talc samples; its surface coated version (NB140Tc) records an improvement in COF because of the lower interaction with slip agent. The best result was achieved with NB240TL (coated).

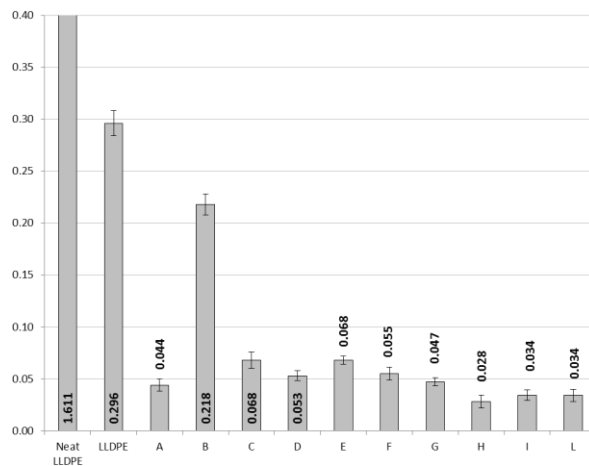


Figure 5: Static coefficient of friction (COF) [-] of 45µm LLDPE blown film, modified with 3000ppm of different antiblocking additives and 800ppm of Erucamide - according to ASTM D1894

In this work, the interaction effect between inorganic antiblocking and polymer processing aids (PPA) was not investigated. PPA are used to improve the melt fracture in LLDPE during extrusions as well as to minimize the die build-up (such as fluoropolymers). The same considerations made on slip properties can be partly extended to PPA, as general behavior. It means that coated talc will exhibit lower interactions with PPAs keeping them more available for their primary function and thus allowing a certain cost saving on PPA lower loading. .

Mechanical properties

Referring to Figure 6, tensile strength (machine direction) of neat LLDPE is always negatively affected by the presence of foreign additives. The slip agent (800 ppm of Erucamide) minimally affects the tensile properties of the film, but the inorganic additives contribution is more visible. In particular, both calcined clay and calcium carbonate show the strongest effect. All the other additives are, more or less, on the same level.

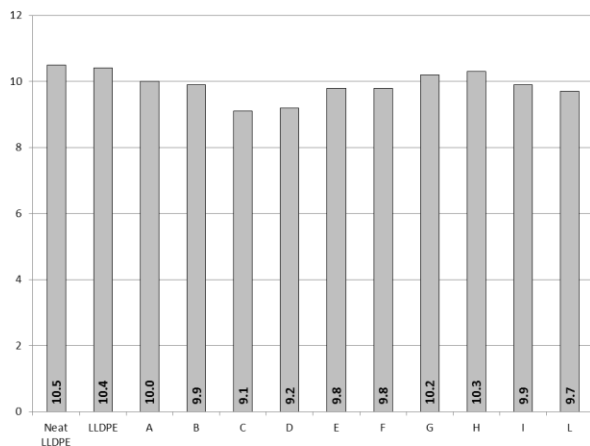


Figure 6: Tensile strength at yield [MPa] (machine direction) of 45 μ m LLDPE blown film, modified with 3000ppm of different antiblocking additives and 800ppm of Erucamide - according to ASTM D882

A similar behavior can be observed in Figure 7 for dart drop test too. Dart drop test records similar data for all the tested additives with the exception of synthetic silica that showed the worse value.

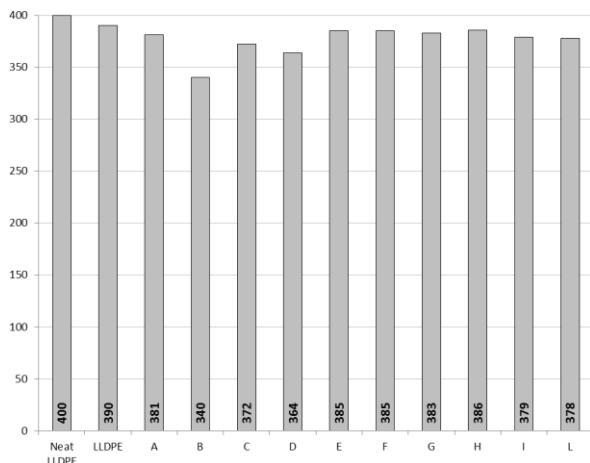


Figure 7: Dart drop[g] of 45 μ m LLDPE blown film, modified with 3000ppm of different antiblocking additives and 800ppm of Erucamide - according to ASTM D882

Conclusions

For a proper evaluation of an antiblocking additive it is necessary to consider a combination of different properties to cover all the different properties of interest for a LLDPE film.

In general, together with antiblocking evaluation, the most important properties refer to both clarity and coefficient of friction. Performing a simple scoring (Table 2), where the scores are meant as a value calculated between the worse (score = 0) and the best (score = 10) in the evaluated series of experimental data, it is possible to rank the different additives under those three properties. A very simple calculation (Table 3) addresses to diatomaceous earth (Sample A) the best in class product, followed by talc NB240L and NB240TL (samples G and H).

Then, considering other properties such as the abrasivity of the different additives, the bulk density for easy handling and the price, the ranking (Table 4) changes in favor of most of the talc samples, recording talc NB240 (sample G) as the best in class. Talc samples show a more balanced set of properties including some side properties not always considered as important during an additive evaluation, but potentially critical during its utilization. In particular, the abrasivity of the inorganic additive could affect both mixing equipment and downstream apparatus used in film handling such as trimming device. The higher bulk density, available for compacted talc, allows to achieve a better handling, especially during the production of concentrates to be used in blown film production.

In this respect, the sample NoBlock-S, showing a good set of properties, is characterized by an exceptional flowability. Because of the spherical agglomerates, NoBlock-S flows in every conditions, allowing its usage even in the more severe handling conditions. Also, it develops very little dust during handling, making this additive perfect for all the environments sensitive to dust pollution.

Key Words: LLDPE, antiblocking, talc, synthetic silica, calcined clay, calcium carbonate,

Additive	ID	bulk density [g/cc]	specific surface [m ² /g]	abrasivity [mg]	fineness		brightness		coated	compacted
					D ₅₀ [μm]	D ₉₈ [μm]	CIE-L [-]	CIE-b [-]		
Diatomaceous earth	A	0.23	2.00	121	11.3	25.9	97.2	1.8	no	no
Synthetic silica	B	0.16	380.79	30	5.7	11.4	98.5	0.3	no	no
Calcined Clay	C	0.50	11.00	57	3.8	15.2	96.5	3.0	no	no
Calcium Carbonate	D	0.91	3.00	25	4.1	15.9	95.6	3.1	yes	no
Talc NB140c	E	0.90	7.62	6	6.1	15.8	97.0	0.7	no	yes
Talc NB140Tc	F	0.90	5.76	5	6.8	18.7	96.9	0.8	yes	yes
Talc NB 240L	G	0.60	6.44	7	8.3	24.1	97.5	0.5	no	yes
Talc NB 240LT	H	0.60	4.59	6	8.3	23.5	97.3	0.8	yes	yes
Talc NoBlock-s	I	0.67	8.05	6	9.2	25.6	96.7	1.6	no	yes
Talc CHB2	L	0.29	6.74	7	11.2	37.2	95.3	0.7	no	no

Table 1: main properties of the different inorganic additives used as antiblocking agents in LLDPE films. Diatomaceous earth, synthetic silica, calcined clay and calcium carbonate are samples secured on the market, while all the talc samples are produced by IMI Fabi SpA.

Property	LLDPE	A	B	C	D	E	F	G	H	I	L
Antiblocking	0.0	10.0	9.7	0.3	5.3	7.3	7.2	9.1	8.6	9.1	9.3
Transparency	10.0	4.9	3.1	5.9	3.0	5.1	5.1	4.7	4.5	0.0	2.5
Slip	0.0	9.4	2.9	8.5	9.1	8.5	9.0	9.3	10.0	9.8	9.8
Abrasivity	10.0	0.0	7.8	5.5	8.3	9.9	10.0	9.8	9.9	9.8	9.9
Handling	9.9	0.9	0.0	4.5	10.0	9.9	9.9	5.9	5.9	1.7	6.8
Price	10.0	8.7	0.0	9.7	10.0	9.5	9.3	9.7	9.5	9.9	9.3

Table 2: relative scoring for different examined properties. For each one, a proportional score in the range 0 (worse) – 10 (best) is recorded among the experimental data recorded in the experiment. For transparency, haze was considered, while for handling, the powder loose bulk density was used for scoring.

Property	Weight [%]	LLDPE	A	B	C	D	E	F	G	H	I	L
Antiblocking	33.34	0.00	3.33	3.24	0.10	1.78	2.45	2.40	3.04	2.86	3.02	3.10
Transparency	33.33	3.33	1.65	1.05	1.95	1.00	1.70	1.70	1.56	1.49	0.00	0.84
Slip	33.33	0.00	3.13	0.97	2.84	3.02	2.84	3.00	3.10	3.33	3.26	3.26
total	100	3.33	8.11	5.25	4.89	5.80	6.98	7.09	7.70	7.69	6.28	7.20

Table 3: Scorecard calculated on the relative scores listed in Table 2 and weighed for each considered properties. In this scorecard, properties such as antiblocking, transparency (Haze) and slip (static COF) were considered at same relative weight. The higher the score, the better the set of properties.

Property	Weight [%]	LLDPE	A	B	C	D	E	F	G	H	I	L
Antiblocking	25	0.00	2.50	2.43	0.07	1.33	1.84	1.80	2.28	2.14	2.26	2.33
Transparency	25	2.50	1.23	0.78	1.47	0.75	1.27	1.27	1.17	1.12	0.00	0.63
Slip	20	0.00	1.88	0.58	1.70	1.81	1.70	1.80	1.86	2.00	1.96	1.96
Abrasivity	10	1.00	0.00	0.78	0.55	0.83	0.99	1.00	0.98	0.99	0.98	0.99
Handling	10	0.99	0.09	0.00	0.45	1.00	0.99	0.99	0.59	0.59	0.17	0.68
Price	10	1.00	0.87	0.00	0.97	1.00	0.95	0.93	0.97	0.95	0.99	0.93
total	100	5.49	6.58	4.58	5.22	6.73	7.73	7.78	7.85	7.79	6.36	7.51

Table 4: scorecard calculated on the relative scores listed in Table 2 and weighted for each considered properties. In this scorecard, properties such as antiblocking, transparency (Haze), slip (static COF), Handling (additive bulk density), additive abrasivity and price were considered at different relative weight. Antiblocking, slip and transparency were set at the highest weight (70% of total), while the other properties were considered for the remaining 30%. The higher the score, the better the set of properties.

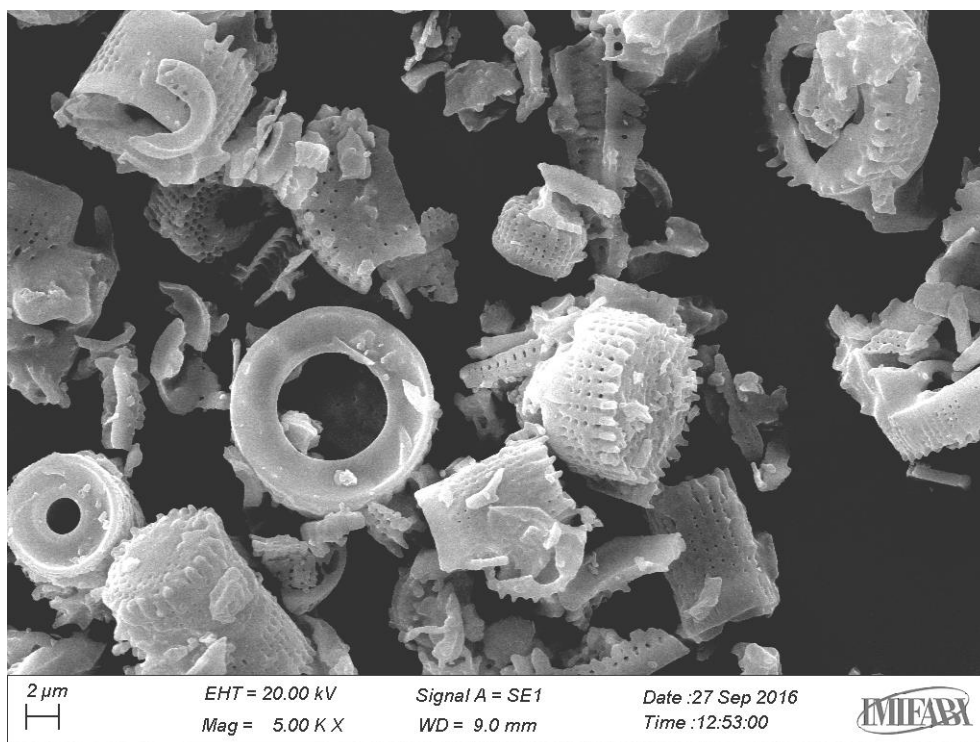


Figure 8: SEM image of a powder sample of diatomaceous earth

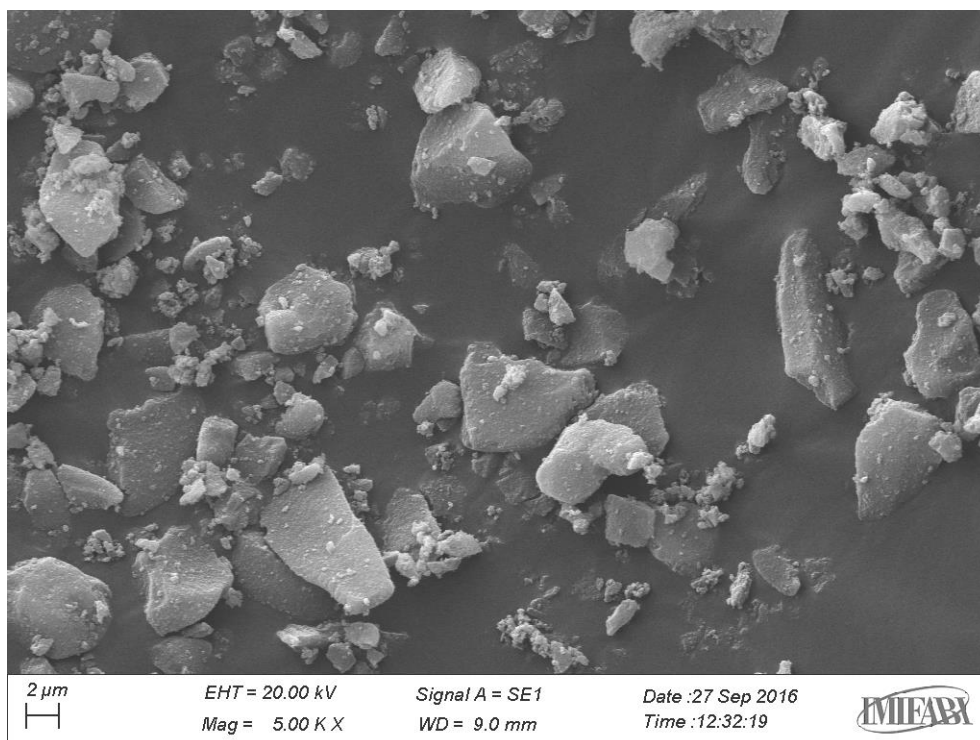


Figure 9: SEM image of a powder sample of synthetic silica

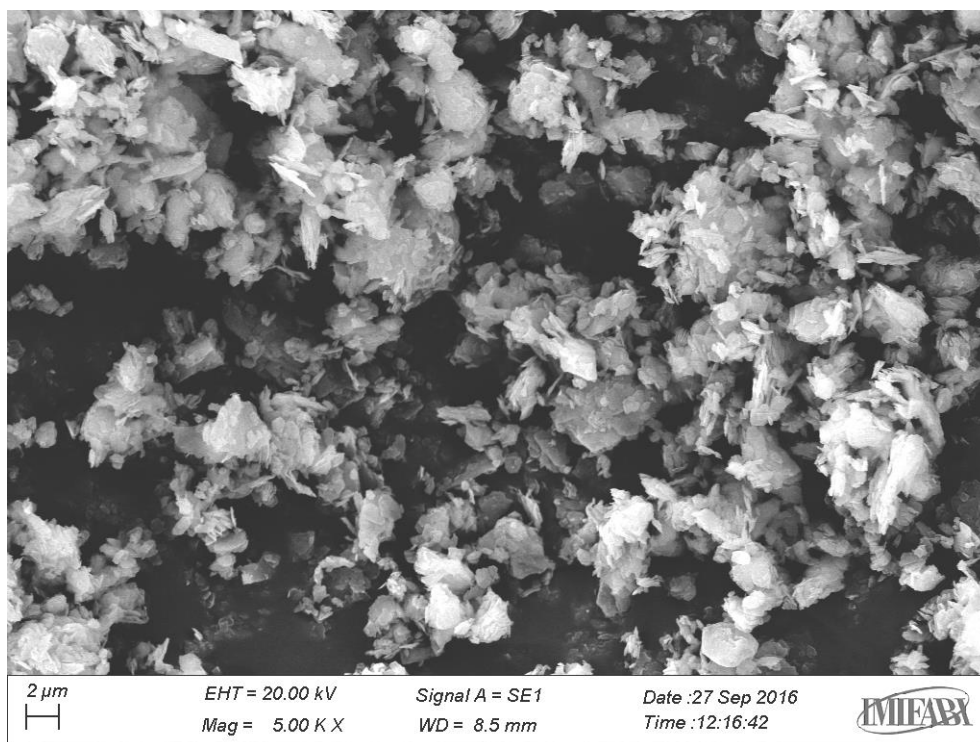


Figure 10: SEM image of a calcined clay

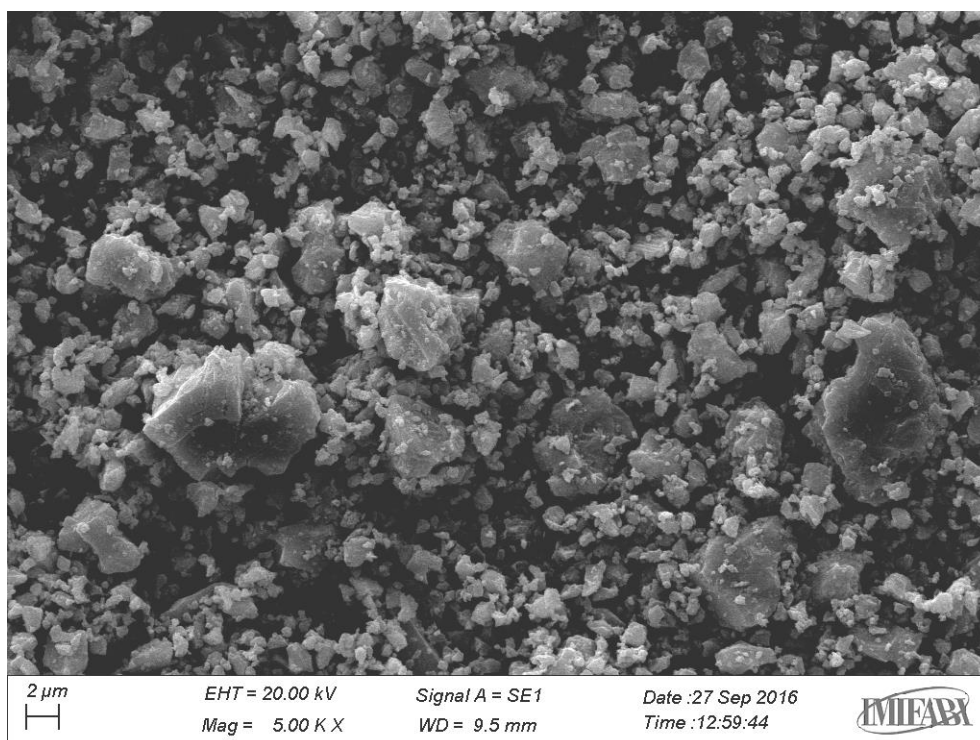


Figure 11: SEM Image of ground calcium carbonate

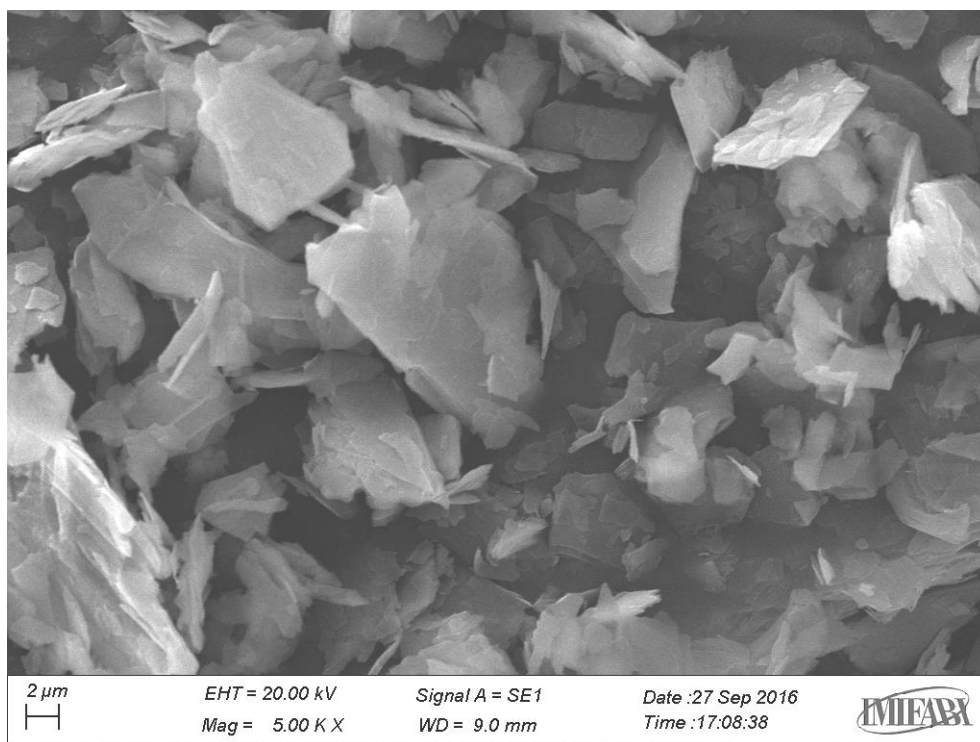


Figure 12: SEM image of micronized platy talc

A New Semi-Crystalline Styrenic Block Copolymer for Elastic Films, Fibers and Compounds

*John E. Flood, Kuitian Tan, Xavier Muyltermans, Sharman K. McGilbert, and Lana Culbert
Kraton Corporation, LLC*

Introduction

Professor Richard Register and his group at Princeton University have been working with polyethylene crystallinity in block copolymers since the late 1990s (1,2). William Gergen et. al., with the Shell Chemical Company, describe polyethylene crystallinity in styrenic block copolymers in the classic book on elastomers “Thermoplastic Elastomers” (3). A new semi-crystalline block copolymer is being developed at Kraton that takes a different approach (4). The new polymer offers polyethylene-like crystallinity but is also elastic, high modulus and strong. It is compatible with polyethylene and can be used in conjunction with polyethylene and oil to make elastic and soft compounds. In addition, unlike conventional styrenic block copolymers, the new polymers are resistant to oil and organic solvents. Other potential applications are elastic film for packaging, automotive soft touch skins, fabric coatings, yarns and nonwoven fabrics.

Experimental

The new semi-crystalline block copolymers (designated SCBC1(6 melt flow rate(MFR)) and SCBC2 (38 MFR) in this study) were made at the Kraton Semi Works plant in Belpre, Ohio. Conventional anionic polymerization chemistry was used to make both polymers. The viscosity-shear rate data were generated on a Dynisco model LCR 7000 capillary rheometer. A TA Instruments model DSC Q20 was used to determine the polymer glass transition temperatures (T_g), melting temperature (T_m), crystallization temperature and heat of fusion. Film samples were made on a 25 cm wide single layer Davis-Standard Killian cast film line. Film mechanical testing was done on an Instron model 4465. ASTM D638 test conditions were used to evaluate the film mechanical properties.

Polymer Descriptions, Rheology and Mechanical Properties

Both SCBC polymers are relatively low molecular weight, low diblock, triblock copolymers. The diblock concentration is less than 10 wt % and the melt flow (230 ° C @ 2.16kg) is between 3 and 7 g/10 min for SCBC1 and 25 to 40 g/10min for SCBC2; refer to Table 1 for a comparison to other conventional poly(b-styrene-b-ethylene-r-butylene-b-styrene) or SEBS styrenic block copolymers. Typical melt processing temperatures are between 220 ° C and 250 ° C. Figures 1 and 2 are DSC scans for SCBC1 and SCBC2 respectively. Note both scans are similar because, except for molecular weight, the molecule designs are similar. There is a distinct melting peak close to 100 ° C and a crystallization peak close to 70 ° C. A typical heat of fusion for these polymers is between 22 to 30 J/g, with percent crystallinity ranging from 8 to 10 wt%. Percent crystallinity in just the crystalline block is between 25 and 30 wt%. As a comparison, selectively hydrogenated SEBS styrenic block copolymers (38-40 wt % butene in the midblock)

have a broad, not well defined, melting endotherm with a crystallization peak between -5 to 0 ° C; see Figure 3 for a DSC scan of MD1653 (5).

Figure 4 is a plot of viscosity versus shear rate for MD1653 (22 MFR), G1652 (2 MFR) and the new SCBC polymers. SCBC1 was designed for compounds and films and has a similar viscosity/shear rate response as G1652 which is used in compounds and coatings. SCBC2 was designed for elastic fiber applications and high flow compounds and has a similar to viscosity/shear rate response as MD1653. All four polymers are melt processable and can be used as standalone polymers.

Table 2 lists the melt cast film tensile properties for the SCBC polymers, G1652 and MD1653. Even though SCBC1 is similar viscosity to G1652, its film properties are more equal biaxial; refer to the 100%, and 300% moduli in Table 2. SCBC1 is probably closer to a single phase melt than G1652 (two phase melts exist above the T_g of polystyrene because of strongly phase separated styrene domains) at the typical process temperatures used to make the films (240 ° C for SCBC1 and 265 ° C for G1652). Both MD1653 and SCBC2 have almost equal biaxial properties because they are single phase melts at typical film processing temperatures (240 ° C for SCBC2 and 260 ° C for MD1653). From a modulus perspective, it probably better to compare the properties of SCBC1 and SCBC2 to MD1653 because all three films have almost equal biaxial mechanical properties. Consequently, except for the 500 % modulus, it interesting to note the SCBC polymers have similar moduli to a 30 % styrene SEBS polymer (MD1653) but lower tensile strength than either MD1653 or G1652. However, even though the tensile strength is lower for the SCBC polymers, the tensile strength is still reasonable for most applications. The 500% modulus is lower for the SCBC polymers because they do not appear to have the same strain hardening mechanism as the SEBS polymers. Lastly, the elongation to break for the SCBC polymers is equivalent to conventional SEBS polymers; refer to Table 2.

Table 3 lists the elastic properties for the polymers in this study. Note the significantly better elasticity of the SCBC polymers compared to MD1653 and G1652; refer to the tensile set and recovered energy in Table 3. MD1653 and G1652 can and are used in many elastic applications and compounds because they are typically compounded with oil and other non-elastic, but compatible, polymers to manipulate their polystyrene domain structure into a domain structure that is more elastic. Similarly, the SCBC polymers can be compounded with oil and compatible polymers to improve their performance for certain applications; refer to the presentation for more details.

Summary

SCBC polymers are a new class of block copolymers being evaluated by Kraton (6). Because of their crystallinity, they are more resistant to oil and organic solvents than conventional SEBS polymers. At the same time, they are elastic and strong like conventional SEBS polymers and can be easily melt processed into compounds, films and fibers.

References

1. D.J. Quiram, G.R. Marchand and R. A. Register, “Crystallization of Asymmetric Diblock Copolymers from Microphase Separated Melts, *Macromolecules*”, **1997**, 30(16), pp 4551-4558.
2. Y.L. Loo, A.J. Ryan, and R. A. Register, “Modes of Crystallization in Block Copolymer Microdomains: Breakout, Templated, and Confined”, *Macromolecules*, **2002**, 35(6), pp 2365-2374.
3. N. R. Legge, G. Holden, and H.E. Schroeder, “Thermoplastic Elastomers”, Chapter 14, *Hanser Publishers*, **1987**
4. K. Tan and J. E. Flood, “ New Styrenic Block Copolymers”, The 2016 Fall Fiber Society meeting, Cornell University, **2016**
5. John E. Flood and Bing B. Yang, A New Styrenic Block Copolymer for Polyolefin Modification, Coatings and Adhesives, *Society of Plastics Engineers*, Annual Technical Conference, Anaheim, California **2017**.
6. Contact Lana Culbert at lane.culbert@kraton.com, 713-724-3646 for more information.

Table 1. Polymer Descriptions. A comparison of the semi-crystalline block copolymers to commercially available styrenic block copolymers.

Polymer/ Property	Molecule Design	MFR (230°C@2.16 kg) (g/10 min)	Polystyrene Concentratio n (wt. %)	Diblock Concentratio n (wt. %)	Shore A Hardness	Polymer Form
G 1652	SEBS, Normal Vinyl	2	30	< 10	73	Crumb
MD1653	SEBS Normal Vinyl	20 - 28	30	<10	73	Dense Pellet
SCBC1	Semi- Crystalline Block Copolymer	4-6	25	<10	63	Dense Pellet
SCBC2	Semi- Crystalline Block Copolymer	22-40	25	<10	N/A	Dense Pellet

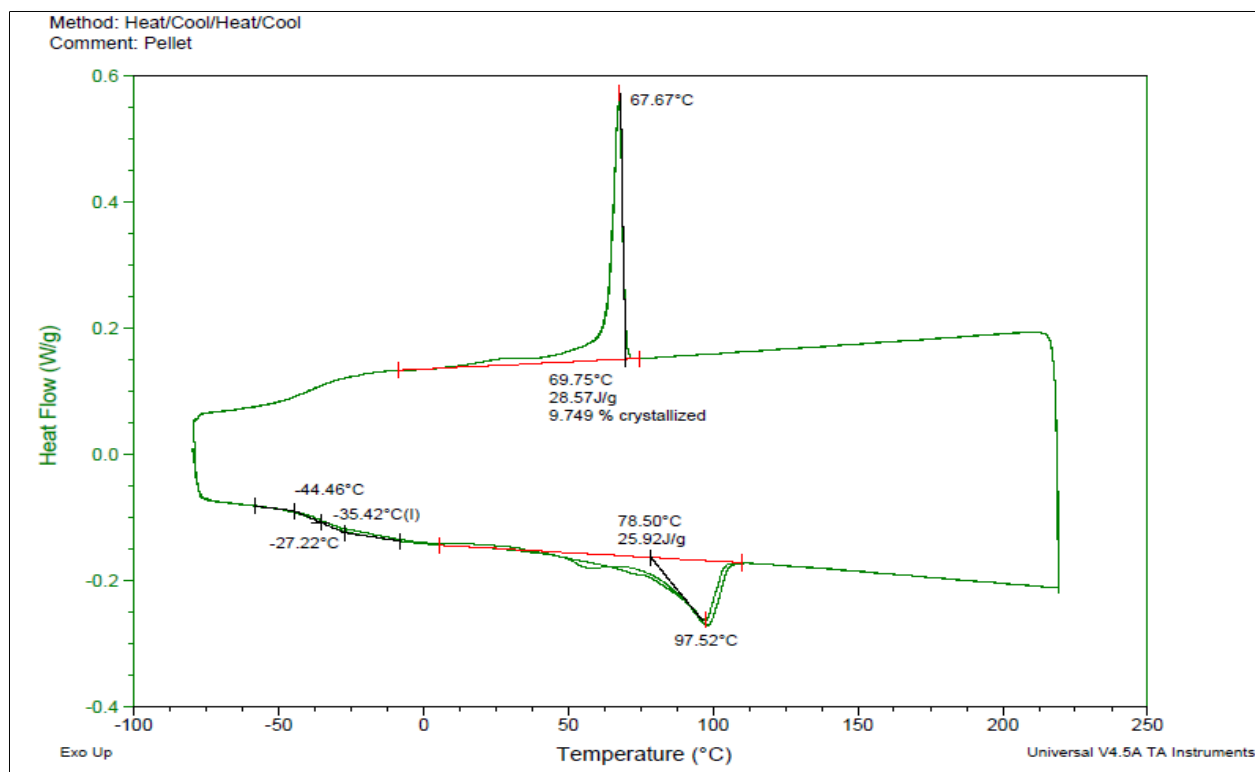


Figure 1. DSC Analysis for SCBC1.

Method: Heat/Cool/Heat
Comment: Pellet

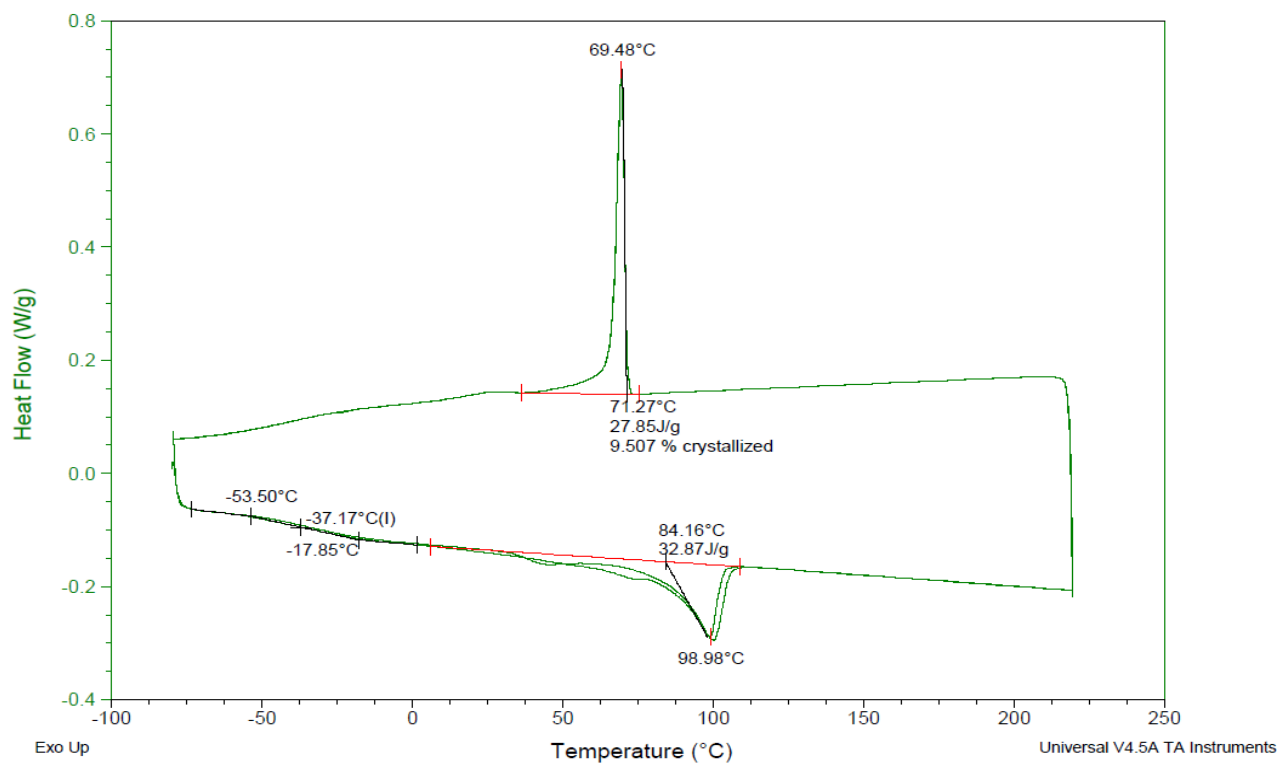


Figure 2. DSC Analysis for SCBC2.

Method: Heat/Cool/Heat/Cool

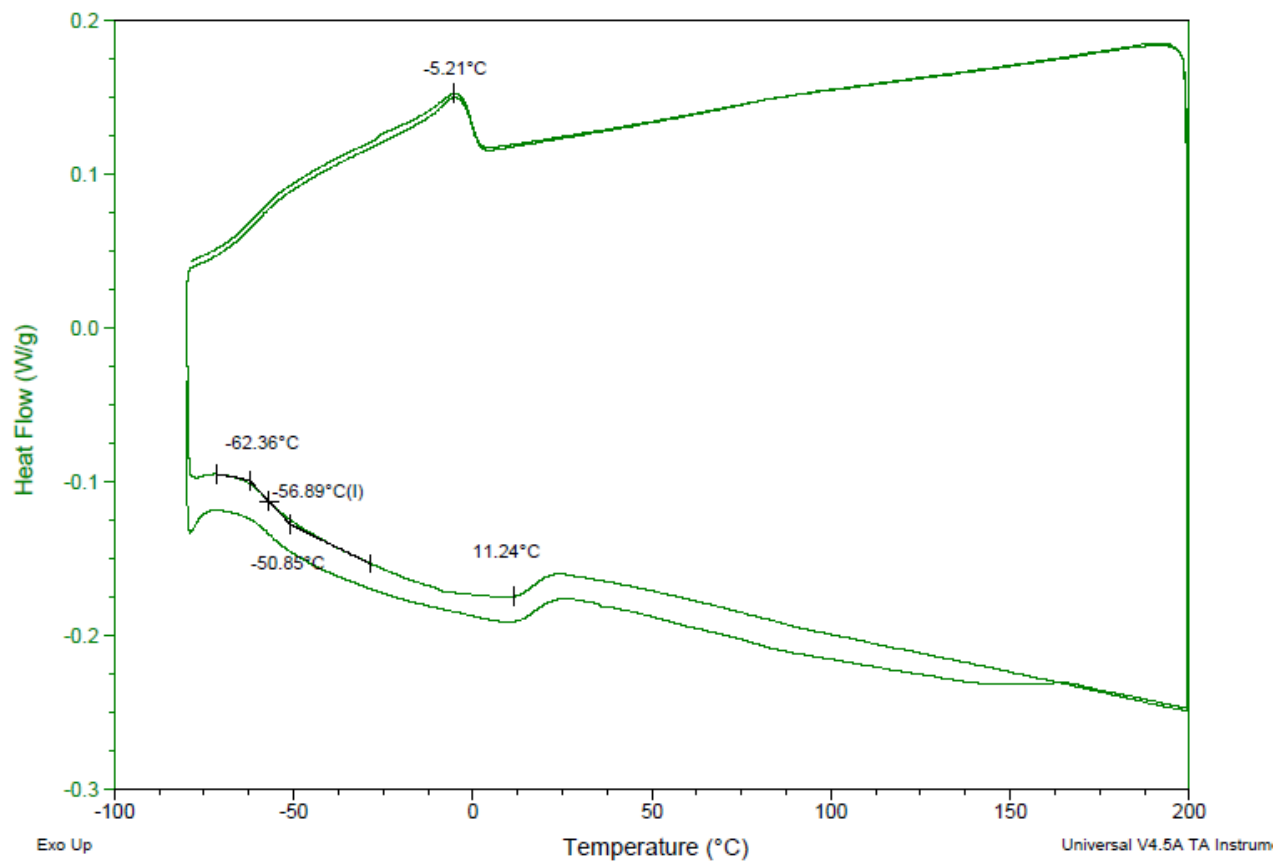


Figure 3. DSC Analysis for a Typical Normal Vinyl SEBS (MD1653).

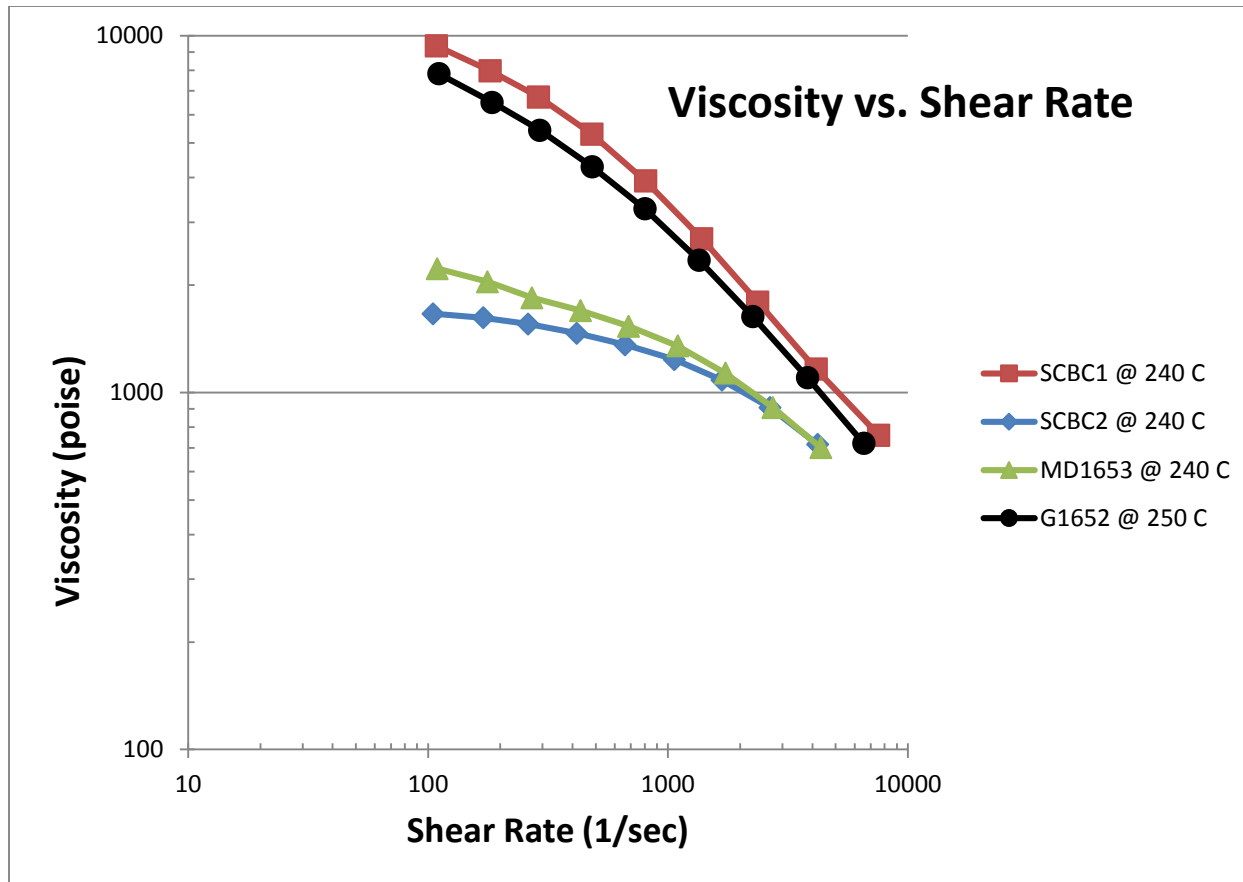


Figure 3. Viscosity vs. Shear Rate for SCBC1 and SCBC2 Compared to G1652 and MD1653.

Table 2. SCBC Mechanical Properties Compared to Commercial MD1653 and G1652 Grades. MD is the machine direction and TD is transverse direction. MD1653 was melt cast at 260° C and G1652 was melt cast at 266° C. The SCBC1 and SCBC2 films were melt cast at 240° C.

Polymers	MD1653		G1652		SCBC1		SCBC2	
Film Direction/Property	MD	TD	MD	TD	MD	TD	MD	TD
100% Modulus, MPa	2.7	2.6	4.9	1.6	3	2.7	3.1	3
300% Modulus, MPa	6.6	5.8	8.4	3.6	6	5.4	6	5.7
500% Modulus, MPa	31	23	17	11	11	9.7	7.3	7.1
Ultimate Stress, MPa	40	38	42	37	19	20	8.3	7.9
Elongation at Break, %	560	620	760	770	610	640	760	770

Table 3. 100 % Hysteresis Properties for Melt Cast Film.

Polymers	MD1653		G1652		SCBC1		SCBC2	
Film Direction/Property	MD	TD	MD	TD	MD	TD	MD	TD
50% Modulus load, MPa	2.2	2.1	3.7	1.4	2.1	2	2.2	2.1
50 % Modulus unload, MPa	1.2	1.1	1.7	1.1	1.6	1.5	1.7	1.6
Tensile Set, %	16	14	11	4	5.7	7.7	6.6	7.2
Recovered Energy, %	52	52	44	82	82	82	78	78

ON-LINE COMPOUNDING OF TPO BLENDS FOR LARGE PART THERMOFORMING APPLICATIONS

*Kurt A. Koppi, Sam L. Crabtree, and Todd A. Hogan
The Dow Chemical Company, Midland, MI*

ABSTRACT

An effort was initiated to explore the viability of compounding a talc-filled thermoplastic olefin (TPO) formulation directly on a sheet extrusion line. This approach would reduce cost by eliminating a separate compounding step. It was found that it is indeed possible to perform on-line TPO compounding on a sheet extrusion line. A simple single-flighted general purpose screw works as well as a high performance dual-wave screw for on-line compounding when using a talc-concentrate. The use of polypropylene-based talc concentrate is preferred over that of an elastomer-based talc concentrate as the former results in sheet with improved tensile modulus. The sag rate of on-line compounded TPO extruded sheet can also match that of pre-compounded TPO extruded sheet if one uses a polypropylene-based talc concentrate. Based on this work, it has been shown that it should be possible to reduce the manufacturing cost of TPO extruded sheet designed for large part thermoforming applications by eliminating a separate compounding step and blending the formulation directly on a sheet extrusion line through the use of a highly-filled talc concentrate.

INTRODUCTION

TPO formulations typically consist of olefin-based thermoplastics, elastomers, and fillers which are blended in twin-screw extruders, continuous mixers, or batch mixers. The focus of this work was to explore the viability of compounding such a formulation directly on a sheet extrusion line. This would reduce cost by eliminating a separate compounding step. In this study, TPO sheet samples were prepared via on-line compounding on a sheet line equipped with a single screw extruder. Experiments were performed with three different screw designs. To further understand on-line compounding of this formulation, experiments were also performed on a shear refiner to study the influence of applied shear stress on mixing quality. The mechanical properties and thermoforming behavior of the TPO sheet samples prepared in this study were quantified and compared to TPO sheet prepared from the same formulation compounded on continuous mixer.

EXPERIMENTAL

Materials: This on-line compounding investigation was performed using a TPO formulation developed for large part thermoforming applications. This TPO formulation consists of 55% polypropylene (PP), 15% polyolefin elastomer

(POE), and 30% talc. The PP used in this formulation is an impact copolymer PP with a 0.5 dg/min melt flow rate (230°C/2.16kg) and the POE used in this formulation is an ethylene-octene copolymer with a 0.868 g/cc density and 0.5 dg/min melt index (190°C/2.16kg).

It would be difficult to compound raw talc on a single-screw extruder sheet line so talc was added as a talc concentrate. Two different talc concentrates were prepared. The first talc concentrate (60% talc) used the PP resin as the carrier resin and the second talc concentrate (67% talc) used the POE resin as the carrier resin. Each of these talc concentrates was prepared on a CP-250 Farrel Continuous Mixer (FCM) using a set point temperature of 210°C.

One of the main questions to be answered in this investigation was to identify which concentrate was best suited for on-line compounding. The main benefit of the first approach is that the talc starts out in the most desirable phase for the TPO formulation – the PP phase. The main benefit of the second approach is that material handling would be easier because one would only need to add two components into the hopper of the single-screw extruder of the extrusion sheet line (talc concentrate #2 + PP) whereas the first approach would require the addition of three components (talc concentrate #1 + PP + POE).

Shear Refiner: It was hypothesized at the beginning of this project that talc would be dispersed well in the talc concentrate and that only distributive mixing of the TPO formulation components would be required at the sheet extrusion line. In the event that this hypothesis was not correct, the level of dispersive mixing required from the single-screw extruder would be identified through the use of a shear refiner (1,2). A sketch of this instrument is presented in Figure 1. It is essentially a decoupled Maddock-type mixer (3) that is fed by a combination of a single-screw extruder and gear pump. This polymer processing assembly allows one to vary the speed of the mixer while holding the output rate of the system constant. Thus, with a shear refiner it is possible to vary the applied shear stress by simply adjusting the rotor speed of the mixer while maintaining a constant output rate.

A significant amount of shear stress is generated during the melting operation of the single-screw extruder that feeds the Maddock-type mixer of the shear refiner. The shear stress developed by the Maddock-type mixer is an additional shear history that can be used to increase the level of dispersive mixing that the material experiences beyond

what is generated in the single-screw extruder. If indeed the level of dispersive mixing developed by the single-screw extruder was not sufficient, the level of dispersive mixing could be adjusted by varying the speed of the Maddock-type mixer of the shear refiner.

The shear refiner was operated with a set point temperature of 210°C and the rotor speed was varied from 20 to 180 rpm in 40 rpm steps. Pellets were collected at each rotor speed and the resulting TPO was characterized. Characterization included rheological testing, mechanical testing (performed on injection molded test specimens), and microscopy. As will be described later, these experiments revealed that the level of dispersion mixing was not altered by rotor speed which indicated that the hypothesis regarding the dispersion of the talc in the talc concentrate was indeed adequate for preparing TPO through on-line compounding on a sheet extrusion line.

Sheet Extrusion: Based on the results of the shear refiner experiments, it seemed clear that dispersive mixing would not be an issue regarding the on-line compounding of the TPO formulation. It was not known, however, what degree of distributive mixing would be required to mix properly the blend. Distributive mixing was investigated by blending the TPO formulation on a sheet line using three different screws: a simple single-flighted screw, a screw containing a single-pass mixing blister ring, and a high performance double wave screw. The sheet line was equipped with a 2.5 inch diameter 30:1 L/D vented single-screw extruder and a gear pump, a coat hanger style sheet die, and a three-roll stack. Each of the screws used for these experiments was a two-stage screw but vacuum was not pulled on the vent.

Extruded sheet was fabricated from three different materials. Two of these were the same blend formulations previously described for the shear refiner experiments. The third was a pre-compounded TPO with the same overall composition. This pre-compounded material was prepared on the same FCM described earlier. Sheet was extruded at two different rates: 45 and 91 kg/hr. The extruder temperature profile was maintained at 210/220/230°C and the sheet die temperature was maintained at 230°C. The first roll was maintained at 140°C while the second and third rolls were maintained at 220°C. Ten sheet samples with dimensions 0.5 cm x 61 cm x 91 cm were fabricated for each material at both extrusion rates. The machine direction mechanical properties of these sheets were measured through Izod and instrumented dart impact as well as flexural and tensile testing. Sheet orientation was also quantified through sheet shrinkage measurements.

Thermoforming: The main thermoforming characteristic quantified in these experiments was sheet sag performance. Sheet samples were thermoformed on a ZMD International Model V223 shuttle thermoformer. Each sheet was placed

in the clamp frame of the thermoformer, and rigidly clamped on all four sides. Next, the clamped sheet was indexed into the heat station of the thermoformer, where the sheet was heated by absorption of infrared radiation supplied by quartz infrared radiant heaters. As the temperature of the sheet increased, the initially flat sheet began to sag under its own weight.

The amount of sag was limited by the equipment configuration and ultimately on the final part quality. The vertical distance of the sheet sag from the initial position in the clamp frame was measured using an infrared profiling scanner (light curtain) that was positioned to detect sheet sag at the middle of the oven. The time required for the sheet to sag from 57 mm below its initial position to 108 mm from its initial position was recorded. Sag rate was determined by dividing the change in the vertical distance of the sheet by the time required for the change in height. The sheet was removed from the oven when the sag reached approximately 108 mm from its initial position and moved to the form station.

The sheet surface temperature on the bottom side of the sheet was measured at the end of the heat cycle using an infrared pyrometer. Once the heated sheet was positioned in the form station, a vacuum box contacted the sheet from below. Vacuum was applied to draw the sheet into the vacuum box and pre-stretch the sheet. A machined aluminum mold was lowered into the top of the pre-stretched sheet and vacuum applied to draw the extended sheet against the mold while the vacuum was simultaneously released from the vacuum box. Details of the mold have been published previously (4). The part was formed and allowed to cool and was ultimately removed from the clamp frame.

RESULTS AND DISCUSSION

Shear Refiner: The shear refiner experiments revealed that varying the amount of applied shear stress experienced by the blend in the melt state did not significantly alter properties of the TPO blend. The viscosity curves of TPO prepared from the PP/talc concentrate formulation on the shear refiner at high and low rotor speeds were nearly identical (Figure 2). The curves overlay perfectly at high shear rates and only a slight difference was observed at low shear rates. This slight difference was likely due to polymer degradation when subjected to a high rotor speed in the shear refiner – an effect which would be more pronounced at low shear rate than high shear rate.

The shear refiner experiments also showed that the choice of talc concentrate type influenced the rheological properties of the TPO formulation (Figure 3). The melt flow rates (MFR) of the TPO formulations prepared from the PP/talc concentrate were higher than those prepared from

the POE/talc concentrate across the full range of rotor speeds explored. It is believed that this difference was due to the PP carrier resin experiencing a greater degree of degradation during the FCM compounding of this concentrate than that experienced by the POE carrier resin during the FCM compounding of the POE/talc concentrate. For each given TPO recipe, no clear trend in MFR with rotor speed was observed.

Similarly, no clear trends in mechanical properties with rotor speed were observed for each of the two TPO recipes. However, the flex modulus (Figure 4) of TPO samples prepared from PP/talc concentrates was higher than those prepared from POE/talc concentrates – despite the speculation that the PP/talc concentrate experienced more degradation during its preparation than the POE/talc concentrate. It is believed that this difference in flex modulus was due to the location of talc in the resulting TPO samples. In order to maximize stiffness, one would want all of the talc to be dispersed in the PP phase of the TPO with no talc located in the POE phase. The contribution that talc particles would make to the stiffening of the TPO formulation would be significantly diminished if the talc was buried within a soft elastomer phase. For TPO samples prepared from the POE/talc concentrate, all of the talc was located within the elastomer at the beginning of the blending process so it stands to reason that the TPO blends prepared via this route would tend to have more talc embedded in elastomer phases than one would achieve using a PP/talc concentrate.

A similar explanation is used to explain the tensile yield data (Figure 5) collected from the shear refiner TPO samples. Again, no trend with rotor speed was observed but the TPO samples prepared from the POE/talc concentrate exhibit a larger tensile yield than those prepared from the PP/talc concentrate. It is also believed that this difference was caused by a difference in talc distribution across the PP and POE phases of the TPO. Samples prepared using the PP/talc concentrate likely contained a high concentration of talc particles (i.e. defects in the stiff phase) which caused yielding to occur at a lower applied tensile stress than that experienced by samples prepared using the POE/talc concentrate.

No clear trends were observed in the Izod impact data (Figure 6) collected from the shear refiner TPO samples: neither with respect to rotor speed nor talc concentrate type. This behavior could be due to two different competing effects counterbalancing each other. TPO samples based on the PP/talc concentrate yielded at a lower stress (due to an increased population of talc defects in the PP phase) but the elastomer phase particles are better impact modifiers (due to a decreased population of talc defects in the elastomer phase) whereas just the opposite

would be the case with TPO samples based on the POE/talc concentrate.

Close inspection of the transmission electron microscopy (TEM) images prepared from the TPO shear refiner samples indicate that the talc particles were more likely to be imbedded in the elastomer phase for the case of samples prepared using the POE/talc concentrate (Figure 7). It was also observed (Figure 8) that rotor speed did not significantly alter TPO morphology. Such a result was no surprise considering that there were no trends observed between rotor speed and mechanical performance for the TPO samples prepared on the shear refiner.

Sheet Extrusion: Unlike what was found regarding Izod impact of injection molded samples prepared from the shear refiner TPO samples, the type of talc concentrate used to prepare extruded sheet TPO samples did exhibit a slight effect on instrumented dart impact performance (Figure 9). Sheet samples prepared using the POE/talc concentrate exhibited a slightly lower total energy to break than those prepared using PP/talc concentrate and those prepared from pre-compounded TPO. The insensitivity of impact performance to talc concentrate type exhibited by the shear refiner samples could be a result of the extra mixing history associated with the injection molding of the shear refiner test specimens. The instrumented dart impact test specimens prepared from the extruded sheets did not undergo any addition mixing – test specimens were simply cut from the extruded sheets. It should also be noted that no trend in instrumented dart impact performance was observed with respect to screw design or extrusion rate.

A significant influence of talc concentrate type on TPO sheet modulus was observed (Figure 10). Similar to what was seen for the injection molded shear refiner TPO samples, a lower modulus was exhibited by the TPO sheet prepared using the POE/talc concentrate whereas that prepared using the PP/talc concentrate was similar to that prepared from pre-compounded TPO. The root cause of this behavior is again believed to be a result of the relative distribution of talc in the PP and elastomer phases of the TPO samples. As was the case with instrumented dart impact, no influence of screw design or extrusion rate on the modulus of TPO extruded sheet was observed.

An influence of extrusion rate on ultimate tensile strength was observed (Figure 11). TPO sheet fabricated using a fast extrusion rate exhibited lower tensile strength than that fabricated using a slow extrusion rate. It is believed that this behavior was due to a difference in orientation developed in the sheet as a function of extrusion rate. It was observed (based on shrinkage measurements) that sheet extruded at a high extrusion rate possessed a lower amount of orientation (17.6% shrinkage) than sheet fabricated at a slow extrusion rate (22.3% shrinkage). All things being

equal, a faster extrusion rate typically causes an increase in sheet orientation. The opposite effect exhibited by these sheets is thought to be due to a difference in extrudate temperature caused by viscous heating of the extrudate. It should also be noted that the tensile strength of the extruded TPO sheet prepared using the POE/talc concentrate was slightly lower than that of sheet prepared using the PP/talc concentrate and sheet prepared from pre-compounded TPO. No influence of screw design on tensile strength was observed.

An influence of talc concentrate type on yield behavior of extruded TPO sheet was observed. Elongation at yield (Figure 12) of TPO sheet prepared using POE/talc concentrate was significantly greater than that of TPO sheet prepared using PP/talc concentrate and sheet prepared from pre-compounded TPO but yield strength showed the opposite trend (note: for these materials the yield strength was the ultimate tensile strength). Both sets of behaviors are believed to be due to differences in talc distribution across the TPO polypropylene and elastomer phases. It should be noted that the yield strength behavior dependence on talc concentrate type was the opposite of what was observed from the injection molded shear refiner TPO samples. It is believed that this difference may be influenced by sheet orientation as it can also be seen that yield strength of extruded TPO sheet reduced with increased extrusion rate (Figure 11). No influence of screw design yield behavior was observed.

Thermoforming: Since no influence of screw design on mechanical performance was observed, it was decided to only perform a thermoforming analysis of TPO sheet extruded with the simple single-flighted screw design. The results of the sag behavior of the TPO sheets in the thermoforming oven are presented in Figure 13. Sheet sag rate is observed to be influenced by the extrusion rate used during the fabrication of the sheet. For pre-compounded TPO sheet, sag rate of the sheet fabricated at a fast rate is faster than that fabricated at a slow rate. The opposite trend is observed for the on-line compounded TPO sheets. For a given extrusion rate, the on-line compounded TPO sheet prepared from the POE/talc concentrate sags at a faster rate than that prepared from the PP/talc concentrate. This difference is believed to be due to differences in talc localization between these two different types of TPO sheet. Sheet surface temperatures were monitored during the sag measurements and it was observed that sheet temperature was consistent for all the samples.

For large part thermoforming applications, a slow sheet sag rate is desirable as a means to maintain uniform thickness across the formed part. Sheet sag of on-line compounded TPO sheet prepared from the PP/talc concentrate nearly matches that of the pre-compounded TPO sheet for the case of a fast sheet extrusion rate.

Likewise, these TPO sheets exhibited less thinning in the corners during the forming operation as compared to the on-line compounded TPO sheet prepared with the POE/talc concentrate which is also as a desirable characteristic.

CONCLUSIONS

It was possible to match the mechanical performance of pre-compounded TPO formulations through the use of on-line compounding. A simple single-flighted general purpose screw works as well as a high performance dual wave screw for on-line compounding. The use of a PP-based talc concentrate is preferred over that of a POE-based talc concentrate as the former resulted in sheet with improved tensile modulus. The sag rate of on-line compounded TPO extruded sheet can also match that of pre-compounded TPO extruded sheet when a PP/talc concentrate is used. Based on this work, it has been shown that it should be possible to reduce the manufacturing cost of TPO extruded sheet designed for large part thermoforming applications by eliminating a separate compounding step and compounding the formulation directly on a sheet extrusion line through the use of a highly filled talc concentrate.

ACKNOWLEDGEMENT

Thanks are given to Mark Spalding for insightful comments regarding extruder mixing as well as Paul Vantol, Dave Headley, Gary Poltorak, Andy Schlader, Robbie Samson, and Bob Cieslinski for help in performing the experiments described in this paper.

REFERENCES

1. G.A. Campbell and M.A. Spalding, "Analyzing and Troubleshooting Single-Screw Extruders," Hanser Publications, Munich, 2013.
2. Chung, C.I., Powell, T.M., and Werling, C.L., *SPE-ANTEC TECH. Papers*, **44**, 76 (1998).
3. X. Sun, Q. Gou, M.A. Spalding, T.W. Womer, and N. Uzelac, *SPE-ANTEC TECH. Papers*, **62**, 856 (2012).
4. T.A. Hogan, *et al.*, *SPE-ANTEC TECH. Papers*, **57**, 1127 (2007).

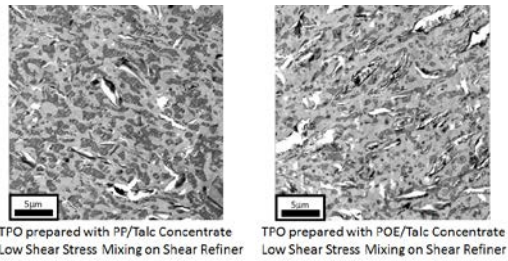


Figure 7: TEM of Shear Refiner Mixed TPO: comparison of two talc concentrates.

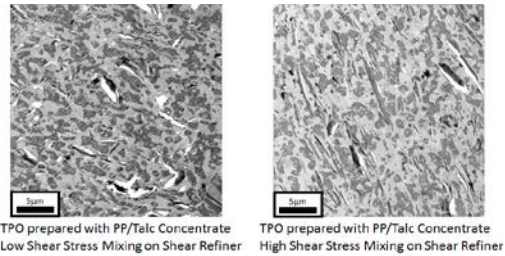


Figure 8: TEM of Shear Refiner Mixed TPO: influence of applied shear stress.

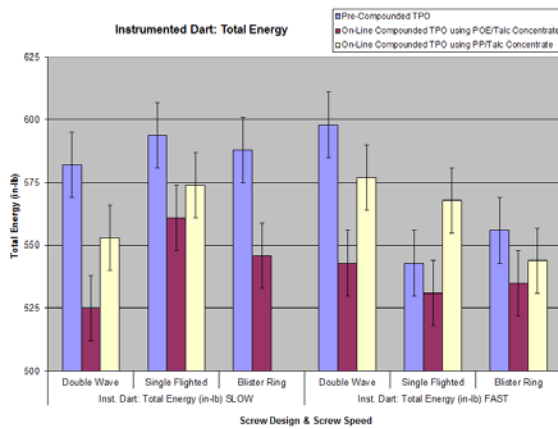


Figure 9: TPO Sheet – Instrumented Dart Impact.

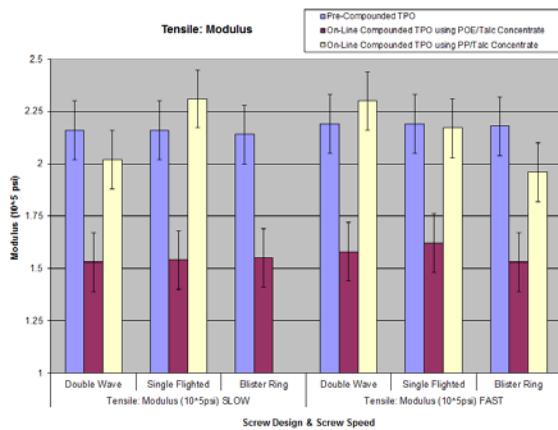


Figure 10: TPO Sheet – Tensile Modulus

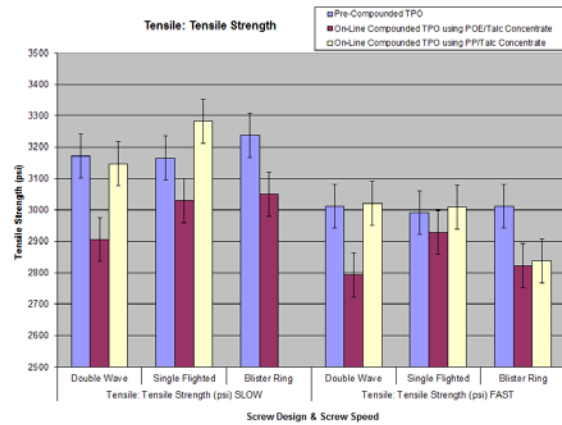


Figure 11: TPO Sheet – Tensile Strength.

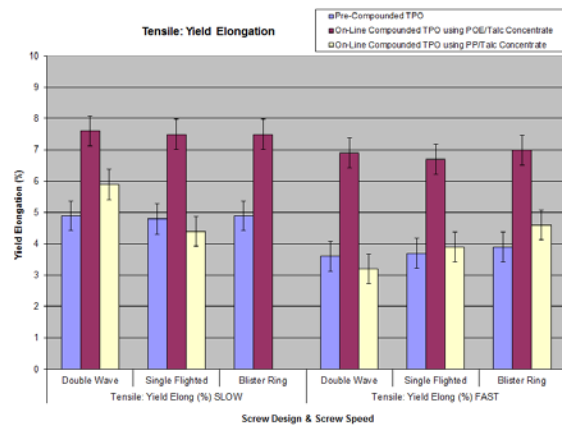


Figure 12: TPO Sheet – Tensile Elongation at Yield.

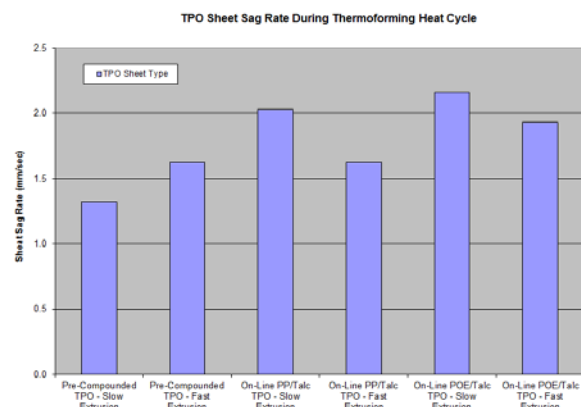


Figure 14: TPO Sheet Sag Rate

POLYOLEFIN DISPERSIONS FOR AUTOMOTIVE INTERIOR APPLICATIONS

*Amit K Chaudhary and Parvinder Walia, The Dow Chemical Company, Midland, MI
Sarah Wakumoto, Colorado State University, CO*

Abstract

HYPOD™ aqueous polyolefin dispersions represent a new class of waterborne polymeric material produced by a proprietary mechanical dispersion process utilizing BLUEWAVE™ Technology. These dispersions are commercially available for use in various coating applications, and have characteristics similar to other water-based dispersions/emulsions (e.g., 40 to 50% solids, particle sizes 0.15 to 2.5 μm , viscosities from 300 to 3500 cP, and pH ranging from 7 to 11). With a wide array of olefin chemistries and crystallinities available from Dow, the polyolefin dispersion (POD) composition can be tailored to a specific application and performance requirements. Experimental POD dispersions have been developed for automotive interior applications, targeting soft skins and other automotive interior applications. The drivers for these applications are light weight, lower emissions, and potential recyclability. In addition, these skins show direct adhesion to polyurethane foams without any pretreatment. These dispersions can be tailored to fit various processing technologies – spray, cast and extrusion. This paper will provide a summary of these unique PODs tailored for the above processes.

Introduction

Traditionally, polyolefins have been available as pellets which are processed by conventional thermoplastic processes such as extrusion, thermoforming, injection molding, and blow molding. The lack of a viable emulsion polymerization process for the production of polyolefins has prevented the availability of these polymers in a waterborne emulsion form, suitable for use in coatings, binders, adhesives, and other applications where emulsion polymers are typically used. BLUEWAVE™ Technology is Dow's proprietary high-shear mechanical dispersion process technology [1, 2] that enables the production of waterborne dispersions of traditional thermoplastic polymers and elastomers, not possible via conventional emulsion polymerization process. The resulting dispersion has a narrow particle size distribution (approximately 1 μm) and solids content of up to 60 wt%. Low surfactant content enables customers to minimize surfactant effects, and maintain a very high level of product performance. When applied to a heated substrate, the water evaporates, forming a coating that is thin and cost effective for a variety of applications. These dispersions when applied to

various substrates offer the exceptional characteristics of polyolefins, including water and chemical resistance, heat sealability, thermoform ability (embossing), adhesion to polyolefin substrates, low temperature flexibility, and others. This technology permits the use of polyolefins in a wide range of new applications including coatings, sealants, binders, adhesives, and foams.

Aqueous polyolefin dispersions have the potential to be utilized for a variety of automotive applications such as soft skins, artificial leather, adhesives, and carpet binders. There are several methods to make soft skins for an automotive interior article, such as an instrument panel, door panel, console, glove compartment cover, and others. Soft skins are used in automotive interior applications for superior touch/feel/haptics. Positive thermoforming, negative thermoforming, slush molding, and spray coatings are four major processes used to make skins. Slush molding and spray processes offer the most design freedom and provide the ability to do complex geometries and fine grain detail (can even imitate stitching). Until recently, polyvinyl chloride (PVC) was the material of choice for interior skins, and is ideally suited for slush molding. However, PVC formulations suffer from migration and volatilization of the plasticizers over time, and this leads both to physical property changes during aging and fogging of the car window glass. PVC also suffers from being heavier than alternative materials. This is an important consideration in the current design of automobiles with the emphasis on lighter materials to reduce the overall weight of the vehicle and thus increase fuel efficiency. Additionally, the low temperature ($-40\text{ }^{\circ}\text{C}$) ductility, and air bag deployment, is an issue with PVC, especially maintaining ductility with time (and heat aging).

Alternatives to PVC include thermoplastic polyurethanes (TPU), thermoplastic polyolefins (TPO), and polyolefin elastomers (POE). TPU has good scratch and mar properties and better low temperature properties than PVC, but aromatic based TPUs have poor ultraviolet (UV) light resistance. Aliphatic isocyanates can be used to prepare TPUs having good UV light resistance but at a significant cost penalty.

Blends of polypropylene (PP) and a polyolefinic rubber, referred to as thermoplastic polyolefin (TPO), is a good alternative [3, 4]. TPO possesses better ductility than PVC. Moreover, it retains its ductility over time since it does not contain any low molecular weight plasticizers, as

does PVC. TPO performs better in comparison to PVC in interior automotive applications. TPO is less expensive as compared to TPU.

Polyurethanes (PU) have been the resins of choice for spray processes. A polyurethane reaction mixture is sprayed onto a mold surface and allowed to cure to produce the skin layer. For PU materials, volatile organic compounds (VOCs) are released and scrap is not recyclable. Further, polyurethane spray process equipment requires complex mixing capabilities as well as the need for solvent flushing.

The polyolefin spray skin approach offers the following advantages over a PU spray process:

- Lighter weight – lower density as compared to PU. Also potential of thin gauging.
- Lower VOCs – aqueous polyolefin system.
- Recyclability - scrap and captured overspray could be recycled in-house (it's a thermoplastic elastomer).
- Eliminate solvent flush needed for PU.
- Simplified process with a single component system with no mixing and curing requirements.

Materials and Methods

An olefin block copolymer (OBC) is used along with ethylene acrylic acid copolymer (EAA) based dispersing agent to produce a polyolefin dispersion using the proprietary BLUEWAVE™ Technology (Figure 1). Material properties of the polymers (supplied by The Dow Chemical Company) used in this study are presented in Table 1. The OBCs used were soft and covered a Shore A hardness range of 60 to 85.

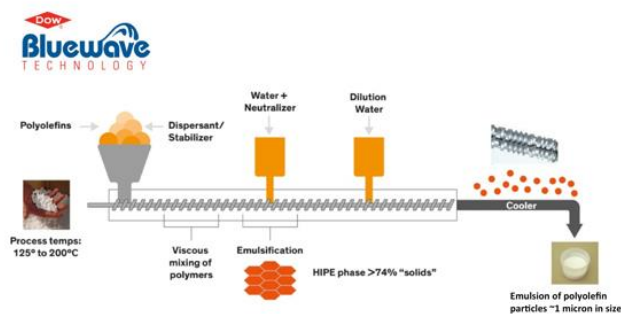


Figure 1. BLUEWAVE™ Technology.

The hydroxyethyl cellulose (HEC) based thickeners used in this study (supplied by The Dow Chemical Company) were:

- (a) CELLOSIZETM QP 15000H (medium molecular weight cellulosic polymer)

- (b) CELLOSIZETM QP 100MH (high molecular weight cellulosic polymer)

Table 1. Raw material properties.

Materials	Material Properties	Flow Rate, g/10 min (1)	Density, g/cm ³
OBC-1	Shore A = 83	5.0	0.887
OBC-2	Shore A = 60	5.0	0.866
EAA Copolymer	20.5 wt% acrylic acid content	300	0.958

(1) 2.16 kg @ 190 °C

Methods used for characterization of the various physical properties of the polyolefin dispersion are described in Table 2.

Table 2. Characterization methods for polymer dispersion.

Measurement	Instrument Used	Condition
Particle Size	LS 13 320 Beckman Coulter particle size analyzer	Test done with dilute solution of sample
Viscosity	Brookfield viscometer	RV2, 50 rpm
Solids	Sartorius moisture analyzer	1 g sample at 120 °C

Results and Discussion

The physical properties of the aqueous dispersion produced using the BLUEWAVE™ Technology dispersion process is presented in Table 3 and the particle size distribution is presented in Figure 2.

Skins were made by spraying the dispersions with a hand held pneumatic spray gun on a 5" x 5" grained tool (Figure 3a) that was pre-heated to 80 °C in a convection oven. The tool was then placed in an oven to remove the excess moisture. Figure 3b shows the quality of the grain in the skins produced using the dispersion.

Table 4 presents the mechanical properties of the two polyolefin spray skins prepared using POD-1 and POD-2 respectively along with aromatic PU skin made via spray process and PVC skin made via slush molding process. As presented in the table, the Shore A and tear strength of all the skins are comparable to each other. The tensile properties are also comparable though it is slightly lower than the PU or PVC skins. Any impact on the part performance, especially air bag deployment, is expected

to be minimal. However, this would have to be validated on an actual part.

Table 3. Physical properties of the polyolefin dispersions.

	POD – 1	POD – 2
Polymer Used	OBC-1	OBC-2
Average Particle Size (µm)	1.07	0.97
Viscosity @ 20 °C (cP)	280	250
Solids (wt%)	40.2	39.8
pH	10.4	10.2

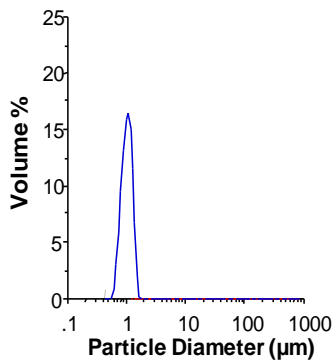


Figure 2. Particle size distribution of the polyolefin dispersion.



Figure 3. (a) Grain pattern of the tool used for producing skin, (b) grain pattern of the polyolefin skin produced.

Table 4. Physical Properties of the Polyolefin Dispersion.

Skin	Shore A	Tear Strength ISO 34-1 (N/mm)	Tensile Strength ISO 527-3 (N/mm ²)	Elongation at Break ISO 527-3 (%)
PO Spray Skin 1	73-78	24	5.0	170
PO Spray Skin 2	73-78	21	4.8	160
Aromatic PU Spray Skin	73-78	14	6.7	240
PVC Slush Skin	73-78	31	11	301

One of the key requirements of such polymeric skins is the thermal stability up to at least 100 °C. Figure 4 presents the DSC scans for the prepared OBC skin –

showing the melting point of the skin to be above 120 °C. To further confirm the thermal stability of the prepared skins, small sections of these skins were aged in an oven at 100 °C for 4 h. The skin, after heat aging, showed excellent grain retention, thereby indicating that these skins are thermally stable up to 100 °C.

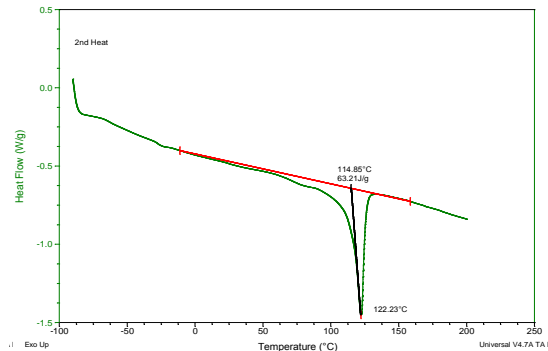


Figure 4. DSC Scan of the Polymer Skin (Tm=122 °C).

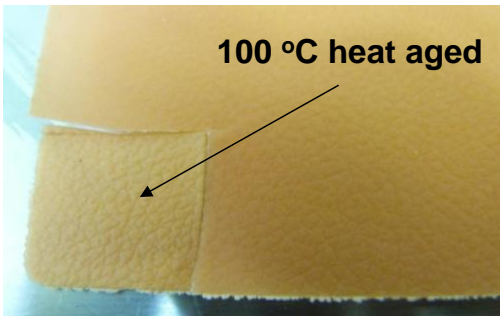


Figure 5. Excellent grain retention after thermal aging

Another critical requirement for interior skins is adhesion to PU foam. A typical instrument panel Dow foam system (NM856: prepared with PAPI-94 isocyanate and NM 858 polyol) was used to back foam these spray skins. Excellent PU foam adhesion (Figure 6) was achieved. Cohesive failure was judged visually (qualitative) based on the amount of area on skin that was covered with foam upon peeling.

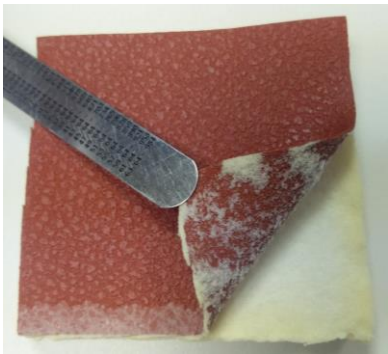


Figure 6. Cohesive Failure of the polyolefin skin and the PU foam.

Further, the possibility of the use of such aqueous dispersions was explored for its use in cast or extrusion process for making skins. Different applications have different viscosity requirements. For instance, dispersions for spray skins must be thin enough to be sprayed, yet thick enough to not drip off of a hot mold surface. Ideal viscosity for spray skins is about 100 to 1000 cP, while for cast skins, it is about 1,500 to 3,000 cP, so the dispersion can be laid onto a release paper and for extrusion process dispersions with significantly higher viscosities (15,000 to 30,000 cP) is required.

Viscosity can be tailored by either changing the dispersion formulation (e.g., solid concentration, surfactant type and concentration, etc.) or by the addition of thickeners which provides the benefit of working with one base polyolefin dispersion formulation. The later approach was investigated to test the viability of the polyolefin dispersion in cast or extrusion process. Two different hydroxyethyl cellulose based thickeners were chosen for this study (medium MW and high MW).

Small amount of the thickeners (0.5 and 1.0 wt%) were dispersed in the aqueous polyolefin dispersion using a Cowles blade mixer. The viscosity of the samples was tested after 24 h using a Brookfield viscometer at 50 rpm. The results are presented in Figure 7. Based on the data it is evident that thickeners can be used for altering the viscosity of such aqueous dispersions. This approach provides flexibility for using either spray, cast or extrusion process.

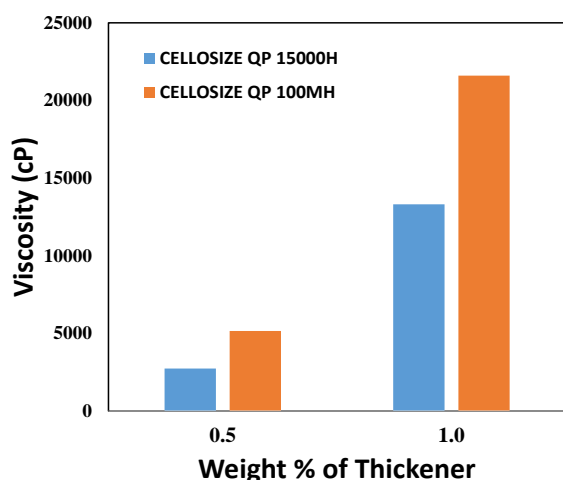


Figure 7. Effect of thickener on the viscosity of the dispersion

Conclusions

Aqueous dispersion of polyolefin elastomers prepared using BLUEWAVE™ Technology could be used to

successfully produce soft skins that can be used in the automotive interior application. The spray skins demonstrated the following features:

- Excellent grain replication
- Good haptics
- Mechanical properties comparable to other soft skin materials and technologies
- Good thermal aging under conditions seen in interior applications (100 °C).
- Direct adhesion to PU foam (typically polyolefin substrates require flaming or primers)

These dispersions can be tailored to fit various processing technologies – spray, cast, and extrusion, by addition of a thickening agent [5]. Future work will focus on further development of the dispersion for validation of OEM specs and incorporation of color/UV package required for interior applications.

™Trademark of The Dow Chemical Company ("Dow") or an affiliated company of Dow

References

1. B. Moncla, M. Kalinowski, D. Speth, C. Diehl, D. Schmidt, K. Maak, W. Liang, G. Strandburg, *Aqueous Dispersion, Its Production Method and Its Use*, US 20070292705A1 (Dow Global Technologies Inc.).
2. A. Neubauer, A. Quaranta, N. Dunchus, M. Kalinowski, G. Strandburg, K. Maak, *Dispersions of Higher Crystallinity Olefins*, US20100255207 A1 (Dow Global Technologies Inc.).
3. R. Eller Associates, "Automotive Interior Skins and Foams", pp. 1-4 to 1-11., Robert Eller Associates, November 1997.
4. S. Shah, N. Kakarala, J. Schneider, "An Overview of Advances in TPO Skin Material and Process Technology," Proceedings of TPO in Automotive '98 Conference, Novi, MI, October 1998.
5. P. Walia, A. Chaudhary, G. Klumb, *Method to Make an Elastomeric Polyolefin Skin*, WO2016148897 A1 (Dow Global Technologies Inc.).

Polypropylene Based Olefin Block Copolymers for Clear Cold Tough Application

*Jihean Lee, Colin Li Pi Shan, Ray Laakso, Lisa Madenjian, Eddy Garcia-Meitin, Michael White
The Dow Chemical Company, Freeport, TX*

Abstract

INTUNE™ Olefin Block Copolymer (OBC) builds upon Dow's proprietary catalyst chain shuttling technology. INTUNE OBC is a block copolymer that contains both polypropylene and polyethylene connected together within one polymer chain. INTUNE OBC is the ideal compatibilizer to connect and balance the properties of blends of polyethylene and polypropylene.

PE and PP each have a material advantage when used alone. PE has toughness and flexibility while PP has stiffness and clarity. With OBCs, a new balance of properties of where one no longer has to choose between toughness and clarity or flexibility and stiffness. OBC technology can provide better dispersion that this correlates to better homogeneity, less stresses, better part esthetics, and more consistent part performance. As an impact modifier, OBC technology can offer balanced solutions of clarity, impact, and flow. This study shows that INTUNE 10510 OBC offers high flow, good dispersion, good optics, and good impact and INFUSE™ 9817 OBC offers moderate optics and excellent impact over the leading high clarity impact copolymer.

Introduction

PP homopolymers or PP random copolymers provide the desirable stiffness and clarity for many applications, but suffer from poor impact properties due to PP's high T_g of 0°C and high degree of crystallinity. To overcome this deficiency, PP homopolymer is blended with PP copolymers and/or elastomers to improve toughness, but often at the expense of clarity, impact properties, and modulus (1-2). Conventionally, to achieve high clarity and impact of PP, the modifier needs to be refractive indexed matched. However clarity can also be achieved using non-refractive index polymer, as long as it is a high flow elastomer where fine dispersion of elastomer domains can be achieved. The performance at freezing temperature is still lacking with these approaches.

INTUNE™ OBC, a polypropylene-based OBC comprising iPP hard blocks and ethylene-propylene soft blocks offers a compatibilization solution to reduce the domain sizes (100-500 nm) of the elastomer phase when blended in PP. These novel compatibilized blends of PP and elastomers offer a wider range of thermodynamically-stable compositions with morphologies finer than those

achievable with classical blends (3), resulting in unique combinations of properties.

The purpose of this study was to compare the relative performance of an RCP impact modified with olefin block copolymers and polyolefin elastomers, targeted for use in a clear freezer application. Impact modifiers based on OBC technology can offer balanced solutions of clarity, impact, and flow that outperforms a leading high clarity impact copolymers (4).

Materials

A 40 MFR, random copolymer (next gen clarified), was impact modified with polymers listed in Table 1. These materials were dry-blended with the PP random copolymer (40 MFR) at 20wt% concentration and then injection molded in a KraussMaffei KM110-390 injection molding machine. The conditions were as follows: injection parameters of 40 mm/s at 2000 bar for 0.78s, hold pressure of 300 bar for 20 s, and cool time of 20s.

INTUNE™ 10510 OBC, is a new PP based olefin block copolymer. INFUSE™ OBC 9817 is an ethylene-based olefin block copolymer containing polyethylene hard segments and ethylene-octene soft segments. ENGAGE™ 8402 Polyolefin Elastomer (to be referred to as POE 1), ENGAGE™ 8200 Polyolefin Elastomer are random copolymers containing ethylene and octene (to be referred to as POE 2). VERSIFY™ 4301 Polyolefin Elastomer is a random copolymer containing propylene and ethylene (to be referred to as PBE).

For comparison, a clarity ICP that is typically used for cold food and storage applications was also tested.

Property Testing

Optical Properties

Plaques of 1.6 and 0.75 mm thickness were compression molded. Clarity, transmittance, and haze was measured using BYK Gardner Haze-gard as specified in ASTM D1746. 60° gloss was measured using BYK Gardner Glossmeter Microgloss 60° as specified in ASTM D-2457.

Tensile Testing

Stress-strain behavior in uniaxial tension was measured using ASTM D638. Injection molded tensile specimens are used (approx. 16.5mm 19mm x 1.6mm). Samples

were stretched with an Instron at 50mm/min at 23°C. Tensile strengths and elongation at break are reported for an average of 5 specimens.

Izod Impact

The notched Izod impact tests were performed on injection molded specimens (63.5 mm x 12.7 mm x 1.6 mm) was used with a milled notch and confirmed according to ASTM D256. The samples were notched using a notcher to produce a notch depth 2.54 +/- 0.05 mm. Ten specimens of each sample were tested using ASTM D256 at room temperature, 23°C, and 0°C.

Transmission Electron Microscopy

Image Collection - TEM analyses were performed on a JEOL JEM-1230 operated at 100kV accelerating voltage and collected on a Gatan-791 and 794 digital cameras.

TEM Sample Preparation - The compression molded films were trimmed so that sections could be collected near the core of the films. The trimmed samples were cryopolished prior to staining by removing sections from the blocks at -60°C to prevent smearing of the elastomer phases. The cryo-polished blocks were stained with the vapor phase of a 2% aqueous ruthenium tetroxide solution for 3hrs at ambient temperature. Sections of approximately 90 nanometers in thickness were collected at ambient temperature using a diamond knife on a Leica EM UC6 microtome and placed on 600 mesh virgin TEM grids for observation.

Discussion

The development of PP impact modifiers to meet the requirements for clear freezer applications is an on-going challenge. Containers and articles for frozen foods or storage are challenged by the balance of toughness and stiffness while having clear optics for consumer appeal. Containers made from polyethylene can certainly meet the needs of toughness but are not clear. Containers made from polypropylene random copolymers have excellent clarity (with the addition of clarifiers and nucleators) but are not tough. Hence, the introduction of elastomer modifiers to toughen the PP to meet the impact requirements is needed. Reactor grade PP impact copolymers can offer a good balance of clarity and stiffness, but the impact properties are limited due to the miscibility of the ethylene-propylene rubber phase and dispersion. To obtain the best impact performance, additional elastomers are compounded and blended with RCP's or ICP's to increase the rubber phase volume and increase the impact toughness. The loading of modifier varies depending on the performance that is required in the given application. Typically, ~3-10 wt% loading of the modifier is sufficient for room-temperature applications, ~10 wt% for refrigerator applications, and greater than 20 wt% for cold freezer applications.

In this work, solutions for the freezer application was targeted and 20 wt% of modifier was blended and tested. The optical and physical properties of blends containing a RCP matrix and 20% dispersed elastomer phase were evaluated (refer to Table 1). It was hypothesized that olefin block copolymer with its Compatibilization attributes, could improve the balance of clarity and toughness. For cold freezer applications, the stiffness is less of a requirement due to the increase in modulus at low temperatures but viscosity build and crystallization setup is important for quick processing and demolding of articles for injection molding.

Table 2 shows the clarity, and haze measurements for plaques from the blended components. Two part thicknesses were tested for optics; thin 0.75mm and thick 1.6mm. At 0.75 mm thickness, the thickness used for thin-wall food containers, all of the parts looked transparent and clear as a stand-alone RCP. At 1.6 mm thickness which is typically used for storage containers, the best optics, highest clarity and lowest haze % was observed with PBE and POE 1, 99% clarity, and 13-14% haze. Next, the INTUNE™ 10510 OBC exhibited a clarity of 99% and 22% haze. Poorer optics were observed with INFUSE™ 9817 OBC and the clarity ICP. The worst optics was with the POE 2, with a reduction in clarity to 90% and greater than 50% haze.

The optical results are in-line with the composition of the modifiers. For the non-refractive index matched polymers, INTUNE 10510 OBC, INFUSE 9817 OBC, POE 2, Clarity ICP, TEM micrographs of the samples were recorded to understand the relationship of optics and the dispersed morphology of the rubber domains. Figure 1 shows the TEM micrographs of the blends at the 1µm scale. The micrographs show that the size and dispersion of the rubber domains are related the optical properties observed. The clarity ICP and the POE 2 modified blend showed the poorest dispersion with large bands in the flow direction. Similarly, the INFUSE 9817 show bands in the flow direction but shows some evidence of droplet break-up; it is suspected that the long and thick domain bands, contributed to higher haze. Unlike the other modifiers, INTUNE 10510 shows the rubber domains been finely dispersed into the matrix with droplet sizes less than 200 nm. Note due to the compatibilization effect of the iPP-EP nature of the polymer, a very fine dispersion results and relates to the lower haze observed in the molded plaques that shows better dispersion is good for optics. However the next question is how the balance of performance changes with the improvement in optics?

Table 3 summarizes the physical properties of the blends. All mechanical testing was completed on the 1.6 mm thickness parts. The tensile modulus (2% secant) of the modified blends ranged from ≈ 1300 – 1500 psi. The

™Trademark of The Dow Chemical Company ("Dow") or an affiliated company of Dow

PBE resulted in the lowest modulus while POE 1, the highest. The INTUNE™ 10510 OBC, INFUSE™ 9817, and POE 2 were all around 1400 psi. However, at the 20 wt% loading of these modifiers, the modulus is lower than that of the clarity ICP. As mentioned, for cold/freezer temperatures, the toughness is more critical than the modulus since the modulus increases with decreasing temperature. The more important factor is the impact strength and failure mode at low temperatures.

Figure 2, 3, and 4 compares the IZOD impact strength and failure type at 23°C, 0°C, and -20°C, respectively. These testing temperatures were chosen to understand the impact performance at room temperature, refrigerator, and freezer conditions.

At room temperature, the INTUNE 10510 and INFUSE 9817 modified blends, and clarity ICP exhibited ductile behavior with high impact strength and partial breaks of the specimens. At room temperature, these materials exhibit high toughness sufficient for storage and food/pantry applications. Conversely, the other modifiers exhibited lower impact strength and brittle behavior, with PBE and POE 2 being similar and POE 1 the lowest.

As expected, the impact strength of all the materials decreased when tested at subambient temperatures. The data shows that the INTUNE 10510 and INFUSE 9817 outperformed the clarity ICP, exhibiting higher impact energies and some partial breaks (indicating more ductility) than the clarity ICP which showed brittle behavior with 100% complete breaks. The observed trend for these three examples is consistent at both 0°C and -20°C. In comparison of the INTUNE 10510 and INFUSE 9817, the INFUSE 9817 exhibited higher impact strength at these subambient temperatures; the increase is attributed to its block architecture and high levels of incorporated octene which results in a low T_g and high flexibility. The INTUNE 10510 and its compatibilization approach for a propylene-based OBC resulted in not only an improvement in impact strength, but in rubber dispersion and homogeneity to result in better optics.

In application to clarity freezer applications, each modifier solution can be tailored to provide a unique feature balance. Figure 5 depicts the property balance and comparison to the clarity ICP. The INTUNE 10510 exhibited the fine particle sizes and excellent dispersion, to result in good optics, room temperature ductility, and an improvement in low temperature toughness. The INFUSE 9817, offers a significant improvement in low temperature toughness (due to its low density, ethylene-octene soft segments), a slight improvement in dispersion

but poorer optics than the clarity ICP. Therefore, depending on the processing and application constraints, a unique and tailored solution can be provided. High flow, good dispersion, good optics, and good impact with INTUNE 10510 or moderate optics and excellent impact with INFUSE 9817, all out performing the clarity ICP.

Conclusions

The olefin block copolymers can be used to modify RCP PP, to improve the performance compared to a clarity ICP. INTUNE™ 10510 OBC compatibilizes the polymer where it results in the fine particle sizes and excellent dispersion, to result in good optics, room temperature ductility, and an improvement in low temperature toughness. INFUSE™ 9817 OBC offers a significant improvement in low temperature toughness with a slight improvement in dispersion, but poorer optics. The processing plays a part in the final performance in the parts, however the OBCs outperform clarity ICP.

INTUNE 10510 and INFUSE 9817 outperformed the clarity ICP, exhibiting higher impact energies and some partial breaks. INFUSE 9817 exhibited higher impact strength at these subambient temperatures of 0 and -20 °C. INTUNE 10510 resulted in not only an improvement in impact strength, but in rubber dispersion and homogeneity to result in better optics than the clarity ICP. INTUNE 10510 rubber domains have been finely dispersed into the matrix that relates to the lower haze observed in the molded plaques that shows better dispersion is good for optics. The benefits of dispersion by the OBCs results in better homogeneity, less stresses, better part esthetics, more consistent part performance.

References

1. Hansen, D.; Huan, Y.; de Groot, H.; Masuko, N.; Southwick, J.; Toughening clear polypropylene random copolymers with styrenic block copolymers, International Conference on Polyolefins 2006 (Feb 26-Mar 1st).
2. Spontak, R.J.; Patel, N. in Developments in Block Copolymer Science and Technology; John Wiley & Sons, New York, (2004), Chapt 5.
3. Pernot, H.; Baumert, M.; Court, F.; Leibler, L.; Nature Materials, 1, 54-58 (2002).
4. Li, P.; Shan, C.; Marchand, G.; Walton, K.; Carnahan, E.; Laakso, R.; Garcia-Meitin, E.; Tuning the compatibility of polyolefins with propylene-based olefin block copolymers, SPE ANTEC 2014 (April 28)

Table 1 – Properties of Matrix Blending Components

	MFR (230°C) or MI (190°C) (g/10 min)	Density (g/cm ³)	Description
Clarity RCP	40	0.902	Random copolymer, PP (clarified)
Clarity ICP	30	0.900	PP Impact copolymer (clarified)
INTUNE™ 10510	90	0.890	Olefin Block Copolymer, propylene-based
INFUSE™ 9817	15	0.890	Olefin Block Copolymer, ethylene-based
POE 1	30	0.902	Random copolymer, ethylene-octene
POE 2	5	0.870	Random copolymer, ethylene-octene
PBE	25	0.868	Random copolymer, propylene-ethylene

Table 2 – Physical and Optical Properties

	Clarity ICP	INTUNE™ 10510 OBC	INFUSE™ 9817 OBC	PBE	POE 1	POE 2
Ten. 2% Sec. Mod. (psi)	1650	1400	1460	1290	1500	1430
Clarity % (1.6mm)	99	99	97	99	99	90
Haze % (0.75mm , 1.6 mm)	13, 31	11, 22	15, 36	6, 14	7, 13	21, 50
Izod (23°C), kJ/m ²	20	21	23	16	5	15
Izod (0°C), kJ/m ²	8	13	20	5	4	7
Izod (-20°C), kJ/m ²	7	7	11	3	3	7

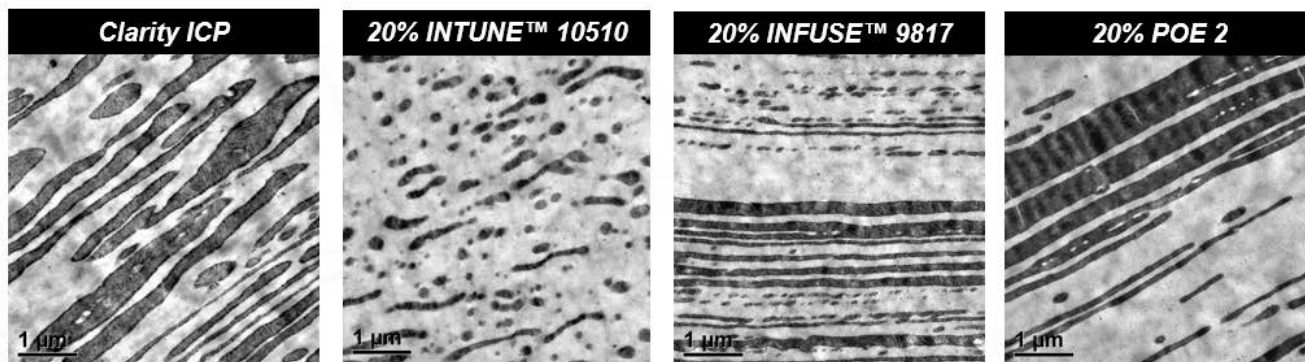


Figure 1 – TEM comparison of RCP modified blends to clarity ICP

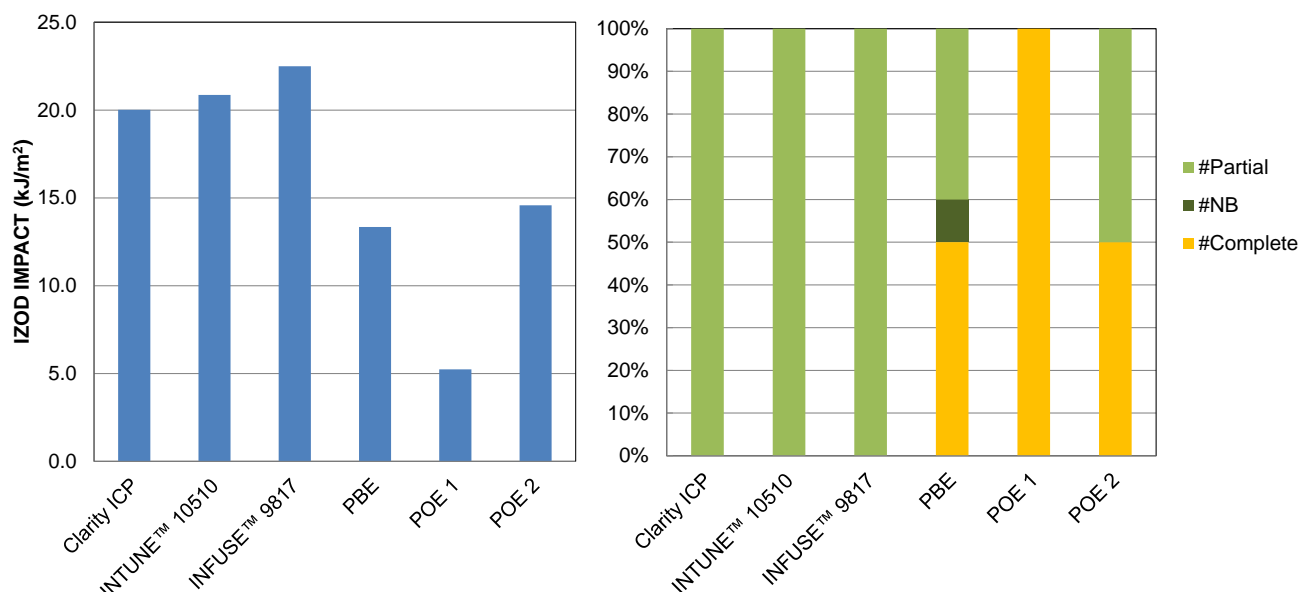


Figure 2 – Izod Impact and Failure type at 23°C

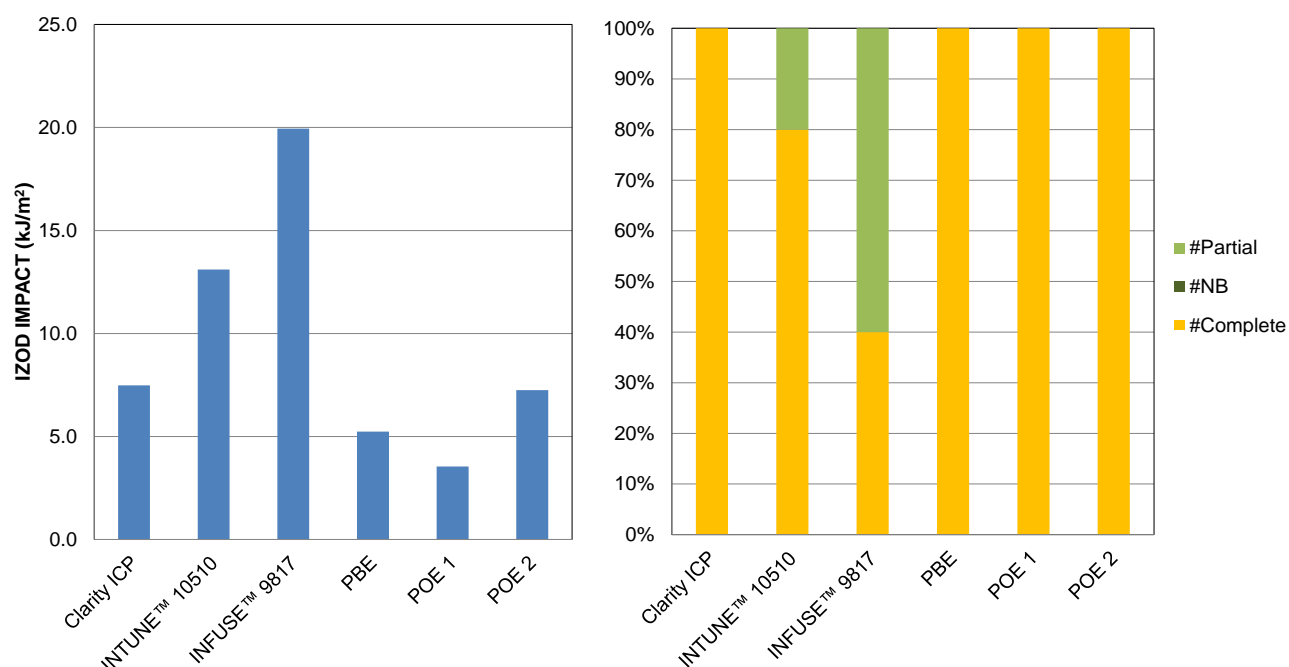


Figure 3 – Izod Impact and Failure type at 0°C

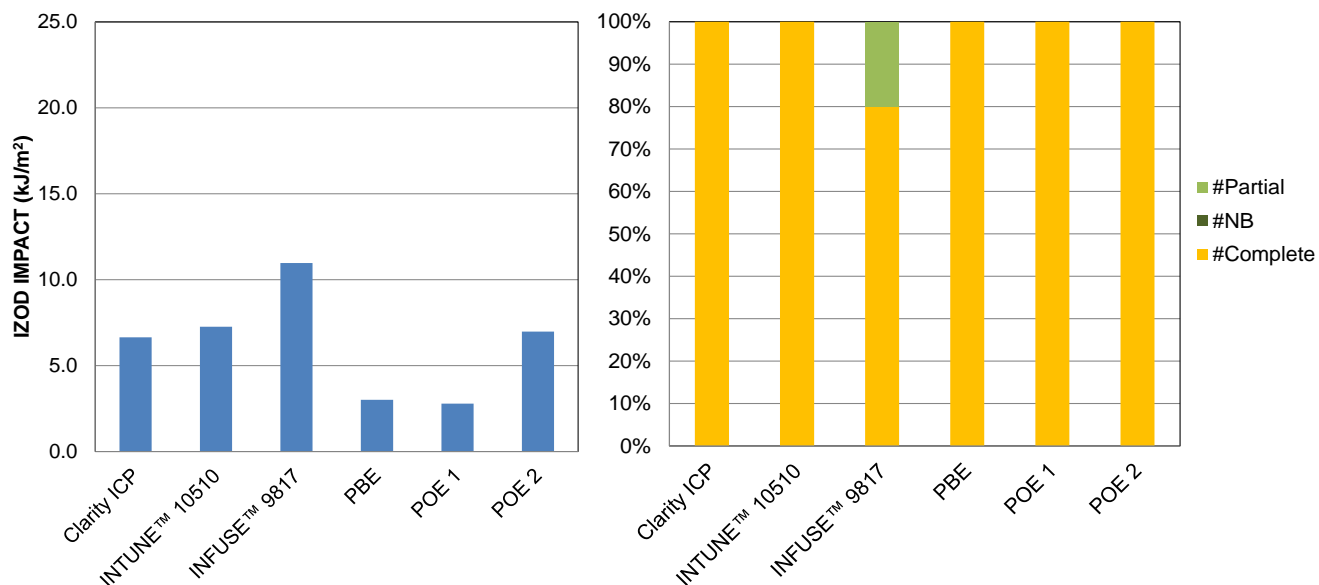


Figure 4 – Izod Impact and Failure type at -20°C

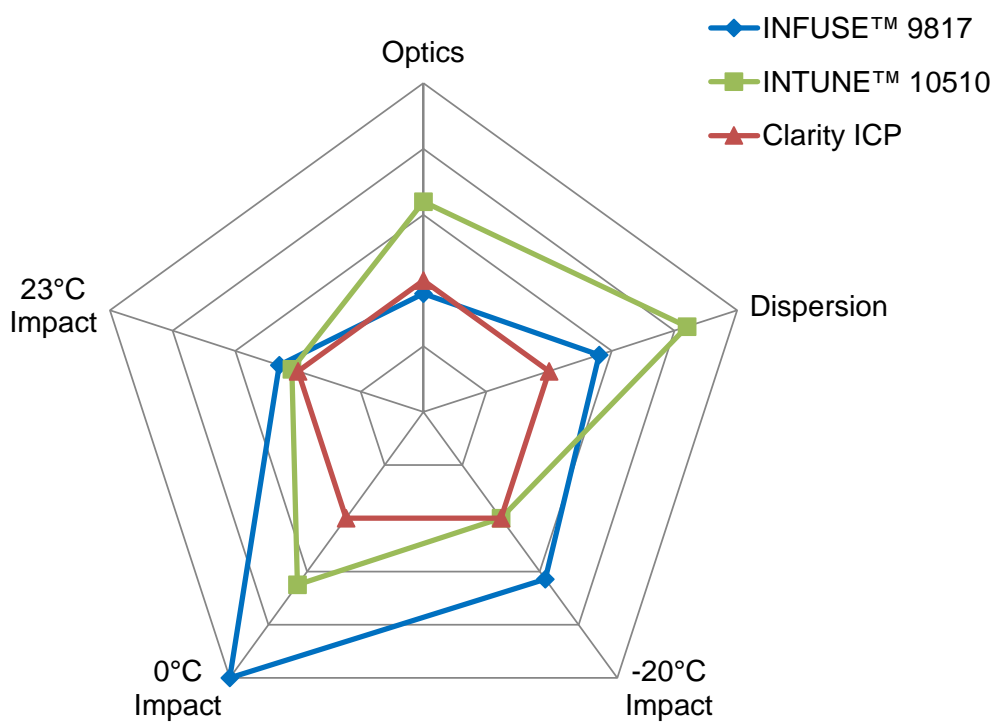


Figure 5 – Performance advantages of INFUSE™ 9817 OBC and INTUNE™ 10510 OBC compared to the clarity ICP.

POLYPROPYLENE RECOVERED FROM SHREDDED END-OF-LIFE DURABLE GOODS

Brian Riise, MBA Polymers Inc., San Ramon, CA

Abstract

Our industry leading separation technology enables us to recover polyolefins and styrenic plastics from complex mixed streams such as shredded end-of-life vehicles and waste electrical and electronics equipment. Plastic flakes recovered using our process are compounded and sold as pellets suitable for use in injection molding and extrusion applications. This paper looks at the challenges and benefits of recovering polypropylene and modifying its properties for use in various injection molded parts in the horticultural, construction, packaging and automotive industries.

Introduction

The volume of plastic produced globally in 2014 was 311 million metric tons [1]. The distribution of plastics demand by segment in Europe from the same study is shown in Figure 1.

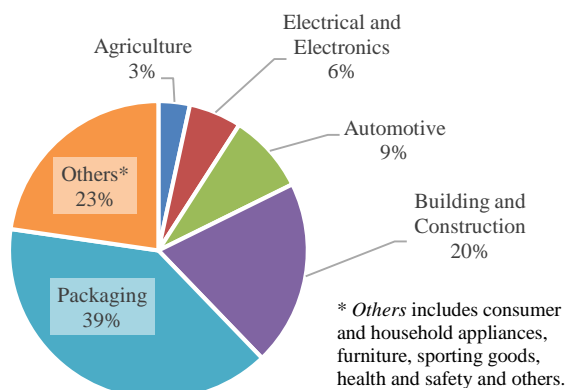


Figure 1. Distribution of European plastics demand by segment in 2014 [1]

Studies have shown that recycling is the preferred environmental option for plastics at the end-of-life [2,3], but the fraction of plastics recycled was only 29.7% in Europe in 2014. Plastics from packaging were the most recycled, with national recycling rates mostly in the range of 25-50%. This suggests that plastics from durable goods such as automobiles and electrical and electronics equipment (E&EE) were recycled at rates well below 30%.

In the US, recycling rates of plastics tend to be even lower. The rate of plastic recycled from municipal solid waste (MSW) was only 9.5% in 2014 [4]. Recycling rates from durable goods in MSW was even lower, at 7.5%.

Many of the plastics in durable goods are highly engineered to meet the long-term performance requirements of these products, so it would be beneficial if these plastics could be recycled at higher rates. Such products can often be used in less demanding applications that might still typically use virgin plastics, but in some cases these plastics can be used in durable goods in applications similar to their original use. Such efforts are also a key part of the Circular Economy [5], as much of the recycled plastic currently used in automobiles is from sources other than durable goods [6].

When automobiles reach the end of their life, parts are often removed for re-use (i.e. replacement parts for running automobiles) or for recycling (e.g. catalytic converters and some larger plastic items such as bumpers). Automobiles also undergo a decontamination step which includes removal of fluids, batteries and tires. After the decontamination step, automobiles are compacted and then shredded (often along with other metal-containing items such as large home appliances and demolition debris along with end-of-life vehicles [7]) to enable recycling of the remaining materials in the automobile. The material remaining after most of the metal is recovered is known as automobile shredder residue (ASR). ASR contains the majority of the plastics from end-of-life vehicles, though it is most often sent to landfill in the US. The recycling industry expects that 1.6 million metric tons of plastic could be recovered annually from ASR in the US [8].

The method of handling waste electrical and electronics equipment (WEEE) depends on the type of product and where the product is recycled. Some handling of WEEE is necessary in order to remove hazardous components such as cathode ray tubes or batteries. Some recyclers take the hand dismantling further and end up recovering large pieces of plastics that can be baled and sold to plastic recyclers [9]. Other recyclers shred the WEEE (after removal of hazardous components) and recover the metals using methods similar to those used by recyclers of automobiles. The remaining material after most of the metal is recovered, which we refer to as electronics shredder residue (ESR), may be further processed by plastic recyclers with automated sorting equipment. The latter method of recycling plastics from WEEE is most common in Europe, whereas both approaches are practiced in the US [9].

European Directives covering end-of-life vehicles (ELV) and WEEE in fact provide targets for recycling of these end-of-life products [10, 11]. The recycling targets are based on the entire weight of these products. The targets can only be partially achieved through the recycling of metals, so some portion of the plastics must also be recycled.

In response to these targets for plastic recycling, a number of recyclers in Europe have been recovering plastics-rich streams for recycling for a number of years. In previous papers [12,13,14], we have described our plastic recycling facilities that recover plastics from upgraded ASR (in the United Kingdom) and ESR (in Austria).

Plastics from ELVs include polypropylene (PP), high density polyethylene (HDPE), acrylonitrile-butadiene-styrene (ABS), polyamides (PA), polycarbonate (PC), blends of PC with ABS (PC/ABS) and many others [15,16]. Other plastics, such as high impact polystyrene (HIPS), are also present in shredder residue because of the shredding of large appliances such as refrigerators.

Plastics from WEEE include acrylonitrile-butadiene-styrene (ABS), high impact polystyrene (HIPS), polypropylene (PP), polyamides (PA), polycarbonate (PC), blends of PC with ABS (PC/ABS), flame retardants grades of ABS and HIPS (ABS-FR and HIPS-FR), mineral and glass filled grades of PP, polyvinyl chloride (PVC), polyoxymethylene (POM) and many others [13].

PP is the largest volume plastic product present in ASR. It is also found in ESR, but in a smaller amount. In this paper, we first summarize the feed materials and separation process used to recover PP from these complex streams. Next we discuss the composition and properties of the PP products. We then discuss some of the limitations and potential improvements to these products. Finally, we give some case studies where the material has been successfully in place of virgin PP in demanding applications.

Compositions of ASR and ESR

Typical ASR only contains a small portion of plastic, so further processing is required to make this stream more interesting economically for plastic recycling. The mixture can be upgraded using processes available in the recycling industry. Such an upgraded ASR mixture is what is fed to MBA Polymers' facility in the UK [14].

Table 1 summarizes typical compositions of mixtures fed to MBA Polymers' facilities in the UK (upgraded ASR) and Austria (European ESR).

Table 1. Example compositions of upgraded ASR and European ESR as fed to the MBA Polymers process

Material	Upgraded ASR	European ESR
"Target Plastics"	77%*	61%†
Other plastics	7%	25%
Rubber	6%	3%
Wood	5%	3%
foam, textiles, paper and film	3%	1%
Other materials	0%	1%
wires and metal	1%	5%
"fines" (<3 mm)	1%	1%

* PP, ABS, 20% filled PP, HIPS and HDPE

† ABS, HIPS, PP, PC/ABS

Process to Recover Plastics from Shredded End-of-Life Durable Goods

MBA Polymers has considerable experience and technical know-how for processing streams of plastics from durable goods such as ESR or upgraded ASR. Some of the technologies employed to create high value products from these streams are covered in more detail in our patents [17].

The MBA Polymers process to recover plastic products from ESR is summarized in Figure 2. The process for recovering plastics from ASR is similar, though PC/ABS is not currently recovered, and both HDPE and PP (20% mineral filled) are recovered as separate products.

Initial steps of the process include size reduction and processes to removal non-plastics such as metal (mostly from wires), wood, rubber and foam. Next, the plastic-enriched stream is separated into streams of plastic "families". These plastic "families" each contain significant amounts of one or more major plastic types as well as minor amounts of other plastics, rubber and wood. The next steps include the removal of the majority of the remaining non-plastics (i.e. rubber and wood) and purification of the plastics by type. The purified flakes are then blended in large blending silos prior to compounding.

Figure 3 is a photograph of a mixture of PP flakes recovered from upgraded ASR using the MBA Polymers separation processes.

Product flakes are compounded using a twin screw extruder. This step includes the addition of additives (usually small amounts of antioxidant, colorant, impact modifier and/or others as required), vacuum de-volatilization and melt filtration.

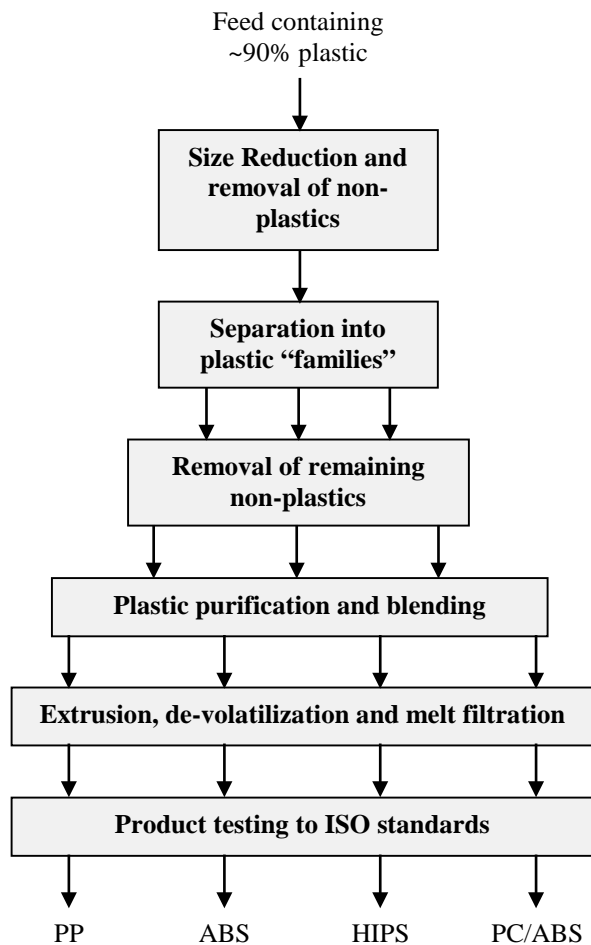


Figure 2. Process for recovering plastics from ESR



Figure 3. PP flakes recovered from upgraded ASR

The final products are tested using ISO standards to ensure product quality. These tests include measurements of moisture, density, melt flow rate (ISO 1133), tensile strength (ISO 527), notched Izod impact strength (ISO 180) and flexural modulus (ISO 178).



Figure 4. PP pellets from upgraded ASR after compounding flakes with small amounts of additives

Polypropylene Products from ASR and ESR

PP Flake Mixtures Prior to Compounding

The purified PP flake mixture recovered from upgraded ASR is a complex mixture that includes various grades of impact copolymer PP from automotive sources (which is itself a multi-phase mix of isotactic PP, ethylene-propylene copolymer, ethylene-propylene-diene copolymer and others [18,19,20]), copolymer PP grades from E&EE and large appliances, mineral filled PP grades and HDPE.

The purified PP flake mixture recovered from ESR is a slightly less complex mixture that includes mostly copolymer PP grades from E&EE.

PP Properties and Applications

Several standard grades are produced by compounding the purified PP flakes with small amounts (typically <2%) of additives. Table 2 summarizes the typical properties of three of the most commonly produced grades.

PP 2126 is the base product from upgraded ASR. PP flakes are compounded with a small amount of antioxidant along with impact modifiers. PP 2126 is suitable for a number of applications requiring good toughness. Specific examples of parts manufactured using PP 2126 include injection molded pallets and plant trays thermoformed from extruded sheet. The fairly low melt flow rate (MFR) prevents its use in some applications (e.g. products with very thin walls), though, so higher flow grades are also available.

PP 2172 is produced from the same flake material as PP 2126, but the MFR is modified to satisfy customers requiring better flowing PP. PP 2172 loses some of its mechanical properties (especially impact strength) due to the additives required to reduce the PP molecular weight,

but it still has sufficiently good mechanical properties for a number of applications in the horticultural, construction and packaging industries. Specific examples include plant pots, waste baskets, storage boxes and crates.

PP 2131 is produced from flake recovered from ESR. This material has a lower impact strength than PP 2126, but has a much higher flexural modulus. Specific applications of this grade include several in new automobiles, including a cable tray used in a luxury automobile.

Table 2. Typical properties of PP products recovered from upgraded shredder residue at MBA Polymers UK

Property	Units	PP 2126	PP 2172	PP 2131
MFR (230/2.16)	g/10 min	7	25	8
Izod impact, notched	kJ/m ²	20	9	6
Tensile strength at yield	MPa	19	18	24
Flexural Modulus	MPa	850	850	1500

Chemical and Thermal Characterization

We have characterized the PP 2126 and PP 2131 products using FTIR. Figure 5 compares the FTIR spectra of PP 2126 and PP 2131 with a virgin copolymer PP. We note that the absorptions overlap reasonably well, though we do note a significant absorption near 1050 cm⁻¹ due to the presence of ~4% talc (based on TGA measurements) in the PP 2126 sample.

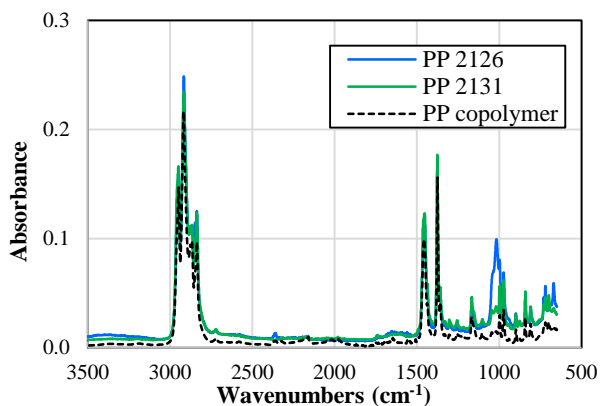


Figure 5. FTIR spectrum of standard PP products from upgraded ASR (PP 2126) and ESR (PP 2131) compared with a virgin PP copolymer

We have also characterized PP 2126 and PP 2131 using differential scanning calorimetry (DSC). Figure 6 shows a DSC thermogram (2nd heat at 10°C/min) with melting endotherms for PE (peak at 127°C) and for PP (peak at 164 or 165°C). The thermograms are typical of PP

copolymers, though there is a higher ratio of crystalline PE to crystalline PP in PP 2126 (as indicated by the higher ratio of PE to PP melting enthalpies). This is consistent with PP 2126 being an impact copolymer grade with a higher impact and lower flexural modulus than PP 2131.

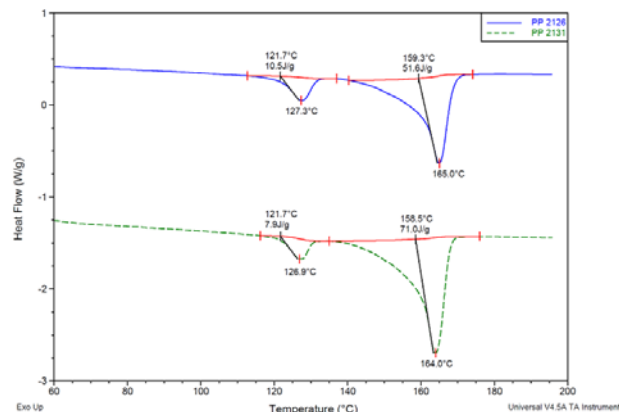


Figure 6. DSC thermogram for PP 2126 and PP 2131 (2nd heat at 10°C/min) showing melting for PE and PP phases

Product Limitations

PP products recovered from ASR and ESR do suffer from a number of limitations that make their use in some applications more challenging. The limitations include:

- Residual semi-volatile organic compounds (SVOCs) and associated odors
- Low flexural modulus (for grades from ASR)
- Color limitations
- Contamination from non-melt particles
- Consistency of properties
- Substances of concern

While PP grades recovered from ASR and ESR can be used in a wide variety of applications, the presence of SVOCs (and associated odors) provides a challenge to their use in demanding applications such as automobile interiors. We are continuing to investigate cost-effective methods to reduce SVOCs and odors for plastics from ASR [21], though we have made significant progress with PP 2131 from ESR (see the Product Development Case Study on “PP from ESR used in Automotive Cable Tray” later in this paper).

The flexural modulus of the PP grades recovered from ASR is approximately 10-20% lower than some virgin high impact PP grades with which we are competing. While this is not an issue for many applications, it can be problematic when the part is under a flexural load and where flexural creep might occur. Later in this paper, we discuss an example of how the flexural modulus and flexural creep resistance were improved for a particular application (see

the Product Development Case Study on “Gray PP with High Flow for Paint Cans”).

The color of the PP products is limited by the existing carbon black, TiO₂ and other pigments present in the PP found in ASR or ESR (see Figure 3). Therefore, the “natural” colors of the PP products are a light black (if from ASR) and a medium dark (if from ESR). Commercially available color sorting equipment can be used to separate the flake mixture into lighter and darker colored mixtures, but this results in added costs and diminished available volumes of any given product. Adding carbon black or TiO₂ pigments in the compounding step also allows for some adjustment of the color, though it is very difficult to achieve deep black colors when TiO₂ is present even in small amounts. Achieving very light gray is difficult even with color sorting and it is not possible to achieve meaningful volumes of white product from either ASR or ESR. Colors other than gray or black are possible by adding colorants to the light colored fraction after color sorting, but these products tend to be expensive and large volumes are not possible.

Although there are a number of process steps to remove non-melts (e.g. wood and rubber) from both flakes and the melt, the PP products contain traces of particulate contamination. These particulates are mostly smaller than approximately 100 microns in size, and have little effect on most mechanical properties, but they are large enough to be visible when extruded or injection molded parts are examined closely.

Even though the flake composition and additive loadings are well controlled in the production of PP products from ASR and ESR, we have observed that the mechanical properties can vary measurably from batch to batch. In a paper presented at ANTEC 2016, we discussed this variation in PP 2126 (up to about $\pm 20\%$ variation in notched Izod) and presented an approach to rapidly measure the mechanical properties of the PP product by statistical analysis of FTIR spectra [22].

PP products from ASR and ESR also contain trace amounts of “legacy” substances of concern such as heavy metals and flame retardants because many of the used vehicles and E&EE comprising the ASR and ESR were manufactured prior to restrictions on these substances. Because of these “legacy” substances of concern, we DO NOT recommend our products for toys, for medical applications or for applications that involve food contact or human oral contact. We do note, however, that our products are RoHS [23] and REACH [24]-compliant and substances of concern are below limits established in the candidate list of substances of very high concern (SVHC) published by the European Chemicals Agency (ECHA) [25] and in the Global Automotive Declarable Substance List (GADSL) [26].

Product Development Case Studies

Gray PP with high flow for paint cans

A manufacturer of plastic paint cans required a dark gray post-consumer recycled PP with a melt flow rate of approximately 20 g/10 min (or higher), sufficient toughness to withstand various impact tests, shrinkage similar to virgin PP grades used to make lids for the can, and sufficient creep resistance to withstand a test designed to mimic the stacking of filled paint cans on a pallet. The recycled PP is to be added at 25% into virgin PP that the molder has historically used for the cans.

Initially, the molder tested PP 2172 at a 25% loading in virgin PP. The molder found that the compound passed tests for shrinkage and impact, but failed the creep test.

As the creep test resulted in failure due to excessive flexing of the walls of the can, we developed a formulation with a 5-10% higher flexural modulus that would better resist any deflection during the test. The formulation included a TiO₂ masterbatch to slightly lighten the color to the desired medium dark gray, a peroxide to control the MFR, an antioxidant to stabilize the end product against oxidation during processing and use, and an additive to increase the flexural modulus by approximately 5-10%. The newly formulated product easily passed the creep (and other) tests performed by the molder.

PP from ESR used in Automotive Cable Tray

A tier 1 molder for a luxury automobile manufacturer required a recycled PP material for use in a cable tray. MBA Polymers facility in Austria sampled their PP 2131 product for the application.

In order to pass the required tests for thermal stability, the product was specially formulated with heat stabilizers.

In order to meet stringent requirements for odors and emissions of volatile organic compounds in this automotive interior application (e.g. VDA 270 and VDA 278), the PP 2131 product was compounded carefully while ensuring optimal vacuum de-volatilization.

Conclusions

PP products recovered from shredded end-of-life durable goods and further compounded into pellets by MBA Polymers are useful for a number of injection molding applications. Though some limitations in properties remain, we continue to improve the products to expand the range of end products in which they can be used. These advancements have resulted in the use of at least one of the PP products as a replacement for virgin PP in an automotive interior application.

References

1. *Plastics – the Facts 2015: An analysis of European plastics production, demand and waste data*, data from PlasticsEurope (the Association of Plastics Manufacturers in Europe) and EPRO (the European Association of Plastics Recycling and Recovery Organisations). Available at <http://www.plasticseurope.org/documents/document/20151216062602-plastics-the-facts-2015-final-30pages-14122015.pdf>, accessed December 1, 2016.
2. P. Shonfield, “LCA of Management Options for Mixed Waste Plastics”, Final Report prepared for WRAP Project MDP017, June 2008. Available at <http://www.wrap.org.uk/sites/files/wrap/LCA%20of%20Management%20Options%20for%20Mixed%20Waste%20Plastics.pdf>, accessed December 1, 2016.
3. P. A. Wäger and R. Hischier, “Life cycle assessment of post-consumer plastics production from waste electrical and electronic equipment (WEEE) treatment residues in a Central European plastics recycling plant”, *Science of the Total Environment* 529 (2015) 158–167.
4. “Advancing Sustainable Materials Management: 2014 Fact Sheet Assessing Trends in Material Generation, Recycling, Composting, Combustion with Energy Recovery and Landfilling in the United States”, US EPA, November 2016.
5. “Communication from the Commission to the European Parliament, the Council, the European Economic and Social Committee and the Committee of the Regions: Closing the loop - An EU action plan for the Circular Economy”, December 2, 2015. Available at http://ec.europa.eu/environment/circular-economy/index_en.htm, accessed December 1, 2016.
6. “Plastics Market Watch: Automotive Recycling: Devalued is now Revalued”, ed. W. Mashek, SPI: The Plastics Industry Trade Association, 2016.
7. C. Duranceau and J. Spangenberg, “All Auto Shredding: Evaluation of Automotive Shredder Residue Generated by Shredding Only Vehicles”, ANL/ES-C0201801, July 11, 2011.
8. R. Damuth, “Economic Impacts and Environmental Benefits of Separating, Sorting, Processing, and Recycling Plastics in the Automobile and Appliance Shredder Aggregate”, prepared by Nathan Associates Inc. for the Institute of Scrap Recycling Industries, December 2010.
9. <http://www.hse.gov.uk/waste/waste-electrical.htm>, accessed December 1, 2016.
10. Directive 2000/53/EC
11. Directive 2002/96/EC and Directive 2012/19/EU
12. B. Riise, and R. Rau, “Plastics Recovered from Shredded Waste Electrical and Electronic Equipment”, ANTEC® 2015 - Orlando, Florida, USA March 23-25, 2015, Society of Plastics Engineers.
13. A. Schwesig and B. Riise, “PC/ABS Recovered from Shredded Waste Electrical and Electronic Equipment”, ANTEC® 2016 - Indianapolis, Indiana, USA May 23-25, 2016, Society of Plastics Engineers.
14. B. Riise, P. Mackrell, R. Rau and I. Patel, “Plastics Recovered from Shredded End-of-Life Vehicles”, ANTEC® 2015 - Orlando, Florida, USA March 23-25, 2015, Society of Plastics Engineers.
15. *Chemistry and Light Vehicles*, Economics & Statistics Department, American Chemistry Council, July 2013.
16. B.L. Riise, M.B. Biddle, M. M. Fisher, N. Simon, C.M. Duranceau, C.S. Wheeler, G.R. Winslow, “Recovery of Plastics from Pre-Processed Shredder Residue”, Paper Number 07ENV-24, Society of Automotive Engineers 2007 World Congress, Detroit, MI, April 2007.
17. US 7,802,685 and US 7,884,140 provide overviews of the separation process and the resulting products.
18. H. Domininghaus, *Plastics for Engineers: Materials, Properties, Applications*, Hanser Publishers, 1993, pp. 105-109.
19. F.M. Mirabella, “Multiphase Polypropylene Copolymer Blends” in *Polyolefins Blends*, ed. D. Nwabunma and T. Kyu, Wiley, 2008, pp. 351-378.
20. C.-S. Ha, S.R. Chowdhury, G.-H. Kim and I. Kim, “Propylene/Ethylene-Propylene-Diene Terpolymer Blends” in *Polyolefin Blends*, ed. D. Nwabunma and T. Kyu, Wiley, 2008, pp. 411-440.
21. Wypych, *Handbook of Odors in Plastic Materials*, ChemTec Publishing, 2013, pp. 147-171.
22. B. Riise, A. Pye, P. Mackrell, H. Herman, and G. Stevens, “Rapid Spectral Measurement of the Mechanical Properties of Polypropylene Recovered from Shredded End-of-Life Vehicles”, ANTEC® 2016 - Indianapolis, Indiana, USA May 23-25, 2016, Society of Plastics Engineers.
23. Restriction of Hazardous Substances Directive 2002/95/EC
24. Registration, Evaluation, Authorisation and Restriction of Chemicals Directive 1907/2006/EC
25. <http://echa.europa.eu/candidate-list-table>, accessed December 1, 2016.
26. <http://www.gadsl.org/>, accessed December 1, 2016.

A NEW METHOD TO MODIFY PP FOR IMPROVED MELT STRENGTH

Anthony Marozsan, Philippe Lodefier, Brett Robb, Virginie Chabrol

Total Cray Valley

ABSTRACT

Total Cray Valley (TCV) has developed a new technology to enable producers and compounders to improve the melt strength of conventional PP. Analytical tools show that the addition of inomeric zinc salts into PP at low loading levels induces behavior similar to long chain branched high melt strength PP (HMS-PP). Foam extrusion testing shows that conventional PP produced can be successfully foamed.

INTRODUCTION

Polypropylene (PP) has long been heralded as an important material within the industrial world. PP is a cost-effective, simple-to-process polyolefin with decent chemical stability and myriad properties. One long-standing deficiency, however, is poor melt strength. There are only a few grades of PP available globally with high melt strength known as High Melt Strength PP (HMS-PP).

The traditional approach to improve melt strength has been the chemical addition of high levels of long chain branching to the polymer backbone. Other strategies have proven efficient but introduce into the polymer large amounts of low molecular weight byproducts. Dymalink® 9200 is a zinc salt widely used in the rubber chemical industry. It reacts with aliphatic polymers and forms a C-C link. Within the polymer the zinc salts, thanks to their polar nature, tend to assemble themselves into ionic clusters promoting the formation of a dynamic network. This leads to unusual melt strength behavior even at very low loadings. The following data highlight the use of this mechanism in PP.

MECHANISM

The general mechanism for ionomeric zinc salts has been demonstrated in the literature by Li et al. [1] Through conventional grafting techniques they abducted maleic anhydride groups to PP and then added zinc to open the anhydride groups and create an ionomeric network.

The ionomeric cross links in this study come from the addition of zinc salts without any peroxide. These cross links are formed with reactive zinc acrylates through reactive extrusion with moderate shear at $>200^{\circ}\text{C}$.

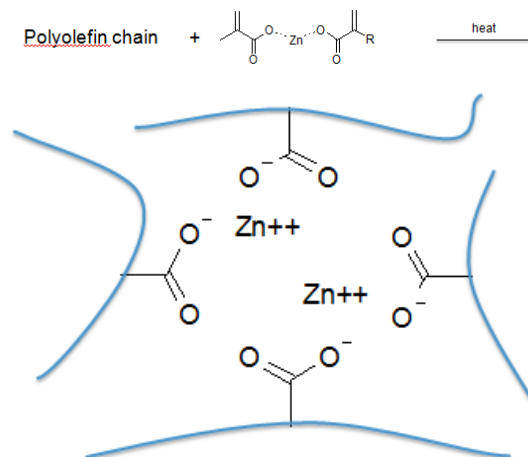


Figure 1. Reaction of zinc salts with polyolefin chain.

The polar zinc salt groups cluster away from the polyolefin chains forming ionomeric domains within the polymer matrix. These domains form as reversible 'crosslinks' with the ionic bonds disassociating at 150°C . With low loading levels of these additives and conventional twin screw compounding equipment and processes ionomeric behavior is introduced to polypropylene.

In this study a conventional 3.5 melt index homopolymer PP was compounded on a twin screw extruder with 2500ppm of an antioxidant blend, 500ppm calcium stearate, and 0.5 to 2% Dymalink® 9200 zinc diacrylate.

RESULTS

Melt elongation and rheology were studied using a Rheotens 71.97 Gottfert instrument with a 2mm die with an L/D of 15. With the addition of even 0.5% of Dymalink a significant melt elongation effect was observed with the elongation speed for the melt strand increasing from ~ 250 to ~ 500 mm/s.

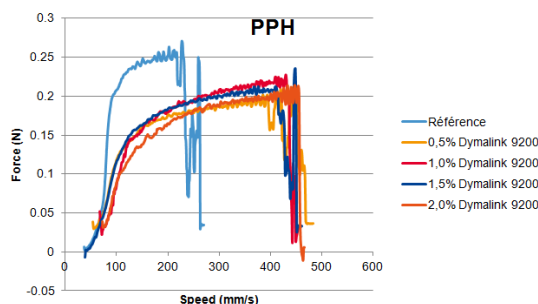


Figure 2. Melt elongation of PPH with and without the addition of Dymalink® 9200

With reactive extrusion one concern is the potential for chain scission of the PP. This is of particular concern with maleinated or peroxide treated PP which typically exhibits an increased low molecular weight fraction. The effect of the reactive extrusion of zinc diacrylate was studied via GPC with the results shown in Figure 3. The molecular weight of the samples was quite constant with the addition of Dymalink and only a small reduction in M_n was observed. The expected cross linking behavior was not observed in the M_z measurement which may be related to the polar solvent used in the GPC method.

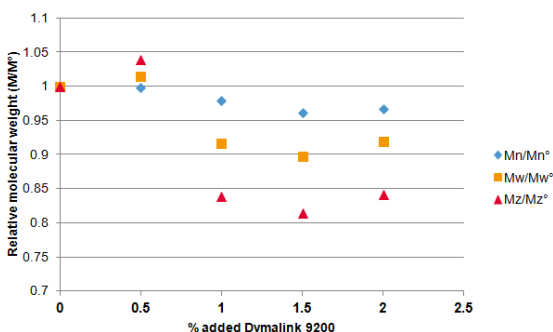


Figure 3. GPC analysis of molecular weight changes in PP with and without Dymalink

One final concern with the addition of salts in PP is the potential nucleating effect of these materials. DSC analysis of the resin with Dymalink added shows no change in melting enthalpy and a small increase of crystallization temperature on cooling for the resin, indicating a slight nucleating effect with Dymalink.

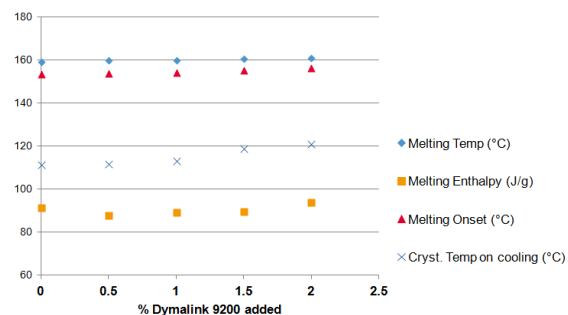


Figure 4. Melting enthalpy effects

A foaming trial was also carried out with 3.5 melt index homopolymer PP, 0.5% talc, and 1% Dymalink 9200. Materials were processed on a single screw extruder at 240°C with a static mixer feeding CO₂ liquid at 74bar. Compared to unmodified resin the extruded material with Dymalink exhibited a smooth surface appearance with better foam morphology indicating successful foaming. Figure 5 and 6 show SEM images of the material with and without Dymalink respectively. Without the improved melt strength imparted by Dymalink the conventional resin has poor cell morphology with open cell content, irregular sizes, and poor surface morphology. With Dymalink the cell structure is homogenous with good closed cell content.

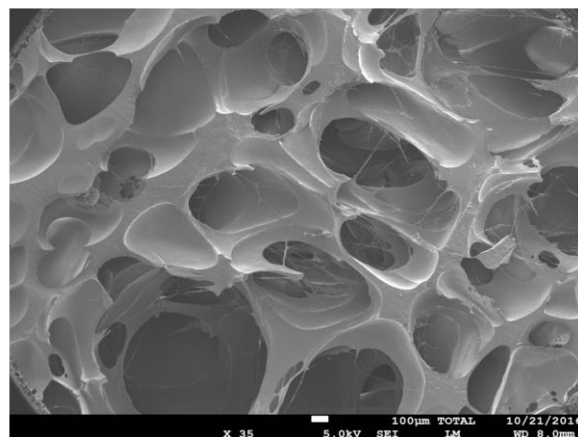


Figure 5. SEM image of conventional PP processed with 0.6mL/min CO₂ at 130 bar die pressure

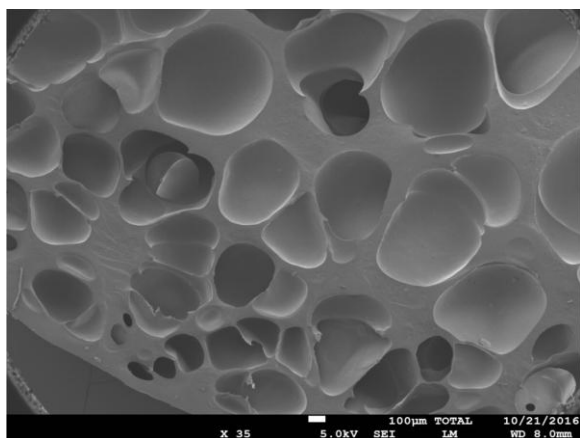


Figure 6. SEM image of conventional PP modified with 1% Dymalink® 9200 processed with 0.6mL/min CO₂ at 130 bar die pressure

MATERIAL AVAILABILITY

Dymalink® 9200 and Dymalink® 9201 are TSCA and REACH registered with global availability. Food contact approval is underway.

CONCLUSIONS

Zinc salts represent a new class of polyolefin additives with a novel set of performance attributes. Addition of zinc salts to conventional PP improves the melt strength of the resin with very few observed drawbacks. This allows a greater freedom to tailor compounds to specific end use needs vs. the use of conventional HMS-PP. These materials are now commercially available globally.

References

1. Li et al, Polymers 70 (2015), 207

COMPARISON OF INJECTION MOLDED CORE LAYER AND ADDITIVE MANUFACTURED CORE LAYER FOR POLYMER SANDWICH PANEL

Min-Young Lyu, Jeoung Hyun Park, Serin Kim, Seoul National University of Science and Technology, Seoul, S. Korea

Jun Sun Hwang, Dong-Yeol Yang, KAIST, Daejeon, S. Korea

Abstract

Additive manufacturing or 3D printing is a new manufacturing process and its application is getting growth. In this study polymer sandwich panel having three dimensional core layer has been designed. And the core layer was fabricated by injection molding and additive manufacturing (AM). The shape of three dimensional core layer was pyramidal kagome structure with semicircle cross-section truss. The materials for core layer were PP for injection molding and ABS for AM. The material for face sheets in polymer sandwich panel were PP. Mechanical robustness has been examined for kagome core strips and polymer sandwich panels.

Introduction

Demand for lightweight material has been rapidly increasing as the price of energy soars and restrictions on carbon emissions are becoming stricter. A promising candidate is high strength polymer materials: engineering plastics and FRP (fiber-reinforced polymer) are examples of such materials.

Even though previous approaches have had common objectives, they have been different in the sense that engineering plastics are produced by design at the nanometer scale (i.e. molecular design) while composite materials are produced by design at the micrometer scale (i.e. design of the micro-structure).

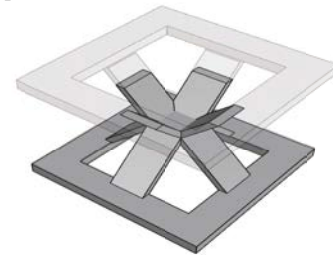
Interestingly, few studies have been done on the structural design of polymers at the millimeter scale. It is definitely possible that excellent mechanical properties could be achieved by proper structural design of polymer, which has not been estimated properly. Fortunately, various design schemes have been suggested for metallic cores such as tetrahedral cores [1, 2], dimple cores [3, 4] or corrugated cores [5]. While the weight-efficiency of structured cores has been analyzed and approved [6-8], many of the structures are not applicable to industrial use due to their complicated fabrication process.

In this study pyramidal kagome core for plastic sandwich panel has been suggested. And the manufacturing method of pyramidal kagome core has been examined. Injection molding and additive manufacturing, so called 3D printing were used for the

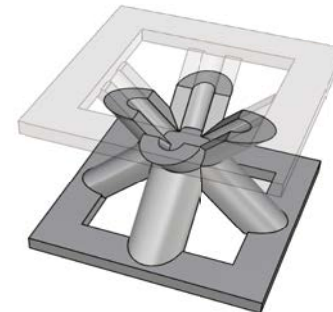
fabrication of plastic pyramidal core. Mechanical property of pyramidal kagome core strips were examined. Plastic panels with pyramidal kagome core strips were manufactured and then the mechanical characteristics were tested. Through these test injection molded and 3D printing manufactured products has been compared.

Experimental and Results

Pyramidal kagome core for three dimensional core layer in plastic sandwich panel was designed as shown in Figure 1 [9, 10].



(a) Rectangular cross-section of kagome truss



(b) Semicircular cross-section of kagome truss

Figure 1. Pyramidal kagome lattice

Pyramidal kagome core strips were fabricated by injection molding and 3D printing. Figure 2 showed injection mold and 3D printer, Connex 500 of Stratasys.



(a) Injection mold and molded product



(b) 3D printer and 3D printing manufactured product
Figure 2. Injection mold and 3D printer

Figure 3 showed plastic kagome core strips fabricated by injection molding and 3D printer. PP supplied by Lotte Chemical was used for injection molding. In the 3D printing photo curing material, VeroWhitePlus RGD835 was used.



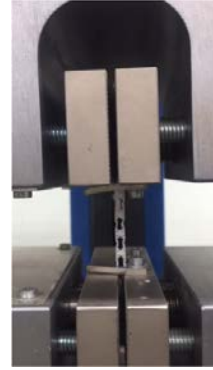
(a) Injection molded core strip



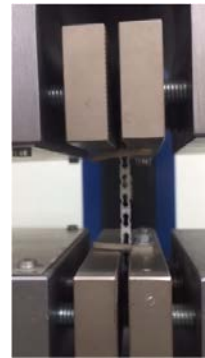
(b) 3D printing manufactured core strip

Figure 3. Fabricated pyramidal kagome core strip

Pyramidal kagome core strips were tested by Instron for the mechanical property. Figure 4 showed tensile test.



(a) Tensile test of injection molded pyramidal kagome core strip



(b) Tensile test of 3D printing manufactured pyramidal kagome core strip

Figure 4. Tensile test of pyramidal kagome core strip

Plastic sandwich panels were manufactured using pyramidal core strips fabricated by injection molding and 3D printing. Figure 5 shows plastic sandwich panel containing pyramidal kagome core.

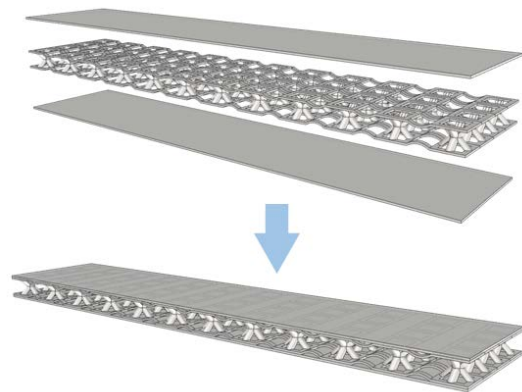
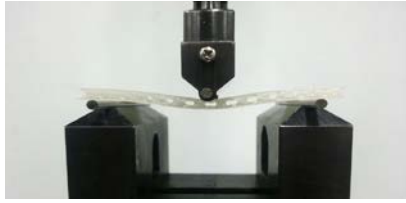
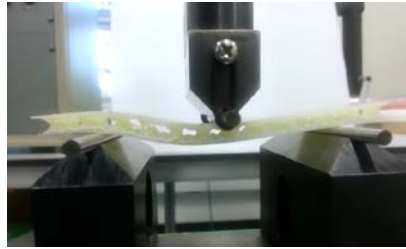


Figure 5. Plastic sandwich panel with pyramidal kagome core

3-point bending test (Compression test) for plastic sandwich panel was performed as shown in Figure 6. Through this test performance of core layer fabricated by injection molding and 3D printing was compared.



(a) Plastic sandwich panel having core layer fabricated by injection molding



(b) Plastic sandwich panel having core layer fabricated by 3D printing

Figure 6 3-point bending test of plastic sandwich panel

Figure 7 shows result of 3-point bending test for plastic sandwich panel which contains pyramidal kagome core layer. Plastic sandwich panel with injection molded core showed higher maximum load than that of the Plastic sandwich panel with 3D printing manufactured core. Plastic sandwich panel 3D printing with manufactured core showed higher stiffness than that of the plastic sandwich panel with injection molded core by 30%.

3D printing manufactured pyramidal kagome core strip has a brittle property and weak mechanical property. However, plastic sandwich panel with this core layer showed reasonable mechanical property. Pyramidal kagome core layer has a role for increasing moment inertial rather than giving a mechanical strength itself.

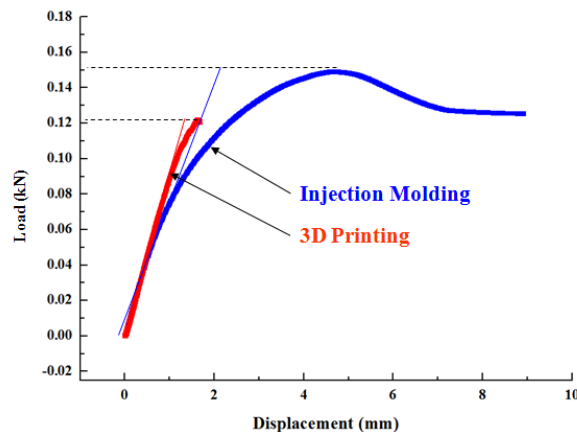


Figure 7 Result of compression test of plastic sandwich panel

Conclusions

Through this study pyramidal kagome core has been designed. Pyramidal kagome core strips were fabricated by injection molding and 3D printing. Mechanical characteristics of two types of pyramidal kagome core strips were compared. 3D printing manufactured pyramidal kagome core showed brittle and weak property compared with injection molded pyramidal kagome core. Plastics sandwich panels have been manufactured by using pyramidal kagome cores that were fabricated by injection molding and 3D printing. Mechanical characteristics of plastic sandwich panels have been examined using 3-point bending test. Plastic sandwich panel with pyramidal kagome core fabricated 3D printing showed higher stiffness than that of the plastic sandwich panel with pyramidal kagome core fabricated injection molding. Plastic sandwich panel with pyramidal kagome core fabricated 3D printing showed reasonable mechanical property even though the 3D printing manufactured pyramidal core strip showed weak mechanical property. The important role of core layer is providing space between face sheets of sandwich panel and it gives high momentum of inertia to the sandwich panel. 3D printing can give a diverse design for the manufacturing of three dimensional complicated core layers. Subsequently it gives a high mechanical property on the plastic sandwich panel.

References

1. Chiras S, Mumm D, Evans A, Wicks N., et al., *International Journal of Solids and Structures*, **39**, 4093 (2002).
2. Kooistra GW, Queheillalt DT, and Wadley HN, *Materials Science and Engineering: A*, **472**, 242 (2008).
3. Seong D, Jung C, Yang D, Kim J., et al., *Scripta Materialia*, **63**, 81 (2010).
4. Seong D, Jung C, Yang D, Nam G., et al., *Journal of Sandwich Structures and Materials*, **13**, 445 (2011).
5. Cote F, Deshpande V, Fleck N, and Evans A., *International Journal of Solids and Structures*, **43**, 6220 (2006).
6. Seong D, Jung C, Yang D, Moon K., et al., *Materials & Design*, **31**, 2804 (2010).
7. Seong D and Yang D., *International Journal of Mechanical Sciences*, (2012).
8. Ahn D-G, Nam G-H, Jung C-G, and Yang D-Y., *International Journal of Precision Engineering and Manufacturing*, **10**, 107 (2009).
9. June-Sun Hwang, Tae-Gyun Choi, Dongyoung Lee, Min-Young Lyu, Dai Gil Lee, Dong Yol Yang, *Composite Structures*, **131**, 17 (2015).
10. June-Sun Hwang, Tae-Gyun Choi, Min-Young Lyu, Dong Yol Yang, *Composite Structures*, **134**, 10 (2015).

FOAM PERFORMANCE OF A NEW HMS-PP

Marcelo Farah^{*(1)}, Ana Paula de Azeredo⁽¹⁾, Steven M. Krupinski⁽²⁾ and Kimberly M. McLoughlin⁽²⁾

1) Polymer Science, Braskem SA, Triunfo, RS, Brazil

2) Product Development, Braskem NA, Pittsburgh, PA, USA.

Abstract

Foaming polymers is an important technological approach with economical and technical advantages in a range of applications, providing qualified products using less material and improving sustainability. Braskem has developed proprietary technology to produce High Melt Strength Polypropylene (HMS-PP), branded as the “AmPPleo” family, with long chain branching (LCB) suitable for foaming processes. The rheological properties have been evaluated in terms of viscosity, elasticity and melt strength, showing good foaming potential. Several large-scale foaming trials have confirmed laboratory results. These results showed stable process conditions, excellent foam properties, cell structure control using different chemical blowing agents and confident correlation of density versus gas amount using different gases (isobutene and CO₂). Foaming process parameters and final structures were very promising and demonstrated a very broad range of low densities (from 150 to 50 kg/m³), cell size control with different cell nucleation agents and the ability to maintain excellent foam characteristics with physical blowing agents.

Introduction

Long chain branch (LCB) insertion in polymer chains is the object of many fields of research, including catalyst systems, process development and post-reactor reactions^{1,2,3,4,5,6,7,8}.

Usually the first technological approach would be reactive extrusion to create branching in PP, but techniques involving free radical generation are usually limited to PP interaction with free radicals, where at temperatures higher than 120°C the β -scission is favorable instead of the branching process. A chemical suitable process might need to be developed.

Braskem developed a post-reactor chemical modification technology⁹ where long chain branching is introduced. The objective of this paper is to discuss the AmPPleo properties and performance in different foaming conditions and compositions.

Materials and Methods

AmPPleo 1020GA HMS-PP produced by Braskem has a MFI of 2.0 g/10min (ASTM. D1238).

Reference linear material data used included a product with usual Molecular Weight distribution (catalyst 1) and one with broad molecular weight distribution (catalyst 2).

Samples were also analyzed in Rheotens 49.11, coupled in a Haake extruder at 190°C, with an acceleration of 60 mm/s² and a die distance of 60 mm in order to determine the Melt Strength following internal methodology.

The foaming processes were characterized in the Krauss-Maffei Berstoff GmbH (KMB) facility in Hannover, Germany, in a tandem system, 1st Extruder- ZE 40, Co-rotating twin screw extruder and a 2nd Extruder, KE 90 – Single Screw Extruder, coupled to an annular die, operating at 100 kg/h, using different gases (Butane and CO₂) as physical blowing agents. Densities were determined by internal KMB methods and it was confirmed by buoyancy gravimetric analyses according to ASTM 792.

Closed cell content was measured in a gas pycnometer Quantichrome Ultrafoam 1200e (V5.04.) following ASTM D6226.

Samples were foamed with special additivation as show in Table 1.

Table 1 – additives used in foaming process

Additive	Commercial name	Supplier
Talc	Finatalc M30	Mondo Minerals
CBA-1	Hydrocerol CF40E	Clariant
CBA-2	Ecocell 20P	PoliFil

Rheological Behavior

The first approach in characterizing HMS-PP is the measurement of the melt strength (MS) as a function of melt flow rate (MFR.)¹⁰ In general, melt strength increases as molecular weight increases and melt flow decreases, as shown in Figure 1. The amount of melt strength increase with decreasing melt flow varies, depending on the specific processing used to produce the polymer. For example, different catalyst systems give different response to the melt flow as shown in

Figure 1. Some catalysts can provide melt strength as high as that of commercially available HMSPP grades at low melt flow. However, these linear materials are not viable options for processes requiring high elongational viscosity. It can be seen that changes in the catalyst system can result in some improvement in MS at levels similar to HMS-PP.

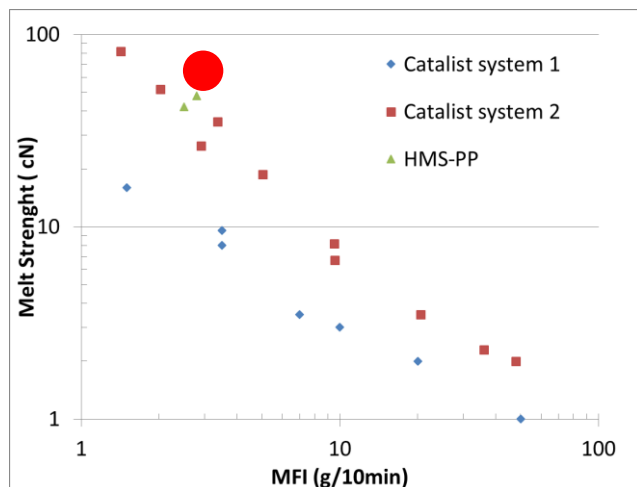


Figure 1 – MFI x Melt Strength for different Polymers.

However, MS data alone is not sufficient to evaluate HMS-PP performance. For processes such as foam, which require high elongational viscosity, melt elongation is also an important feature.

As reported in Figure 2, branched PP is differentiated from linear PP by the drawability at peak melt strength.

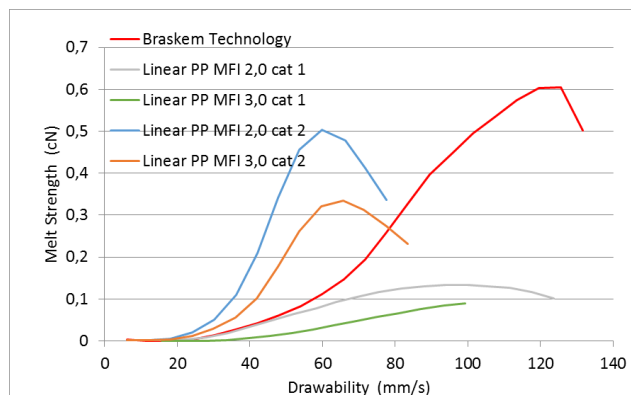


Figure 2 – Melt Strength profile for a HMS-PP compared to linear PP using different catalyst systems

Other rheological methods can also be used to characterize HMSPP. Both shear rheology and elongational viscosity measurements demonstrate the significant effects of branching on the melt behavior of HMSPP. These methods can be used to predict processing performance.

In addition to rheological properties, foam performance depends on crystallization control and gas solubility.^{11,12,13}

Crystallization of Braskem AmPPleo 1020GA has been developed to provide a broad foaming window (crystallization control) and high gas solubility as shown in

Figure 3.

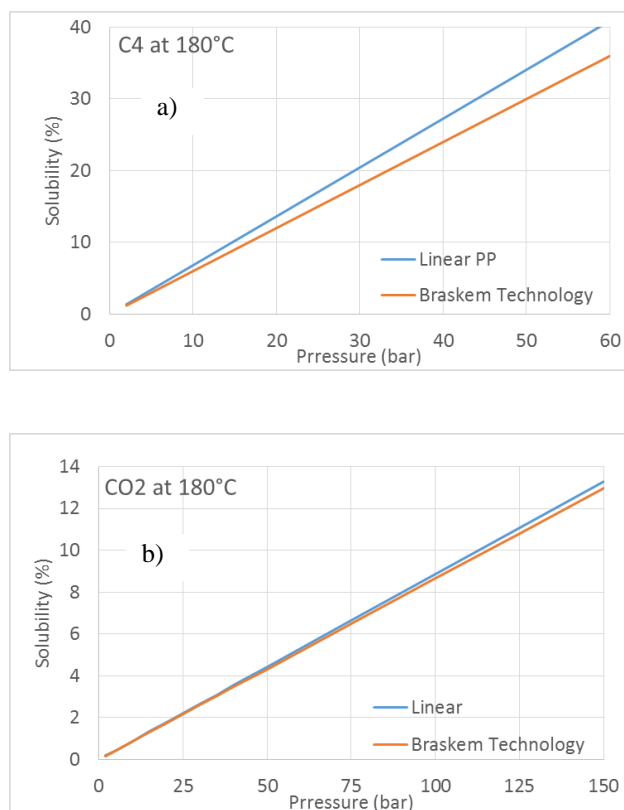


Figure 3 -AmPPleo 1020GA solubility in different gases
a) Butane and b) CO₂.

Foaming Performance

Foam performance can be evaluated by measuring the response of density to gas feed content, process temperatures, and formulation including talc and chemical blowing agents.

Density x Gas amount

Figure 4 demonstrates that AmPPleo can achieve a wide range of densities, using several different physical blowing agents, specifically, CO₂ and isobutene.

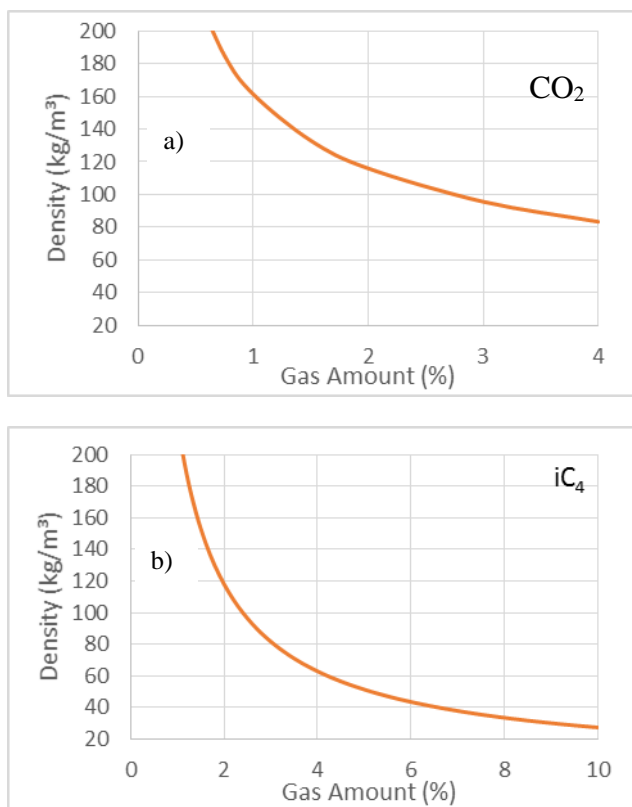


Figure 4 – Effect of gas feed amount on foam density for a) CO₂ and b) Butane.

Optimum Foaming Temperature

Figure 5 confirms that the optimum foam temperature for AmPPleo HMSPP decreases with increasing gas feed concentration. The trend is expected, because higher gas feed leads to decreased melt viscosity. The optimum foam temperature also depends on the specific formulation, including the presence of nucleating agents.

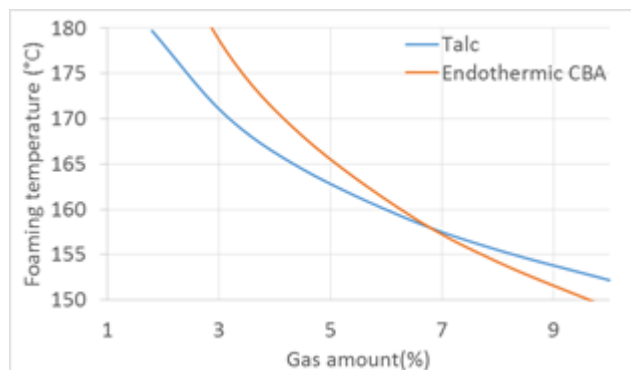


Figure 5 – Optimum foam temperature response to feed amount of C4 1.

Foam Characteristic with C4

Foam performance depends strongly on cell structure as well as density. Therefore, an HMSPP grade that is effective for low-density foam must offer the possibility of generating a high level of closed cells that support foam process performance or open cells for special applications.

Two key factors affect cell structure. The first is the cell count. The higher the cell count, the thinner the cell walls, which makes it much more difficult to maintain an intact structure. The second driver is the cell nucleation mechanism. For example, using talc as a cell nucleation agent presents another problem, because the talc can promote some defects in cell structure such being a source of open cells. The effect of talc concentration on AmPPleo cell count is shown in Figure 6.

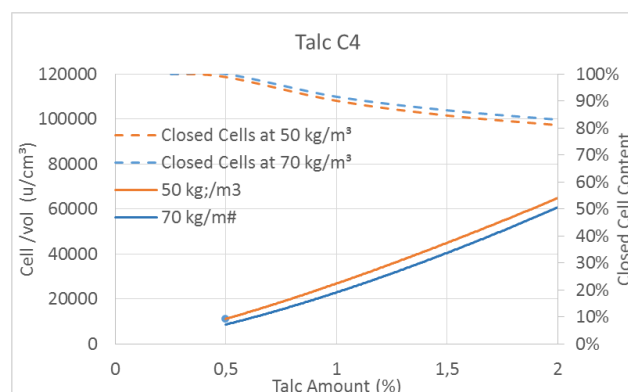


Figure 6 – Cell count and close cell content against Talc loading to C4 densities.

For both densities, there is a slow decrease in cell count, indicating that the talc effect on closed cell content is stronger than the decrease in cell wall thickness. It is an important conclusion which indicates how robust the AmPPleo may be for different final applications, mainly for large/medium cell sizes.

However, some applications require a more fine structure with a larger numbers of cells and also do not allow reduction in closed cell content. A solution is the use of CBA's. These two CBA's, 1 and 2, give different density responses using Butane, as shown in Figure 7.

Using different CBA's the cell count increases at different rates. This is important for process control. It is one more important aspect in final product development.

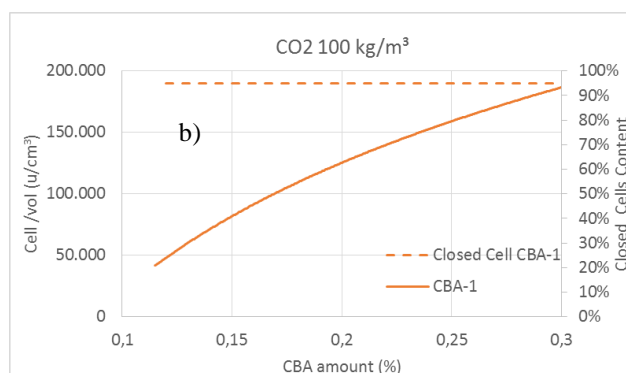
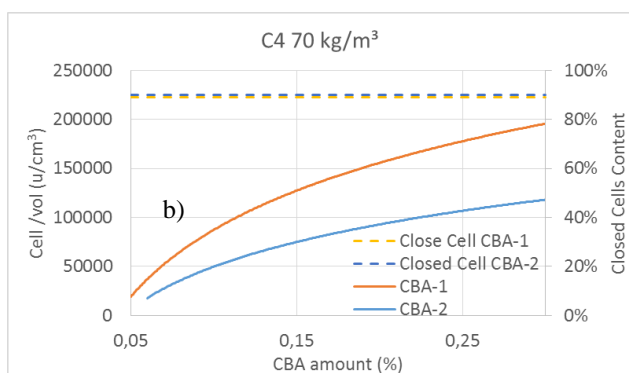
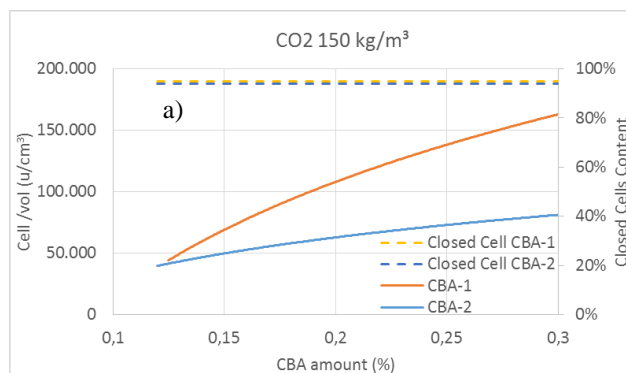
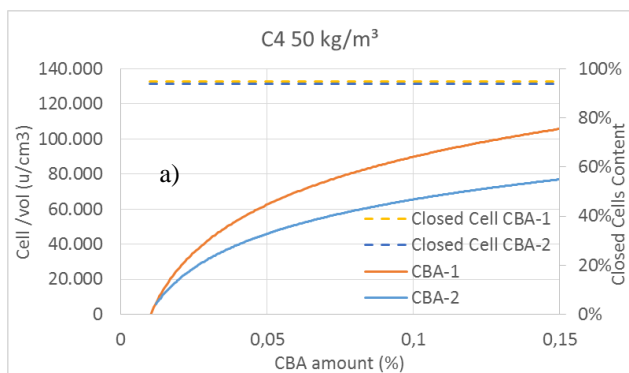


Figure 7 – Closed cell content and cell count using Butane and different CBA's at a) 70 kg/m³ and b) 50 kg/m³.

Figure 9 – Effects of CBA's on cell count and closed cells content using CO₂ as PBA: a) 150 kg/m³ and b) 100 kg/m³.

Foam Characteristic with CO₂

The effects of density and cell nucleating agent on cell morphology are somewhat different for foams produced using CO₂ than for foams produced using butane. As shown in Figure 8, the cell count is more dependent on density, and less so on talc feed concentration. Also, using CBA's increases the cell count to a greater extent than using talc; however, no changes in closed cells were observed.

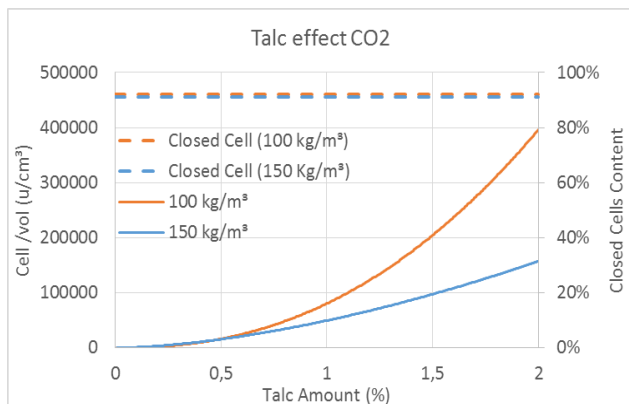


Figure 8 - Talc effect on cell count using CO₂ as PBA for different densities.

Conclusions

This paper demonstrates the melt rheological attributes and foam processing and performance properties of Braskem's new high melt strength PP, AmPPleo 1020GA. It also demonstrates the very good performance of the Braskem AmPPleo 1020GA in different foaming densities, compositions and structures. The broad processing window, with a suitable response to foaming temperature and nucleation create multiple density possibilities. AmPPleo is a new option in the market for PP foams development.

References

1. BORSIG, E. et al. Long chain branching on linear polypropylene by solid state reactions. European Polymer Journal, 44, 2008, 2012, 2008.
2. LAGENDIJK, R. P. et al. Peroxydicarbonate modification of polypropylene and extensional flow properties. Polymer, 42, 10035-10043, 2001.

3. TIAN, J.; YU, W.; ZHOU, C. The preparation and rheology characterization of long chain branching polypropylene. *Polymer*, 47, 7962-7969, 2006.
4. AUHL, D. et al. Long-chain branched polypropylene by electron beam irradiation and their rheological properties. *Macromolecules*, 37, 9465-9472, 2004.
5. LANGSTON, J.A. et al. Synthesis and characterization of long chain branched isotactic polypropylene via metallocene catalyst and T-reagent. *Macromolecules*, 40, 2712-2720, 2007.
6. LI, S. et al. The melt grafting preparation and rheological characterization of long chain branching polypropylene. *Polymer*, 50, 6121-6128, 2009.
7. ZHANG, Z. et al. A new grafting monomer for synthesizing long chain branched polypropylene through melt radical reaction. *Polymer*, 53, 121-129, 2012.
8. WENG, W. et al. Long chain branched isotactic polypropylene. *Macromolecules*, 35, 3838-3843, 2002.
9. MABROUK, K. et al. Chemical modification of PP architecture: strategies for introducing long-chain branching. *Polymer*, 50, 5390-5397, 2009.
10. AZEREDO, A. P., FARAH, M. Process for producing modified poly(propene), the modified poly(propene) and the use thereof, and the polymer blend. US20160355644. Dec 8, 2016.
11. WONG, B., BAKER, W.E. Melt rheology of graft modified polypropylene. *Polymer*, 38, 2781-2789, 1997.
12. TABATABAEI, S.; CARREAU, P.J.; AJJI, A. Rheological and thermal properties of blends of a long-chain branched polypropylene and different linear polypropylenes. *Chemical Engineering Science*, 64, 4719-4731, 2009.
13. STADLER, F., KASCHTA, J., MÜNSTEDT, H. Thermorheological behavior of various long-chain branched polyethylenes. *Macromolecules*, 41, 1328-1333, 2008.
14. W. Zhao, Y. Huang, Q. Yang. The molecular structure characteristics of long chain branched polypropylene and its effects on non-isothermal crystallization and mechanical properties, *Polymer*, 2013, 54, 1455.

SEPARATING PROCESS STEPS LEADS TO NEW FOAM EXTRUSION MACHINERY

Frank van Lueck, AIXtrusion Consulting, Kaarst, Germany

Abstract

The consumption of resources can only be reduced by not using them at all. Therefore foaming is the key technology of the 21st century. Life Cycle analysis confirm this view: foamed oil based polymers are equal or better in carbon footprints compared with non-foamed bio-polymers. As a result, more and more research is dedicated to foaming technologies (injection molding, autoclave, rubber foaming,...). Only in foam extrusion, the most common and since 50 years industrial successfully used technology, still only is able to use a few polymers. In the last 25 years, only PP and PET material developments have enabled to use these polymers on top of PS and PE.

During the same time period, the only new machine development was the use of twin screw extruders, that have been substituting single screw extruders in foam tandem lines, as the twin screw extruders have shown major advantages using CO₂ as blowing agent in the XPS insulation board industry.

When in Europe due to the reach regulation since 2015 new fire retardants ("FR") must be used, now even the twin screw extruders show disadvantages: the higher speeds, that enable better mixing, is increasing the melt temperature, which is critical above 190°C, leading to thermal degradation of the FR (bio-polymers are equal to FR) - as a result twin screw extruders are running less than half speeds.

The solution is to separate the process steps melting from mixing. The Gneuss MRS PET recycling extruder was further developed as a mixing extruder that is replacing the connection pipe between primary extruder and cooling extruder (or static coolers).

As a result, melt temperature is below 190°C, blowing agent is much better dispersed so that lower densities with similar product properties can be achieved. As well the process pressures in the system can be reduced, enlarging the process window.

Introduction

The biggest application of extrusion foaming is the production of insulation boards. While other extrusion

foamed products are made by a variety of different extrusion technologies, insulation boards are mainly produced on tandem extrusion lines. Only a few machines have static coolers instead of cooling extruders, mainly made in the early years - with thicker boards, more output is needed to produce "thickness" which only cooling extruders can give.

Machine technology today

The primary extruders of these tandem foam extrusion lines are extended in length compared to regular extruders: a "regular" extruder, in which the solid ingredients (material, color, nucleant, flame retardants,...) are processed, an extension is added, in which the blowing agent(s) are injected into the melt and the material recipe is mixed. Single screw extruders are having a process length for example about 32 to 36 L/D compared with 24 to 27 L/D of regular extruders.

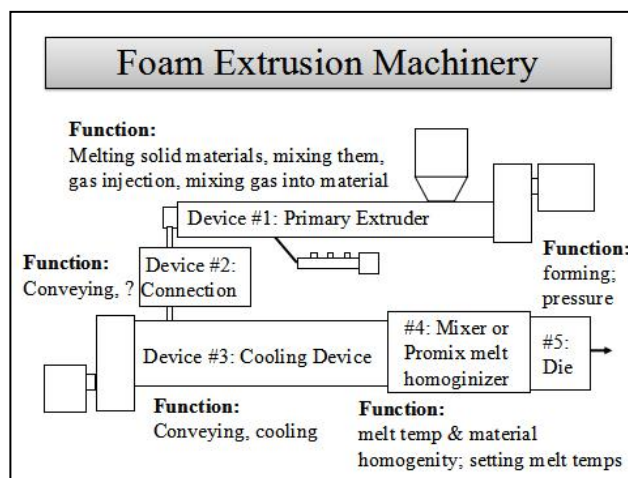


Figure 1: Process functions of foam extrusion machinery

One main target in foam extrusion is to keep the melt temperature low. If flame retardants are used (Polystyrene "PS"), melt temperatures are requested to remain about 190°C (new flame retardants in Europe) to 200°C (HBCD flame retardants). Even if no flame retardants are used, temperatures should remain low, as the foaming materials have elongated polymer chains that allow better foaming - and these longer chains are sensitive against shear and high temperatures. Moreover, in average 35% of the material comes from internal recycling, containing regrind that has been internally recycled in average 5 times and as such was stressed significantly.

The melt is then transferred into the second extruder.

Here the melt temperature is being reduced: the blowing agent has significantly reduced the melt viscosity. Without increasing the melt viscosity by dropping the melt temperature the melt would not have enough resistance to withstand the bubble expansion of the blowing agent behind the die. If e.g. CO₂, that has the biggest foaming / expansion pressure, is used as blowing agent, the final melt temperature needs to be dropped to about 110°C.

Some research on small and medium output production lines has been made, showing that the melt that exits the cooling extruder varies from screw to barrel by more than 20K. To compensate, a mixer is used behind the cooling extruder. Most mixers are followed by a “sleeping tube”, as the mixers are too short for thermal homogenization. Making them longer would create significant pressure drop, that most extrusion lines can not overcome, so that the sleeping tubes help to uniform the melt temperature a bit more.

Insulation boards are produced on flat dies. The exiting gap mainly is a slot (PS, PET), but for some materials, a perforated plate is used (PE, PET, SAN).

The “Cross Over”

If the pressure drops too much before reaching the die, the blowing agent would vaporize before exiting the die and the bubbles would be crashed when forced through the die gap so that no or bad foam products would be obtained. If a machine design does not allow to control the pressure or to build up pressure, pressure drop must be watched carefully. The most critical area here is the connection between the 2 extruders (“cross over”): to allow maintenance work, a spacing of minimum 1 meter is required, that has been extended now to more than 2m.

This connection has been mainly a heated pipe. A pipe is causing a significant residence time distribution: the material in the middle is flowing 10 times faster than the material at the side. This leads to mechanical and thermal de-mixing. Thermal critical materials like the flame retardants can be stressed significantly. As well blowing agents are de-mixed, so that in best case more blowing agent must be injected. In the worst case, the foam product contains gas pockets and can not be sold.

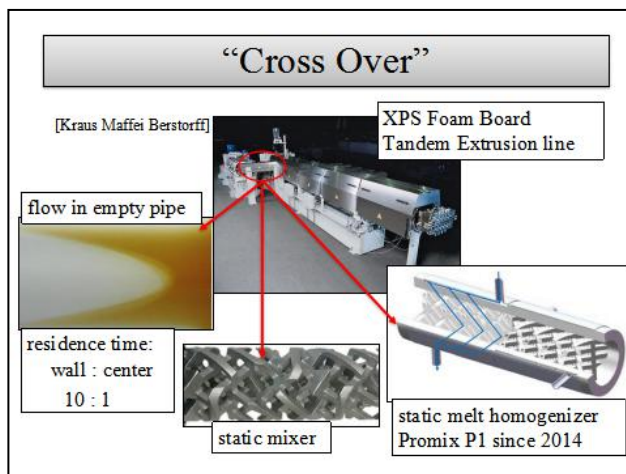


Figure 2: Options for the connection pipe

If pressure drop is not critical, mixers can be used to avoid de-mixing. As the mixing effect is lost about 1 L/D after the last mixer, the whole pipe should be fully equipped with mixers. Due to the shear stress, mixers are increasing the melt temperature, again resulting in negative stress that just should have been avoided by using the mixer - if the distance is not too long, mixers are always better than an empty pipe.

To avoid the melt temperature increase, the use of static coolers is an option - not replacing the cooling extruder but the empty pipe. Static coolers on the other hand are bad material mixers, so that a static cooler should be followed by a mixer. In 2014 Promix has launched the “melt homogenizer P1”, combining a mixer with temperature control and as such avoided all negative effects of residence time distribution. Replacing a 2m long melt pipe with the P1, the flame retardant consumption (EU) was dropped by 50%!

Unluckily, about 90% of all insulation board tandem foam extrusion lines have “open” cooling screws. These “open” screws are pressure consuming screws and as a result, pressure drop is a significant problem. As both mixers and melt homogenizers are pressure consuming, they can not or only limited be used in these machines. Adding a melt pump increases shear stress that has again similar negative stress effects and is therefore not the right solution (besides cost, maintenance and leakage problems).

The “Foam MRS” device

To overcome this problem, a new solution was developed. In 2007 the company Gneuss has developed a recycling extruder, that e.g. can transfer any kind of PET regrind into FDA approved sheets of pellets on 100% regrind. This extruder is a single screw extruder with a special part in the center, the “MRS” unit: for a short section, the diameter of the single screw is increased. In

this part, small screws / spindles are counter rotating inside the bigger screw. The small spindles are hold inside the housing, so that single extruder gear boxes and motors can be used, reducing significantly the cost of the extruder compared with planetary, multi or twin screw extruders, that need special gear box designs.

In this section, vacuum is applied to take out the volatile contamination of the melt. Due to this special design, the MRS is producing a surface exchange area, that is about 40 times bigger compared with twin screws and as such guarantees to take out 100% contamination.

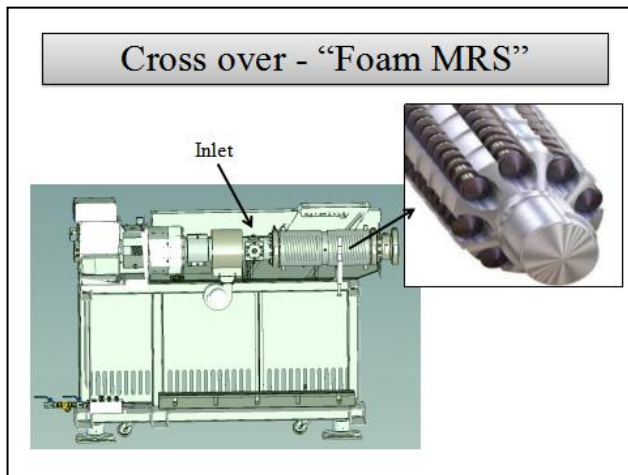


Figure 3: "Foam MRS Concept"

For foam extrusion, only the heart, the MRS part was used. In the "foam MRS" the de-gassing function was transferred into a mixing function with conveying potential, minimizing residence time distribution and overcoming the pressure limitations.

The "foam MRS" is fed with melt from the primary extruder - it does not have melting capabilities. As such the unit is short and can be retrofitted into existing machines without or only slightly moving any equipment. So the "foam MRS" is an add-on unit, that cannot stand alone.

In 2015 a XPS tandem foam line was retrofitted with a "foam MRS", replacing the cross over pipe between the 2 extruders. Most primary extruders are put on wheels so that they can slide backwards and forwards 30 to 50 cm. This was unluckily not the case here. On top due to production pressure the request was to shorten any down time and return to the original situation within a few hours in case of failure. So the "foam MRS" was in this case even build around a platform.

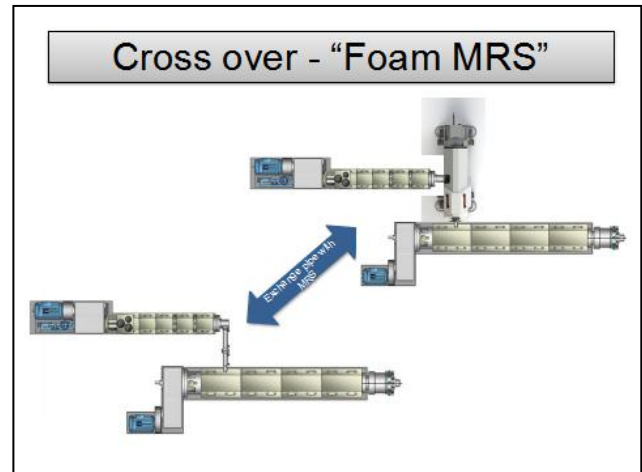


Figure 4: Foam MRS for retrofit

The speed of the center screw can be increased up to 50 rpm. At that speed, the small spindles are running on approx. 200 rpm. By changing the speed, the pressure at the "foam MRS" exit can be varied. Regular exit / inlet pressure into the secondary extruder was on the old set up about 150 bar.

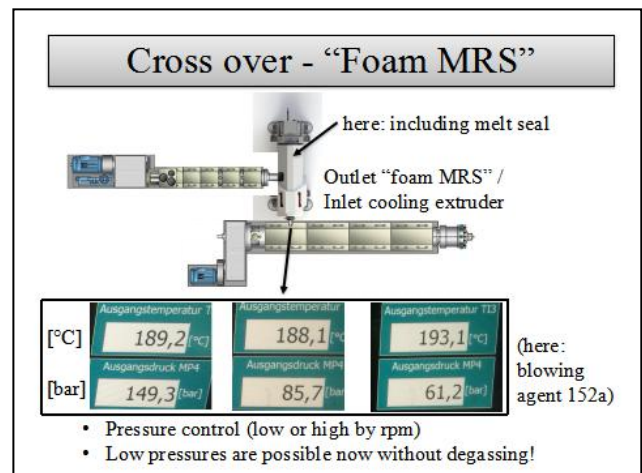


Figure 5: Process pressure independence

By screw speed, pressures could be lowered down to 60 bar. As the secondary extruder did contain a melt pump at the end, the die pressure could be kept high enough for foaming. It was found out, that even at 60 bar good foam was achieved! The pressure was independent from the melt temperature, which was started at about 200°C. The melt was in production successfully lowered below 190°C in the MRS to avoid the degradation of the flame retardant.

Comparison of technology

So with the foam MRS a device was developed that allows a precise residence time & melt temperature distribution as well as pressure control and as such overcomes the limitations of the alternative technologies.

Summary “Process”						
Device option	Active			Passive		
	mixing in / into	melt temp	pressure	residence time distribution / de-mixing	melt temp	pressure
empty pipe	-	-	-	significant increase	wide spread	big drop
mixer	neutral / little improved	-	-	avoided	homogenized	medium drop
melt homogenizer P1	neutral / little improved	adjustable	-	avoided	homogenized	medium drop
Foam MRS	adjustable	adjustable	adjustable	avoided	homogenized	no drop / independence

Figure 6: Comparison of machinery options

Important to explain more in detail at this point is the word “mixing”.

Explanation of “Mixing”

The word “mixing” implies an active function. This is not correct for foam extrusion! “Mixing” as active function is given only when the blowing agent is injected and dispersed into the melt - so being “mixed in / into” in the primary extruder. Once the blowing agent is inside the melt it must be kept fine dispersed in it. Assuming, it was “mixed in”, from now the reversed effect, the “de-mixing”, must be avoided. So behind the primary extruder, “mixing” is now getting the passive function “de-mixing”. To avoid further complications, the melt temperature is not “mixed” by static mixers, but “homogenized” by them.

Homogeneous mixing

Working with the “foam MRS”, interesting results were found. Foam boards were produced without using nucleation at all! As R152 was used as blowing agent, that is not self-nucleating in PS, the result only allows one conclusion: the “foam MRS” is now enabling a homogeneous mixing, as otherwise no regular foam structure could have been made! This on the other hand leads to the understanding that the mixing of blowing agents into the melt before was only heterogeneous - even using twin screws as primary extruders!

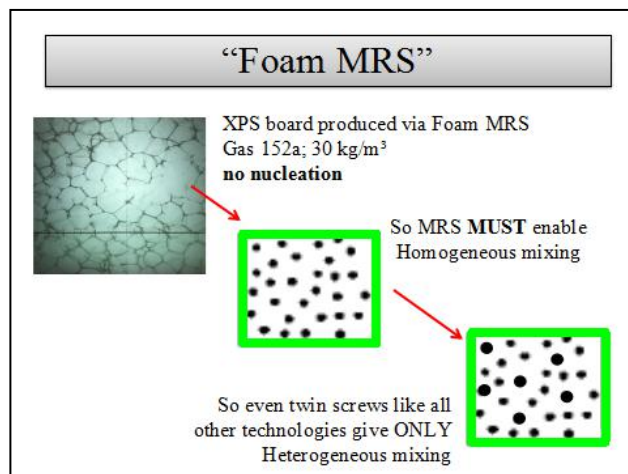


Figure 7: Mixing - the new quality showing our reality

With the potential shown of the “foam MRS”, more tests have been made with blowing agents that are more difficult to be used. All of these blowing agents can be mixed easy into the melt.

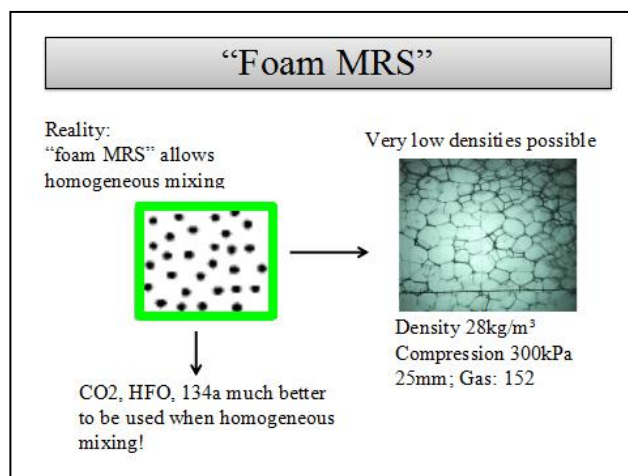


Figure 8: Results of homogeneous mixing

As well the density of the foam board could be reduced significantly, keeping all requested properties on low densities and this even on low board thicknesses!

Product benefits

Summarizing the benefits, inserting the “foam MRS” between primary extruder and cooling extruder (device), lower densities can be achieved, keeping all needed properties due to a better foam structure.

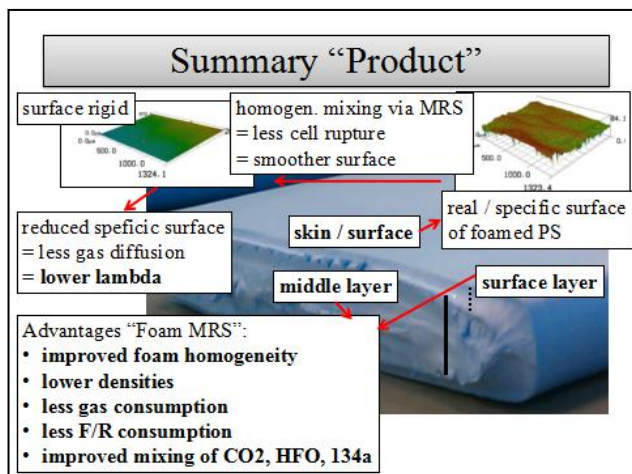


Figure 9: Product benefits

By the homogeneous mixing and improved residence time distribution, less blowing agent is needed and even HFO as one of the most difficult to use blowing agents can now be mixed easily into the melt. With controlling the melt temperature, critical additives like flame retardants can be reduced in consumption as well.

Separating the process steps

So by adding the “foam MRS” into tandem foam lines, it is possible to now separate process functions. When all mixing can be done in the MRS, the primary extruder would only need to melt the material and the solid additives. So then even regular length single screw extruders can be used with 24 to 27 L/D process length.

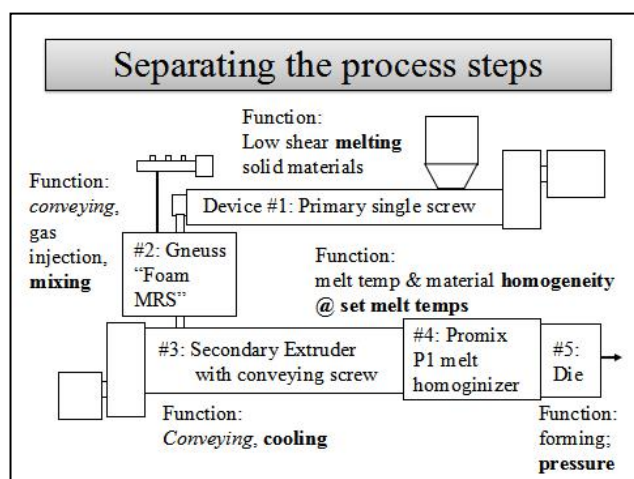


Figure 10: Advised machinery set up

The “foam MRS” can increase the pressure / reduce the pressure need for the following sections, so that a Promix P1 melt homogenizer can be added after the cooling extruder even if pressure consuming “open” cooling screws are used.

Nevertheless are “open” cooling screws increasing the residence time distribution and as such leading to demixing, which at the end will get to the bottle neck when using CO₂ or other “difficult” blowing agents like R134a or HFO. So optimum is then to cool the melt in a cooling extruder, that is equipped with a conveying screw.

The Promix P1 melt homogenizer is then used to adjust the desired, homogenized melt temperature, separating the cooling step (cooling extruder) from adjusting the melt temperature.

As well the die is solely used to set the foaming pressure, if conveying screw plus Promix P1 is keeping material flow and melt temperature stable.

“Open flighted” cooling screws on the other hand are behaving different. Changing the die pressure leads to a pressure change throughout the whole extrusion line back to the position of maximum pressure build up inside the primary extruder. As a result, local residence time within the different machinery sections is changing. Changing the residence time in cooling zones leads to a change in heat transfer, resulting in a change of melt viscosity. This again is influencing the pressure drop. So the result is a non-constant process that requires permanent operator adjustments.

Conclusions

The possibility to overcome this unstable, swinging system are presented in the paper. Even not having a conveying cooling screw, adding a “foam MRS” into the system allows the use of a P1 and as such enabling now much better process control.

Outlook

At present, the European regional developing fund (EFRE) and the German federal state Northrhine Westphalia (NRW) are funding a research project (OP EFRE “Schaum MRS Reaktor”) to further develop the “foam MRS” into a reactor. If residence time can be precisely defined, chemical reactions can be controlled. One example is the chain extension process that is needed for PET foam extrusion, where IV ~ 1.0 is desired. The bigger the machine, the bigger is the residence time window and the more uncontrolled the extension process takes place. Negative example is the presentation of a PLA foam line on a conference in Europe in 2015, where a molecular weight increase by factor eight (!) was pretended to be found on a 800kg/hr production line - in reality this was a “cross-linking” of PLA chains by uncontrolled chain extension. With the control of the residence time distribution, chemical reactions can be controlled and such problems can be avoided, opening up the foaming technology for new applications.

Vision

A regular length single screw extruder with batch gravimetric dosing station plus “foam MRS” is an alternative in terms of costs and functionality to a twin screw extruder with loss-in-weight dosing stations! So there might be in the future an alternative for twin screw extruders for compounding functions!

ATYPICAL TWIN SCREW EXTRUSION COMPOUNDING SYSTEMS FOR POLYOLEFINS

Charlie Martin, Leistritz Extrusion, 175 Meister Avenue, Somerville, New Jersey 08876, U.S.A.

Abstract

Plastics is a major worldwide industry that plays a role in all facets of modern life, from health and well-being, nutrition, shelter and transportation, to safety and security, communication, sports, and leisure activities. Almost every polyolefin based polymer has been processed at some stage on a twin screw extruder to mix materials to impart desired properties into products such as packaging films, fibers for carpets, car interiors and windshields, structural decking, conductive parts, and synthetic wine corks. These are all high-tech products!

Introduction

Developed almost 100 years ago, twin screw extrusion (TSE) is now the industry standard to perform mixing, devolatilization and reactive extrusion processes for polyolefin and other polymer based formulations. The vast majority of TSEs make pellets. Some are configured to directly extrude continuous shapes or “parts”. In both instances, TSE technologies are being applied to non-traditional operations to manufacture a variety of new products.

The high speed co-rotating intermeshing twin screw extruder is the most prevalent device for continuous compounding applications. The intense inter-screw mixing associated with the short mass transfer distances inherent with a TSE and the possible use of low or high screw speeds (i.e., 1000+ rpm) makes the TSE a highly efficient and versatile mixing device. Entrapped air, moisture and volatiles are also removed via venting.

The TSE process is dependent upon the rotating screws contained within barrels to impart energy into the materials being processed. Screws are segmented and assembled on high torque shafts. Screw designs can be made shear

intensive and/or passive. Mixing elements may be dispersive, distributive, or a balance of each/both. (Fig. 1)

Process control parameters include screw speed (rpm), feed rate, barrel/die temperatures, and vacuum levels. Typical readouts include melt pressure, melt temperature, and motor amperage. Monitoring these values ensures what's being produced is consistent and repeatable.

A metering system sets the rate to the TSE. Feeders utilize various delivery mechanisms, including: vibratory trays, single screw and twin screw augers. Loss-in-weight (LIW) feeders maintain a constant mass-flow rate to the TSE by adjusting the feed mechanism based on materials usage from the hopper that is situated on a load cell. Liquid feed streams use various types of pumps (i.e., piston or gear pump) depending upon the viscosity of the liquid. Crammer feeders can also be used for highly filled and/or low bulk density materials.

The TSE is referred to as “starve-fed” because the TSE screw rpms are independent from the feed rate. The pressure gradient along the length of the TSE process section (barrels/screws) is primarily influenced by the selection of screws. Flighted screw elements are strategically placed so that the screw channels are not filled, which results in a zero-pressure underneath feed and downstream vent/feed sections, facilitating strategic sequential feeding and preventing vent flooding. (Fig. 2)

The addition of materials into the melt stream of a TSE is often facilitated by a side stuffer. A side stuffer is a twin screw auger that “pushes” material into the process melt stream to minimize screw/barrel wear, residence time and shear exposure for sensitive materials. Liquid injection into the process section is also possible. In some cases, sequential feeding may eliminate the need for premixing of feedstocks.^[1]

Downstream systems size and cool the extrudate, with a multitude of high-tech equipment options available to make high-quality,

precision parts. Pressure generating devices, such as a gear pump or screw pump can also be mated to the twin screw extruder to help manage melt pressure and temperature.

In the context of the above discussion the following statements generally apply to co-rotating, intermeshing twin screw extruders:

- Recycling is an area where TSEs have not been widely used due to difficulties/limitations associated with processing contaminated feedstocks
- The starve fed TSE is a better mixer than a pump, as compared to a single screw extruder (SSE)
- TSEs tend to run at much higher screw speeds than SSEs
- Almost every TSE integrates venting/devolatilization into the process, with multi-stage venting being common
- Most TSEs make pellets where dimensional tolerances are a secondary concern as compared to achieving a homogenous mix (without degrading the product)
- TSEs, compared to SSEs, are low pressure machines, rated for operation at less than 3500 psi and very seldom operated above 2000 psi
- Probably 99% of TSEs are the only extruder in the system, as opposed to part of a tandem or co-extrusion system
- Almost all TSEs process plastics, as compared to rubbers, due to torque and cooling limitations

In the context of the above the following are examples of TSEs that have been integrated into atypical system configurations.

Using the TSE to purposely increase the MFI of HDPE

In virtually every process the goal of the TSE is to mix materials together with minimal degradation and maintain mechanical properties. Too much shear often results in degradation. However, the TSE can be purposely used to “intensively” mix the polymer and increase the MFI in a controlled and purposeful way to match its’ flow properties

to a subsequent process.

For example, a fractional melt HDPE scrap material from an in-house process can be ground and metered into a TSE that will operate at very high speeds (800+ rpm) with elevated temperature set points (i.e., 100°C higher than normal). The screw design will include high energy input neutral and reverse kneading elements to maximize the energy imparted by the rotating screws and motor. The resulting melt temperature might be 100°C above what’s typically deemed optimal. (Fig. 3)

By using the TSE in this process as described a fractional melt HDPE scrap was modified into a molding grade MFI so that the materials could be reused in a molding process, facilitating close to 100% utilization of the raw materials coming into the facility.

Integrating a TSE into a coextruded foamed profile

TSEs can be used to mix supercritical fluids with PE and PP to produce foamed parts. The screw design will integrate a dynamic seal prior to the injection of sCO₂ at high pressure. High pressures necessitate the use of a one-piece barrel or modified barrel flanges. Once the supercritical fluid is mixed and dissolved, the TSE screws pump and cool the melt. Near the end of the screws, high-distributive rate mixers are used to thermally homogenize the melt prior to discharge.^[2] (Fig. 4)

Unlike most high speed TSEs, for this application screws are operated with filled screw channels and at lower speeds (200 rpm or less). The TSE barrels are used as a heat exchange device to cool and condition the melt and maintain viscosity into the die. For rates below 200 kg/hr, the TSE may be able to directly pump into the die.

Customized coextrusion dies may be specified to accept melt streams from single screw extruders to facilitate unique multi-layer structures. For instance, a thermoplastic elastomer might be added as an external layer of a coextruded structure to facilitate texture and printing capabilities.

The usage of a TSE in this example is unique because: the TSE is both mixing and serving as a high-pressure pump to make a

precision part, and is also being integrated with a SSE to make a unique, multi-layer structure.

Recycling and devulcanization of tire rubber with in-line Thermoplastic Vulcanizate (TPV) production

A patented thermo-mechanical devulcanization process, with no chemical agents, was developed for recycled ground tire rubber using a TSE.^[3] Ground tire rubber particles are metered into a TSE and conditioned via shear prior to injection of sCO₂ that acts as a plasticizer to facilitate and complete the devulcanization process. The resulting devulcanized rubber can then be processed/revulcanized.

By extending the length of the TSE process section to 60/1 L/D, a second extruder can meter a molten PP feed stream into the TSE process section to prepare a TPV material. Resulting volatiles are controlled and removed via multi-stage venting, and the TSE is now be mated to a traditional downstream system to make a profile, sheet or pellets.

This system as described is unique for a number of reasons: TSEs are generally not used to process rubber formulations, the process as described has never been done before and the extended L/D facilitates its' integration as part of an in-line TPV compounding system. (Fig. 5)

High level filler compounding of Post Consumer Reclaim (PCR)

Processing of HDPE, PE and PP Post Consumer Reclaim (PCR) materials present particular challenges for a TSE. The materials must be thoroughly washed and dried. Metals must be removed from the feed stream as severe damage will result if these are metered into a closely meshing, high speed TSE. Residual moisture from the washing step can be problematic from a processing perspective.

In every instance, filtration will play a key role in making a good product, which often requires high pressures. Accordingly, it may be preferable to use a SSE to melt and pump the PCR feedstock through a screen changer prior to mixing the fillers in the TSE. A gear pump would

then be mated to the exit of the screen changer to "meter" a specific rate of the "clean" melt to the twin screw extruder. The TSE will mix fillers (up to 80%) and additives with the polymer and the TSE can pressurize an underwater pelletizer.

The process as described is different from a traditional TSE compounding system for a number of reasons. The melting and filtration of the PCR materials are performed upstream of the TSE. A gear pump then functions as a metering feeder, pumping into the TSE feed zone. The TSE can now use a shorter L/D and smaller horsepower motor because of the upstream melting and filtration unit operations being performed before the melt enters the TSE. The TSE now only needs to complete traditional mixing and devolatilization functions.^[4] (Fig. 6)

Conclusion

Twin screw extrusion is a battle hardened, well proven, manufacturing process that has been validated in 24 hour/day industrial settings for more than half a century. The superior mixing characteristics inherent to a co-rotating intermeshing twin screw extruder has resulted in this device being the preferred manufacturing methodology for polyolefin and plastics compounds. The dominance of the TSE in this capacity has spawned intensive machine development efforts and extensive industry research, which is responsible for the current level of understanding and experience with TSE mixing technology. The continued expansion of TSE technology as part of atypical extrusion systems will help improve manufacturing efficiencies in a wide variety of new applications that benefit from the consistent and less costly TSE in-line mixing process.

References

1. C. Martin, *Twin Screw Extruders as Continuous Mixers for Thermal Processing: a Technical and Historical Perspective*, **AAPS Pharm SciTech** (2016)
2. W. Thiele, C. Martin, *Extrusion Equipment for Foam Processing*, **Pharmaceutical Extrusion Technology**, **10**, 293 (2007)

3. Tyromer Patent # US20130023595 A1, Method and Apparatus for Regenerating Vulcanized Rubber, (2013)
4. C. Martin, presentation “Integrating

Compounding Twin Screw Extruders Into PCR/PIR Reclaim Systems”, SPI Refocus Recycling Summit & Expo, Orlando, FL (April 25-27, 2016)

Figures



Figure 1: Co-rotating intermeshing twin screw extruder screws

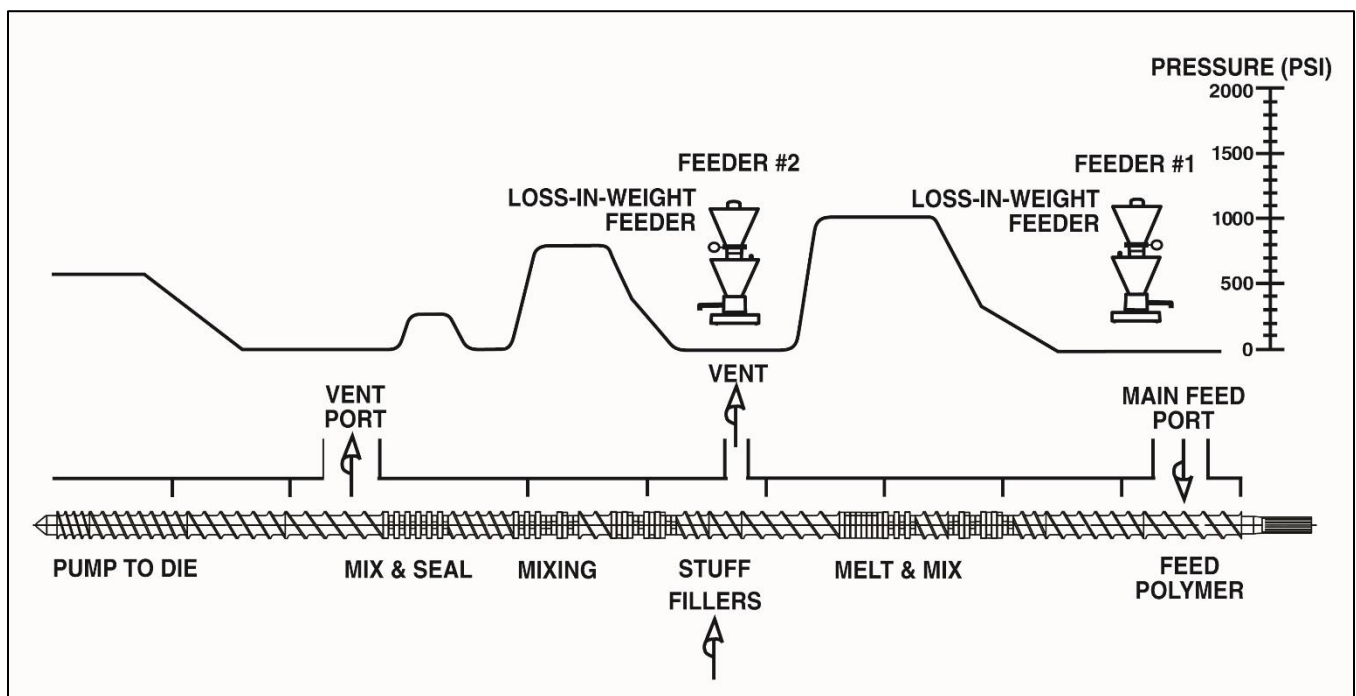


Figure 2: Pressure gradient in a typical twin screw extruder system

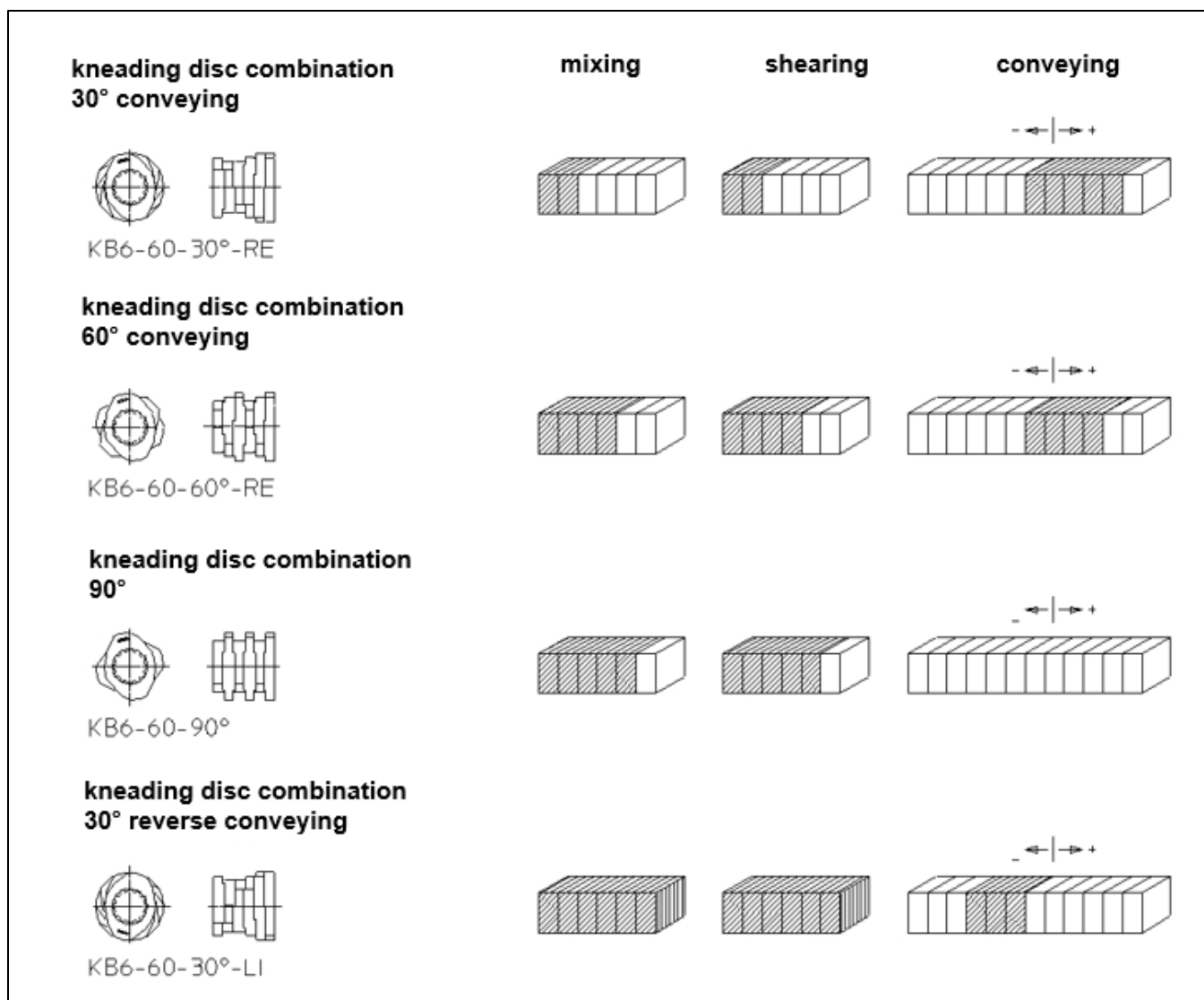


Figure 3: Examples of forward, reverse and TSE mixing elements

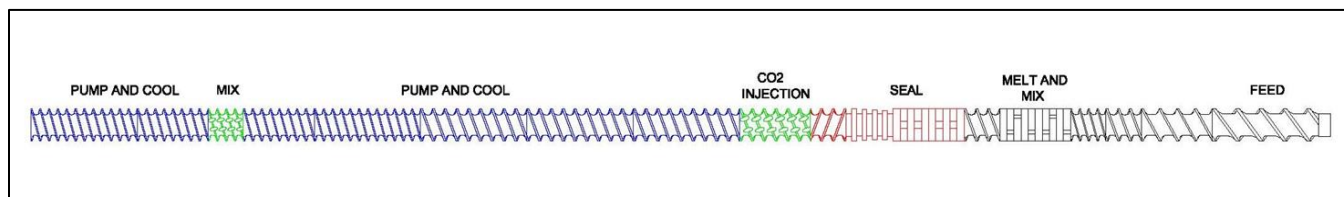


Figure 4: Screw design for sCO₂ injection for direct profile extrusion

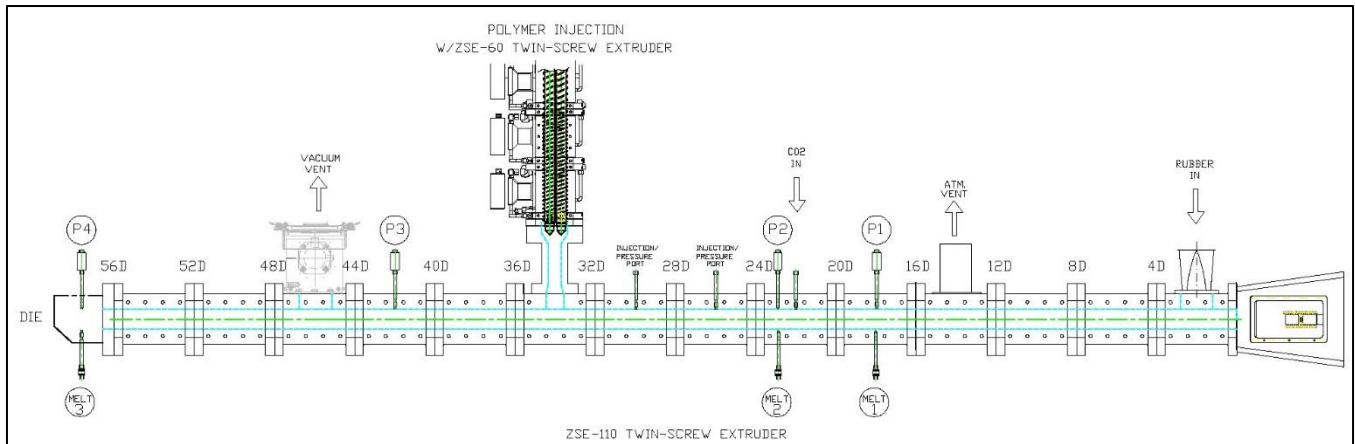


Figure 5: Process schematic for devulcanizing tire rubber and TPV processing

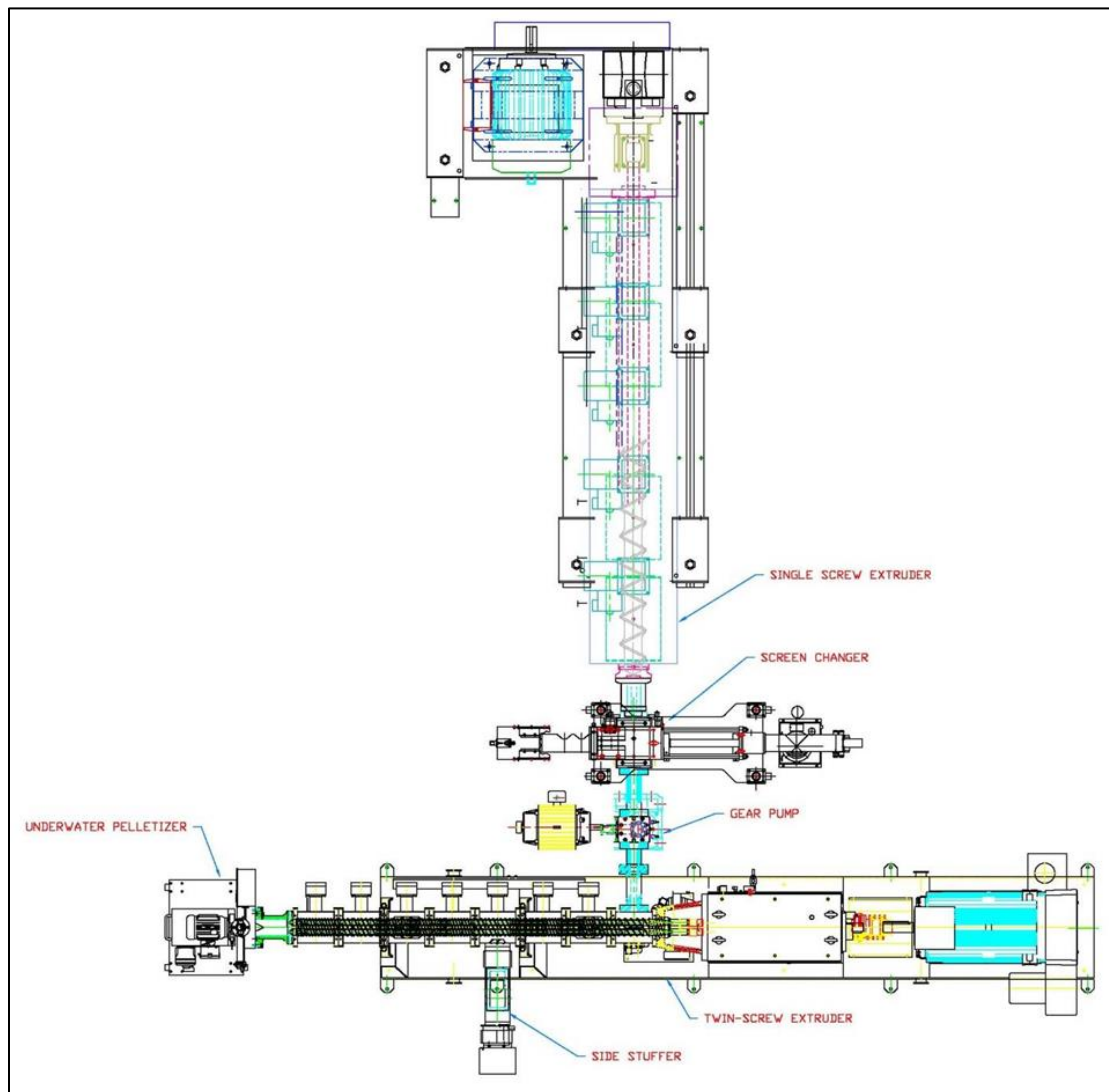


Figure 6: System design for PCR reclaim and high-level filler compounding

CHANGEOVER TIME FOR SINGLE AND TWIN-SCREW EXTRUDERS

*Christopher Thurber, Hyunwoo Kim, Jin Wang, Bob Wrisley, Eric Marchbanks, Xiaoyun Chen
The Dow Chemical Company, Midland, MI*

Abstract

Changing extrusion formulations causes downtime and wasted materials before a new steady state is achieved. Accurate determination of changeover times minimizes these negative impacts. In this work, changeover times are compared for single and twin-screw extruders by online Raman spectroscopy. Our results show that twin-screw extruders usually purge more quickly than single-screw extruders, attributed to their self-wiping design.

Introduction

The purpose of this work is to determine factors that influence downtime when changing extrusion formulations. Minimizing this downtime has the potential to increase production and reduce waste. In particular, this work aims to quantify changeover times for a single-screw extruder (SSE), and compare these times to those found previously for a twin-screw extruder (TSE). Our hypothesis is that TSEs will changeover more quickly, as a result of their self-wiping design.

Due to the complex, transient nature of extrusion formulation changes, theory is inadequate for accurately predicting residence times and changeover times. Therefore, an experimental approach is usually implemented, in which a step change is imposed on the feed formulation and the discharge composition is monitored until a new steady state is reached.

Several papers have reviewed online methods for measuring exit composition in extruders [1-3]. Some of the most sensitive and robust techniques include spectroscopic methods [4]. For example, Alig et al. demonstrated online near-infrared (NIR), Raman, and ultrasonic spectroscopy to quantify antioxidant and carbon black concentrations in polymer extrudates [5]. Coates et al. also utilized online NIR, Raman, ultrasonic, and attenuated total reflectance infrared (ATR-IR) spectroscopy to monitor a variety of mixtures and reactions for molten polymers [6].

Gilmor et al. used a charge coupled device spectrometer to study changeover times between red and blue colored masterbatches in a SSE.[7] They found changeover times ranging from 3 – 20 minutes when transitioning between a white purge material and 95 / 5 blends of linear low density polyethylene (LLDPE)

DOWLEX™ 2045 resin and colored masterbatch. Changeover time depended on the screw speed (throughput) and the type of masterbatch used. The authors attributed the masterbatch differences to viscosity and type of colorant, although viscosity correlations with changeover time were not established.

Changeover time has also been studied in TSEs [8]. Wang et al. used online Raman spectroscopy to measure the time to change between polyethylene (PE) and polystyrene (PS) on a 25 mm TSE. Of the four factors studied, screw speed and mixing zone location showed no significant effect on changeover time, whereas increasing the end/initial viscosity ratio and the throughput significantly decreased changeover time. Measured changeover times ranged from 1 – 3 min for rates between 4.5 and 9 kg/h. This study also validated the Raman quantitation of exit composition via offline ATR-FTIR.

This study uses the same Raman instrument to measure changeover times between PE and PS in a SSE, with the purpose of finding factors that reduce time and waste in material transitions.

Materials and Methods

LLDPE DOWLEX™ 2247G resin (MFI = 2.3 dg / min / 190 °C / 2.16 kg, density = 0.917 g/cm³) and LLDPE DOWLEX™ 2045G resin (MFI = 1.0 dg / min / 190 °C / 2.16 kg, density = 0.920 g/cm³) were used to examine changeover time as a function of viscosity. PS STYRON (Trademark of Trinseo) 685 D resin (MFI = 1.5 g / 5 min / 200 °C / 5 kg, density = 1.05 g/cm³) was alternately fed with the polyethylenes to produce strong, distinct Raman peaks.

A 25.4 mm diameter, 24:1 L:D single-screw extruder with a general PE screw was placed in series with a 1.28 cm³/rev gear pump (Maag 22-6) and a die. The extruder speed was automatically controlled by the gear pump inlet pressure, set to a target of 1.72 MPa. All temperatures were set to 220 °C, except the first two extruder zones, which were 168 °C and 204 °C, respectively.

Changeover times were studied by changing the feed from 100% PE → 50/50 wt% PE/PS → 100% PS → 50/50 wt% PE/PS → 100% PE. This was done at two sets of flow rates (30 and 80 gear pump rpm) for two different LLDPEs. During changeovers, the feed level was allowed to decrease to the top of the screw flights. Then, the new

formulation was added to the hopper and the start time was recorded. Blends were dry mixed in zippered bags before feeding. This differs from twin-screw feeding procedures, which rely on gravimetric feeders to control flow rate. The melt temperature, gear pump outlet pressure, and average extruder speed were recorded for each steady state.

A BWTek iRaman Pro with Kaiser optical probe was connected to a pressure gauge port at the extruder outlet to monitor composition (<2 s between spectra). More information on the instrument and optical probe may be found in Wang et al. [8]. Pure component spectra were obtained by averaging sample spectra over several minutes at steady state.

Raman signal was used to calculate percent PE and PS near the probe location (i.e., extruder exit). First, classical least squares (CLS) was used to fit sample spectra with a linear combination of PE and PS reference spectra within the 2750-3150 cm^{-1} spectral region (Figure 1) [9-11]. Raw CLS signal strength is sensitive to sample transparency, which changes dramatically from the pure materials (transparent melt, strong signal) to the blends (opaque melt, weaker signal). Therefore, one additional corrective term is necessary to fix the 50/50 wt% blend steady state signal at 50% PS (α_{PS}/α_{PE} , where α is Raman response factor). Percent PS is calculated from CLS signal by Equation 1.

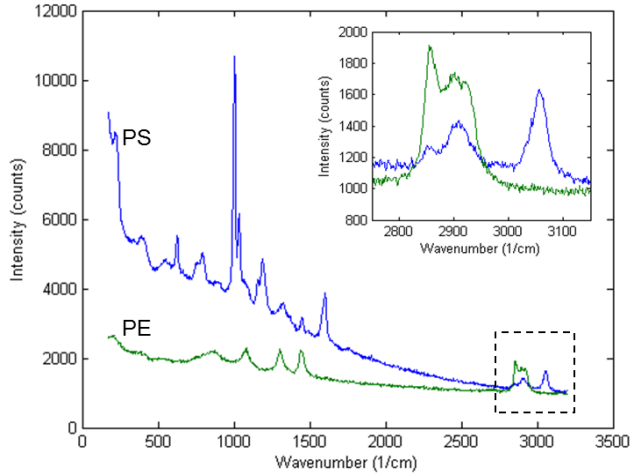


Figure 1. Raman spectra of pure PE and PS

$$\% \text{ PS} = \frac{(\text{PS CLS signal})}{(\text{PS CLS signal}) + (\text{PE CLS signal}) \times \frac{\alpha_{PS}}{\alpha_{PE}}} \quad (1)$$

Changeover start times were manually recorded in a text file, and read as input to an online MATLAB analysis program. The MATLAB program parses the Raman data between changeover start times, calculates percent PS for each time-point, normalizes percent PS and time, fits a curve to the data, and finally extracts a changeover time. This program runs online, to provide operators with feedback for when changes are complete.

Noise in the Raman signal makes it difficult to pick a changeover time value from raw data. Therefore, a Double Weibull curve was fit to the data for each changeover. It is clear that the standard deviation is larger for 50/50 blends than pure materials (opaque melt leads to a weaker signal), so bi-square weightings were given to the errors. The fitted curve is monotonic, so picking a time from the fitted curve is easy and more accurate. The 99% changeover time (99% COT) is defined in Equation 2, where percent PS initial and final values are averages of the first or last 10 data points.

$$\% \text{ PS}(99\% \text{ COT}) = [\% \text{ PS}(\text{final}) - \% \text{ PS}(\text{initial})] \times 0.99 + \% \text{ PS}(\text{initial}) \quad (2)$$

Figure 2 shows a sample output of CLS raw response and percent PS versus time. The black vertical dashed lines indicate a change in feed formulation, and the black vertical solid lines indicate a 99% COT. The red solid line indicates the Double Weibull curve fit. Three fitted changeover time curves showed significant deviation from the raw data, due to a large number of points after the changeover was complete, coupled with drift in the raw data signal at steady state. These three curves were fit using only 400 data points, which resulted in more reasonable fits and changeover times.

Viscosity ratio was calculated as a function of temperature, shear rate, and composition. Pure component shear viscosities were obtained at 200 °C, 220 °C, and 240 °C by parallel plate rheology (Figure 3). Cross model and Arrhenius fits were used to extrapolate viscosity over a range of shear rates and temperatures (Equation 3), where η_0 is zero shear viscosity, $\dot{\gamma}$ is shear rate, E_A is a fitted activation energy, R is the Ideal Gas constant, K is a Cross model material constant, m is the power law exponent, and T_0 is the reference temperature. T was the extrudate hand-held melt temperature for each run.

$$\eta(\dot{\gamma}, T) = \frac{a_T \eta_0}{1 + (K a_T \eta_0 \dot{\gamma})^{1-m}} \quad (3)$$

$$a_T = \exp \left[\frac{E_A}{R} \left(\frac{1}{T} - \frac{1}{T_0} \right) \right]$$

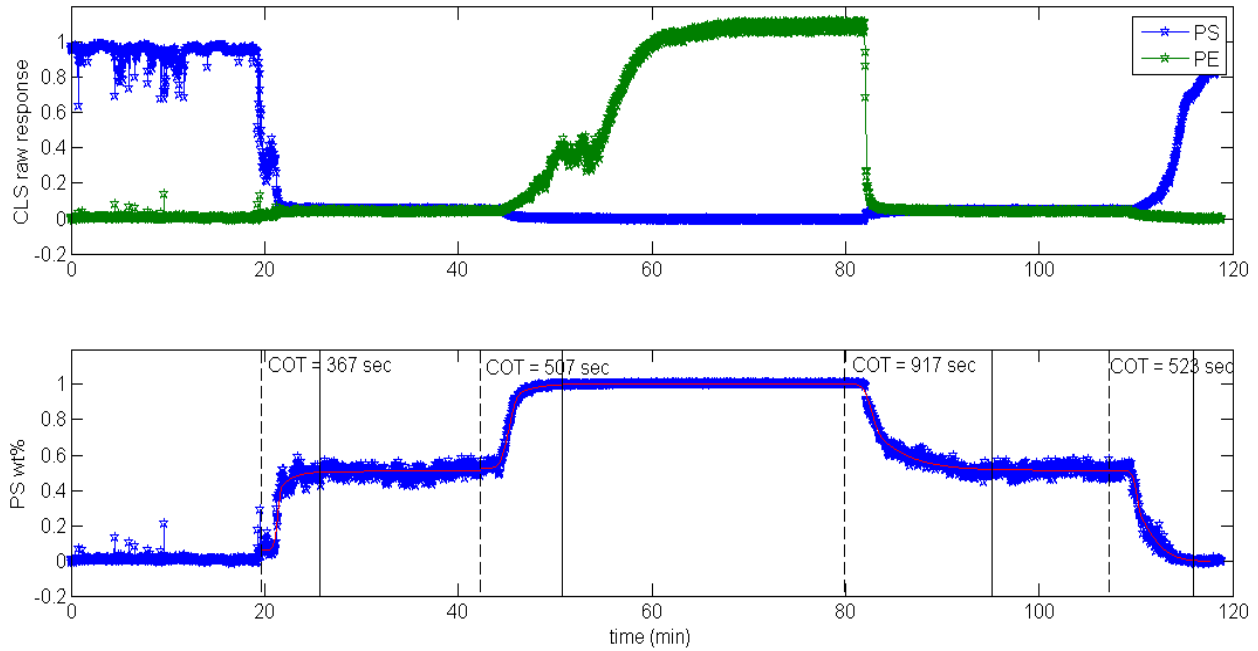


Figure 2. Sample changeover time results for the first five entries in the Appendix; (top) Raw signal response versus time. (bottom) Percent PS versus time.

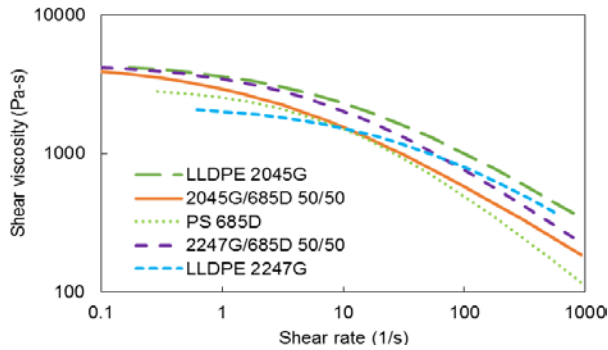


Figure 3. Shear viscosity Cross model fits of pure materials and blends at 240 °C.

The average shear rate in the extruder is estimated as the metering section shear rate (Equation 4), where D_c is the screw core diameter, N is the extruder speed (rpm), and H is the distance from the screw root to the barrel [12]. For this particular SSE, $D_c \approx 22.8$ mm and $H \approx 1.27$ mm. Finally, viscosity ratio is calculated as the steady state viscosity of the final material divided by the steady state viscosity of the initial material.

$$\dot{\gamma} = \frac{\pi D_c N}{H} \quad (4)$$

There are many errors associated with these viscosity estimations. The values are extrapolated outside the temperature range of experimental rheology data (200 – 240 °C). This is also true for the shear rates, which are

estimated to be much higher than any measured in rheology. Both of these parameters are not constant, and vary spatially in the extruder. However, the estimated shear viscosity ratios are expected to correlate with true viscosity ratios in extrusion, and therefore are still included as a factor for changeover time.

Results and Discussion

Changeover times for the SSE experiments are summarized in the Appendix, along with the relevant processing parameters. The measured melt temperatures show significant shear heating (up to 74 °C), similar to previous TSE trials.[8] The mass flow rates are not constant due to density differences between PE and PS, but were generally around 1.8 and 4.5 kg/h for the two given gear pump speeds (30 and 80 rpm, respectively). As expected, the gear pump outlet pressure varies directly with viscosity. Changeover times ranged from 2.5 to 15 minutes, generally longer than those found for a 25 mm TSE.

Changeover times were analyzed in the Fit Model platform of SAS JMP, with factors viscosity ratio and gear pump rpm (results shown in the Appendix, Figure A). ANOVA shows that there is at least one significant factor at a 95% confidence level ($p < 0.0001$). Effects tests show that both viscosity ratio and gear pump speed are significant factors ($p = 0.0024$ and $p < 0.0001$, respectively). Other measured factors, such as melt temperature, were either not significant or highly collinear

with the two significant factors. Higher order terms were not appropriate for this screening, and independent cross terms were not significant. The final prediction expression shows that changeover time increases with decreasing flow rate and increasing viscosity ratio.

Flow rate is a strong effect, indicated by the large prefactor in the model prediction and the low p -value in the effects test. It is somewhat surprising that the viscosity term shows the opposite effect as the analogous TSE experiments. Several factors that may have affected this result are the different softening/melting temperature profiles of PE and PS, pellet sizes and shapes, and melt densities. Also, as stated before, there is a large degree of uncertainty in the viscosity calculations.

There are several differences between the SSE and TSE experiments, which must be highlighted. First, the residence volume of the 25 mm TSE is approximately 390 cm³ (assuming 50% fill fraction), compared to 220 cm³ for the SSE. This would favor the SSE for shorter changeover times. Secondly, the TSE has gravimetric feed control whereas the SSE is flood fed, but this is ameliorated by using gear pump speeds that roughly matched the 4.5 kg/h settings on the TSE feeders. Third, a different analysis method was used for determining changeover time for these two experiments. For the TSE, the data was fit to a Sigmoidal curve and changeover times were defined when a composition change of less than 0.1% occurred between time points. The SSE changeovers from this study were fit using both equations and criteria (Sigmoidal / 0.1% change between points, Double Weibull / 99% of concentration change), and there was about 22 s difference on average. This is not enough to affect the main conclusions of our work (that SSEs change over slower than TSEs). Fourth, the control system on the SSE is a feedback loop, where the extruder speed is controlled to keep the gear pump inlet pressure constant. This control loop may have caused the system to take more time to equilibrate, but a steady inlet pressure was achieved within a minute, so this is not considered to be a large factor. Lastly, the SSE had more discharge pressure than the TSE (due to the die and gear pump), which has an unknown effect on changeover time.

If a comparison is to be made between TSE and SSE changeover time, it should be at similar mass throughput with the same materials, since both are significant factors for changeover time in SSEs and TSEs. This occurred for four changeovers at 4.5 kg/h, between 685D and 2045G resins, compared in Figure 4. From this data, the twin-screw extruder appears to change over more rapidly.

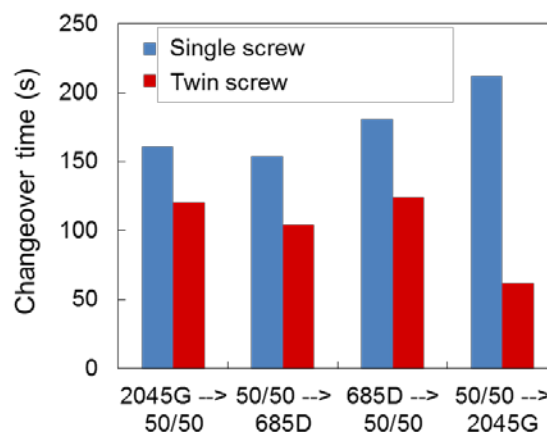


Figure 4. Comparison of changeover time for single-screw and twin-screw extruders at approximately 4.5 kg/h throughput.

Conclusions

Changeover times for a SSE were estimated by online Raman, analyzed in MATLAB and JMP. Increasing throughput and decreasing viscosity ratio decreased changeover time.

Changeover times ranged from 2.5 – 15 min, and were generally longer than those found in a 25 mm TSE. This confirmed our hypothesis; that TSEs change formulation more quickly, attributed to their self-wiping capability.

Acknowledgements

The authors would like to thank Frank Kincade for compression molding rheology samples and Wenyu Su for support with statistical analysis.

TM Trademark of The Dow Chemical Company (“Dow”) or an affiliated company of Dow.

References

1. L. Saerens, C. Vervaet, J. P. Remon, T. De Beer, *Journal of Pharmacy and Pharmacology*, **66**, 180 (2014).
2. A. Poulesquen, B. Vergnes, P. Cassagnau, A. Michel, O. S. Carneiro, J. A. Covas, *Polymer Engineering & Science*, **43**, 1849 (2003).
3. M. D. Wetzel, C. K. Shih, U. Sundararaj, *ANTEC Papers*, **3**, 3707 (1997).
4. D. Fischer, K. Sahre, M. Abdelrhim, B. Voit, V. B. Sadhu, J. Pionteck, H. Komber, J. Hutschenreuter, *Comptes Rendus Chimie*, **9**, 1419 (2006).
5. I. Alig, D. Fischer, D. Lellinger, B. Steinhoff, *Macromolecular Symposia*, **230**, 51 (2005).
6. P. Coates, S. Barnes, M. Sibley, E. Brown, H. G. Edwards, I. Scowen, *Polymer*, **44**, 5937 (2003).

7. C. Gilmor, S. T. Balke, F. Calidonio, A. Rom-Roginski, *Polymer Engineering & Science*, **43**, 356 (2003).
8. J. Wang, C. Thurber, X. Chen, M. Read, N. Horstman, C. Pavlicek, J. Stanley, *SPE ANTEC Papers*, **1**, 863 (2016).
9. D. M. Haaland, R. G. Easterling, *Applied Spectroscopy*, **34**, 539 (1980).
10. D. M. Haaland, R. G. Easterling, D. A. Vopicka, *Applied Spectroscopy*, **39**, 73 (1985).
11. K. R. Beebe, R. J. Pell, M. B. Seasholtz, "Chemometrics: A practical guide", Wiley (1998).
12. G. A. Campbell, M. A. Spalding, "Analyzing and troubleshooting single-screw extruders", Cincinnati, OH, Hanser (2013).

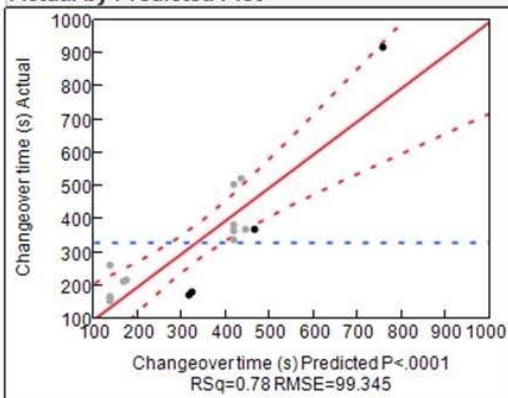
Appendix

Table 1. Changeover time results

Material	Gear pump (rpm)	Melt T (°C)	Mass flow (kg/h)	Gear pump outlet pressure (MPa)	Viscosity ratio (-)	Changeover time (s)
2045G	30	269	1.54	8.8		
50/50	30	270	1.71	6.2	0.14	367
685D	30	262	2.02	4.8	0.02	507
50/50	30	265	1.80	5.6	89	917
2045G	30	277	1.55	8.2	4.4	523
2045G	80	294	3.79	12.3		
50/50	80	284	4.47	7.93	0.12	161
685D	80	275	5.15	6.76	0.02	154
50/50	80	284	4.59	7.65	49	181
2045G	80	294	3.88	12.1	8.4	212
2247G	30	264	1.57	6.27		
50/50	30	268	1.67	4.76	0.10	339
685D	30	263	1.96	4.55	0.11	385
50/50	30	265	1.75	4.62	12	369
2247G	30	279	1.60	5.79	7.3	372
2247G	80	289	4.01	8.96		
50/50	80	281	4.13	6.48	0.09	261
685D	80	280	5.16	6.55	0.02	166
50/50	80	281	4.27	6.62	47	171
2247G	80	293	3.82	8.96	9.9	218

Whole Model

Actual by Predicted Plot



Summary of Fit

RSquare	0.781059
RSquare Adj	0.747375
Root Mean Square Error	99.34537
Mean of Response	331.4375
Observations (or Sum Wgts)	16

Analysis of Variance

Source	DF	Sum of Squares	Mean Square	F Ratio
Model	2	457714.39	228857	23.1883
Error	13	128303.54	9870	Prob > F
C. Total	15	586017.94		<.0001*

Effect Tests

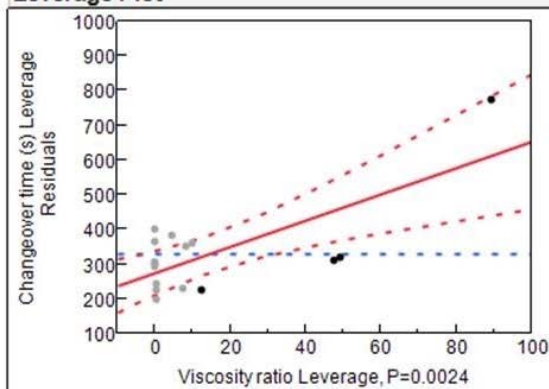
Source	Nparm	DF	Sum of Squares	F Ratio	Prob > F
Viscosity ratio	1	1	139900.33	14.1750	0.0024*
Gear pump speed (rpm)	1	1	319347.76	32.3570	<.0001*

Prediction Expression

588.104426059433
 + 3.78437038453293 * Viscosity ratio
 + -5.6511237333843 * Gear pump speed (rpm)

Viscosity ratio

Leverage Plot



Gear pump speed (rpm)

Leverage Plot

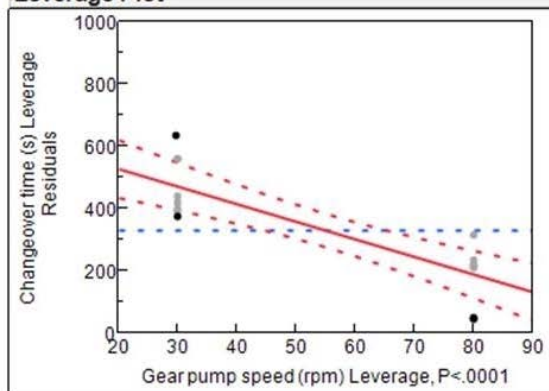


Figure A. Model fit for SSE changeover time, as a function of viscosity ratio and gear pump speed

Latest technology innovation for counter rotating continuous mixer

Yoshinori Kuroda, Tsugushi Fukui, Kazuo Yamaguchi, Hideo Funahashi

Industrial Machinery Division, KOBE STEEL, LTD. Kobe, Japan

Sayaka Yamada, Kazuhide Sekiyama, Shiori Watanabe

Mechanical Engineering Research Laboratory, KOBE STEEL, LTD. Kobe, Japan

Abstract

The new generation continuous mixer has been developed in response to Bi-modal HDPE property progressions, this by means of a new mixing concept, which has been studied and realized through empirical experiments. By using the developed continuous mixer, the gel number and gel size of film samples have exhibited improved film appearance. The White Spot Area (WSA), a method used for evaluation of pipe grades with black pigment, has also been improved.

Introduction

Although the basic concept of the continuous mixer for the polyolefin post-reactor extruder/pelletizer has not been changed significantly from the original mixer configuration, mixing and homogeneity performance, especially for Bi-modal HDPE extrusion, has been largely improved by 1) longer L/D, 2) applying a gate valve, and 3) rotor geometry optimization ^[1].

In the latest conferences, homogeneity performance advantages of the counter rotating Long Continuous Mixer (LCM) compared with co-rotating Twin Screw Extruder (TSE) were presented ^[2], and an investigation of the mixing mechanism difference between LCM and TSE has been attempted by a numerical analysis ^[3].

In recent years Bi-modal HDPE has been polymerized with broader molecular weight distribution and 1-Hexene (C6) instead of 1-Butene

(C4) has been applied as a co-monomer component in order to improve the post-extrusion processability and the strength of the final product.

However both modifications have brought about difficulties from the point of view of homogenization.

The new generation continuous mixer has been developed to respond to the above Bi-modal HDPE progress by means of a new mixing concept, which has been studied and obtained through basic experiments using a two-dimensional test mixer. And these obtained operation and mixing performance data from two-dimensional mixer have been applied to the development of a new generation continuous mixer.

This paper introduces improvements in the mixing performance of bi-modal HDPE extrusion by a new generation continuous mixer.

1. 1 Two-dimensional test mixer experiment

The schematic view of the two-dimensional test mixer is shown in Fig. 1 ^[1], that is composed of i) mixer barrel, ii) twin rotor counter rotating elements, the various dimensions of which may be changed by varying the element sets, and iii) main motor, which is connected through gear reducer to the twin rotor mixing elements. Motor speed can be controlled variably and the torque and the power could be measured during the experimental operation.

Bi-modal HDPE powder, 2.25 wt% of Carbon black and an appropriate amount of anti-oxidant were mixed by the two-dimensional test mixer.

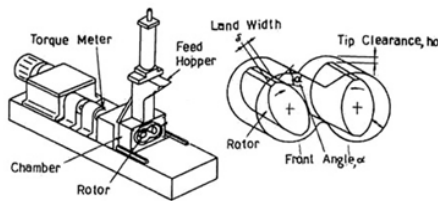


Fig.1 Two-dimensional test mixer

1. 2 Two-dimensional mixer experiment results

The positive effects of rotor dimensions for Bi-modal HDPE mixing homogeneity performance were investigated. Rotor element dimensions, which were a) Tip clearance, b) Rotor front angle, and c) Tip land width, were varied. Additionally the new concept rotor shape was introduced to the experiments. The rotor element dimension matrix is shown in Table 1.

Mixing performances of each of the different mixing elements and mixing conditions were evaluated by WSA (White Spot Area; [%]) measurement, which were observed and calculated

from a total white spot area, versus well mixed black background in the microscope views. Ten (10) small samples, which were sliced from respective tested mixtures, of 20 micron thickness by the Microtome, were measured.

Table 1 Various rotor element dimensions matrix

		Front angle			Land width	New concept shape
		Small	STD	Large	Large	
Tip clearance	Narrow	Rotor # 15A	Rotor # 15B	Rotor # 15C	Rotor # 15L	Rotor # 15P
	STD	Rotor # 15E	Rotor # 15F [STD]	Rotor # 15G	Rotor # 15M	Rotor # 15Q
	Wide	Rotor # 15H	Rotor # 15J	Rotor # 15K	Rotor # 15N	Rotor # 15R

Among rotor element code numbers from ‘15A’ to ‘15N’, the best mixing performance, that showed smallest WSA value with shortest mixing time, was by the rotor code ‘15F’ element. In fact, the ‘15F’ 2D shape has already been applied for the MIXTRON™ LCM series of KOBE STEEL, LTD.

New mixing concept element profiles were also tested using 2-D mixer and interesting WSA evaluation results were obtained. Fig. 3 shows the relation between mixing time and WSA [%] evaluation by the standard 2D profile of ‘15F’ element and the new concept 2D profile of ‘15Q’ element.

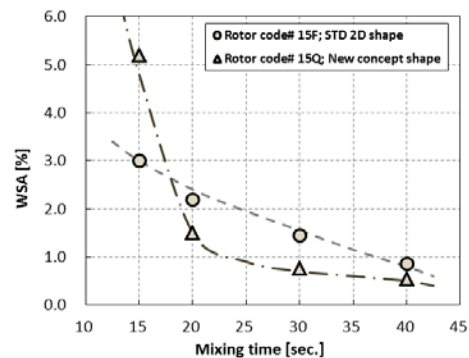


Fig.3 WSA reduction by mixing time

Until 15 seconds of mixing time, the 15F rotor profile provided better homogeneity performance than the 15Q rotor profile. After 20 seconds of mixing time, the 15Q rotor profile brought about better mixing performance than 15F rotor profile. The mixing performance features of respective rotor profiles are summarized in Table 2, below.

Table 2 Respective rotor features

	Melting performance	Mixing performance
15F profile	++	+
15Q profile	+	++

++ superior performance
+ standard performance

2.1 Continuous mixer development

The results from the two-dimensional test mixer suggested how to apply and arrange both rotor profiles to the continuous mixer.

The MIXTRON™ LCM is a two stage continuous mixer, in which the respective process parts have independent and different functions. Major role of the 1st process part is melting and mixing, while the role of 2nd process part is mainly mixing. The ‘15F’ profile rotor has been applied to both the 1st and the 2nd process parts for the conventional LCM mixer.

The new generation LCM applies the ‘15Q’ profile in the 2nd process part. The 1st process part should keep the 15F profile, because the 15F profile provides superior melting performance. Now, Fig. 4 is a schematic view, which compares the conventional LCM and the new generation LCM.

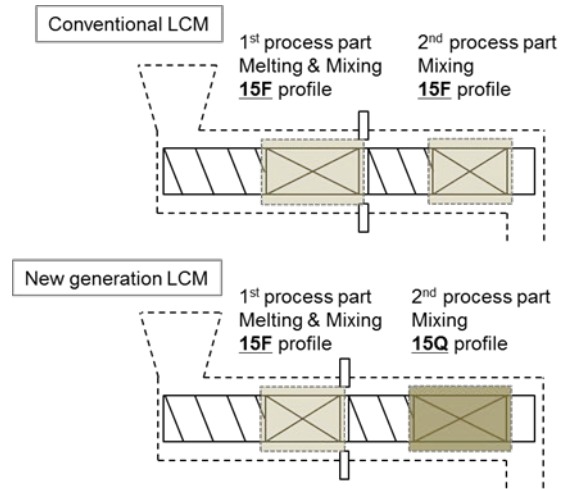


Fig. 4 Comparison between conventional LCM and new generation LCM

2.2 Mixing performance of new generation LCM

Mixing tests were performed on the newly designed continuous mixer MIXTRON™ LCM-IM (Intensive Mixing) to confirm improvement of the homogeneity performance. Bi-modal HDPE pipe grade without black pigment was used. Homogeneity performance was evaluated by film appearance, which was investigated by on-line gel analyzer (made by OCS GmbH, Germany) on cast film appearances.

Fig. 5 shows the relationship between total gel area [ppm] and SEI [kwh/kg] depending on the types of LCM. A significant improvement of LCM-IM was not observed below 0.230 kWh/kg of SEI, however for SEI above 0.230 kWh/kg regions, the LCM-IM the reduction in the gel number was dramatic. The mixing performance comparison result from both continuous mixers agreed well with the result from two-dimensional test behaviors.

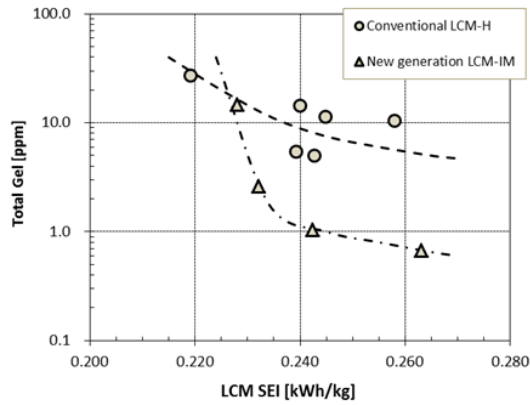


Fig.5 Gel reduction in casting film by mixer SEI

3. Summaries

Improvement of homogeneity performance has been confirmed through lab trials.

The significant development concepts of LCM-IM are not only superior mixing performance but also “easy retro fitting” to existing LCM-H lines. L/D of both the LCM-H and the LCM-IM is 8.0. Moreover adjusted raw material feed point / mixer support foot-print and the same rotor center-distance mean that rotor replacement may be implemented easily. Users of the LCM-H are able to re-use their existing ‘main motor, melt pump system, screen changer and under water pelletizer system’. Such easy retro fitting policy promises minimized replacement down time of the production line.

4. Reference

- [1] Inoue, K. et al., Kobe Steel Engineering Report 44, 53 (1994).
- [2] Yamaguchi, K. et al., SPE International Polyolefins Conference, Houston, TX, USA (2015).
- [3] Sekiyama, K. et al., SPE International Polyolefins Conference, Houston, TX, USA (2016).

TAKING GEAR PUMP TECHNOLOGY TO THE NEXT LEVEL

Ryan Emerick, MaagAutomatik Inc., Charlotte, NC

Abstract

Processes in the manufacture of virgin polyolefin resins require high-pressure gear pumps which build up pressure for the pelletizing units downstream. Maag Pump Systems has recently redesigned each component featured in its gear pump portfolio, from gears and shafts to bearings and seals, fine-tuning how all components interact, culminating in a new, state of the art technology. The new performance-driven geometry of Maag Pump Systems' "x6 class" gear pump, pronounced six class, enables higher throughput rates of high viscosity polymers and can convey low viscosity polymers where classic pump technology failed. This paper describes features of this latest design and the benefits they bring to polyolefin post reaction processing.

Introduction

The use of a gear pump in a continuous Polyethylene compounding process improves mixing performance of the twin screw extruder and reduces overall energy consumption, while in Polypropylene compounding it increases production capacity when processing high-viscosity resins. When a gear pump is installed between the outlet of a twin screw extruder and the inlet of the screen changer prior to the pelletizing die, the outlet pressure of the extruder is greatly reduced. When the gear pump takes over the task of pressure building, energy consumption of the unit is cut by one-half to two-thirds and the temperature of the polymer resin entering the pelletizer is reduced significantly. The extruder can then more effectively melt and mix the resin and at a higher production capacity.

While a gear pump brings these clear benefits to the compounding operation, it does require additional initial investment, occupies additional space on the production floor and adds to overall system complexity which add to concerns about plant reliability. The new x6 class of gear pumps were developed to minimize each of these costs while maximizing each of the benefits. The purpose of this paper is to describe the limits which classic gear pumps were facing, how they are being overcome, as well as to quantify the benefits which today's polyolefin compounding operations stand to gain from the new technology.

Redesigning to Raise the Limits

Flow rate

The maximum achievable flow rate of a gear pump of a given size is governed by the pump's speed limit, typically in the range of 40 to 50 rpm for polyolefin compounding applications. The pump's speed limit is determined by the rpm at which the maximum allowed bearing temperature is reached. If the gear pump of a given size cannot reach the desired flow rate, one of the following two solutions are often employed, both of which involve a significant investment cost:

1. A larger size gear pump is installed, operating at slightly slower speed.
2. A shaft and bearing cooling system is added to reduce bearing temperature and effectively raise the pump's speed limit.

The x6 class pump technology makes it possible for a gear pump of the same basic size to achieve significantly higher rates without additional investment. This allows a different approach to be taken:

1. Increase gear pump output per revolution, to increase flow rate without increasing rpm.
2. Enhance the transfer of heat out of the bearings to reduce the bearing temperature and thus raise the maximum allowable pump speed.

The output per revolution, or specific volume capacity of a gear pump, is determined by the volume between the gear teeth. One way to increase that volume is to design the pump with longer gear teeth. There is a limit to tooth length, however, because longer teeth have always meant reduced differential pressure capability due to the resulting higher shaft deflection and bending stress. To circumvent this limitation, the shaft journal diameter of the x6 class pump is larger so that it resists deflection under load and allows the use of longer gear teeth without sacrificing pressure capability. The longer teeth add 25 to 30% in specific volume and the inlet-to-outlet width of the gear pump remains the same as classic pumps.

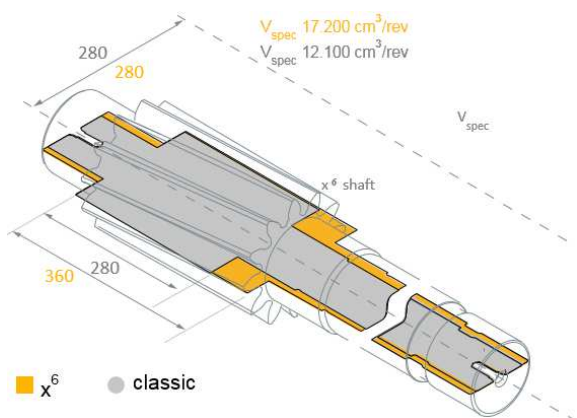


Figure 1: The larger shaft journal diameter of the x6 class pump makes it possible to have longer gear teeth for higher specific volume, without sacrificing the pump's pressure-building capability.

Working against the gear pump's output per revolution is the back-flow of polymer through the pump's internal clearances from the high pressure discharge side of the gears back to the low pressure inlet side of the gears. Actual pump output per revolution in polyolefin compounding is typically 10 to 35% less than the theoretical specific capacity, depending on differential pressure and resin viscosity. By identifying the back-flow paths and reshaping the geometry of the pump's internal components, the back-flow paths which existed in classic gear pumps have been dramatically reduced. The x6 class pump operates with roughly half the amount of back-flow thereby regaining 5-15% of the gear pump's output per revolution.

In order to maintain thermal balance and to avoid excessive thermal growth of the bearings which would close off the pump's internal clearances and possibly lead to pump seizure, the temperature of the pump's bearings must not exceed a certain limit. Heat which accumulates in the bearings during operation is generated from the shearing of polymer as it flows through the gap between the rotating gear shaft journals and the stationary journal bearings. The heat is transferred out from the inner to outer diameter of the bearings and into the pump housing and covers. The geometry of the x6 class pump bearing has been redesigned to reduce the bearing temperature by:

1. Increasing the inner diameter to reduce the thickness of the bearings, so that heat is more quickly transferred out of the bearings.
2. Speeding the flow of polymer through the bearings.

Smaller Bearing Section with Increased Heat Transfer

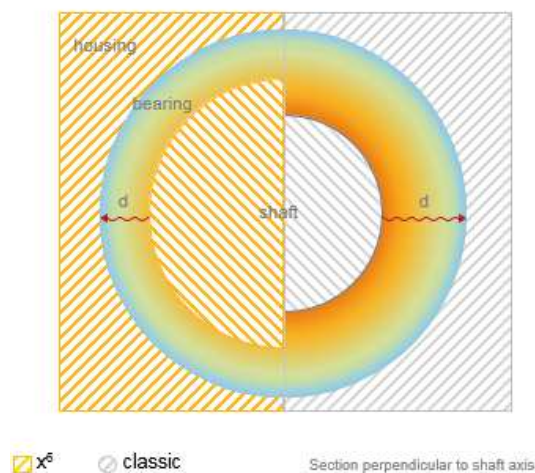


Figure 2: Modified bearing design reduces bearing temperature and effectively increases the pump speed limit to make higher flow rates possible.

Reliability

The shafts and bearings of a gear pump are lubricated by the polymer which it pumps, as 2 to 4% of the overall polymer flow is directed through internal lubrication channels into the gaps between shaft and bearing. Here it forms the thin lubricating film which lifts the rotating shaft journal away from the surface of the bearing.

Pump failures often result from process upsets such as sudden changes in pressure, viscosity or ingestion of foreign material which either disturbs the lubricating film or exerts an extreme load on the shafts, overcoming the lubricating film and resulting in metal-to-metal contact between shaft and bearing.

The redesigned shaft and bearing geometry in the x6 class pump improves reliability by reducing the likelihood of such a failure by:

1. Increasing resilience to process upsets by increasing the thickness of the lubrication film between gear shaft O.D. and bearing I.D.
2. Increasing resilience to foreign material by increasing axial gap between gear teeth side face and bearing face.
3. Increasing bearing load capability by increasing the bearing I.D. surface area.

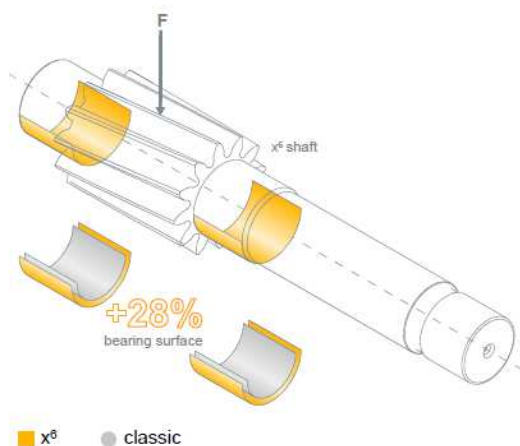


Figure 3: Increasing the bearing surface area to improve pump reliability.

Size and Cost of the Pump System

Controlling total investment cost is important to polyolefin plant design. The addition of a gear pump involves additional initial investment, but the payback time of a gear pump is typically less than one year due to energy savings and increased production rate. Furthermore, its investment cost may be partially offset by the use of a smaller drive unit for the twin screw extruder, since the pump reduces the power requirement of the extruder. The x6 class pump technology can further offset the investment cost in the following ways:

1. A smaller and therefore more economical x6 class gear pump can achieve the same production rate as a larger classic pump.
2. A production rate for which a classic pump requires a shaft and bearing cooling unit may be achievable with an x6 class pump without shaft and bearing cooling.
3. An x6 class pump can often be driven with a smaller drive unit than a classic gear pump would require, due to higher efficiency and lower pump speed requirement.

Quantifying the Benefits

To illustrate the benefits to be gained from x6 class pump technology and to make a side-by-side comparison to classic pump technology, two compounding processes were considered for this paper:

Plant 1: High Density Polyethylene

Product: High density Polyethylene

Capacity: 60 tons per hour

Grades: HLMI=9, MI=0.2, MI=18, MI=30

Pressure: 120 bar for MI 18 and MI 30

250 bar for MI 0.2 and HLMI 9

Temp: 200 – 260°C

Classic: PR 50 (450/450) with shaft & bearing cooling

x6 class: PR 450-6EP (450/450) with no cooling

In this HDPE plant, a classic pump would require the addition of a shaft and bearing cooling system to maintain the bearing temperatures below the 320°C alarm limit for the high viscosity grades HLMI=9 and MI=0.2 at a flow rate of 60 tons/hr. Removal of a cooling system from the gear pump system scope can amount to 10% to 15% lower investment cost, as well as 10 to 15% lower energy consumption for the pump system.

Using a higher gear ratio in the gearbox, a 1500 kW motor would be sufficient to power the x6 class pump, while the classic pump would require a larger 1750 kW motor. This is another way in which the new pump design is reducing investment cost and energy usage.

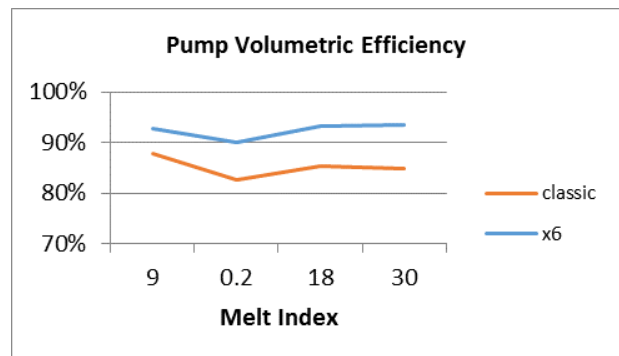


Figure 4: In the 60 tph HDPE plant, a classic pump operates at 85% volumetric efficiency, while the x6 class pump operates at 92% volumetric efficiency.

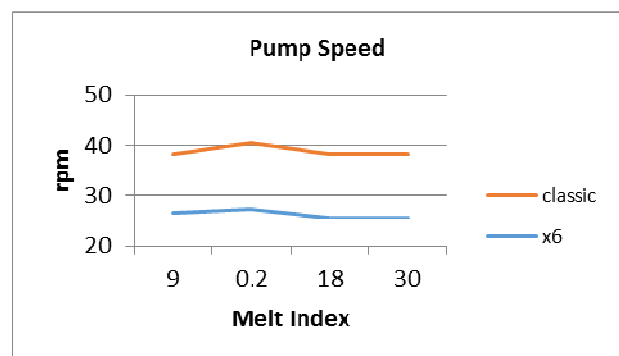


Figure 5: In the 60 tph HDPE plant, a classic pump operates at 39 rpm, while a x6 class pump of the same size operates at 26 rpm.

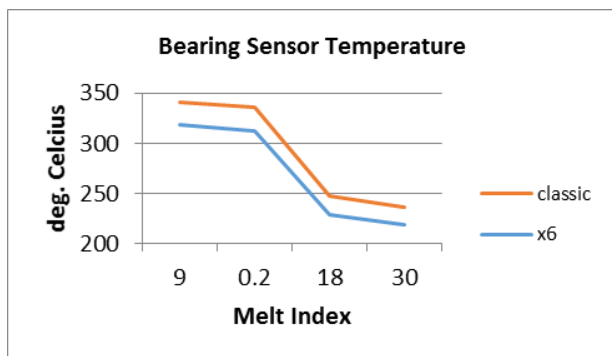


Figure 6: Without cooling, the classic pump would operate with > 340°C bearing temperature for low MI grades of HDPE, while the x6 class pump maintains temperatures comfortably below the 320°C limit with no need for cooling.

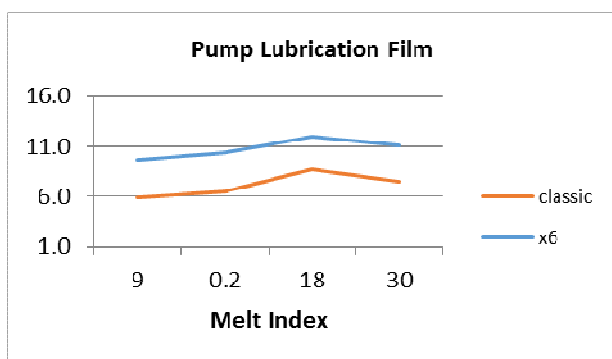


Figure 7: In the 60 tph HDPE plant, the x6 class pump operates with approximately 1.5 times the lubrication film thickness of a classic pump.

Plant 2: Polypropylene

Product: Polypropylene

Capacity: 20 tons per hour

Grades: MI=0.7, MI=2, MI=8, MI=25, MI=75

Pressure: MI=0.7 to MI=8 at 195 bar
MI=25 and MI=75 at 150 bar

Temp: 195 – 265°C

Classic: PR 25 (360/250) with shaft & bearing cooling

x6 class: PR 360-6SP (360/280) with no cooling

In this example, a classic pump would require the addition of a shaft cooling system to maintain the bearing temperatures below the 320°C alarm limit for the high viscosity grade MI=0.7 at a flow rate of 20 tons/hr.

The increase in volumetric efficiency makes it possible to operate at further reduced RPM, shear rates and temperatures, and consequently a narrower polymer residence time distribution. This favorably impacts production rate, polymer quality, pump reliability and lifetime, while reducing energy consumption, as losses are reduced by 50%.

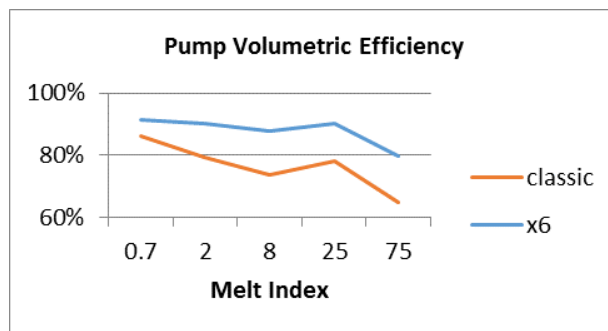


Figure 8: In the 20 tph PP plant, a classic pump operates at 76% volumetric efficiency, while the x6 class pump operates at 88% volumetric efficiency.

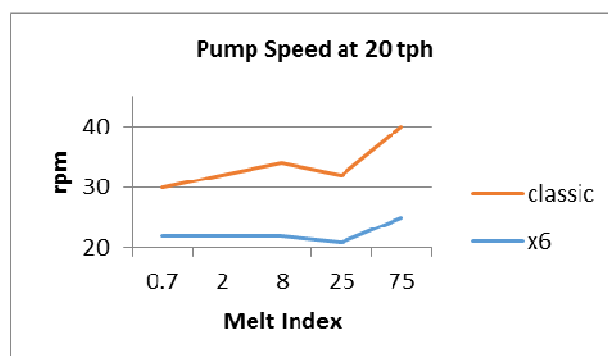


Figure 9: In the 20 tph PP plant, a classic pump operates at 34 rpm, while an x6 class pump of the same size operates at 22 rpm.

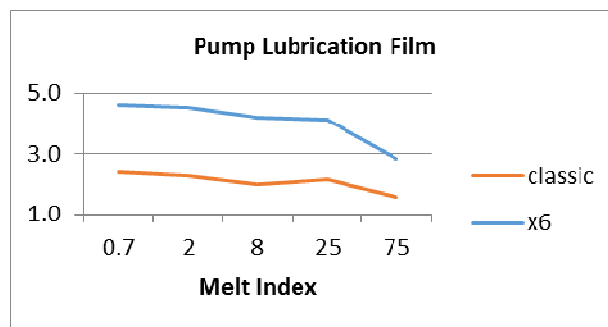


Figure 10: In the 20 tph PP plant, the x6 class pump operates with approximately 2 times the lubrication film thickness of a classic pump.

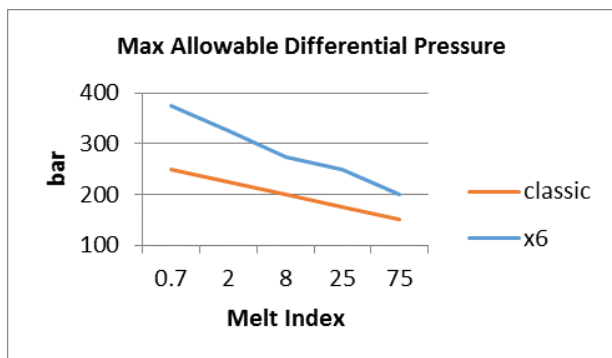


Figure 11: In the 20 tph PP plant, the x6 class pump gives the user the possibility to operate with 1.5x higher differential pressure than a classic pump.

Conclusions

Gear pumps based on classic technology face limitations in flow rate and differential pressure. Those limitations have made it necessary to use larger, more expensive, less efficient machines to deliver the polymer at flow rates and pressures required in polyolefin post reaction processing.

Maag's x6 class pump technology raises the limits of flow rate and differential pressure. The same machine size as before is now capable of higher flow rates, thanks to optimized shaft and bearing geometry which give the pump a higher specific volume capacity and higher volumetric efficiency. Furthermore, improved heat transfer reduces bearing temperature and makes it possible to operate the pump at higher speeds.

Being a critical component of a polyolefin plant, a gear pump must be a highly reliable machine in order to avoid costly unexpected plant down time. The pump is expected to operate with minimal maintenance for years between scheduled plant turn-arounds, but it can reliably do so only if operated safely within its process limits. The process limits that exist for classic pumps being relatively narrow, a small deviation from the expected operating parameters can threaten a pump's reliability.

The process limits have been widened for the x6 class pump. Thicker bearing lubrication film and increased bearing surface area give the x6 class pump a larger operating window and make it more resilient to process upsets or deviations from typical operating conditions. A larger axial gap between shafts and bearings make it less susceptible to damage, should foreign materials ever make their way into the pump.

For debottlenecking existing plants, Maag offers housing designs with matching interfaces to classic pumps, making it possible in some cases to increase flow

rate by 30% with a drop-in replacement pump and using the existing drive unit.

For new plants, x6 class pump technology will give users more choices in selecting the best pump to suit their needs, whether the situation calls for a smaller, more economical pump or for a machine size comparable to a classic pump but with higher capabilities for future rate expansions and greater flexibility to process new polymer grades. Compared to gear pumps based on classic technology, x6 class pumps give polyolefin manufacturers the possibility to reduce investment cost through machine size, reduce operating cost through energy savings and increase productivity through higher reliability.

Supercritical Washing of Polymers within a Twin Screw Extruder

Jacob C. Kohl, Christopher S. Tucker, NFM Welding Engineers, Inc., Massillon, OH

Abstract

For some applications, resin purity is critical because contaminants such as residual solvent, monomer, and dimer strongly affect product quality. Volatile contaminants can be removed by devolatilization under vacuum, which can be enhanced through stripping with a medium such as water or alcohol. Some contaminants, however, are difficult to remove by vaporization because they have low vapor pressures or interact strongly with the polymer. For components with low vapor pressures, liquid extraction is a viable alternative to stripping. The drawbacks of injecting conventional solvents like water or alcohol include the addition of a new component which must be volatilized and complications from handling flammable materials. Washing with supercritical fluids can address both of these problems for systems designed to accommodate polymer/SCF separations. SCF extraction has been demonstrated for polypropylene and shows good potential for a number of other applications.

Introduction

The development and optimization of reliable, efficient separation technologies are critical to the production of highly pure polymers. A number of unit operations have been designed to accomplish these separations, and a number of techniques for improving separation performance have been developed as well. Co- and counter-rotating twin screw extruders have been employed for decades as reliable equipment for devolatilizing polymers [1-3].

Direct devolatilization is a staged operation that relies on multiple approaches toward phase equilibrium to achieve a desired product purity [1-3]. These approaches are limited by contaminant volatility, surface area, and diffusion. Volatile vapor pressure, P_1 , follows from the Flory-Huggins model, which predicts the relationship in Equation 1 for low concentrations:

$$P_1 = P_1^0 \phi_1 e^{1+\chi} \quad (1)$$

where P_1 is the partial pressure of a volatile contaminant; P_1^0 is the ideal vapor pressure of the contaminant; ϕ_1 is the volume fraction of the contaminant in the polymer matrix; and χ is a dimensionless interaction parameter that accounts for interactions between the contaminant and polymer [2, 3].

When the partial pressure of a contaminant reaches or exceeds the total venting pressure, volatiles will foam even at very low concentrations. This phenomenon is strong contributing factor for efficient devolatilization because is very rapid compared to simple diffusion [2-5].

Typically achieving residual volatile levels below 500 ppm requires either very strong vacuum, very low throughput rates, or both. Carrier substances such as stripping agents can improve devolatilization by (1) reducing the partial pressure, P_1 , over the polymer, thereby shifting the equilibrium concentration of contaminant towards zero; and (2) acting as nucleation aids, enhancing the formation of bubbles which contributes to foam formation and increased surface area for mass transfer [3].

Despite its widespread use, devolatilization with and without the benefit of inert stripping aids is limited by its reliance on volatility for separation. Some contaminants such as monomer, short chain oligomers, and high-boiling solvent can be difficult to remove by boiling alone due to their low vapor pressures and strong polymer interactions, χ . Extraction into a condensed phase offers a solution to this challenging separation.

Extraction with liquids such as water, alcohols, and organic solvents can be incomplete and can complicate separation. Water extraction is inefficient for non-polar contaminants due to their low solubility. Extraction with organic solvents is often effective, but further devolatilization steps are required following the extraction stage in order to remove residual extraction solvent. Supercritical fluids (SCF) offer a solution to all of the problems

An SCF is chosen for suitable compatibility with the polymer and good contaminant solubility. The SCF is highly volatile at low pressures, so it does not require extensive downstream separation. The high vapor pressure of the SCF also contributes to foam formation during the rapid decompression following extraction. SCF extraction can also accelerate the migration of contaminants through diffusion out of the polymer matrix by swelling the polymer [6]. Supercritical carbon dioxide has a solubility in PP around 8 wt% under the conditions studied, which can swell the polymer as much as 20% [6, 7].

Supercritical fluid stripping, which has been studied extensively, still relies on contaminant volatility as the ultimate driving force for separation. The technology described in this article seeks to overcome the limited

volatility of certain contaminated species by washing a polymer stream within a TSE and mechanically separating the SCF-rich phase from the polymer-rich phase above the critical temperature and pressure of the wash medium.

The objective of following studies was to identify whether SCF washing could improve the reduction of the outgassing organics contaminating a commercial grade of polypropylene (PP) versus a more traditional inert stripping process.

Experimental

Equipment and Materials

Experiments were conducted in two phases on a 48:1 L/D NFM Welding Engineers TEM-26SS co-rotating twin screw extruder (TSE). The extruder comprised 12 barrel segments, 4 L/D each, outfitted with cast aluminum heaters and cored for water cooling. Both phases of experiments used a K-Tron loss-in-weight feeder positioned over a feed hopper in barrel 1 of the 26mm TSE. A countercurrent flush of nitrogen was injected in the second barrel of the extruder 6D from the feed location to purge oxygen from the system. Strands were extruded through a water bath into a Rieter Primo 100 pelletizer.

Nitrogen and carbon dioxide were supplied by Matheson Tri-Gas in liquid Dewars. These gases were pressurized by a Haskel AGD-14 gas booster, measured by a Micro Motion Coriolis mass flow meter, and regulated using a manual micrometer needle valve. LC/MS grade methanol was purchased from Fisher Scientific (A456-4). Deionized water was produced on-site through a 4-tank ion exchange resin system provided by Culligan. An Eldex piston pump, capable of 10 mL/min at 5000 psi, was used to volumetrically meter methanol and water during Phase 1. A commercially available grade of polypropylene (MFR 28 g/10 min @ 230°C) with low residual outgassing organics (100-150 ppm) was used throughout the study.

In the first phase of experiments, a traditional co-current stripping process was evaluated using nitrogen, carbon dioxide, methanol, and deionized water as stripping media. In the second phase of experiments, supercritical carbon dioxide and nitrogen were compared in a novel co-current SCF washing/stripping process.

Phase 1 (Stripping)

In Phase 1, stripping agent was injected at 1% or 3% of the polymer feed rate 12 D from the feed location. Nitrogen and carbon dioxide were metered through a Micro Motion mass flow meter, and methanol and water were metered through a calibrated Eldex positive displacement pump. At the injection location, the screw was designed to provide gentle mixing to incorporate the stripping agent

into the melt. Four vacuum vents were positioned 8 D apart downstream of the injection point with polymer seals separating them. See Figure 1. The vent pressures were maintained between 3 and 6 torr (absolute).

Phase 2 (SCF Washing)

In Phase 2, SCF was injected at 12 D from the feed location, and SCF effluent was removed under 1200 psig back pressure 12 D downstream of the injection point through an NFM Welding Engineers 0.8" mechanical filter. The mechanical filter is a vertically mounted counter-rotating twin screw extruder designed with tight clearances in order to allow low viscosity materials such as liquids and vapors to be removed from the extruder by pressure flow while retaining solids and high-viscosity polymer melts.

The screw configuration in this set of experiments was designed to provide a melt seal before and after the SCF extraction section. Three kneading sections provided mixing between the SCF injection location and the mechanical filter. A strong melt seal was created under barrel segment 9 using highly restrictive screw elements in order to maintain critical pressure within the extraction zone. One vacuum vent was positioned downstream of the SCF washing section in barrel 11. See Figure 1.

SCF was dosed into the extruder at two different levels, low and high: 32 wt% and 41 wt% for nitrogen and 32 wt% and 48 wt% for carbon dioxide. The high dosing levels were set by the pumping capacity of the Haskel gas booster.

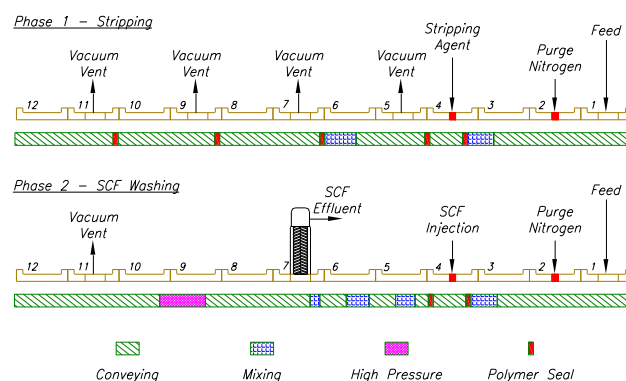


Figure 1. Extruder configurations for experimental phases 1 and 2.

Analysis

PP sample outgassing organic concentration was measured by thermal desorption coupled gas chromatography mass spectroscopy (TD-GC-MS) by a collaborator outside NFM. Outgassing organic values were normalized for pellet surface area, a technique confirmed by the analysis of cryogenically pulverized samples.

Results

Phase 1 (Stripping)

Vacuum devolatilization was evaluated in concert with two gas and two liquid stripping aids: nitrogen, carbon dioxide, methanol, and water. Vacuum devolatilization alone using four vents without any stripping aids achieved an outgassing organic contaminant reduction of 38%. Compared to vacuum alone, nitrogen, carbon dioxide, and water stripping did not improve organic contaminant removal, while stripping with methanol potentially demonstrated some slight improvement. See Figure 2.

Increasing the stripping ratio from 1% to 3% adversely impacted outgassing reduction with nitrogen and showed no effect with carbon dioxide. The behavior was reversed for methanol and water; increasing the dosing level from 1% to 3% improved the outgassing reduction for both.

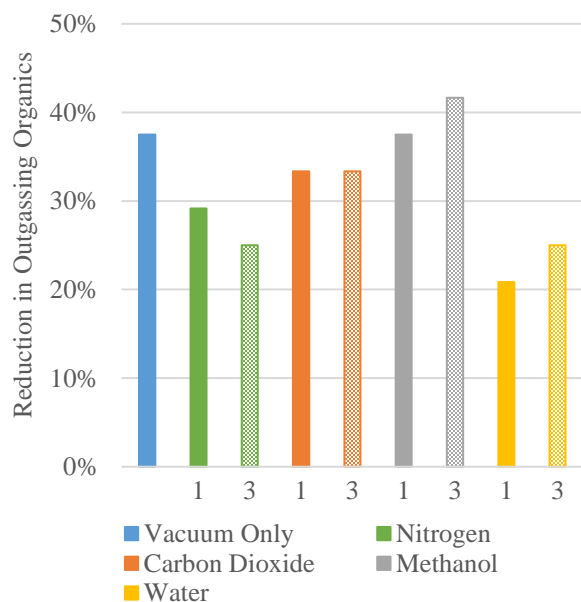


Figure 2. Reduction in outgassing organics by vacuum devolatilization and by stripping with nitrogen, carbon dioxide, methanol, and water. Stripping agents were evaluated at 1% and 3% of the polymer throughput rate.

Phase 2 (SCF Washing)

Supercritical carbon dioxide and nitrogen each significantly reduced the levels of outgassing organics. Nitrogen was more effective than carbon dioxide, reducing the outgassing organic levels by 65% vs 57%. Increasing the SCF ratio from 32 wt% to 41/48 wt% did not significantly improve washing performance for either nitrogen or carbon dioxide SCF. See Figure 3.

Washing with both supercritical carbon dioxide and nitrogen demonstrated significant gains over simple vacuum devolatilization, which reduced outgassing organics by 38%. See Figure 4.

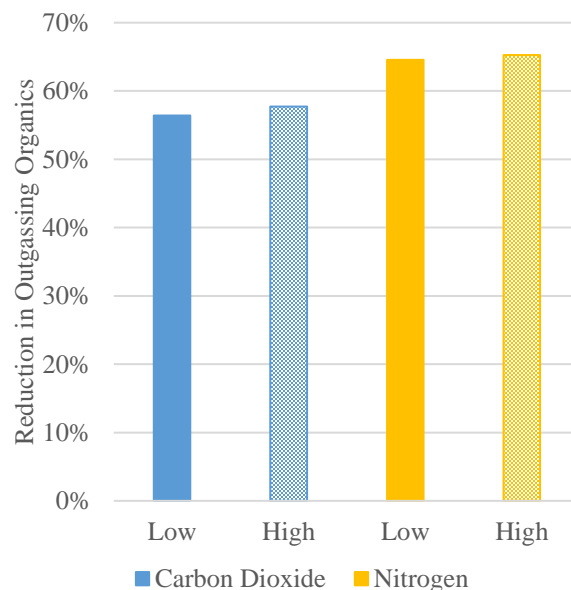


Figure 3. Reduction in outgassing organics by SCF washing with carbon dioxide and nitrogen. Both fluids were evaluated at low and high levels.

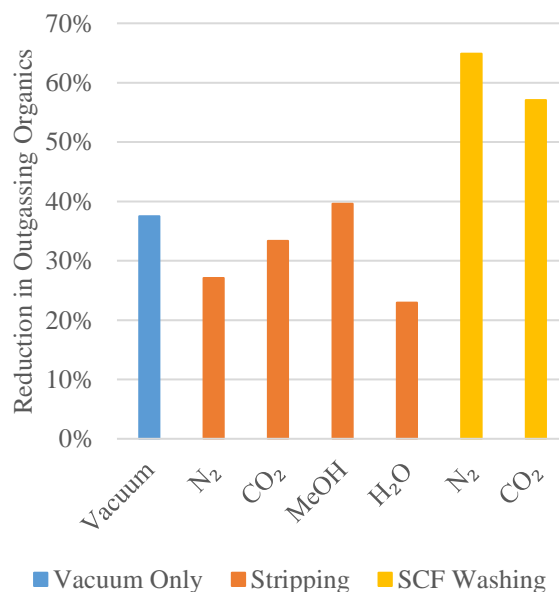


Figure 4. Comparison between outgassing organic reduction using stripping and SCF washing.

Discussion and Conclusions

The polypropylene used in these experiments was selected for its relatively low level of residual organic

volatiles. These organics were known to comprise a range of short chain oligomers, some of which have very low vapor pressures. Around 38% of these outgassing organics could be removed by vacuum devolatilization alone, but the remaining 62% was more difficult.

Conventional stripping was ineffective, if not counterproductive, compared to simple vacuum for all but one of the stripping media studied. Methanol was likely more successfully dissolved into the polymer melt than water, nitrogen, or carbon dioxide under the processing conditions. This would have resulted in enhanced foam formation. Stripping performance with water was the worst of all media evaluated. This could be attributed to the poor compatibility of PP and water, and the high latent heat of water, which will result in melt cooling on boiling.

The modest gains in outgassing organic reduction from 1% to 3% stripping ratio for methanol and water is likely due to proportionally enhanced foaming and/or surface area expansion due to boiling.

Supercritical fluid washing performed very well compared to vacuum alone and traditional stripping. Vacuum devolatilization was able to remove 38% of outgassing organics in four vent stages. These components likely had the highest vapor pressures, leaving behind higher molecular weight oligomers. With only one vacuum stage, SCF extraction was able to improve the reduction of outgassing organics by an additional 30%. Some of this improvement can be attributed to the rapid expansion of dissolved nitrogen/carbon dioxide during decompression out of the extraction zone [6].

From these studies, traditional stripping techniques were not well-suited for improving the devolatilization performance of a twin screw extruder for high-purity PP. SCF extraction, however, enhanced organic contaminant removal by more than 70% versus vacuum alone. This technology shows promise for a number of applications including the removal of monomer, oligomers, and high-boiling solvent, which have been difficult in the past to separate via devolatilization alone.

References

1. J.A. Biesenberger, *Polymer Engineering and Science*, **20**, 1015 (1980).
2. J.A. Biesenberger, *Devolatilization of Polymers*, Hanser Publishers, New York (1983).
3. R.J. Albalak, *Polymer Devolatilization*, Marcel Dekker, New York (1996).
4. J.A. Biesenberger, *Polymer Engineering and Science*, **26**, 582 (1986).
5. I. Gestring and D. Mewes. *Journal of Reinforced Plastics and Composites*, **21**, 409 (2002).
6. S. Alsoy and J.L. Duda, *AIChE Journal*, **44**, 582 (1998).
7. G. Li, F. Gunkel, J. Wang, C.B. Park, and V. Altstädt, *Journal of Applied Polymer Science*, **103**, 2945 (2007).

Twin Screw Extruder “TEX” in a Wide Variety of New Processes

Yoshitaka Kimura, Daigo Saga, Yasufumi Fujita, Makoto Tojo, Kouhei Muranaka

The Japan Steel Works, LTD, Hiroshima, Japan

Satoshi Takami, Japan Steel Works America, Inc., Houston, TX, USA

Synopsis

The twin screw extruders “TEX” have originally been developed for plastics compounding and have been significantly improved together with active demands for further development and rationalization in the plastics manufacturing processes. Because of the high flexibility, such as the changeable operation conditions, and excellent mixing function, TEX series have been increasingly applied to a wide variety of new processes including reaction, devolatilization, and concentration of surfactant additives. We introduce new mixing processes with the advantages of TEX in comparison with conventional processes using batch mixers.

Introduction

When first introduced in 1978, TEX twin screw extruders were primarily used for molten plastics mixture purposes. While various polymer producers and compounding producers are very active in plastics processing technology development and its improvements, processes using TEX has been significantly extended. Nowadays, it is widely used in compounding, polymer alloying, devolatilizing, dewatering, and reaction applications. In recent years, in addition to conventional applications, TEX has been used for applications where twin screw extruders have not been used before. For instance, a reactive and devolatilizing process for surface active agents previously manufactured using conventional batch reactor vessels, has been shifted to continuous process by using TEX technology. Moreover, several conventional mixing processes using intensive batch mixer and roll mixer have been changed to continuous process using TEX technology. In this paper, we will introduce how conversion to new mixing process from conventional batch mixer has been demonstrated by using features of TEX technologies.

Changes made on TEX technology

The first TEX proto type twin screw extruder with counter-rotating, intermeshing design was named TEX65 (screw diameter 65mm). Photo 1 shows appearance of the first generation TEX65.

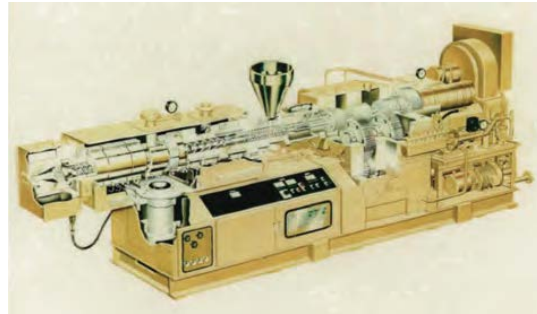


Photo 1: First generation TEX65

TEX series were initially developed mainly for compounding applications but gradually started using for various applications. In 1984, devolatilizing machine TEX305S has been delivered for solution L-LDPE devolatilization application (Photo 2).



Photo 2: TEX305S for devolatilizing

Since then TEX series have made its evolution to present 9th generation, which is called TEX-α III, released in 2011 by adopting the latest design and production technologies. Development of the 9th generation TEX-α III, which has the world's highest level torque made the technology more frequently to be used for engineering plastics and super engineering plastics compounds applications. Also, in high-

performance elastomer compounds such as TPV, which is much used in automotive components, use of TEX technology is remarkably increased. Therefore, we are seeking opportunity in areas of plastics where twin screw extruders were not used, also new materials other than plastics.

This is a technology to shift to twin screw extruders with continuous production from conventional batch type (non-continuous) mixers. Conventional batch mixer has a feature of making residence time as long as required and sufficient reaction and mixing can be achieved. On the other hand, due to long residence time, productivity is inferior to continuous and there are some environmental and safety issues due to manual handling of material. In case of twin screw extruders, this will be a continuous process and enhanced productivity and improved work environmental and safety can be expected. There is a slight concern of insufficient reaction due to shorter residence time than batch mixer, but it is possible to overcome the concern and improve reactivity by means of optimization of screw configurations, barrel configurations and barrel temperature settings.

Batch versus continuous mixers

Batch mixers are classified between low and high viscosity material mixers and used depending on material viscosity. Here is a comparison between batch mixer and continuous mixer, namely TEX and its process.

Batch mixer: For low viscosity materials

In general, reactor vessel is famous for paddle type blender. The vessel itself has jacket structure and materials are heated by injecting hot oil or steam into jackets. Also there is a blending blades located inside of the vessel and by blending, materials are molten, mixed and reacted. Materials are fed from material inlet on the top of vessel and spending certain time and proceeding with reaction and mixing. Due to structure of blending blades, torque and strength of blending blades are not high and there is a limitation of mixing high viscosity materials. Therefore, it is only used mainly for low viscosity materials, basically, liquid materials. By blending blades, high speed disturbed flow turbulence is

generated among a fluid that makes main material and sub-materials such as additives and oils can be blended fairly with a flexibility of mixing duration setting as you like. However, in order to get fair blending, sometimes residence time is required for a few hours and this is an issue for poor productivity. Also, feeding materials and discharging products are done manually, this will be a concern of high cost due to less automated and less productivity. Specially, when it comes to discharging high viscosity materials after mixing, materials may stick to inside of vessels that makes difficult to discharge and such removal and cleaning for material transition will take some time. This will be an environmental and safety issue. Also, more manual work will cause higher defect risk on product due to human error.

Batch mixer: For high viscosity materials

In batch type high viscosity material mixers, there are two types, namely twin roll mill and closed batch mixer. Twin roll mills are still widely used as laboratory and R&D purpose mixer while for production, closed type mixers are used.

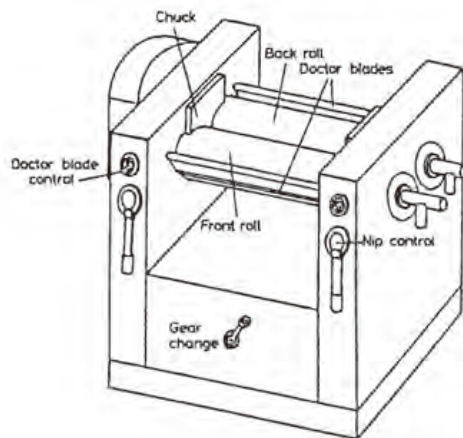
Twin roll mill is an origin of all the closed type mixers. As shown on Drawing 1, the structure is to have two rolls with counter rotation which are installed horizontally and surface is polished. Materials are inserted between rotating rolls that provide shear and mixing.

Closed type mixer is generally called as intensive mixer and represented by Banbury mixer. Its fundamental principal is same as roll mills but its mixing performance is far stronger than roll mills. As shown on Drawing 2, mixing cell with closed cross sectional "8" shaped with two parallel kneading rotors built-in, hopper, ram for pressurizing materials and outlet door for either falling or sliding discharge.

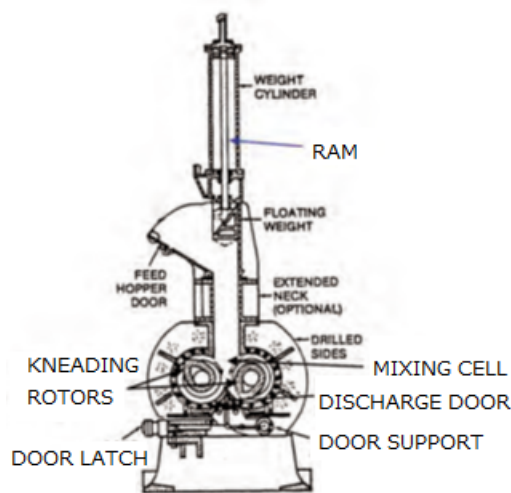
Material is mixed by shear between two kneading rotors rotating like roll mills. Mixing strength can be adjusted by pressurize system called ram that can move up and down. The mixer is capable to change mixing level by using kneading rotor configuration, speed, ram pressure and mixing cell temperature, etc.

Since mechanical structure is robust, it is capable to sustain torque and mechanical

strength and is suitable for low temperature mixing of high viscosity material and mixing involving plasticizing of solid materials. However since it is batch type similar to reactor vessel, material discharge needs to be done by hand and there are issues for productivity, environment and safety. Also, similar to reactor vessel, operation is mainly done by manually and there will be a concern of stable quality of mixing product as it is depending on operators experience and skills.



Drawing 1: Twin roll mill



Drawing 2: Banbury mixer

Continuous mixer: Twin screw extruder, TEX

In case of twin screw extruder, residence time is determined by throughput per hour, and L/D , which is a ratio of, machine size; i.e., length (L) and screw diameter (D). L/D has a limitation and in general, it is difficult to get the same

residence time as reactor vessel and Banbury mixer. To overcome this, applying necessary energy onto mixing product by optimizing screw and barrel configuration is a supplement for shortage of reaction time.

Since continuous mixers have significant advantage for users, they are active in process development by using additives to expediting reaction and mixing in shorter time. The structure of TEX, which is co-rotating and intermeshing type has superior self-cleaning capability and discharge for material transition can be done easily. This can overcome challenges of product discharge and self-cleaning of batch mixers.

Process using twin screw extruders possible to get stable product quality continuously by feeding material automatically by feeder, making integrated controls onto twin screw extruder controller for feeding material and necessary parameters for operation conditions of extruders and discharged product reaction and mixing controls. That will help reduction of off specification products and increase productivity drastically.

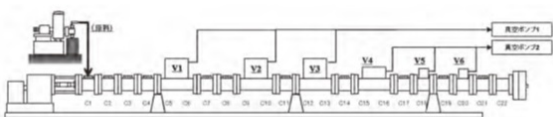
In the next section, we will introduce example of changing process from conventional production process using reactor vessels and Banbury mixers to TEX twin screw extruder for enhanced productivity and improved quality.

Example of changing process from batch process to twin screw extrusion process; Devolatilization process for specialty purpose additives

Devolatilization is typically required to remove by-products from produced material from reactor vessel. Thin film evaporators are often used and produced high purified products by taking long time. The process has an issue of productivity and in order to avoid off-product during grades change, there were studies for better efficiency production system. Also, operational environment upon grade change needs to be improved in the recent years. Therefore, enhanced productivity by use of continuous twin screw extruders has brought attentions.

Drawing 3 shows equipment outline for TEX twin screw extruders upon experiment of material used for actual process. Material is liquid and fed into TEX continuously by plunger pump

which can keep quantitative. Supplied material including by-products heated by shear heat by rotating screw and external heating by heater inside of TEX and devolatilized by reduced pressure grades and transformation to thin film at vent. In order to reduce residual concentration of by-products below target, multiple vent ports are located on extra long L/D extruder. Production with targeted residual concentration of by-products is made possible by improving devolatilizing efficiency significantly by setting off shorter residence time than thin film evaporator with use of intermittent compressional heating by screw and swelling (foaming) resulted from decompression at multiple vent ports and use of screw configuration that increased vacuum exposure area.



Drawing 3: TEX devolatilizing process

It is obvious that devolatilization zone length (L) and exposure area under vacuum atmosphere (S) has large effect on outlet volatile content as shown from the well known equation below.

$$\ln \frac{C_0 - C^*}{C - C^*} = K D_p \frac{SL N^{1/2}}{Q}$$

Aspects affecting to efficiency of devolatilization can be mainly heating applied on the materials and exposure area under vacuum atmosphere. Chart 1 shows relationship between screw speed and residual concentration of by-products. As the screw speed increases shear speeds increase also that makes heating value increased and easier to evaporate solvents. Also, increased renewal of polymer surface makes solvent easier to evaporate under vacuum atmosphere and because of improved devolatilizing efficiency, residual concentration of by-products among products is reduced. However, excessive application of heat for improved devolatilization efficiency will be a concern of degradation of quality.

Chart 2 shows relationship between different exposure sized screw configurations under vacuum venting and residual concentration of

by-products. Use of screw elements that makes larger exposure areas, improves devolatilization efficiency without applying excessive heat and achieved low by-products residual concentration of less than 300 ppm lowering extrusion product limited polymer temperature of 160°C. In this case, larger exposure area screw has twice as large area than smaller exposure area screw.

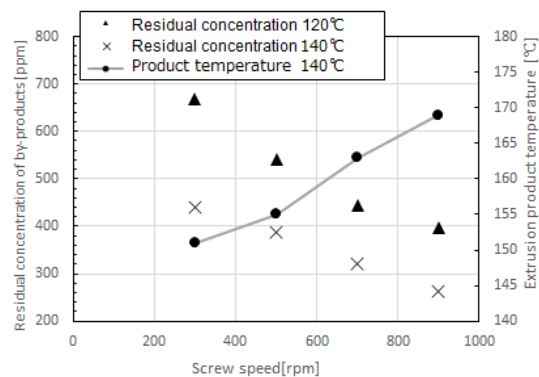


Chart 1: Relationship between screw rpm and residual concentration of by-products

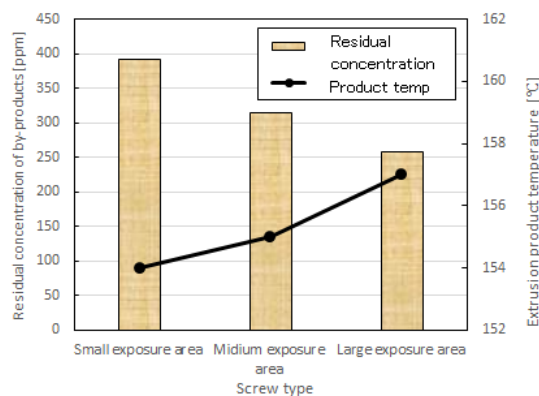


Chart 2: Relationship between screw configuration and residual concentration of by-products

Example ABS+SAN compounding

From the past, twin screw extruders are used for mixing of ABS (Acrylonitrile Butadiene Styrene Resin) and SAN (Styrene Acrylonitrile Copolymer). However such are still produced by batch process such as Banbury mixers. Banbury mixers are capable for melting and mixing solid material with viscosity such as ABS. By mixing parallel kneading rotors as per Drawing 2 with extra time for mixing under low speed, it makes possible to mix uniformly under low polymer temperature.

However, for the purpose of shifting process to continuous production by use of twin screw extruders for better productivity, we have demonstrated an experiment.

Such experiment was demonstrated by TEX54 α III made by JSW. ABS and SAN materials are fed into twin screw extruders quantitatively and continuously by gravity feeder. The quality of mixing of ABS and SAN is evaluated by number of unmolten objects (so called gels) with the size larger than 100 μm on a sheet surface made from sample pellets produced by evaluation type extruder. In order to achieve equivalent mixing performance with Banbury mixer, eccentric 3 lobe kneading elements are used as shown on Photo 3. This screw element has an effect of lowering local pressure generated inside of barrels and kneading tip position. Also, in case of mixing high viscosity ABS and relatively low viscosity SAN, extra precaution on screw configuration is required as mixing dispersion is challenging. Guideline for mixing dispersion is shear stress represented by:

$$\tau = \gamma \times \eta \text{ (shear rate x shear viscosity)}$$

By keeping viscosity of mixing products will make higher shear stress and increase dispersion performance. Since mixing of ABS is disturbed by lowering viscosity from progressed melting of SAN, screw configuration is intended to mix ABX by keeping viscosity of SAN with use of 3 lobe kneading elements.



Photo 3: Eccentric 3 lobe kneading elements

Chart 3 shows extrusion polymer temperature with eccentric 3 lobe kneading elements and conventional kneading elements. Polymer temperature in case of changing screw speed is indicated also. As shown on Chart 3, polymer temperature was effectively reduced with eccentric 3 lobe kneading element rather than screw configuration with conventional kneading elements.

Also, limited polymer temperature of 290°C was achieved by parameters with lower screw speed. By using latest TEX series which has ultra high torque, speed can be reduced by 10% and that made possible to lower polymer temperature.

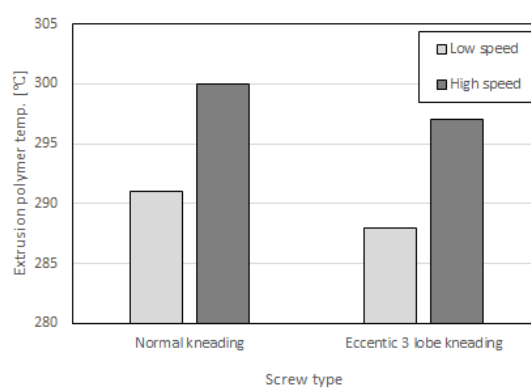


Chart 3: Relationship between screw configuration and polymer temperature.

Chart 4 shows relationship between screw configuration and number of gels from sheet evaluation. It also show relationship between screw speed and number of gels. Targeted gel number was achieved by use of screw configuration including eccentric 3 lobe kneading elements. Since equivalent mixing performance has been observed with products made from conventional batch mixer, the experimental result has been applied to actual production machine. This is the first achievement thanks to JSW's unique technology of eccentric 3 lobe kneading element and use of TEX α -III technology which has the world highest level torque.

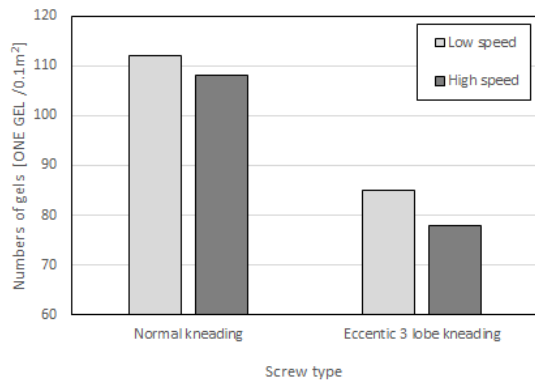


Chart 4: Relationship between screw configuration and number of gels on sheet

Example: Compounding of plant derived material

In recent years, compounds made from plant derived, environmentally friendly materials are getting attractions. In this paper, we will report one instance that fiber made from a plant derived material is used as sub-material and compounded with main material of olefin. Conventional batch process has been demonstrated by its laboratory experiments for optimization of blending olefin, fiber and additives. In order to aim continuous mixing of such materials, we came to a need of performance evaluation of mixers and we have studied improvement of productivity and fiber dispersion by using twin screw extruder technology.

Experiment was conducted by using JSW made TEX30α. Optimized material is fed into twin screw extruder quantitatively, and continuously through gravity feeder. There was no improvement on dispersion for process of mixing molten olefin and fibers after melting and adding fiber (Process 1) because of inefficient application of shear towards fibers due to reduced viscosity from molten olefin.

On the other hands, a development was made to molten mixing fed fibers before melting olefin and breaking down fibers in the extruder and after that mixing olefins fed from side feeder (Process 2). Chart 2 shows experimental operation parameters by using TEX30α. Samples obtained from experiments have been hot pressed and converted to thin film of approx. 0.15 mm thickness and observed fiber dispersion as per Photo 4. It is a comparison of

dispersion between fiber mixing process after melting olefin (Process 1) and melt mixing process of olefin and breaking down fibers before olefin melting (Process 2). In result, the less white spot is the better dispersion and it is assumed that fiber dispersion is better for Process 2. Chart 5 is a result for comparison of specific energy (required power per mass rate) on individual experimental processes. Here is specific energy equation:

$$ESP[kWh/kg] = \frac{kW}{kg/h}$$

From the result, it can be concluded that process (Process 2) breaking down plant fiber before melting olefin has better dispersion performance as per Photo 4 as specific energy is improved by approximately 14% than Process 1 and giving sufficient energy input to fiber and olefin.



Photo 4 Fiber dispersion on each mixing processes

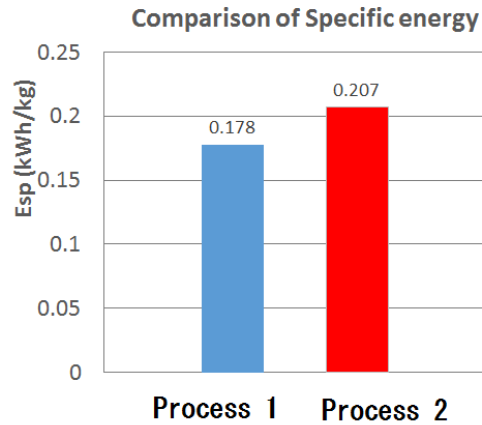


Chart 5: Comparison of specific energy

Conclusion

Twin screw extruder TEX series have made achievement of high torque, high speed and kept on developing its hardware. TEX is expected to be utilized for various application because of such the world leading performance. One of potential applications is for those where twin screw extruder technologies were not used so far. Such application should have potential benefit of enhanced productivity by means of process upgrade and improvement on environmental aspects and suppliers are encouraged to meet with such demands. We will be committed for further improvement of TEX series and upgrading of process technologies.

References

- 1) Sumida, Tomomitsu, Saga, Tojyo, Shimizu, Kodate, Ishibashi, Kakizaki, Inoue JSW Technical Report Vol. 64 (2013)
- 2) Ministry of Health, Labor and Welfare of Japan Workplace Safety, anzeninfo.mhlw.go.jp/
- 3) Kimimasa Ito: Compounding (1993)
- 4) "Devolatilization of Plastics", VD-VERLAG BmbH (1980), p16
- 5) Dr. Sunghoon Kim, Dr. Costas G. Gogos: Polymer Mixing Study Polymer processing Institute (1998), p102

Polypropylene Nanocomposites Containing 0D, 1D, and 2D Nanoparticles

By

P. Liu, K.L. White, M. Wong, C.-C. Chu, J.-I. Weon, M.J. Mullins, and H.-J. Sue

Polymer Technology Center
Department of Materials Science and Engineering
Texas A&M University
College Station, TX 77843

Abstract

Significant academic and industrial efforts have been made in the past three decades to prepare various types of polymer nanocomposites with the goal being greatly improved physical and mechanical properties for demanding engineering applications. However, little success has been achieved, especially for polyolefins. One of the many difficulties is our inability to achieve consistently good dispersion of nanoparticles in polymer matrices. In some cases, even when there is some evidence of good dispersion of nanoparticles, the level of improvements in physical and mechanical properties are disappointingly small. The above facts point to our lack of fundamental knowledge in regard to structure-property relationship of polymer nanocomposites. In this presentation, examples of polypropylene nanocomposites that exhibit outstanding physical and mechanical properties will be demonstrated based on CaCO_3 , MWCNT, and synthetic clay. Possible commercial significance of the present findings will also be discussed.

New Developments in Strain Hardening Modulus for Polyethylene Pressure Piping Applications

Dr. Bryan E. Hauger, Bryan Hauger Consulting, Inc., Longmont, CO

Abstract

Strain Hardening Modulus (SHM) is of increasing international interest for its capability to provide a useful index of the slow-crack growth (SCG) performance of polyethylene (PE) materials. Recently, a broad industry initiative has started to formalize an ASTM International test method to measure SHM. This effort likely is driven by several benefits to industry including the significant reduction in time required for SHM measurement in comparison to traditional SCG test methods. This paper will update the literature establishing the capabilities of SHM to replace traditional SCG test methods and provide a progress report in creating a North American standard for this useful test.

Introduction

PE piping has three distinct advantages over archaic pipe materials; 1) reduced lifetime costs 2) installation complexity and installation sensitivity are dramatically reduced resulting in faster construction especially when trenchless methods are utilized, and 3) very low failure rates per mile of installation when installed using industry best practices. PE pipe has the added benefit of being essentially inert across a broad range of fluids including market penetration in drinking water distribution, natural gas distribution and hydrocarbon production. Based on these benefits and others, PE piping has captured significant infrastructure market share in North America over the past decades. Market share gains in Western Europe for plastic piping have been faster, deeper and continue to grow due to an ever increasing application to new materials to new application environments.

Aside from occasional poor installation practices and third party damage, the ultimate limit on the lifetime of high-density PE (HDPE) piping systems is slow crack growth (SCG) resistance. A variety of index tests have been developed that industry uses for both material qualification and new material development including the Notched Pipe Test¹ (NPT), the Cracked Round Bar (CRB) Test² and Full-Notched Creep Test (FNCT)³. The latter two tests, CRB and FNCT have received attention due in part to reduced testing times.

North America regulations are summarized in ASTM D3350 "Standard Specification for Polyethylene Plastics Pipe and Fittings Materials"⁴. In this standard, HDPE resins used for pressure pipe rely solely on qualification according to ASTM F1473 "Standard Test Method for Notch Tensile Test to Measure the Resistance to Slow

Crack Growth of Polyethylene Pipes and Resins", more commonly called the PENT test⁵. A new index test based on elevated temperature tensile testing called Strain Hardening Modulus (SHM) test has been formalized by the 2015 publication of ISO 18488⁶. This test proposes to provide slow-crack growth (SCG) performance information in a fraction of the time required for all other methods. In 2016, I provided a review and presentation at the Polyolefins Conference which provided a detailed consideration of the microstructural relationship between SCG resistance and strain hardening modulus⁷. In this review, we will illustrate two critical improvements of the SHM when compared to PENT. The SHM test provides a test method with a strong correlation to PENT in a fraction of the time required for PENT. Also, the SHM test provides a reliable index of SCG well beyond the level of performance when PENT is no longer reliable – for example for PE100 RC materials with PENT testing times in excess of 1 year. However, the next section will review the meaning of the term SHM within the context of the more familiar tensile coupon testing found in ASTM D638⁸.

Strain Hardening Modulus

A series of familiar features are observed in the load / displacement plot obtained when polyethylene tensile bars are elongated in a cross-head displacement testing station (see Figure 1). Initially, the modulus of elasticity is observed to start at the origin as the load quickly rises with increasing displacement. After yielding, the strain localizes and the material shows strain softening followed by neck stabilization and drawing of the material into the neck region⁹. This is followed by an extended drawing or necking region with the load becoming fairly stable under further elongation resulting in the gage section of the test specimen converting into a long fiber. The drawing region is terminated at a strain we will refer to as the Natural Draw Ratio (NDR) when the load is observed to increase significantly with incremental elongation. Eventually, the test specimen will rupture or break with the ultimate load sometimes exceeding the load at yield. It is this final feature which is the focus of the ISO 18488 test method⁶. In our previous Polyolefins paper⁷, we discussed the early literature starting in the 1990s which documented a relationship measure of slow crack growth resistance and drawing characteristics from the tensile curve. We also summarized the results of a significant 2001 paper published in the Plastic Pipes conference¹⁰ which related a lower value of NDR to an increased failure time in NPT testing. Most importantly, our previous Polyolefins paper

underlined the nearly universal acceptance of mechanical reinforcement of the damage zone ahead of the crack tip is by “tie molecules” which participate in two crystalline regimes and improve SCG resistance. Generally speaking, as tie molecule density increases, the SCG resistance of the PE material also increases. More recent literature suggests that the strain hardening regime is also mainly governed by the density of tie molecules and entanglements. Thus, the SHM can be used as indirect measure for the SCG resistance.

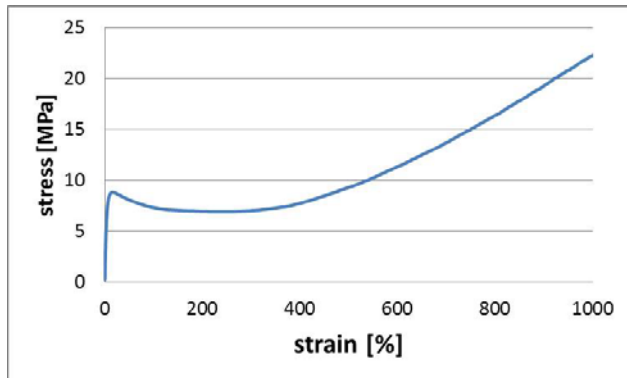


Figure 1. Drawing of a typical PE stress-strain curve illustrating the broad region of fiber drawing that follows yielding.

The Origins of ISO 18488

In fact, the ISO test method reworks the familiar features of Figure 1 into a report of true stress and true strain assuming volumetric conservation. Then a linear fit of the slope of the true stress-strain curve above the NDR is created and this value is referred to as SHM. As stated in the test method “the strain hardening modulus . . . is used as a measure for the resistance to slow crack growth of polyethylene. The strain hardening modulus is obtained from stress-strain curves on compression moulded samples . . . and . . . provides a method that is valid for all types of polyethylene. . . that are used for pipes and fittings applications”.

The ISO test method is clearly based on the 2005 publication¹¹ by researchers from Sabic and DSM and closely mirrors several elements originated in that work including 120°C annealing of the polyethylene sheet prior to stamping out specimens, 80°C elevated temperature during testing, slight modification of an ISO37 type 3 tensile bar, and the preference for optical extensometer measurement. Table 1 contains the data from the 2005 paper and the data is plotted in Figure 2. It is potentially important to note that the authors refer to the testing they conducted as ESCR testing (we continue that terminology) but the testing is not equivalent to the familiar ASTM test method D1693 in several ways¹². The reader is referred to the original paper for the details of this testing. However, the high value for goodness of fit illustrates the quality of

the correlation between SHM in MPa and the log of the time to failure in ESCR testing reported in hours. Our interest in this alternative testing approach is underlined in this quotation from the publication “The slow crack resistance of polyethylene is usually . . . time consuming . . . the findings reported in this publication offer a possibility to assess the information on slow crack propagation in much simpler and faster way”.

ESCR (hrs)	G _p , MPa	Log ESCR
58	18.8	1.763
103	20.6	2.013
10	13.1	1.000
20	15.4	1.301
50	19.0	1.699
47	19.5	1.672
112	26.0	2.049
300	30.7	2.477
1000	35.8	3.000
>2000	47.2	NA

Table 1. Data from Reference 11. The data point reported as “>2000 hrs” was not including in the analysis in Figure 2.

While this 2005 publication provides the first correlation of SHM to ESCR values, the pressure piping industry is more interested in other measures of stress crack resistance aside from ESCR commonly applied to pressure pipe resins. In North America, the most commonly applied test method is PENT.

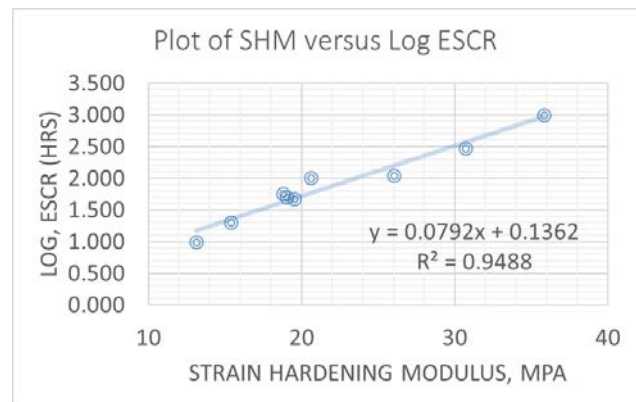


Figure 2. Plot of the log ESCR values against the strain hardening modulus from Reference 11.

SHM and Statistics

Of course, one of the most important considerations for establishing a correlated relationship between SHM and any other measures of SCG resistance will be the statistical variation in the measurement of both values. One of the best publications¹³ on this subject was provided during the Plastic Pipes XVI conference by authors from Kiwa Technology. These authors reported the findings of a round robin study conducted on three generations of

pressure pipe resins; PE80, PE100 and PE100RC. Eight laboratories conducted testing on all three materials with individual replicate measurements varying in number from a minimum of three to a maximum of nine. The reader is directed to the publication for further details but the results summarized in Table 2 are worthy of further discussion.

	Resin A	Resin B	Resin C
G _p , MPa	82.7	46.6	25.1
Stan. Deviation	8.0	2.3	1.1
% Stan. Deviation	9.7	4.9	4.4

Table 2. Summary of Statistical Data from Reference 13.

For a start, it is worth mentioning that the paper describes some reasons for exclusion of some data results from the round robin which fairly significantly reduce the standard deviation for Resin A. The standard deviation for Resin A is then reported to drop to 4.4% of the average value. For the sake of simplification, let us consider that the standard deviation for all three resins was approximately 5% and does not increase significantly as the value for SHM increases. In this data, the standard deviation appears fairly constant over a range of SHM that extends over nearly all modern pressure pipe resins and covers greater than a 300% change in the value. Perhaps a standard deviation value of 5% reflects a good estimate for the experimental error in multiple replicate studies. We will return to this standard deviation value later in the discussion.

SHM and PENT Correlations

In 2015, a case study was published¹⁴ that explored the potential for a correlated relationship between SHM and Log PENT failure times. Unfortunately, the data we are interested in are not published in the paper directly in table format. Instead, the data for both SHM and PENT failure time is estimated here based on Figure 6 from the paper. Table 2 contains the data from the 2015 paper and the Log PENT versus SHM is plotted in Figure 3. The high value

PENT (est.) (hrs)	Est. G _p , MPa	Log PENT
35	28.0	1.544
225	32.2	2.352
230	33.4	2.362
475	34.5	2.677
600	33.9	2.778
950	34.4	2.978
1250	37.6	3.097
1875	38.0	3.273
2000	37.4	3.301
3025	36.9	3.481

Table 2. Data estimates prepared based on Figure 6 of Reference 14

for goodness of fit illustrates the quality of the correlation between SHM in MPa and the log of the time to failure in

PENT testing reported in hours. This implies that one can assess the likely failure time of pipe resins in PENT testing, likely taking thousands of hours in some cases, by conducting the quick and low cost SHM test.

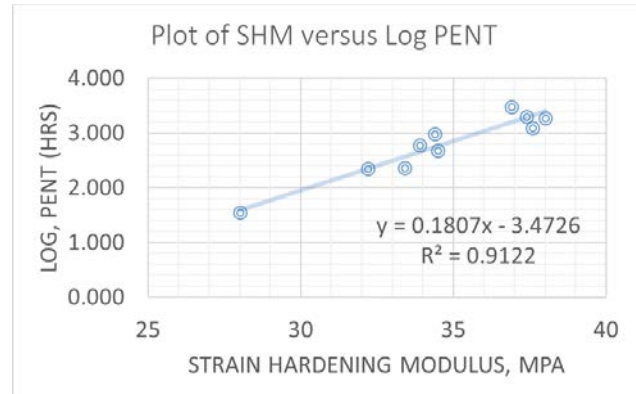


Figure 3. Plot of the log PENT values against the strain hardening modulus from Reference 14

There are other interesting details to mention regarding this case study. The researchers from Rey Juan Carlos University in Spain stated that the resins used in the study were “polyethylene grades from blow molding up to PE-80, PE-100, and higher resistant to crack grades”. However, the values of SHM reported reach a maximum of 36.9 MPa which does not address the full range of SHM values available in the current market or in their later publications. Tensile tests were conducted on ISO37 type 3 tensile bars in an 80°C chamber at a rate of displacement of 10 mm/min measured using an optical extensometer. But it is interesting to note that the thickness used for tensile specimens in this paper was 2 mm which does not comply with the requirements of ISO 18488 which allows a maximum of 1.0 mm and recommends 0.3 mm. Also, it was not mentioned if there was annealing done after initial molding in spite of the fact that this is required by ISO 18488. Otherwise, the details of sample preparation and testing are aligned with the ISO test method. It should be clearly stated that the testing in this paper is not conducted in strict accordance with ISO 18488 and, therefore, the absolute correlation between log PENT and SHM by ISO 18488 provided in Figure 3 must remain in doubt. Additionally, it is unfortunate that, in spite of the fact that the researchers mention that they measured SHM in triplicate, there are no error bars provided in Figure 6.

An additional important case study was provided by the researchers from Rey Juan Carlos University at the 2016 Plastic Pipes Conference¹⁵. In this case study, “a wide range of PE resins grades” was studied using the ISO 18488 test method and compared to PENT testing. As discussed below, this publication introduces additional complexity to the 2015 case study. Shown below is Figure 4 from that paper in which the SHM is compared to the log of PENT failure times for three families of resins; 1) Ziegler-Natta (ZN) resins made using a 1-butene comonomer, 2) chromium catalyzed resins made using a 1-hexene

comonomer and 3) an extrusion blended system prepared from two component polymers. The paper further clarifies that an un-named “iron based catalyst” was the source of a homopolymer PE blended with a low density ethylene-hexene copolymer made using an un-named metallocene catalyst. The paper makes the point that is clearly illustrated in Figure 4, not all polyethylene materials follow an identical relationship between SHM and Log PENT.

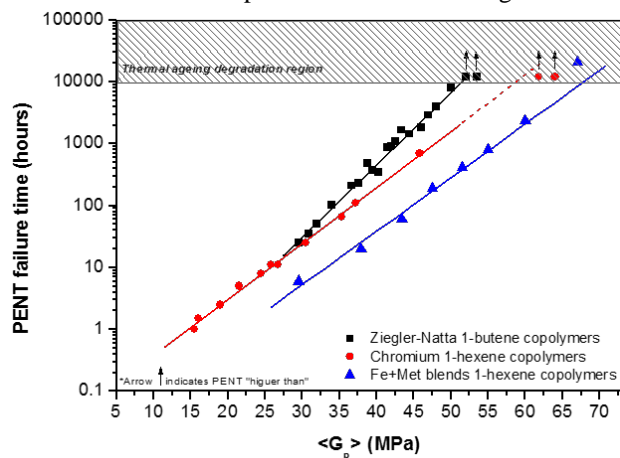


Figure 4. Reprint of the log PENT values against the strain hardening modulus which originally appeared as Figure 4 in Reference 15.

While the paper concludes “Correlation between SH method and classic SCG tests are reported on this work. It is proved that the method guarantees a rapid and accurate evaluation” it is also clear that there is an apparent relationship to the precise nature of the polymer which is not fully explained. It is possible that the SHM may differ for two PE materials with essentially equivalent PENT values due to some relationship to either the catalyst (and its effect on the microstructure of the polymer) and/or the co-monomer. However, for the most common commercial systems, the differences between families of resins is relatively minor up to a PENT failure time of 100 hours or even 500 hours. Perhaps even more critical is to understand if the amount of statistical variation is low when SHM is measured, then this might allow industry to accept a conservative value for SHM in order to obtain a result that is essentially equivalent to a PENT testing time (that may take thousands of hours to generate) by SHM testing consisting of a very rapid tensile test.

Statistical Implications for SHM Correlations

If we now apply the statistical conclusion from the Kiwa publication to the 2015 case study, then the results become even more interesting. If we assume that the errors in these measurements of SHM are normally distribution about the mean, then 3 times the standard deviation should account for 99.7% of the sample population being studied.

It might therefore be reasonable to multiply 15% by the SHM should then account for approximately 99.7% of the measured value for SHM to estimate a measure of statistical relevance that may be applied to our previous Figure 3. It is important to recall that the standard deviation value incorporates both positive and negative variations. These values have been provided in Table 3 as a new column that was not present previously. Next we can superimpose an oval on our previous Figure 3 to represent the positive and negative statistical variation about the mean value for SHM. Then lines are drawn to define the positive and negative boundary for the data variation. These changes to figure 3 are illustrated below as Figure 5.

PENT (est.) (hrs)	Est. G_p , MPa	3 X Est. Stan. Deviation, MPa	Log PENT
35	28.0	4.2	1.544
225	32.2	4.8	2.352
230	33.4	5.0	2.362
475	34.5	5.2	2.677
600	33.9	5.1	2.778
950	34.4	5.2	2.978
1250	37.6	5.6	3.097
1875	38.0	5.7	3.273
2000	37.4	5.6	3.301
3025	36.9	5.5	3.481

Table 3. Data Estimated from Figure 6 of Reference 11 including an estimated standard deviation column equal to 15% of the SHM.

Let us consider the implications of Figure 5 for an illustrative example - a Log PENT value that is equal 2.0 would represent a PENT value of 100 hours. If we wish our SHM values to represent 99.7% of all outcomes, then we must acknowledge that values falling between approximately 28.2 MPa and 32.5 MPa are statistical results one might obtain for that resin.

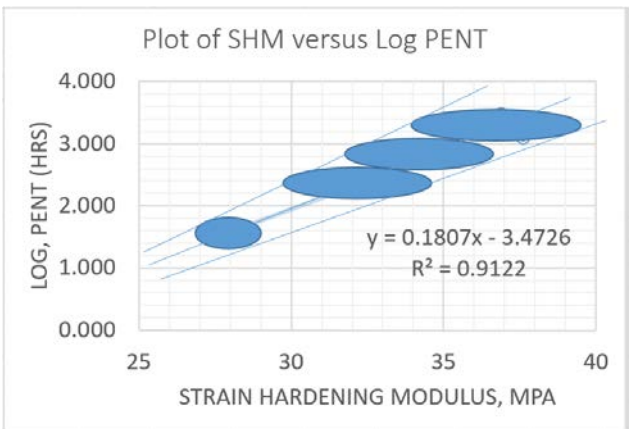


Figure 5. Re-plot of the log PENT values against the SHM for Figure 3 of this paper including superposition of ovals on top of some previous data points to illustrate error bars equal to 15% of the SHM measured value.

Conversely, if one wished to set a minimum SHM value such that statistics provided a 99.7% likelihood that a PENT result would be obtained that exceeds 1000 hours, then one first substitutes 3.0 for the value of y in the equation in Figure 4 and solving for x obtains a value of 35.8 MPa. However, then one must increase this value by 7.5% to account for the possible statistical negative variation. This leads to a calculated value of 38.5 MPa. To those who are more gifted in statistical analysis, it will be clear that the above discussion assumes no variation in the measured value of PENT which is obviously not correct. ASTM F1473 precision statement indicates that standard deviation of the average values within laboratories for round robin testing was $\pm 16\%$ while the standard deviation of the average values between laboratories was $\pm 26\%$. In other words, substantially greater standard deviation than observed for SHM. However, it is hoped that the above discussion illustrates that the statistical consequences of the data analysis are not intractable.

As already noted previously, it is uncertain that the testing conditions in this case study match the ISO 18488 conditions, but for the sake of illustration we will use the values provided in Figure 3 of this paper as if they were reliable without attempting to assure their correctness. If one wished to provide reasonable statistical assurance of a PENT value greater than 1000 hrs by first measuring SHM, the minimum acceptable average value is 38.5 MPa once the possibility of statistical variation is accounted for. While this approach might not be appealing in all circumstances, the opportunity to obtain this result in perhaps 72 hours rather than waiting 1000 hours for the PENT result is likely attractive in some scenarios. Intractable but are, rather, merely complex. Perhaps the attractiveness of such an approach becomes more clear if the desired PENT value is 2000 hours, 5000 hours or 10,000 hours. It should also be mentioned that such an approach unlocks the possibility of selecting SCG resistance that is currently unamenable to PENT testing by thoughtful application of the SHM test.

Current Efforts Underway

The publication of test method ISO 18488 removed a critical barrier to North American industry acceptance of the SHM. The two case studies presented here from 2015 and 2016 remove another barrier by providing a detailed correlation between SHM and log of PENT. Finally, the publication from Kiwa researchers removes an additional barrier by providing confidence that a version of ISO 18488 can be conducted with relatively reasonable statistical variation. What then is lacking for North American industry to start the adoption of SHM into PE piping standards.

One answer might be merely familiarity with the ISO 18488 test method. The author of this review has solicited independent quotations from six North American laboratories to conduct ISO 18488 testing and received

back four valid quotations. One laboratory declined to provide quotation due to limitations relating to the elevated temperature oven required during testing. One laboratory shifted the quotation to a European laboratory. In a very interesting development, this European lab asked if it was necessary for the laboratory to compression mold the initial sheet of material indicating that clients often provide the sheet of material directly and the lab only conducts in-house annealing as required in ISO 18488.

At first glance, this seems an odd response since the compression molding is written as a mandatory component of the ISO test method. However, on further consideration, it seems plausible that the required sheet annealing steps (ie. 1 hour at 120°C followed by slow cooling at a rate less than 2°C / minute) may reasonably be expected to remove any processing history from the initial sheet molding. Perhaps the mandatory conditions for the initial compression molding of the PE sheet are not critical to performance of the testing with high statistical relevance.

It seems that a critical barrier which persists is to obtain an ASTM test method which is vetted by an industry consensus process and eliminates any overly proscriptive requirements that can be shown are not critical to the results of testing. Therefore, the author has initiated a project to create an ASTM test method titled "Measurement of Strain Hardening Modulus on Polyethylene Materials used in the Manufacture of Stress-Rated Pipe". It is hoped that this effort will provide ASTM participants access to a test method which meets the needs of industry. At the point that the test method reaches finalization, it is anticipated that a round robin study will again be conducted on the strict scope of the ASTM SHM test method. A particularly favorable outcome would be to obtain an ASTM test method that retains any critical aspects of the ISO test method.

Discussion and Conclusions

In this review, we have provided some critical case studies to update the reader on the SHM literature. To all appearances, the potential continues to exist to replace traditional SCG test methods such as PENT with SHM and obtain results in less than a 100 hours which can be used to verify thousands or tens of thousands of hours of PENT performance. Additionally, the author has introduced his own efforts at ASTM as a progress report in creating a North American standard for SHM testing. Although the path may take several years and much effort, the pathway for progress seems reasonably straight-forward.

References

1. ISO 13479:2009 "Polyolefin pipes for the conveyance of fluids – Determination of resistance to crack propagation – Test method for slow crack growth on notched pipes".

International Organization of Standardization, Geneva, Switzerland, 2009.

2. ISO 18489:2015 “Polyethylene (PE) materials for piping systems -- Determination of resistance to slow crack growth under cyclic loading -- Cracked Round Bar test method”. *International Organization of Standardization, Geneva, Switzerland, 2015.*

3. C.J.G. Plummer, A. Goldberg, A. Ghanem, “Micromechanisms of slow crack growth in polyethylene under constant tensile loading”, *Polymer*, 2001, 42, 9551-9564.

4. ASTM D3350 – 14, “Standard Specification for Polyethylene Plastics Pipe and Fittings Materials” *2014 Annual Book of ASTM Standards, Volume 08.02, Plastic Piping Systems.*

5. ASTM F1473 – 16 “Standard Test Method for Notch Tensile Test to Measure the Resistance to Slow Crack Growth of Polyethylene Pipes and Resins” *2016 Annual Book of ASTM Standards, Volume 08.04, Plastic Piping Systems.*

6. ISO 18488:2015 “Polyethylene (PE) materials for piping systems — Determination of Strain Hardening Modulus in relation to slow crack growth — Test method”. *International Organization of Standardization, Geneva, Switzerland, 2009.*

7. B. E. Hauger, “Strain Hardening Modulus and Natural Draw Ratio for Polyethylene Pressure Piping Applications” *SPE Polyolefins Retec*, 2016.

8. ASTM D638 – 14, “Standard Test Method for Tensile Properties of Plastics” *2014 Annual Book of ASTM Standards, Volume 08.01, Plastics.*

9. A. Chudnovsky et al “Lifetime Assessment of Engineering Thermoplastics”, *International Journal of Engineering Science*, Volume 59, (2012) pp 108–139,

10. E. Laurent, “Comprehensive Evaluation of the Long-Term Mechanical Properties of PE100 Resins”, *Plastics Pipes XI, Munich, Germany, September 2001.*

11. Kurelec L, Teeuwen M, Schoffeleers H, Deblieck R; “Strain Hardening Modulus As a Measure of Environmental Stress Crack Resistance of High Density Polyethylene” *Polymer*, 46, (2005), 6369-6379.

12. ASTM D1693-15, “Standard Test Method for Environmental Stress-Cracking of Ethylene Plastics” *2015 Annual Book of ASTM Standards, Volume 08.01, Plastics.*

13. E. van der Stok and F. Scholten; “Strain Hardening Tests on PE Pipe Materials” *Plastics Pipes XVI, Barcelona, Spain, September 2012.*

14. A. Adib, C. Dominguez, J. Rodriguez, C. Martin, and R. Garcia; “The Effect of Microstructure on the Slow Crack Growth Resistance in Polyethylene Resins” *J. Polym. Eng. Sci.*, 55, 1018 – 1023 (2015).

15. C. Domínguez, N. Robledo and R. A. García-Muñoz “Limits on the Slow Crack Growth Resistance Evaluation for the PE100 and PE100RC Polyethylene Resins”. *Plastics Pipes XVIII, Munich, Germany, September 2016.*

Key Words: Strain Hardening Modulus, ISO 18488 Test Method, ASTM F1473 Test Method.

7/9/11 layer blown film lines - Which are the most suitable applications?

It's the age old question... "Which came first, the chicken, or the egg"? Are 7/9/11 layer films lines being sold because they are needed for a product, market or economic reason, or because they are the newest and latest equipment technology?

Through the years, film manufacturing has evolved from monolayer films to multilayer films for a variety of reasons. The confluence of machining technology, equipment development, computer technology, process development, polymer chemistry, economic forces, market needs, and education all came together over time to yield what we now know today as modern coextrusion. This is true across the entire spectrum of polymer film production, including blown film, cast film, double bubble, oriented cast sheet and extrusion coating. The technology developed by Roberto Colombo (Turin, Italy) [1] in 1958, Walter Schrenk (Bay City, Michigan, USA) [2] in 1967, and many others has forever changed film manufacturing, and the markets which they serve.

Three and even five-layer films have been common for many years, and are commonly used in a number of packaging applications all around the world, either as stand-alone films, or as part of a lamination to another film or foil. Film structures such as shown in Figure 1 are commonly used for food and non-food packaging either as they are, or as laminations with oriented films. Until now, these 3-layer and 5-layer films have taken full advantage of coextrusion technology, machinery development, polymer properties, and have satisfied market needs.

So, how did we go from one to three and five layer films to 7, 9, and 11-layer films? What is driving the market to films with more and more layers? It seems all the major manufacturers are offering 7, 9, and 11 layer machines. The big question is why? Is there a real benefit to be gained from the additional capital expenditure, or is it marketing hype?

Introduction

All films offer certain properties that make them desirable for various end uses [3]. These properties include:

- Product protection
- Puncture and abuse resistance
- Vapor barrier
- Moisture barrier
- Grease barrier
- Light barrier
- Printability
- Heat seal
- Hot tack
- Machinability

Monolayer films have traditionally been used for the most simple applications, such as agricultural film, construction films, and garment bag films. Very few new lines are sold today as monolayer lines, if for no other reason than for increased output and flexibility of product capability. In fact, surveys show that sales of mono-layer blown film lines have fallen to less than 4% today, whereas the sales of 5/9/11-layer lines has grown to about 30% of the market today [4]. The remainder of the lines sold today are 3-layer lines, whose market share has fallen from about 75% in the year 2000 to about 60% today. Clearly, the trend is to purchase equipment capable of coextruding more and more layers. There are many benefits of multilayer films, as shown in Table 1 below.

Table 1. Benefits of Multilayer Films [4, 7]

- Improved physical properties
- Optimization of film structures for specific applications
- Improved Gelbo flex resistance (reduced flexural failures)
- Reduced layer thickness of expensive resins
- Improved barrier properties
- Controlled respiration (O_2 & CO_2 transmission)
- Use of new polymers
- Thinner, stronger films
- Combining incompatible polymers in one step
- Improved gloss
- Additional attributes, such as anti-fog, anti-block, COF, two-sided color
- Reduced cost
- Quick response of new product structures as new applications are developed

A complete review of all these benefits is beyond the scope of this article. However, if we focus only on barrier properties, the benefits that 7/9/11-layer coextrusion offers become obvious. While EVOH is a very effective oxygen barrier material, its drawbacks are that it is stiff, relatively difficult to process, possesses poor moisture vapor barrier properties, and is expensive. Table 2 below shows the oxygen transmission values of various polymers.

Table 2 - Oxygen Transmission Rate of Various Polymers, [5]

POLYMER	OTR @ 20°C, 65%RH (cm ³ 20μ / m ² day atm)	GAS BARRIER
27 Mol% Ethylene EVOH	0.2	Excellent
44 Mol% Ethylene EVOH	1.5	
PVDC	2.6	
PA	38	Fair
PET	54	
HDPE	2300	Poor
PP	3000	
PC	5000	
PS	8000	
LDPE	10000	
EVA	18000	

As can be seen on Table 2 above, the oxygen transmission rate of 27 Mol% ethylene vinyl alcohol resin is 50,000 times less than traditional LDPE, so that a very thin layer of EVOH provides excellent oxygen permeability. The modulus of elasticity shows that thinner layers of material are more flexible than thicker layers [6], so improved Gelbo flex resistance is anticipated with thinner layers of stiff materials. Also, it can be seen in Table 2 that the oxygen transmission rates of polyamide and polyester films are similar. This means that the possibility exists for polyamides, which are inherently tough and stiff, to be substituted for polyesters in multilayer films, for its oxygen transmission rate and stiffness, thereby producing a finished lamination in the one-step blown film process. This is but one advantage of multilayer coextrusion. As machinery technology developments allow for more and more layers to be coextruded, more and more properties and uses of blown film are being discovered.

What are the advantages of a 3 or 5 layer line over 7/9/11 layer lines?

To be sure, 3- and 5-layer films are not going to disappear anytime soon. The installed base of these machines is very large, and the adhesive laminators that they feed is likewise so large, that it is difficult to imagine these lines disappearing. In addition, 3- and 5-layer lines are perfectly suitable for commodity, non-barrier products such as institutional liners, T-shirt bags, garment bags, stretch films, construction film and agricultural films. They also require less capital outlay, less floor space and ancillary equipment such as material handling, so the overall cost of the equipment is less. In those applications requiring some degree of barrier properties, especially those that are adhesively laminated to metallized films, 5-layer structures as shown in Figure 1 are more than adequate for many applications.

Three-layer film blown lines are capable of either a 2-layer or 3-layer structure, in the form of an A/B/A or A/A/B structure, by simply using the same material in 2 extruders. These structures are commonly used as frozen meat and fish packaging films, frozen vegetable bags, cereal liners, forming webs, Modified Atmosphere Packaging (MAP) for fresh cut produce and poultry, boil-in bags, and much more [3]. Three-layer film capability also provides the option to "bury", or sandwich in between, a low-cost material or post-industrial waste in the middle layer to reduce cost, or to bury a pigmented layer between two layers of virgin polymer to reduce cost, increase gloss, or meet regulatory requirements.

It has long been recognized that 3-layer films have limits, such as with oxygen barrier, or print quality. To solve this issue, many 3-layer films were used as part of an adhesive lamination to reverse-printed films to achieve higher quality structures, either to other 3-layer films, or to metallized-oriented films and foil for improved barrier properties.

Conventional wisdom would say that if three layers are good, five layers must be better. Though this is not necessarily true, it can be said that five layers can offer more options and flexibility over 3 layers. Figure 1 shows a typical 5-layer film structure, showing a core layer of EVOH as a barrier layer, inner and outer layers of LLDPE, and "tie" or adhesive layers to join together the otherwise incompatible LLDPE & EVOH. This structure is ubiquitous today, and is used in many applications.

Figure 1 - Typical 5-Layer Coextruded Structures



Fig 1A. Typical frozen food structure



Fig 1B. Typical processed and cook-in meat structure

For the many basic package structures, a 5-layer film obviates the need for an adhesive lamination step. Figure 2 shows a typical 5-layer coextrusion blown film line. Some might argue that the modulus of oriented PP & PET films are greater than unoriented nylon films, and that laminations are superior to unoriented blown films, and that the film structure shown if

Figure 1B above is inadequate for many packaging applications. However, careful examination of data [6] shows that the secant modulus of nylon is greater than polypropylene and about 10% less than PET. This difference is easily replaced by the traditionally thicker nylon abuse layer, and in practice, nylon-based packages exhibit good toughness and stiffness.

Figure 2. A traditional 5-layer coextrusion blown film line showing a nested spiral die, air ring and bubble. Courtesy Alpine American.



What are the benefits of 7/9/11 layer lines over 3- or 5-layer lines

Given what we know today, 5-layer structures are limited as to their performance and cost saving ability. From a simple cost standpoint for example, whereas the structure in Figure 1A is an [LLDPE – Tie – EVOH – Tie – LLDPE] structure, a 7-layer structure can utilize a lower-cost LLDPE in the second layer and an expensive, high-performance metallocene LLDPE as the skin layer, which has superior hot tack and heat seal properties. This structure, [mLLDPE – LLDPE – Tie – EVOH – Tie – LLDPE – mLLDPE] shown in Figure 3A below, optimizes performance and cost, and is used for milk packaging.

Alternatively, if improved barrier properties and toughness are desired, an [LLDPE – Tie – Nylon – EVOH – Nylon – Tie – mLLDPE] structure can be made with a 7-layer die, shown in Figure 3B. This structure is used as a lidding film with excellent barrier properties and gloss. If ethylene vinyl acetate (EVA) is substituted for the mLLDPE layer in this previous structure, the film can be used as a thermoformable cheese tray, shown in Figure 3C. The point made here is that more layers offers the package designer more options.

Figure 3. 7-layer structures for various applications and uses



Fig. 3A Cost reduction over the 5-layer analog



Fig. 3B High barrier lidding structure



Fig. 3C Thermoformable cheese tray



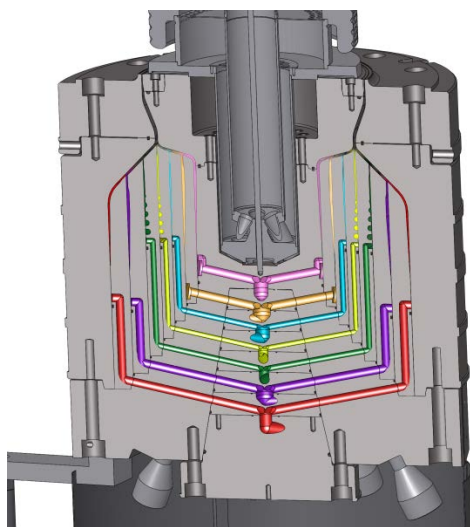
Fig. 3D 9-layer rigid, high barrier structure using cost/performance optimized PE resins



Fig. 3E 11-layer retortable, high-barrier structure using cost/performance optimized PP and copolymer PP resins

In the final analysis, the application determines the performance requirements, which in turn determine the function requirements. The ability to split an expensive sealant layer into two layers, one of which is less expensive, reduces the cost of the overall film and package. Assuming a single line that can produce 362 kg/hr x 22 hours/day up time x \$0.0272/kg = \$380,000/year savings [7]. This is achieved by substituting lower cost resins in a 9-layer structure as compared to a 7-layer structure. Figure 4 shows a schematic of a 7-layer die.

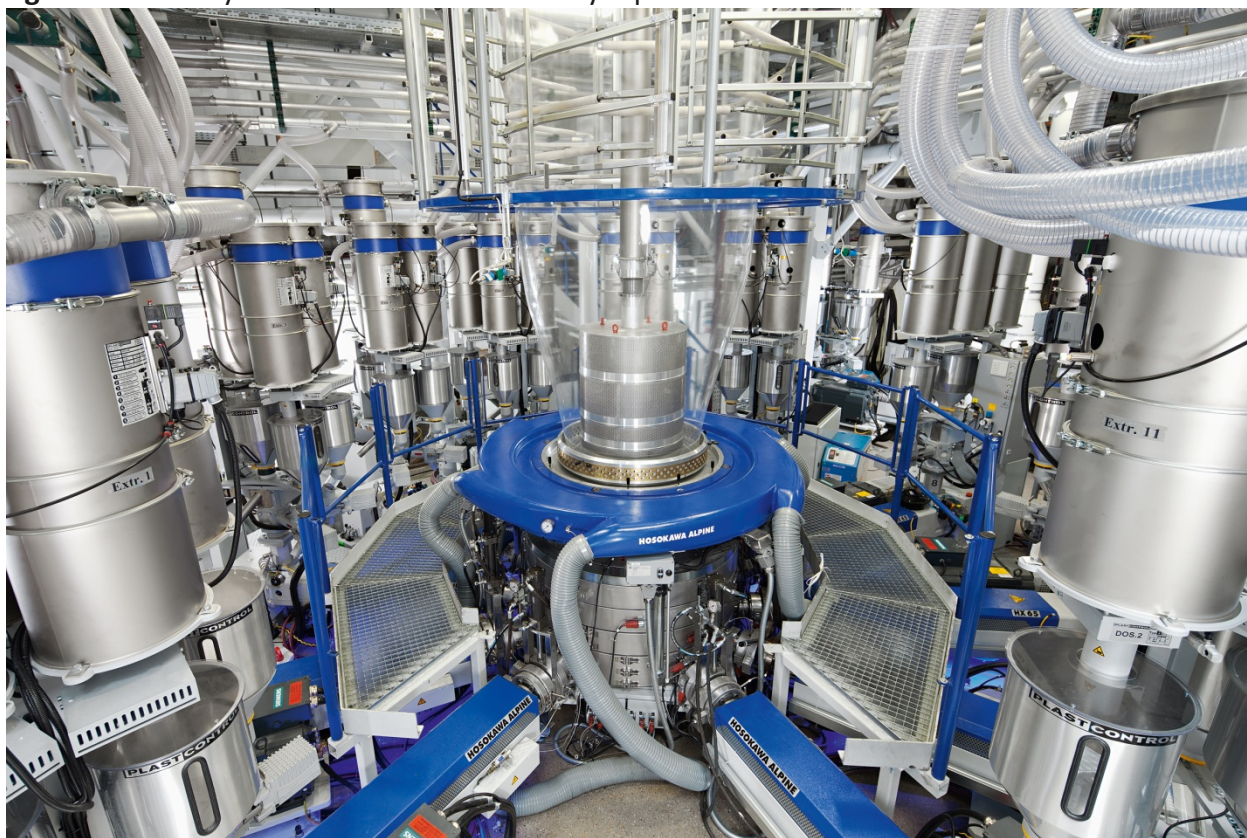
Figure 4. A cross-section of a 7-layer, nested spiral, blown film die. Courtesy Gloucester Engineering



In some parts of the world, some resins are simply not available, so substitution becomes a necessity. Moving to 9-layers gives further flexibility to the blown film manufacturer without sacrificing film properties. According to David Nunes, President of Alpine American in Boston, Massachusetts, USA, "There are dozens, perhaps more than 100, 7-layer blown film lines in use today. They offer the converter excellent flexibility in terms of product structure, asymmetric layer ratios, and film properties".

It is estimated that there are less than fifty (50) 9-layer lines in use in the world today, and 11-layer blown film lines are basically brand new entrees into the market place, so little practical information exists to report on today. It is envisioned that 11 layer structures will provide the ultimate in flexibility in terms of structures that can be made, with advances, asymmetric barrier structures being the target market. One technical source envisions a structure as shown in Figure 3 for use as a retortable pouch with superior barrier properties to be made on 11-layer blown film lines [4]. One configuration for an 11-layer blown film line is shown in Figure 5. It is readily discernible that manufacturing space becomes more and more crowded as the number of extruders is increased, creating a challenging operational and maintenance environment.

Figure 5. A 11-layer blown film line. Courtesy Alpine American



While none of the major manufacturers report any sales, or even the development of, a 13-layer die, a small development company in South Carolina, USA has been working on a 77-layer die which uses nano-technology via a series of layer-splitting rings to produce films of superior strength.

According to Henry Schirmer, CEO at BBS Corporation in Spartanburg, South Carolina, USA, "It has been shown that it is feasible to produce blown film configurations with up to 77 layers using our new Layer Sequence Repeater (LSR). This technology allows the polymer molecules to align without stress in a nanolayer film structure. This provides many advantages, such as increased blow-up ratio in blown film, higher orientation ratios on biax film lines, higher strength films, thinner films, and also improved clarity". Mr. Schirmer, who is author or co-author of nearly 100 patents, further indicates that "Nanolayer coextrusions of nylon 6 and EVOH can be made with higher-than-standard blow-up ratios on a blow film line, which yield high-strength, crystal-clear film, overcoming a present limitation of standard coextrusions of those two materials"[8, 9,10].

Nano-layer films are truly novel and exciting. Because the surface contact area within a nano-layer melt is so great and the mass is so small, instantaneous air quenching reduces crystallinity in a similar manner to water quenched films and high clarity is the result. Even DSC polymer signatures have been altered with nylon/EVOH combinations consistent with forming a co-polymer between these 2 active polymers, which is nothing short of miraculous.

Are there any alternatives to advanced multilayer blown film lines?

While there is a lot of technical merit to 7/9/11-layer blown film lines, the market will have to sort out the utility of this new technology. Until then, there is a very large installed base of 3- and 5-layer blown film lines, dozens or more oriented film machines, vacuum metallizers, adhesive laminators and extrusion laminators that, when taken together, can produce any combination of bulk layers, barrier layers, adhesives and sealants to satisfy any need without any further capital expenditure. And while not as Green or environmentally friendly perhaps as a single-step blown film operation, cost is quite often a driving factor in any product design or market category.

Conclusion

Technology exists today to produce blown films with up to 77 layers. The most common number of coextruded layers in use today is 3 layers, with a trend to 5- and 9-layer films. As machinery advances are made, new product structures are created to fulfill various market needs. A balance will be struck between cost of new capital equipment required to make 7/9/11-layer films, and the benefit derived from doing so. The competition is not necessarily another machine supplier, or from a lower cost producer, but from another technology that can laminate unlike films to produce similar structures, namely adhesive lamination and extrusion lamination. These technologies have coexisted for many years, and are likely to do so for the foreseeable future.

Bibliography

1. US Patent 2820249
2. US Patent 3308508
3. "Blown Film Training", The Dow Chemical Company
4. "Rethinking Technology Innovations for High Barrier Applications", Kurt Freye, Reifenhäuser Kiefel Extrusion
5. "Properties, Processing and Handling of EVAL™ EVOH Resins", Medlock, G., AIMCAL Fall Technical Conference, October 2014
6. "The Influence of Sealant Modulus on the Bending Stiffness of Multilayer Films", Morris & VanSant, DuPont Packaging White Paper, 2009
7. "Coextrusion - The Pros and Cons of More Layers", Bill Hellmuth, Gloucester Engineering

8. "Nano-layer - Micro-layer Structural Advances in Shrink Films, Schirmer et al, 2013 SPE International Polyolefins Conference, Houston, Texas, USA
9. <http://plasticsengineeringblog.com/2013/01/04/new-technologies-in-stretching-and-touching/>
10. US Patent number 8870561, issued 28 OCT 2014

POLYOLEFIN DISPERSIONS FOR AUTOMOTIVE INTERIOR APPLICATIONS

*Amit K Chaudhary and Parvinder Walia, The Dow Chemical Company, Midland, MI
Sarah Wakumoto, Colorado State University, CO*

Abstract

HYPOD™ aqueous polyolefin dispersions represent a new class of waterborne polymeric material produced by a proprietary mechanical dispersion process utilizing BLUEWAVE™ Technology. These dispersions are commercially available for use in various coating applications, and have characteristics similar to other water-based dispersions/emulsions (e.g. 40-50% solids, particle sizes 0.15-2.5 μm , viscosities from 300 to 3500 cP, and pH ranging from 7-11). With a wide array of olefin chemistries and crystallinities available from Dow, the polyolefin dispersion (POD) composition can be tailored to a specific application and performance requirements. Experimental POD dispersions have been developed for automotive interior applications, targeting soft skins and other automotive interior applications. The drivers for these applications are light weight, lower emissions, and potential recyclability. In addition, these skins show direct adhesion to polyurethane foams without any pretreatment. These dispersions can be tailored to fit various processing technologies – spray, cast and extrusion. This paper will provide a summary of these unique PODs tailored for the above processes.

Introduction

Traditionally, polyolefins have been available as pellets which are processed by conventional thermoplastic processes such as extrusion, thermoforming, injection molding, and blow molding. The lack of a viable emulsion polymerization process for the production of polyolefins has prevented the availability of these polymers in a waterborne emulsion form, suitable for use in coatings, binders, adhesives, and other applications where emulsion polymers are typically used. BLUEWAVE™ Technology is Dow's proprietary high-shear mechanical dispersion process technology [1, 2] that enables the production of waterborne dispersions of traditional thermoplastic polymers and elastomers, not possible via conventional emulsion polymerization process. The resulting dispersion has a narrow particle size distribution (approximately 1 μm) and solids content of up to 60 wt%. Low surfactant content enables customers to minimize surfactant effects, and maintain a very high level of product performance. When applied to a heated substrate, the water evaporates, forming a coating that is thin and cost effective for a variety of applications. These dispersions when applied to

various substrates offer the exceptional characteristics of polyolefins, including water and chemical resistance, heat sealability, thermoform ability (embossing), adhesion to polyolefin substrates, low temperature flexibility, and others. This technology permits the use of polyolefins in a wide range of new applications including coatings, sealants, binders, adhesives, and foams.

Aqueous polyolefin dispersions have the potential to be utilized for a variety of automotive applications such as soft skins, artificial leather, adhesives, and carpet binders. There are several methods to make soft skins for an automotive interior article, such as an instrument panel, door panel, console, glove compartment cover, and others. Soft skins are used in automotive interior applications for superior touch/feel/haptics. Positive thermoforming, negative thermoforming, slush molding, and spray coatings are four major processes used to make skins. Slush molding and spray processes offer the most design freedom and provide the ability to do complex geometries and fine grain detail (can even imitate stitching). Until recently, polyvinyl chloride (PVC) was the material of choice for interior skins, and is ideally suited for slush molding. However, PVC formulations suffer from migration and volatilization of the plasticizers over time, and this leads both to physical property changes during aging and fogging of the car window glass. PVC also suffers from being heavier than alternative materials. This is an important consideration in the current design of automobiles with the emphasis on lighter materials to reduce the overall weight of the vehicle and thus increase fuel efficiency. Additionally, the low temperature (-40 °C) ductility, and air bag deployment, is an issue with PVC, especially maintaining ductility with time (and heat aging).

Alternatives to PVC include thermoplastic polyurethanes (TPU), thermoplastic polyolefins (TPO), and polyolefin elastomers (POE). TPU has good scratch and mar properties and better low temperature properties than PVC, but aromatic based TPUs have poor ultraviolet (UV) light resistance. Aliphatic isocyanates can be used to prepare TPUs having good UV light resistance but at a significant cost penalty.

Blends of polypropylene (PP) and a polyolefinic rubber, referred to as thermoplastic polyolefin (TPO), is a good alternative [3, 4]. TPO possesses better ductility than PVC. Moreover, it retains its ductility over time since it does not contain any low molecular weight

plasticizers, as does PVC. TPO performs better in comparison to PVC in interior automotive applications. TPO is less expensive as compared to TPU.

Polyurethanes (PU) have been the resins of choice for spray processes. A polyurethane reaction mixture is sprayed onto a mold surface and allowed to cure to produce the skin layer. For PU materials, volatile organic compounds (VOCs) are released and scrap is not recyclable. Further, polyurethane spray process equipment requires complex mixing capabilities as well as the need for solvent flushing.

The polyolefin spray skin approach offers the following advantages over a PU spray process:

- Lighter weight – lower density as compared to PU. Also potential of thin gauging.
- Lower VOCs – aqueous polyolefin system.
- Recyclability - scrap and captured overspray could be recycled in-house (it's a thermoplastic elastomer).
- Eliminate solvent flush needed for PU.
- Simplified process with a single component system with no mixing and curing requirements.

Materials and Methods

An olefin block copolymer (OBC) is used along with ethylene acrylic acid copolymer (EAA) based dispersing agent to produce a polyolefin dispersion using the proprietary BLUEWAVE™ Technology (Figure 1). The material properties of the polymers (supplied by The Dow Chemical Company) used in this study are presented in Table 1. The OBCs used were soft and covered a Shore A hardness range of 60-85

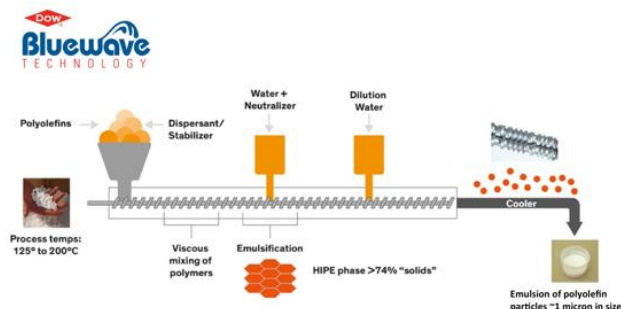


Figure 1. BLUEWAVE™ Technology.

The hydroxyethyl cellulose (HEC) based thickeners used in this study (supplied by The Dow Chemical Company) were:

- CELLOSIZETM QP 15000H (medium molecular weight cellulosic polymer)
- CELLOSIZETM QP 100MH (high molecular weight cellulosic polymer)

Table 1. Raw material properties.

Materials	Material Characteristics	Melt Index, g/10 min (2.16 Kg@ 190°C)	Density (g/cm ³)
OBC-1	Shore A = 83	5.0	0.887
OBC-2	Shore A = 60	5.0	0.866
EAA Copolymer	20.5 wt% acrylic acid content	300	0.958

Methods used for characterization of the various physical properties of the polyolefin dispersion is described in Table 2.

Table 2. Characterization methods for polymer dispersion.

Measurement	Instrument Used	Condition
Particle Size	LS 13 320 Beckman Coulter particle size analyzer	Test done with dilute solution of sample
Viscosity	Brookfield viscometer	RV2, 50 rpm
Solids	Sartorius moisture analyzer	1g sample at 120°C

Results and Discussion

The physical properties of the aqueous dispersion produced using the BLUEWAVE™ Technology dispersion process is presented in Table 3 and the particle size distribution is presented in Figure 2.

Skins were made by spraying the dispersions with a hand held pneumatic spray gun on a 5"x5" grained tool (Figure 3a) that was pre-heated to 80 °C in a convection oven. The tool was then placed in an oven to remove the excess moisture. Figure 3b shows the quality of the grain in the skins produced using the dispersion.

Table 4 presents the mechanical properties of the two polyolefin spray skins prepared using POD-1 and POD-2 respectively along with aromatic PU skin made via spray process and PVC skin made via slush molding process. As presented in the table, the Shore A and tear strength of all the skins are comparable to each other. The tensile properties are also comparable though it is slightly lower than the PU or PVC skins. Any impact on the part performance, especially air bag deployment, is expected to be minimal. However, this would have to be validated on an actual part.

Table 3. Physical properties of the polyolefin dispersions.

	POD – 1	POD – 2
Polymer Used	OBC-1	OBC-2
Average Particle Size (µm)	1.07	0.97
Viscosity @ 20°C (cP)	280	250
Solids (wt%)	40.2	39.8
pH	10.4	10.2

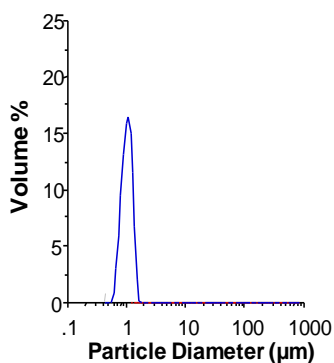


Figure 2. Particle size distribution of the polyolefin dispersion.



Figure 3. (a) Grain pattern of the tool used for producing skin, (b) grain pattern of the polyolefin skin produced.

Table 4. Physical Properties of the Polyolefin Dispersion.

Skin	Shore A	Tear Strength ISO 34-1 (N/mm)	Tensile Strength ISO 527-3 (N/mm ²)	Elongation at Break ISO 527-3 (%)
PO Spray Skin 1	73-78	24	5.0	170
PO Spray Skin 2	73-78	21	4.8	160
Aromatic PU Spray Skin	73-78	14	6.7	240
PVC Slush Skin	73-78	31	11	301

One of the key requirements of such polymeric skins is the thermal stability up to at least 100°C. Figure 4 presents the DSC scans for the prepared OBC skin – showing the melting point of the skin to be above 120 °C. To further confirm the thermal stability of the prepared skins, small sections of these skins were aged in an oven

at 100 °C for 4 h. The skin after heat aging showed excellent grain retention, thereby indicating that these skins are thermally stable up to 100 °C.

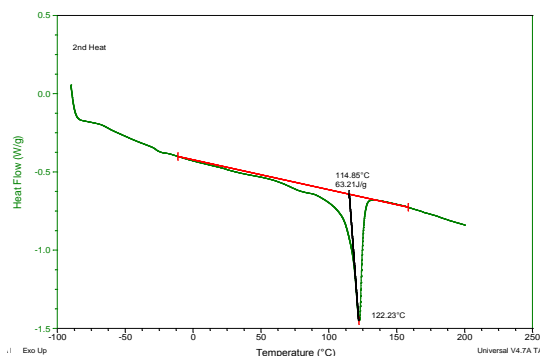


Figure 4. DSC Scan of the Polymer Skin (Tm=122 °C).

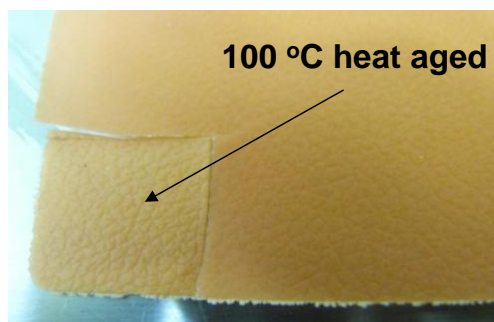


Figure 5. Excellent grain retention after thermal aging

Another critical requirement for interior skins is adhesion to PU foam. A typical instrument panel Dow foam system (NM856: prepared with PAPI-94 isocyanate and NM 858 polyol) was used to back foam these spray skins. Excellent PU foam adhesion (Figure 6) was achieved. Cohesive failure was judged visually (qualitative) based on the amount of area on skin that was covered with foam upon peeling.

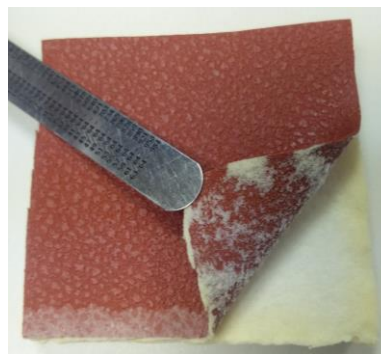


Figure 6. Cohesive Failure of the polyolefin skin and the PU foam.

Further, the possibility of the use of such aqueous dispersions was explored for its use in cast or extrusion

process for making skins. Different applications have different viscosity requirements. For instance, dispersions for spray skins must be thin enough to be sprayed, yet thick enough to not drip off of a hot mold surface. Ideal viscosity for spray skins is about 100-1000 cP, while for cast skins, it is about 1,500 to 3,000, so the dispersion can be laid onto a release paper and for extrusion process dispersions with significantly higher viscosities (15,000-30,000 cP) is required.

Viscosity can be tailored by either changing the dispersion formulation (e.g. solid concentration, surfactant type and concentration, etc.) or by the addition of thickeners which provides the benefit of working with one base polyolefin dispersion formulation. The later approach was investigated to test the viability of the polyolefin dispersion in cast or extrusion process. Two different hydroxyethyl cellulose based thickeners were chosen for this study (medium MW and high MW).

Small amount of the thickeners (0.5 and 1.0 wt%) were dispersed in the aqueous polyolefin dispersion using a cowles blade mixer. The viscosity of the samples were tested after 24 h using a Brookfield viscometer at 50 rpm. The results are presented in Figure 7. Based on the data it is evident that thickeners can be used for altering the viscosity of such aqueous dispersions. This approach provides flexibility for using either spray, cast or extrusion process.

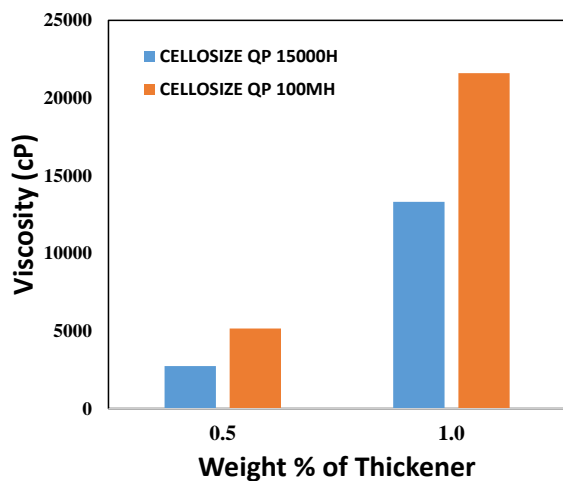


Figure 7. Effect of thickener on the viscosity of the dispersion

Conclusions

Aqueous dispersion of polyolefin elastomers prepared using BLUEWAVE™ Technology could be used to successfully produce soft skins that can be used in the

automotive interior application. The spray skins demonstrated the following features:

- Excellent grain replication
- Good haptics
- Mechanical properties comparable to other soft skin materials and technologies
- Good thermal aging under conditions seen in interior applications (100 °C).
- Direct adhesion to PU foam (typically polyolefin substrates require flaming or primers)

These dispersions can be tailored to fit various processing technologies – spray, cast, and extrusion, by addition of a thickening agent [5]. Future work will focus on further development of the dispersion for validation of OEM specs and incorporation of color/UV package required for interior applications.

™Trademark of The Dow Chemical Company ("Dow") or an affiliated company of Dow

References

1. B. Moncla, M. Kalinowski, D. Speth, C. Diehl, D. Schmidt, K. Maak, W. Liang, G. Strandburg, *Aqueous Dispersion, Its Production Method and Its Use*, US 20070292705A1 (Dow Global Technologies Inc.).
2. A. Neubauer, A. Quaranta, N. Dunchus, M. Kalinowski, G. Strandburg, K. Maak, *Dispersions of Higher Crystallinity Olefins*, US20100255207 A1 (Dow Global Technologies Inc.).
3. R. Eller Associates, "Automotive Interior Skins and Foams", pp. 1-4 to 1-11., Robert Eller Associates, November 1997
4. S. Shah, N. Kakarala, J. Schneider, "An Overview of Advances in TPO Skin Material and Process Technology," Proceedings of TPO in Automotive '98 Conference, Novi, MI, October 1998
5. P. Walia, A. Chaudhary, G. Klumb, *Method to Make an Elastomeric Polyolefin Skin*, WO2016148897 A1 (Dow Global Technologies Inc.).